REGULATION OF THE HUMAN NEK8/NPHP9 PROTEIN DURING CELL CYCLE PROGRESSION AND CILIOGENESIS

Thesis submitted for the degree of
Doctor of Philosophy
at the University of Leicester

by

Detina Zalli BSc (Hons) (SUSSEX)
Department of Biochemistry
University of Leicester

November 2011

DECLARATION

The accompanying thesis submitted for the degree of Doctor of Philosophy, entitled *"Regulation of human Nek8/NPHP9 protein during cell cycle progression and ciliogenesis"* is based on work conducted by the author in the Department of Biochemistry at the University of Leicester during the period October 2008 to October 2011. All of the work recorded in this thesis is original unless otherwise acknowledged in the text or by references. None of the work has been submitted for another degree in this or any other University.

Signed:

Date:

Department of Biochemistry
University of Leicester
Lancaster Road
Leicester
LE1 9HN

REGULATION OF THE HUMAN NEK8/NPHP9 PROTEIN DURING CELL CYCLE PROGRESSION AND CILIOGENESIS

Detina Zalli

Summary

The primary cilium, once considered an evolutionary vestige, has re-emerged as an essential organelle for the normal functioning of a wide variety of cellular processes. It is now clear that it has important roles in the control of cell proliferation and signalling during development, with defects in primary cilia being a major cause of many human diseases. These disorders, collectively referred to as ciliopathies, include the cystic kidney diseases that are characterized by aberrant cell proliferation and cyst formation. Mutations in the NIMA-related kinase, Nek8, are associated with cystic kidney disease in both humans and mice, with Nek8 being the candidate NPHP9 gene in the human juvenile cystic kidney disease, nephronophthisis. Previous localisation studies have shown that Nek8 localises to centrosomes and cilia in dividing and ciliated cells, respectively, strengthening the ciliary hypothesis of cystic kidney disease. However, the role of Nek8 in ciliogenesis remains to be defined and no substrates for this kinase have yet been identified. In this thesis, I present data from a series of biochemical and cell biology experiments aimed at investigating the regulation and function of Nek8 with respect to cell cycle progression and ciliogenesis. I first of all show that localization of Nek8 to centrosomes and cilia is dependent upon both its kinase activity and its C-terminal non-catalytic RCC1 domain. Interestingly, Nek8 was capable of phosphorylating the RCC1 domain, which in isolation also localized to centrosomes and cilia. This leads us to propose that centrosome recruitment is mediated by the RCC1 domain, but requires a conformational change in the full-length protein that is promoted by autophosphorylation. I then established conditions required for measurement of Nek8 catalytic activity. Besides confirming the predicted activity of catalytic site mutants, this revealed that the three NPHP9-associated point mutants did not exhibit loss of activity. However, as one of these mutants, H425Y, failed to localize correctly, we predict that this mutation, which lies in the RCC1 domain, alters the RCC1 conformation such that it disrupts its centrosome targeting motif. Importantly, I also show that serum starvation induces proteasomal degradation of Nek8, specifically in cell lines in which serum starvation induces quiescence and ciliogenesis. Strikingly, serum starvation also induces Nek8 kinase activity, whilst maintained expression of Nek8 appears to suppress ciliogenesis. Taken together, these findings not only reveal important mechanisms through which Nek8 activity and localization are regulated, but suggest that Nek8 itself may have both positive and negative activities in the process of ciliogenesis.

ACKNOWLEDGEMENTS

Above all, I want to thank the person who hired me for the project, and then stood beside me during the whole period, and on each level: from the participation in the project, through developing my ideas and learning to present them, Prof. Andrew Fry. Andrew, I cannot express enough how valuable it has been to have the door always open to your guidance, help, and expertise. You spent time contemplating my ideas, both those with some possible future and the hopeless ones, always coming back with inspiring comments. Knowing them made my life richer and my faith in science and mankind much stronger. This thesis would have not been possible without you. I couldn't have wished for a better supervisor.

Thank you to my committee members, Dr. Martin Dickens and Dr. Sally Priger for their insightful criticism throughout the duration of this project. I would like to thank Dr. Raj Patel, Dr. Kees Straatman and Barbara Birch for their high spirit and jollity.

Thanks are also due to all members of the Fry lab, past and present. I would like to especially thank two lab members, Carlo and Tara, who have been by my side continuously providing support and encouragement from the day that I arrived till the last day of my stay in Leicester. Thanks also to Laura, Jo, Magali, Nav, Suzy and Sarah. Laura, you have been absolutely brilliant with me. Jo, you are one of the most wonderful persons I have met in my life. Thanks for everything you have done for me guys. I would also like to thank all members of lab 2/43, Samrein, Eva, Juhwan and Dalhee for their support and encouragement throughout this PhD.

A special thanks goes to my fiancé Sai, for his love, encouragement and patience. Thanks also to my in laws for being always there for me when I needed advice and encouragement and taught me to look at things in a positive manner even when things didn't look good. Also thanks to my brother-in law, Redi, who have constantly encouraged and support me. Redi, without your help, I wouldn't have made it.

Finally, I would like to thank my Mom, Dad and twin sister for their patience, encouragement and unwavering support through the years. You are my compass. Mom, Dad and Gita, I feel the luckiest person of the world, because I have you.
"Mami-Babi-Gita, Keni qene, Jeni dhe Do Te Jeni gjithmone drita e syve te mi!"

I devote this PhD to you.

TABLE OF CONTENTS

ABBREVIATIONS

A	absorbance
aa	amino acid
ab	antibody
ADPKD	Autosomal dominant polycystic kidney disease
ALMS	Alström Syndrome
ARPKD	Autosomal recessive polycystic kidney disease
APS	ammonium persulphate
APC/C	Anaphase promoting complex/cyclosome
ATP	adenosine triphosphate
bp	base pairs
BBS	Bardet-Biedl Syndrome
BCA	bicinchoninic acid
BSA	bovine serum albumin
BCIP	5-bromo-4-chloro-3-indolyl phosphate
C-	carboxy
CC	coiled-coil
Cdk	cyclin-dependent kinase
cDNA	complementary deoxyribonucleic acid
CE	convergent extension
CEP/Cep	centrosomal protein
C-Nap1	centrosomal Nek2-associated protein 1
cm	centimetre
CNS	central nervous system
CPC	chromosome passenger complex

DMEM	Dulbecco's modified eagle's medium
DMSO	dimethylsulfoxide
DNA	deoxyribonucleic acid
dNTPs	deoxynucleotide triphosphates
dsRNA	double stranded ribonucleic acid
DTT	dithiothreitol
EDTA	ethylene diamine tetraacetic acid
EGTA	ethylene glycol tetraacetic acid
EST	expressed sequence tag
FACS	fluorescence activated cell sorter
FBS	foetal bovine serum
FL	full length
GFP	green fluorescent protein
GL2	firefly luciferase
GST	glutathione-S-transferase
HEK293	human embryonic kidney 293 cells
Hh	Hedgehog
HRP	horseradish peroxidase
hFF	human foreskin fibroblasts
hTERT-RPE1	telomerase-immortalized human retinal pigment epithelial
HU	hydroxyurea
Hz	hertz
IF	immunofluorescence
IFT	Intraflagellar transport
IMCD3	renal inner medullary collecting duct cells
INCENP	Inner centromere protein

IPTG	isopropyl 1-thio-β-D-galactopyranoside
IVT	in vitro translation
JATD	Jeune asphyxiating thoracic Syndrome
JBTS	Joubert Syndrome
kDa	kilo Daltons
KESTREL	kinase substrate tracking and elucidation
K-fiber	kinetochore fiber
LB	Luria Bertani
LCA	Leber congenital amaurosis
LisH	Lissencephaly-1 homology
LMB	Leptomycin-B
LB	Luria Bertani
MAP	microtubule-associated protein
MBP	myelin basic protein
MEK	MAP kinase kinase
MKS	Meckel-Gruber Syndrome
mRNA	messenger ribonucleic acid
mg	milligrams
mM	millimolar
MT	microtubule
MTOC	microtubule organizing center
µM	micromolar
µg	microgram
NBT	nitroblue tetrazolium
N-	amino
Nek	NIMA-related kinase

NIMA	Never in mitosis A
ng	nanogram
nM	nanomolar
NP-40	nonidet P-40
NPHP	Nephronophthisis
OD	optical density
OFD1	oral-facial-digital syndrome type 1
O/N	overnight
PBS	phosphate buffered saline
PC1	polycystin 1
PC2	polycystin 2
PCD	Primary cilia dyskinesia
PCM	pericentriolar material
PCM-1	pericentriolar material protein 1
PCP	planar cell polarity
PCR	polymerase chain reaction
PDGFRα	Platelet-derived growth factor receptor α
Pen/Strep	penicillin/streptomycin
PKD	Polycystic kidney disease
Plk	polo-like kinase
PMSF	phenylmethylsulphonyl fluoride
Ptc	Patched
$p70^{S6K}$	p70 ribosomal S6 kinase
RCC1	regulator of chromatin condensation-1
RNA	ribonucleic acid
RNAi	ribonucleic acid interference

RP	Retinitis pigmentosa
RPGR	Retinitis pigmentosa GTPase regulator
rpm	revolutions per minute
RPTEC	Renal proximal tubule epithelial cells
SAC	Spindle assembly checkpoint
SDS	sodium dodecyl sulphate
SDS-PAGE	sodium dodecyl sulphate polyacrylamide gel electrophoresis
sec	seconds
SIN	septation initiation network
SGBS2	Simpson-Golabi-Behmel Syndrome type 2
siRNA	small interfering ribonucleic acid
Smo	Smoothened
SNLS	Senior-Løken Syndrome
Shh	Sonic hedgehog
SPB	spindle pole body
TACC	transforming acidic coiled coil
TEMED	N, N, N, N,-tetramethylethylenediamine
TBS	tris-buffered saline
Tris	Tris (hydroxymethyl) aminomethane
U	unit
U2OS	osteosarcoma cells
µg	micrograms
µM	micromolar
µl	microlitre
UV	Ultraviolet
V	Volts

v/v	volume/volume
w/v	weight/volume
WT	wild-type
γ-TuRC	γ-tubulin ring complex

TABLES AND FIGURES

Tables:

Figures:

Chapter 1

Introduction

1.1 Organization and generation of cilia

The word cilium, meaning eyelash in latin, was first named in 1968 by Sergei Sorokin to describe tiny hair-like projections that extend like antennae from the surface of most cells in the body (Sorokin, 1968). Indeed, with the exception of higher plants and fungi, these evolutionary conserved organelles can be found on most eukaryotic cells (Baker and Beales, 2009). They generally fall into two types: motile cilia, of which there are many per cell, and primary non-motile cilia, which are present in single copies per cell. Although the biological function of motile cilia in cell motility and fluid transport have long been recognized, most primary cilia were long considered as vestigial organelles of little functional importance. However, this has changed dramatically in the last decade since the crucial role of primary cilia in cell signalling pathways has been highlighted. Furthermore, increasing evidence suggests that as primary cilia are key coordinators of signalling pathways during development and in tissue homeostasis, then defects in primary cilia are a major cause of many human diseases and developmental disorders, collectively referred to as ciliopathies (Baker and Beales, 2009; Satir, 2008; Singla and Reiter, 2006). In this section, I will provide a general introduction to the cell biology of cilia.

1.1.1 Structure of cilia

The cilium is an organelle that extends from the cell surface and is composed of a microtubule-based cytoskeleton, the axoneme, enclosed within a specialized section of the plasma membrane. Although contiguous, the ciliary membrane is both structurally and functionally distinct from the plasma membrane (Figure 1.1A). This distinction is made possible by the presence of a “transition zone” or “ciliary necklace”, located at the junction between the cilium and the plasma membrane. The transition zone contains a ciliary-pore complex that marks the compartment border at which access from the cytoplasmic compartment to the ciliary compartment, is controlled. The axoneme of the cilium extends from a basal body which sits at the cell surface. It therefore mirrors the organization of the basal body and consists of nine doublet microtubules arranged in a ring, with or without a central pair of microtubules (designated as 9+2 or 9+0, respectively). At the distal end of the cilium is a cap structure that links the axonemal microtubules to the ciliary membrane and is the major site of axonemal microtubule subunit addition and subtraction (Fliegauf et al., 2006; Marshall and Nonaka, 2006).

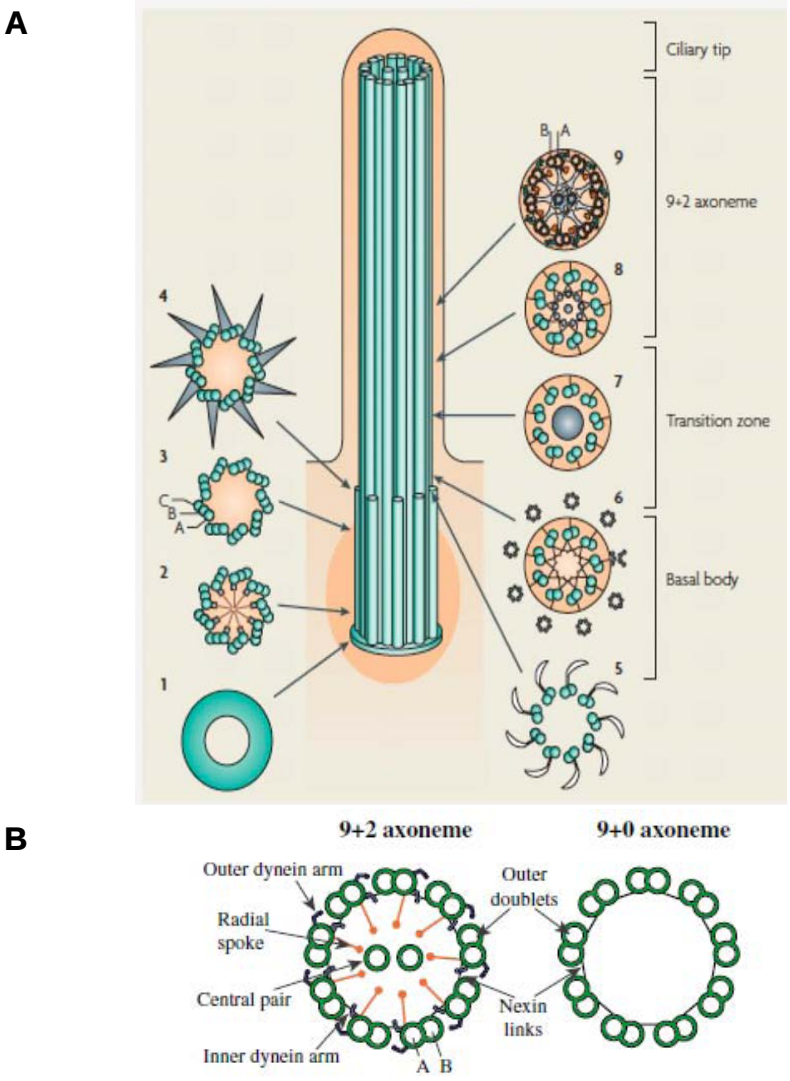

Figure 1.1 The general architecture of a cilium
(A) Schematic diagram showing a longitudinal section through a motile cilia. The ciliary tip contains microtubule plus (+) ends (from which axonemes grow) and is the site where the switch between the anterograde (kinesin) and retrograde (dynein) intraflagellar transport (IFT) occurs. The axoneme (9) which is the structural core of the cilium, extends as a continuation of the basal body. Each doublet microtubule is made of an α and β tubule that are linked together by nexin filaments. They are also held in place by radial spokes that extend into the axoneme centre. At the junction between the cilium and the basal body is the transition zone (7), the place where the triplet microtubules of the basal body are converted into the axonemal doublet microtubules. In the lower part of the transition zone, transition fibres (4 and 5) connect each microtubule doublet to the membrane and mark the ciliary gateway, the place where the IFT proteins accumulate. In the upper part of the transition zone, stellate fibre arrays (6 and 8) and an amorphous disk structure (7) are present and give rise to the central microtubules in 9+2 axonemes. The basal body (1-4), has a microtubular structure typical of a centriole with nine triplets of microtubules (tubules of each triplet depicted as A, B, and C). It is embedded in pericentriolar material (dark orange) with a proximal amorphous disc (1), a cartwheel structure (2), a middle piece that lacks appendages (3) and transition fibres at the distal end (4). **(B)** Schematic diagram of a transverse section through a motile 9+2 axoneme and an immotile 9+0 axoneme. Adapted from Fliegauf et al. (2007) and Dawe et al. (2007).

The main role of the axoneme is to serve as a scaffold to organize associated protein complexes. Specifically, it acts as a binding site for microtubule-based molecular motors. Therefore, it functions in intraflagellar transport (IFT) and also allows the cilia to bend in response to luminal fluid flow. Ciliary microtubules are nucleated at the distal end of the transition zone. Each doublet microtubule consists of $\alpha\beta$ tubulin heterodimers assembled into linear protofilaments that then associate laterally to form a hollow tube. The A tubule is a complete microtubule made up of 13 laterally associated protofilaments, whereas the B tubule, is an incomplete tubule, and consists of 10 protofilaments but which shares part of its wall with the A tubule (Fliegauf et al., 2006; Marshall and Nonaka, 2006; Satir and Christensen, 2007). Ciliary microtubules are highly stable and don't undergo the rapid growth and shrinkage typical of cytoplasmic microtubules. This is due to post-translational modifications such as acetylation and polyglutamylation (Hagiwara et al., 2002; Hoyer-Fender, 2010). In this sense, ciliary microtubules are very similar to those found in centriole and basal bodies. In eukaryotes, cilia and flagella are structurally similar, and the terms "cilia" and "flagella" refer to very similar organelles. Typically, though, flagella are long structures whereas cilia tend to be short. For example, the mammalian spermatozoon has a single long flagellum, which aids in its swimming, whereas the unicellular *Paramecium* is covered with a few thousand short cilia, which are used both to move and to bring in food particles. Large numbers of cilia are also found in the respiratory passages (the nose, pharynx, and trachea) of humans, where they aid in mucus clearing (Baker and Beales, 2009; Marshall and Nonaka, 2006). As indicated above, based on their structure and ability to move, cilia have been classified in two main types: motile cilia, consisting of a 9+2 axoneme, and immotile/primary cilia, which contain a 9+0 axoneme (Figure 1.1B). Recently, two other classes of cilia have been described, known as nodal cilia and the kinocilium. The nodal cilium has a 9+0 axoneme and is motile, whereas the kinocilium generally consists of a 9+2 axoneme but is immotile.

1.1.1.1 Motile cilia

Motile 9+2 cilia have been the most studied of all cilia. They are found on the apical surface of epithelial cells of the trachea, ependymal cells in ventricles of the brain, and on cells lining the oviduct and epididymis of the reproductive tracts. Normally they are present in large numbers that consist of 200-300 individual cilia per cell and beat in an orchestrated wave to move material over the surface of the cell. The main function of these 9+2 cilia is to promote movement of fluids or substances, e.g. for mucociliary clearance in the lung, cerebrospinal fluid

movement in the brain, and ovum and sperm transport along the reproductive tract (Figure 1.2A) (Baker and Beales, 2009; Davenport and Yoder, 2005). Motile cilia are usually 10-15 μm long and beat at approximately 10-20 Hz. The 9+2 microtubule pattern, where nine microtubule doublets surround a central pair of microtubules, is important for the generation of forces needed to induce motility. A number of protein complexes important for motility attach to the outer double microtubules, including the outer and inner dynein arms (ODAs and IDAs, respectively), the radial spokes, and the central-pair projections. These all act coordinately to create the rhythmic beating of the motile cilia. The radial spokes connect the outer doublets with the inner doublet and allow the generation of shear forces needed to bend the cilium. Furthermore, they contain a solid-state signal transduction pathway that regulates motility by linking the position of the central pair to the activity of dynein arms. The ODAs and IDAs are force-producing molecular motors that cause the doublet microtubules to slide with respect to one another, in a process dependent on ATP hydrolysis (Figure 1.3A and 1.3B) (Baker and Beales, 2009; Marshall and Nonaka, 2006; Satir and Christensen, 2007). This inter-doublet sliding is normally constrained by inter-doublet nexin linkages and attachment to the basal body, thereby leading to cilium bending. The latter is coordinated by the radial spokes and central-pair projections, with an effective stroke and a recovery stroke. When active, the dyneins on one side of the axoneme are responsible for the generation of the effective stroke, whereas the dyneins on the opposite side generate the recovery stroke (Figure 1.3C). Upon bending, cilia will cause the bending of the adjacent cilia, initiating a wave along the epithelium, thus resulting in unidirectional flow of fluid (Guirao and Joanny, 2007; Satir and Christensen, 2007). Thus, cilia beat as part of a metachronal wave and ciliary beating is coordinated. However, this is not necessarily the case for cilia on different cells if these ciliated cells are not next to each other, suggesting that the close spatial relationship of cilia is important for coordinated beating. This might explain why cilia are densely packed and close together on all naturally occurring ciliated surfaces e.g., in the fallopian tubes, the airways, and the ventricles (Salathe, 2007). This plays an important role in initiating a defence mechanism against respiratory pathogens, toxins, and particulate matter. Indeed, defects in motile cilia can lead to many associated diseases. For example, defects in ciliary motility in the respiratory tract produce failure in mucus clearance, leading to bronchiectasis and chronic sinusitis. Defects in ciliary motility in the node can cause situs inversus (the reverse of organ laterality) and defects in ciliary motility in the brain can cause hydrocephalus (Baker and Beales, 2009; Ishikawa and Marshall, 2011; Salathe, 2007; Satir and Christensen, 2007).

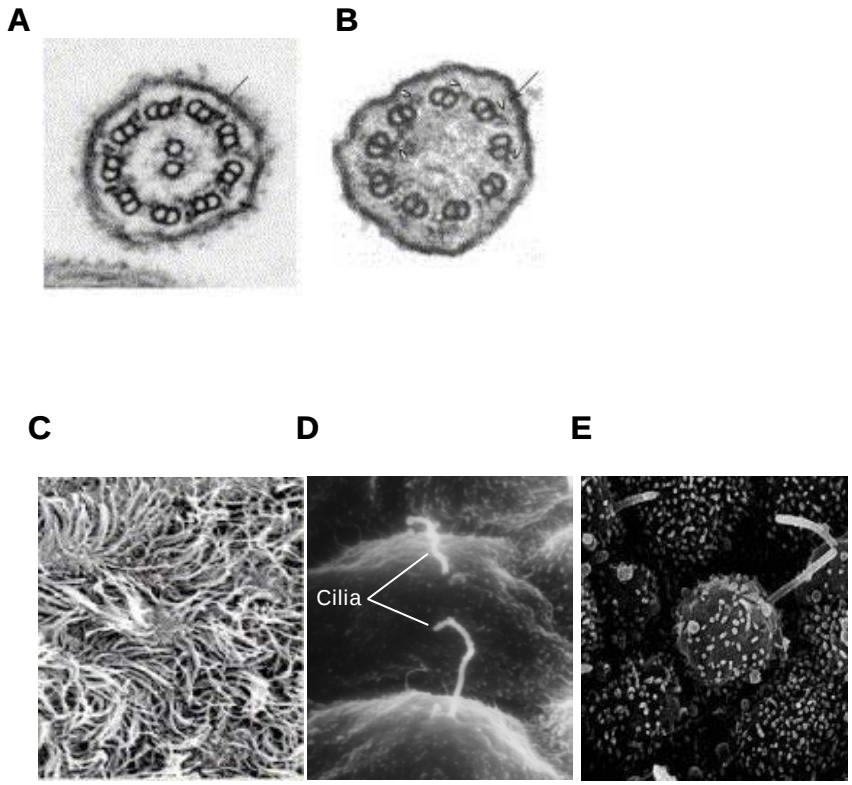

Figure 1.2 The different types of cilia
Transmission electron micrographs showing cross-sections through the (9+2) motile cilia **(A)** and the (9+0) primary cilia **(B)**. Scanning electron micrographs of motile cilia lining the oviduct showing multiple cilia per cell **(C)**, a primary cilium located on the apical surface of the renal tubule epithelium **(D)**, and a nodal cilium projecting from the surface of the node in a mouse embryo **(E)**. Adapted from Huangfu and Anderson (2005) and Zhang et al. (2005).

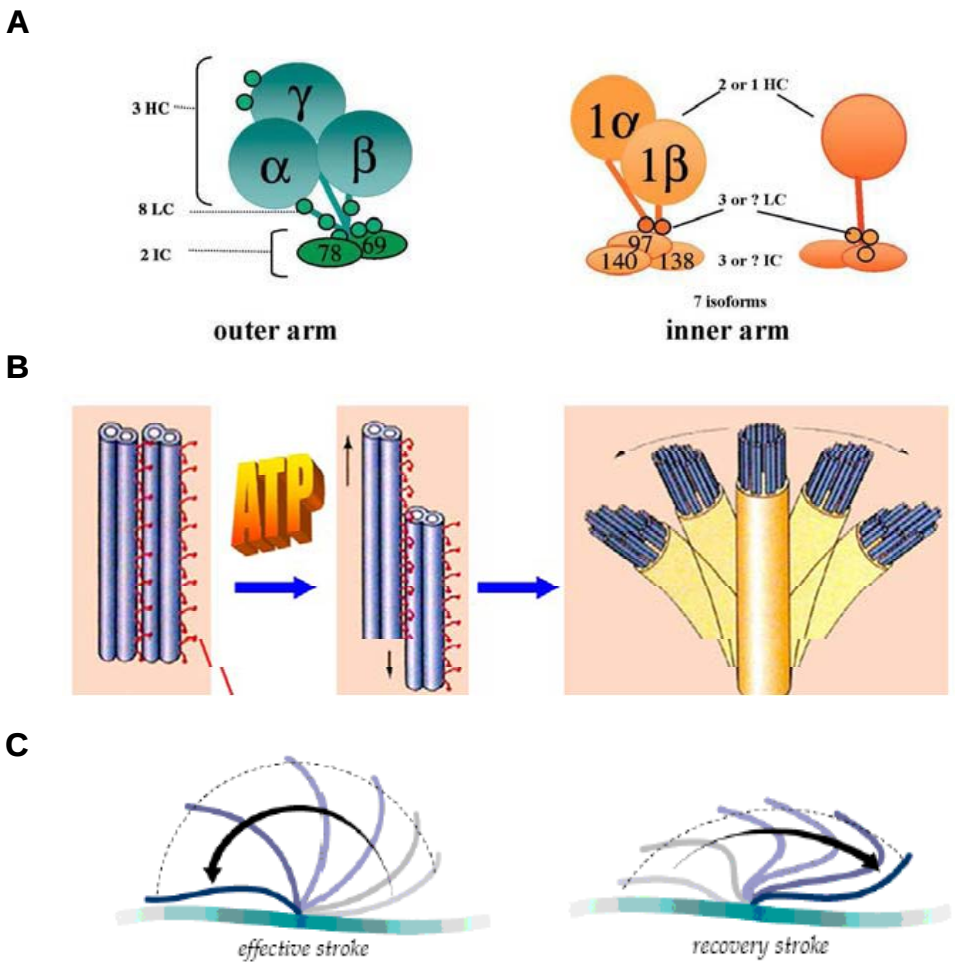

Figure 1.3 The mechanism of cilia movement
(A) Schematic diagram showing the outer and inner dynein arms that are found in the ciliary axoneme. Note that the molecular structure of the dynein is different for the inner and outer arms. **(B)** The dyneins change conformation by converting energy released by hydrolysis of ATP. The change in conformation leads to a relative change in position of the pairs of microtubule, resulting in a bending motion of the axoneme. **(C)** Schematic diagram showing the movement of an individual motile cilium. The motion is asymmetric, consisting of an effective stroke and a recovery stroke, leading to a "metachronic wave". Adapted from Guirao (2007).

1.1.1.2 Primary cilia

The primary cilium was so named by Sergei Sorokin (Sorokin, 1968) to highlight the initial single cilium (therefore called “primary”) that precedes the formation of large numbers of additional cilia which appear in multiciliated epithelial during differentiation (also called secondary cilia).

The primary cilium is a ~3-10 µm long solitary, non-motile organelle that extends from the cell surface of most differentiated post-mitotic mammalian cell types. For example, it is found on epithelial cells lining the kidney tubule, the bile duct, the endocrine pancreas, and the thyroid, but is also present on non-epithelial cells such as chondrocytes, fibroblasts, smooth muscle cells and neurons. Unlike motile cilia, primary cilia have a 9+0 microtubule structure and lack the key elements required for ciliary motility, such as the central pair of microtubules, the radial spokes, and the outer and inner dynein arms that power microtubule sliding (Figures 1.1B and 1.2B). For this reason, primary cilia are immotile and for a long time scientists considered them to be rudimentary or vestigial organelles since they do not show the typical wave motion seen with motile cilia.

All this has now changed with the discovery that mutations that induce failure of primary cilia formation give rise to diverse human diseases. In fact, the primary cilium plays an essential role in multiple cell signalling pathways, since a variety of receptors, ion channels and transporter proteins, as well as some of their downstream effector molecules, localize to the cilium or basal body. Thus, primary cilia are now understood to be predominantly sensory organelles (Marshall and Nonaka, 2006; Satir, 2008; Satir and Christensen, 2007). In fact, because the cilium protrudes from the cell surface, it is thought of as being a cell’s antenna that receives signals from the periphery and converts them into signalling cascades that are initiated within the ciliary compartment and transduced into the cell body. In this way, primary cilia can coordinate many key processes during development and in tissue homeostasis, such as cell migration, differentiation and/or re-entry into the cell cycle, specification of the plane of cell division and apoptosis (Fliegauf et al., 2006; Satir et al., 2010). Another rationale that supports the sensory function of cilia is the fact that the sensory structures of the vertebrate visual and olfactory systems are modified cilia. In fact, our ability to see and smell depends on the continuous transport of proteins through the connecting cilium of photoreceptors, and by the odorant receptors that are localized in cilia extending from the sensory neuron dendritic knob, respectively (Jenkins et al., 2009; Singla and Reiter, 2006). In addition, primary cilia can also respond to other sensory modalities, including

mechanical stimulation (bending of the cilium) as is the case for renal primary cilia that detect fluid flow through the lumen of the kidney tubule. The fact that it protrudes from the cell surface, together with the high surface to volume ratio that allows more effective concentration of receptors and signalling components, makes the primary cilium the ideal organelle for detection of extracellular signals (Satir et al., 2010; Zhang et al., 2004).

1.1.1.3 Nodal cilia

Nodal cilia are short cilia of 2-3 µm that are found in the embryonic node on the ventral surface of early embryos (Figure 1.2E). The embryonic node is a small triangular indentation that forms transiently in the early development of mammalian embryos and is involved in determining the normal left-right (LR) asymmetry. Just like motile cilia, it is thought that nodal cilia know left from right and convey information to the developing embryo, thus playing a crucial role in body axis determination.

Like primary cilia, nodal cilia are solitary organelles with 9+0 axonemes, but unusually they are motile, as they possess unique outer dynein arms as well as radial spokes, that make them able to move, generating a leftward flow across the node. In contrast to the motile 9+2 cilia, motile nodal 9+0 cilia do not move in the forward/return waveform, but exhibit a characteristic clockwise twirling movement. It is this type of motility that directs nodal flow “leftward” across the node, which is necessary for establishment of proper (LR) asymmetry. This model is supported by studies in mice. For example, when the mouse intraciliary transport motor KIF3B was disrupted by gene targeting, the node lacked cilia, and LR asymmetry was randomized (Hashimoto et al., 2010; Hirokawa et al., 2006; Leigh et al., 2009; Pazour and Witman, 2003; Satir and Christensen, 2007; Satir et al., 2007; Satir et al., 2008).

Exactly how nodal flow induces LR asymmetry is still uncertain, but so far two models have been proposed. The first model predicts that the leftward nodal flow, generated by motile cilia at the centre of the node, is mechanically sensed through passive bending of non-motile mechanosensory cilia at the periphery of the node. Bending of the cilia on the left side leads to a left-sided release of Ca^{2+} that initiates the establishment of body asymmetry. In the second model, it is hypothesised that the leftward-directed flow mediated by the motile nodal cilia sets up a gradient of morphogen that initiates Ca^{2+} signalling specifically on one side of the developing embryo. This asymmetric Ca^{2+} release is thought to be involved in

the subsequent events of asymmetric expression of signalling molecules and transcription factors (Figures 1.4A and 1.4B, respectively) (Bloodgood, 2010; Fliegauf et al., 2006; Satir, 2008; Satir and Christensen, 2007; Satir et al., 2010).

1.1.1.4 The kinocilium

Mammalian hearing relies on the sensory cells found in the inner ear. These cells are composed of a staircase array of 50-200 actin-based modified microvilli known as stereocilia, and are densely packed to form a bundle. Each bundle contains a single true cilium, referred to as the kinocilium (Figure 1.5) (Dabdoub and Kelley, 2005; Muller, 2008; Nayak et al., 2007). The kinocilium is the only true cilium in the cells being the only structure that has microtubules as its backbone (Sobkowicz et al., 1995). It is thought to have 9+2 microtubule architecture, although some reports indicate a 9+0 structure. A more likely scenario is that the mature kinocilium contains the central pair of microtubules but this is lacking in the immature kinocilium. Unlike motile cilia, the kinocilium is immotile; it is located on one side of the stereocilia bundle, and it degenerates when the hair bundle has matured. These findings led to suggestions that the kinocilium is not required for mechanotransduction, but may play an important role in establishing polarity (Axelrod, 2008; Muller, 2008; Nayak et al., 2007).

1.1.2 The centrosome

It was in 1888 when Theodor Boveri first observed a small dense focus of material located near the centre of the cell, and named it the centrosome. This non-membranous organelle of 1-2 μm^3 volume is known as the “especial organ of cell division”. However, it was more than a century later before biologists properly understood that centrosomes act as the major microtubule organizing centres (MTOCs) of animal cells, and are thus implicated in most microtubule-based activities, including the maintenance of cell shape and polarity, cell motility, intracellular transport of vesicles and cell division (Bettencourt-Dias and Glover, 2007; Loncarek and Khodjakov, 2009; Nigg and Raff, 2009). The centrosome contains a pair of centrioles that differ in age: the older centriole is named the mother while the younger centriole is called the daughter. Both centrioles are tethered through their proximal ends by a fibrous, intercentriolar linker and are surrounded by a meshwork of proteins, called the pericentriolar material (PCM) (Doxsey, 2001a; Doxsey et al., 2005). Centrioles are short, cylindrical structures and are approximately 0.5 µm long and 0.2 µm in diameter; their walls are made up of nine sets of triplet microtubules (Doxsey, 2001a). Mother and daughter centrioles are structurally distinct in that, unlike the daughter, the mother centriole

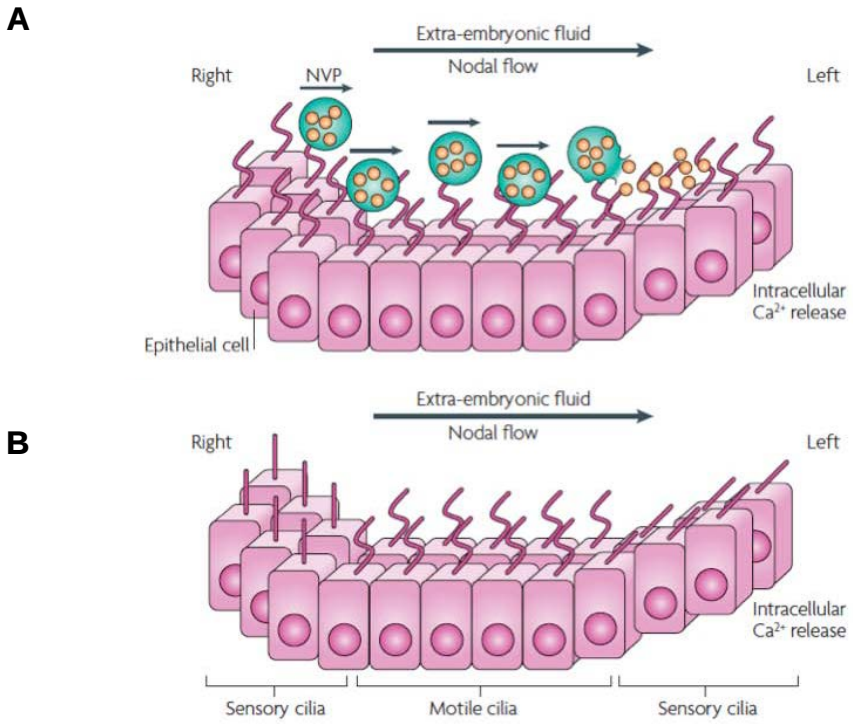

Figure 1.4 Schematic illustration of nodal flow
Due to their vigorous circular movements, motile monocilia in the embryonic node generate a leftward flow of extra-embryonic fluid called the nodal flow. **(A)** The nodal vesicular parcel (NVP) model predicts that vesicles filled with morphogens (such as sonic hedgehog and retinoic acid) are secreted from the right side of the embryonic node and transported to the left side by nodal flow, where they are smashed open by force. The released contents bind to specific transmembrane receptors in the axonemal membrane of the cilia on the left side. This will result in an increase in concentration of Ca^{2+} in the left hand side, and this will induce downstream signalling events that break bilaterality. In this model, the flow of extra-embryonic fluid is not detected by cilia-based mechanosensation. **(B)** In the two-cilia model, non-sensing motile cilia in the centre of the node create a leftward nodal flow that is mechanically sensed through passive bending of non-motile sensory cilia at the periphery of the node. Bending of the cilia on the left side leads to a left-sided release of Ca^{2+} that initiates the establishment of body asymmetry. Adapted from Fliegauf et al. (2007).

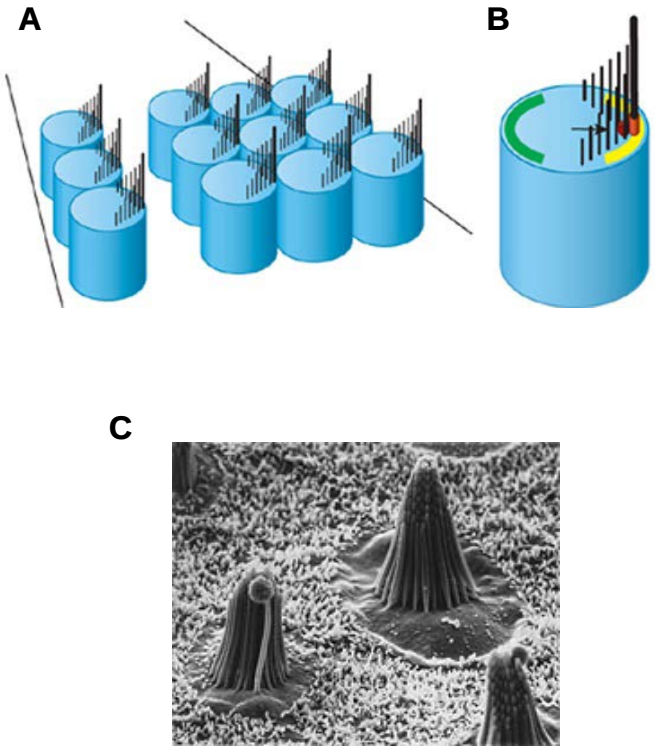

Figure 1.5 The kinocilium
(A and B) Sensory hair cells in the organ of Corti each have a single kinocilium (thick black vertical line) located on the abneural side of the cell and an associated stereociliary bundle (thin black vertical lines), forming a chevron pattern that points abneurally (right). Green and yellow crescents show PCP proteins. **(C)** Scanning electron micrograph of a stereociliary bundle with kinocilium. The ciliary bundle of each cell is composed of about 60 stereocilia, and one kinocilium (with bulb). Adapted from Axelrod et al. (2008) and http://neuro.med.harvard.edu/faculty/corey.html.

has two sets of distal appendages close to its distal ends; these are the “subdistal appendages” that are required to anchor the microtubules, and “distal appendages” that play an important role in cells undergoing ciliogenesis by participating in the association of the centriole, otherwise known at this time as the basal body at the plasma membrane (Figure 1.6) (Bettencourt-Dias and Glover, 2007; Crasta et al., 2008; Doxsey, 2001b; Moser et al., 2009). It is thought that the PCM is the main functional component of the centrosome as it contains the sites of microtubule nucleation. It has a lattice-like structure mainly consisting of coiled-coiled proteins. In fact, evidence indicates that the PCM acts as a scaffold for anchoring of well over 100 proteins (Andersen et al., 2003), including importantly γ-tubulin which is required for microtubule nucleation (Blagden and Glover, 2003; Dictenberg et al., 1998; Doxsey, 2001a). Since the centrosome lacks a clear boundary, such as an encapsulating membrane, its architecture is maintained simply through specific protein-protein interactions. Moreover, centrosomes act as a docking centre for many regulating proteins even though they do not directly contribute to centrosome structure or formation. In fact, some proteins may dock with the centrosome through non-specific interaction, especially if they are present in high abundance in the cytoplasm. However, most core centrosomal components are present in low concentration in the cell and it is possible that their delivery to the centrosome at the correct rate and time occurs via active mechanisms. The amount of PCM associated with the centrosome also changes with the cell cycle (Schatten, 2008; Urbani and Stearns, 1999).

1.1.2.1 Centrosome and microtubule organization

The centrosome is able to organize the cytoplasmic microtubule arrays through its ability to nucleate, anchor and release microtubules. The differences between interphase and mitotic microtubule assembly and organization are thought to be due in part to a cell cycle dependent regulation of the γ-tubulin ring complex (γTuRC) (Schatten, 2008). The γ-TuRC is a complex ring structure with a diameter similar to that of microtubules and are conserved components of microtubule organizing centres (MTOCs) (Cuschieri et al., 2007) that are also capable of nucleating microtubules *in vitro*. In interphase, the centrosome contains fewer numbers of γTuRCs and thus they nucleate fewer microtubules that tend to be relatively long. In contrast, in mitosis, the PCM enlarges in a process known as centrosome maturation and recruits more γTuRCs. These form highly dynamic microtubules which are shorter, but larger in number and are needed for spindle assembly (Schatten, 2008). In order for a γ-TuRC to form, γ-tubulin needs to first form a tetrameric complex with two γ-tubulin proteins and one each of the two

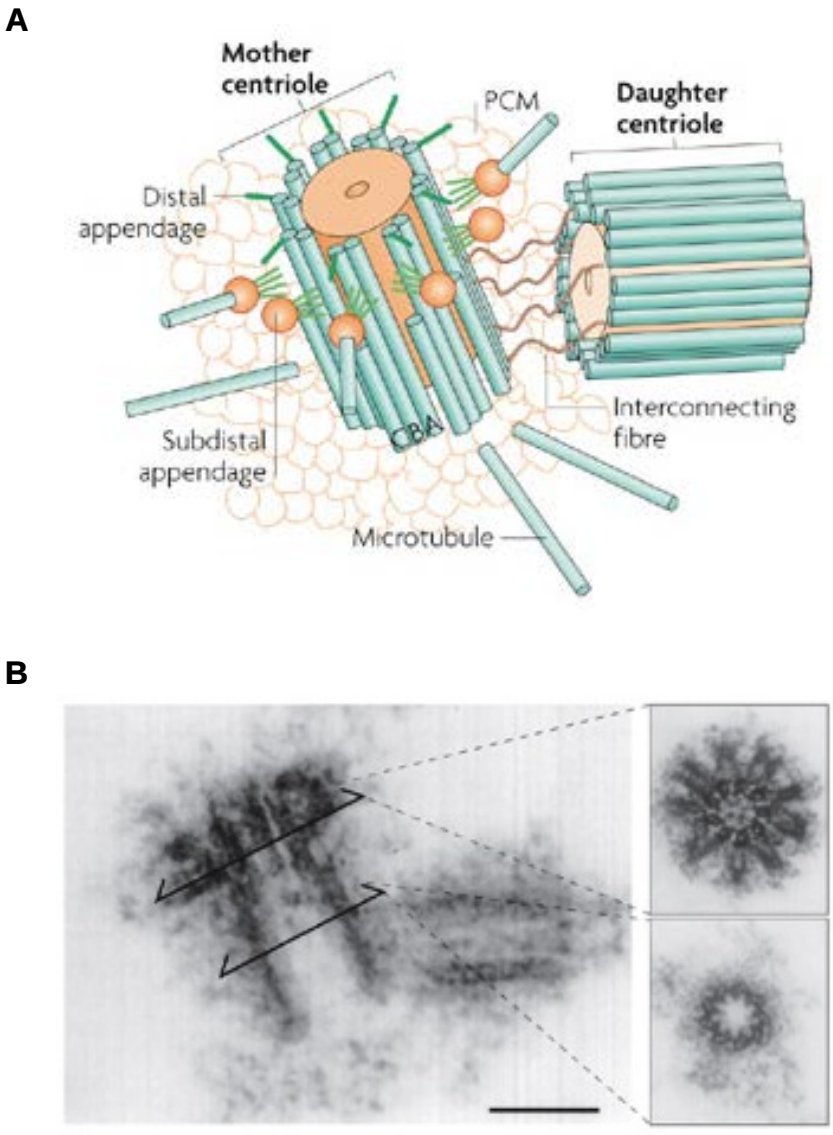

Figure 1.6 Centrosome structure
(A) Schematic representation of the centrosome. In each microtubule triplet, the inner-most microtubule is called the A-tubule, the one following is the B-tubule, and the most external microtubule is the C-tubule. At its distal end, the centriole is made of microtubule doublets. **(B)** Electron micrograph of the centrosome. The top and bottom insets indicate cross-sections of the subdistal appendages and the proximal part of the centriole, respectively. Scale bar, 0.2 μm. Adapted from Bettencourt-Dias and Glover (2007).

proteins, GCP2 and GCP3; this creates the γ-tubulin small complex (γ-TuSC) (Bettencourt-Dias and Glover, 2007). Vèrollet and collegues (2006) have shown that in *Drosophila melanogaster*, depletion of γ-TuSC subunits block microtubule nucleation. In higher eukaryotes, these γ-TuSCs assemble in a ring to form the γ-TuRCs which facilitate the initiation of microtubule filaments by capping the minus end of the microtubules (Bettencourt-Dias and Glover, 2007). Once nucleated by the γ-TuRC, microtubules are either released into the cytoplasm by microtubule severing proteins, such as katanin which is found at the centrosome (Ahmad et al., 1999; Hartman et al., 1998), or are recaptured and anchored at the centrosome. The mechanisms of this remain unclear. However, ninein, a component of the subdistal appendages of mother centrioles, has been shown to interact with the γ-TuRC and is required for microtubule anchoring (Delgehyr et al., 2005; Mogensen et al., 2000). This has led to the hypothesis that the subdistal appendages are the major site of microtubule anchoring within the centrosome.

1.1.2.2 Centrosome duplication and the cell cycle

During the cell cycle, the centrosome undergoes remarkable changes in organization. In order to organize an effective bipolar mitotic spindle it must duplicate once per cell cycle with each centrosome receiving an old centriole and a new centriole, a process known as semi-conservative duplication. The centrosome cycle can be divided in discrete consecutive steps: centriole disengagement, centriole duplication, centrosome disjunction, and centrosome separation (Bettencourt-Dias and Glover, 2007; Nigg, 2007; Nigg and Raff, 2009). The stages of centrosome duplication can be summarized as follows. Initially the loss of an orthogonal relationship between the mother-daughter centriole pair occurs upon exit from M phase, or during early G1, a process which is referred to as centriole disengagement. Nevertheless, the disengaged centrioles remain connected by a "base-to-base" highly dynamic structure composed of centrosome cohesion proteins, including C-Nap1 and rootletin. In order for centriole duplication to proceed, centriole disengagement must occur first. Importantly, this disengagement is thought to license the two centrioles for a new round of duplication. In this model, once centrioles are engaged in S-phase, the engaged centrioles prevent further duplication throughout the remainder of the cell cycle until passage through M-phase and centriole disengagement issues a license for a new round of duplication (Azimzadeh and Bornens, 2007; Lim et al., 2009; Tsou and Stearns, 2006). Centriole disengagement is thought to be triggered by separase, a protease previously shown to release sister-chromatid cohesion in anaphase. Whether separase activity acts directly or indirectly on the linkers

between orthogonal centriole pairs, is not known, however it is thought to be the "licensing event" for allowing further duplication of centrioles (Tsou and Stearns, 2006). Centriole disengagement also requires activity of the mitotic kinase Plk1 (Tsou et al., 2009).

Centrosome duplication, like that of DNA replication, is semi-conservative, with each new centrosome receiving one old centriole and one new centriole. However, unlike DNA synthesis, the duplication of centrosomes does not usually occur by template reading and assembly. The mother centriole simply aids in the accumulation of materials required for the assembly of the daughter centriole (Rodrigues-Martins et al., 2007). Morphologically, the duplication of centrioles is first seen at the G1/S transition, around the same time as the initiation of DNA synthesis. Here, a single new centriole (procentriole) forms at the proximal end of each parental centriole at an orthogonal angle, establishing tight "base-to-side" connections between parental and progeny centrioles (Azimzadeh and Bornens, 2007; Blagden and Glover, 2003; Nigg, 2007). Once formed in S phase, each new centriole elongates throughout the remainder of S and G2 phases until they reach full length in late G2. At this stage, the younger of the two parental centrioles acquires distal and subdistal appendages, thereby reaching full maturity.

At the G2/M transition, the centrosomes increase in size. This is because the PCM expands as it recruits numerous proteins that enable the nucleation of sufficient numbers of mitotic microtubules, a process referred as centrosome maturation (Sankaran and Parvin, 2006). At about the same time, the two parental centrioles lose physical cohesion, a process termed centrosome disjunction. Studies have shown that centrosome cohesion is regulated by phosphorylation of C-Nap1 and rootletin, which in turn, depends on the balance between activities of the Nek2 kinase and protein phosphatase 1 (Bahe et al., 2005; Fry et al., 1998a; Helps et al., 2000; Yang et al., 2006). Following centrosome disjunction, microtubule-based motor proteins generate antiparallel microtubule sliding forces that separate the two centrosomes to two ends of the cell. These thereby form the poles of the mitotic spindle, ensuring that each daughter cell will receive one centrosome when the cell divides. Throughout these events, the parental and new centrioles of each pair remain physically linked. It's only at late mitosis, just before the completion of cytokinesis, that disengagement of centrioles occurs, thus "licensing" the duplication of centrioles in the following cell cycle. At the end of mitosis, each daughter cell has one centrosome containing two centrioles, a newly formed centriole in the previous cycle, and an older centriole formed at least two cycles

prior (Figure 1.7) (Azimzadeh and Bornens, 2007; Blagden and Glover, 2003; Lim et al., 2009; Nigg, 2007)

1.1.2.3 Centrioles and basal bodies

Formation of primary cilia is closely linked with the cell cycle. Primary cilia typically form in cells that are in the G0 stage of the cell cycle, but occasionally can be identified in cells in G1 (Pedersen et al., 2008). All cilia extend from the distal end of the basal body which are equivalent structures to centrioles. At specific cell cycle or developmental stages, centrioles give rise to basal bodies and vice-versa. The mother centriole migrates to the cell surface and it differentiates into a basal body, nucleating microtubules to give rise to the primary cilium. On the other hand, the basal body that anchors a cilium in interphase can revert to a mother centriole prior to mitosis in order to form the mitotic spindle (Hoyer-Fender, 2010; Plotnikova et al., 2008). In cells with multiple cilia, several hundred basal bodies are generated. These migrate to the apical cell surface, acquire accessory structures, and dock to the cell surface. Centrioles are referred to as basal bodies once they dock to the cell membrane (Dawe et al., 2007; Debec et al., 2010). The basic structure of centrioles and the basal bodies is highly conserved in eukaryotes with both compromising nine microtubule triplets organized in a nine-fold symmetrical configuration. However, in vertebrates, only the mother centriole is able to nucleate primary cilia. On the other hand, the daughter centriole becomes competent for ciliary assembly when it acquires distal appendages in the following cell cycle. Therefore, the maturation process takes 1.5 cycles (Bettencourt-Dias and Glover, 2007; Dawe et al., 2007; Hoyer-Fender, 2010). At the foot of a primary cilium, the basal body remains associated with its daughter centriole through filamentous bundles, called the striated connector. This is likely to bear strong similarity to the intercentriolar linker present between parental centrioles during interphase. In order to aid its anchorage to the plasma membrane, the basal body acquires accessory structures including (i) transitional fibres, that might provide a filter for molecules that go into the cilium, since protein synthesis does not occur within cilia; (ii) basal feet that link the primary cilium to the microtubule cytoskeleton by directly contacting cytoplasmic microtubules; and (iii) striated rootlets that help in positioning and orientation of the basal body (Dawe et al., 2007; Debec et al., 2010; Hoyer-Fender, 2010).

1.1.3 Ciliogenesis

Ciliogenesis is the process that describes the formation of cilia. Although different mechanisms of ciliogenesis exist that enable the production of many kind of cilia

A

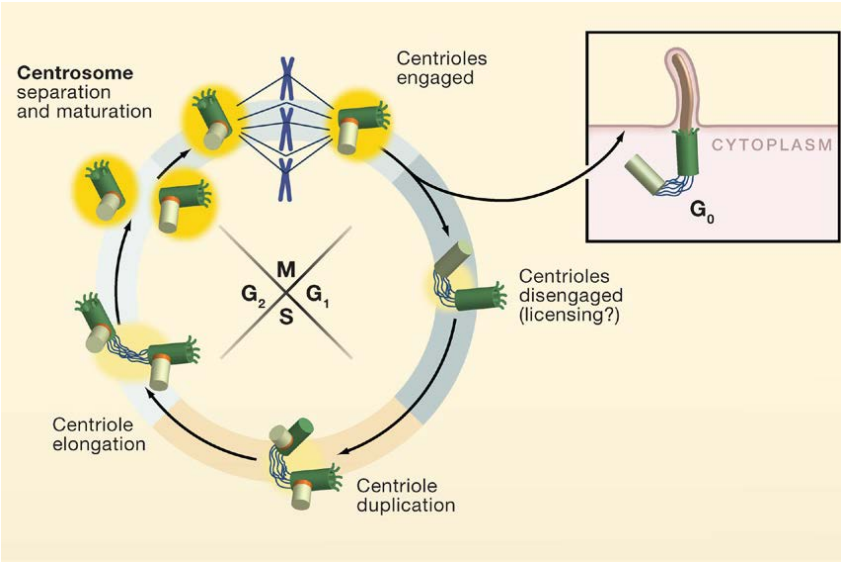

B

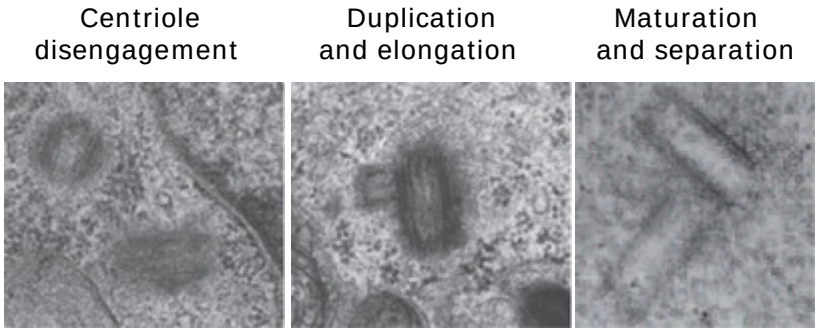

Figure 1.7 The centrosome cycle
(A) Schematic representation of the centrosome cycle. At the end of cell division, each daughter cell inherits one centrosome compromising a single pair of "disengaged" centrioles. Cells then either progress into G_1-phase, or enter G_0 (quiescent stage), when cells form a cilium. In cycling cells, centriole duplication occurs in S-phase. Here, the newly born procentrioles (light green) remain engaged tightly to the parental centriole (dark green) in an orthogonal arrangement. These elongate throughout S and G_2 phase. In late G_2, the centrosome undergoes a process of maturation, involving the recruitment of additional PCM components (yellow) and the two centrosomes start to separate from one another, eventually forming the two poles of the bipolar spindle in mitosis. The pair of centrioles remain in an engaged configuration until late mitosis or G_1, thus preventing re-duplication within the same cycle. When centrioles disengage (early G_1), centrosome duplication is licensed to take place in the following cell cycle. **(B)** Electron micrographs from HeLa cells showing distinct steps in centriole duplication. Adapted from Nigg and Raff (2009) and Bettencourt-Dias and Glover (2007).

and flagella, electron microscopy studies in different cells have shown that the course of ciliogenesis is similar among different animals. Ciliogenesis is therefore divided into four stages: (i) generation of centrioles, (ii) migration of centrioles, (iii) formation of basal body-associated structures, and (iv) elongation of cilia. The main differences between the generation of primary cilia and the cilia of multiple-ciliated epithelia are seen in the centriologenesis step, when the centrioles are generated. In contrast to generation of a primary cilium, which forms from a pre-existing centriole, hundreds of centrioles are required for the generation of several hundred cilia in epithelial cells (Figure 1.8) (Dawe et al., 2007; Hoyer-Fender, 2010).

1.1.3.1 Centriole duplication and multiplication

A primary cilium can be formed in quiescent somatic cells, but can also be identified in proliferating cells in interphase which are able to make a primary cilium in G1 phase. It's therefore only at these specific stages of the cell cycle that the mature mother centriole migrates to the cell surface and is converted into a basal body. The centrioles that are destined to become basal bodies in cells with primary cilia are therefore generated through semi-conservative duplication, where pre-existing centrioles function as a template for the formation of one daughter centriole each (Bettencourt-Dias and Glover, 2007; Dawe et al., 2007; Hoyer-Fender, 2010). Hence, in cells that will form primary cilia, the duplication of centrioles is cell cycle regulated. In contrast, in terminally differentiated multiciliated epithelia cells, such as those in vertebrate respiratory and reproductive tracts, centriole duplication is regulated during differentiation and is mostly independent of pre-existing centrioles. In fact, two distinct mechanisms exist for generation of the multiple centrioles required in multiciliated epithelia: (i) the centriolar pathway, where the pre-existing centriole is used as template, and (ii) the acentriolar pathway, where centrioles are produced de novo. The centriolar pathway plays a minor role in ciliogenesis and occurs when new centrioles are produced around an existing centriole. Unusually though, during ciliogenesis, several centrioles develop simultaneously around one parent centriole, with the daughter centrioles being released into the cytoplasm to mature. This is different from the cell cycle-dependent centriole duplication, where only one daughter centriole buds from the lateral side of each mother centriole. In the acentriolar pathway, which represent the major pathway for centriole generation, with 95% of centrioles generated this way, centrioles are formed without contact with the pre-existing centriole (Bettencourt-Dias and Glover, 2007; Dawe et al., 2007; Hagiwara et al., 2002; Hoyer-Fender, 2010). In this pathway, some irregularly

shaped, small, non-membranous granules with a diameter of 70-90 nm first appear in the cytoplasm. These are called fibrous granules and initially appear in low numbers; however, they then increase in number and cluster to form aggregates. One of the molecular components of these dense granules is PCM-1 (pericentriolar material protein 1), a known centriolar satellite protein. Therefore, fibrous granules appear to be equivalent structures to those electron dense centriolar satellites scattered around centrosomes in proliferating mammalian cells (Hagiwara et al., 2002; Hagiwara et al., 2004; Kubo et al., 1999). Following clustering, the fibrous granules fuse to create dense, spheroidal bodies called deuterosomes. Deuterosomes somehow organize the growth of new centrioles around them and depending on the size of deuterosomes, different numbers of centrioles are formed (Figure 1.8B) (Bettencourt-Dias and Glover, 2007; Dawe et al., 2007; Hagiwara et al., 2004; Kubo et al., 1999).

1.1.3.2 Transformation of centrioles to basal bodies

Once formed, centrioles separate from deuterosomes and migrate to the cell surface where they acquire three types of accessory structures: (i) alar sheets, (ii) basal feet, and (iii) striated rootlets. These serve as plasma-membrane anchors enabling the attachment of centrioles to the cell membrane. Once a centriole has acquired the structures and docked with the cell membrane, it is known as a basal body (Figure 1.9A, B, C and D) (Dawe et al., 2007; Hagiwara et al., 2004). The alar sheets are also known as transition fibres and correspond to the distal appendages of the mother centriole. They are wing-like trapezoidal sheets that extend from the lateral side of each triplet microtubule of the basal body to the cytoplasmic face of the plasma membrane. Their role is to act as docking platforms to enable the docking of the basal body to the cell membrane. This docking is achieved either by directly attaching to the apical membrane, or by first docking with the membrane of ciliary vesicles that in turn, fuse with the apical membrane. Moreover they are thought to be part of a “ciliary pore complex” allowing only selected proteins to pass through into the ciliary compartment (Satir et al., 2010; Seeley and Nachury, 2010). The basal foot is formed by fibrous granules. It is a conical structure that originates laterally from the midregion of the basal body. Ultrastructure analysis has revealed that cytoplasmic microtubule ends are embedded in each basal foot suggesting that the basal feet can play an important role in the firm anchorage of cytoplasmic microtubules to the base of the cilium. For coordinated movement of cilia, the basal feet must point in the same direction, which corresponds to the direction of the effective stroke of ciliary beat. The striated rootlets extend from the proximal end of the basal body toward the

A

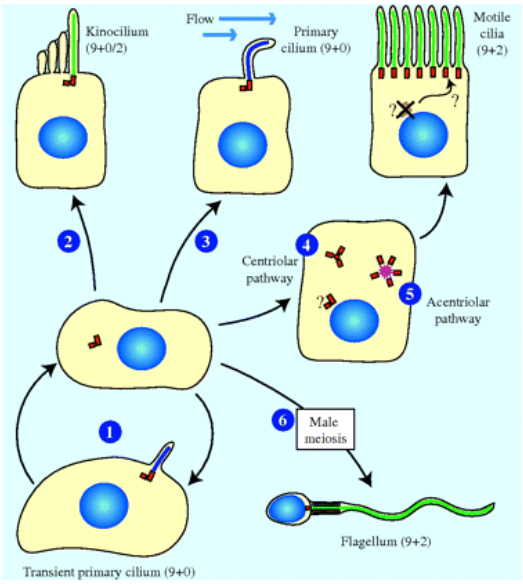

B

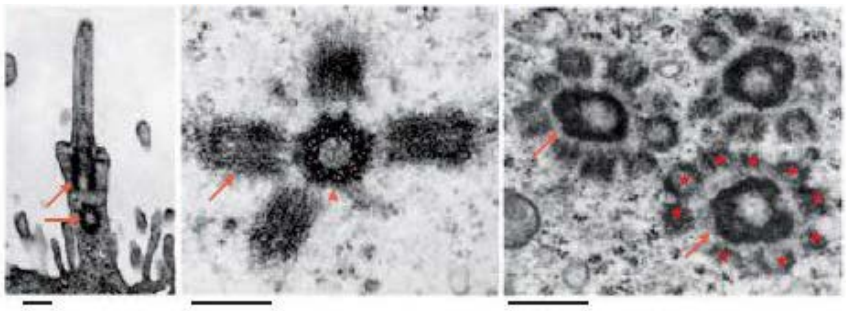

Figure 1.8 Pathways of ciliogenesis

(A) Diagram representing multiple pathways of ciliogenesis. Quiescent somatic cells use a single pre-existing mature centriole to subtend a transient primary cilium (1) lacking central pair microtubules, which is lost as the cell re-enters the cell cycle. In differentiated cells, a mature centriole can give rise to several different types of single cilia, such as the temporary (9+2 or 9+0) kinocilium (2), which may or may not possess the central pair of microtubules and the primary (9+0) cilium produced on the luminal epithelium of kidney tubules (3). In mammalian airways, the epithelial cells have several hundred cilia. Here, hundreds of centrioles are produced, that are duplicated either using the pre-existing centriole as a template (4), or formed via a non-templated method (5). The sperm flagellum produced in male meiosis is depicted at (6). Green denotes 9+2 axonemes; dark blue denotes 9+0 axonemes; centrioles are shown in red; the deuterosome is shown in purple. **(B)** Electron micrograph showing the formation of cilia in monkey oviduct cells. Left hand side shows two basal bodies at the base of a cilium (red arrows). Middle panel shows the nearly mature basal bodies (arrows) associated with a centriole (arrowhead). Right hand panel shows three deuterosomes (red arrows) with several nascent centrioles (asterisks). Scale bar, 0.25 µm. Adapted from Dawe et al. (2007) and Bettercourt-Dias & Glover (2007).

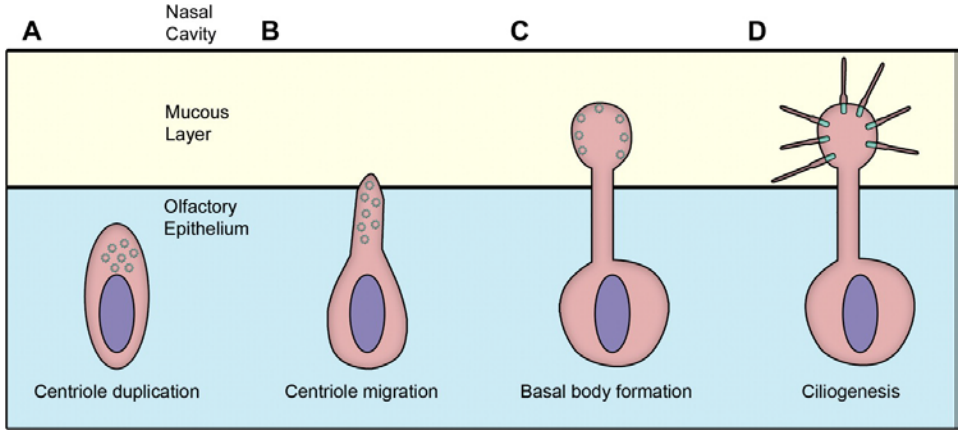

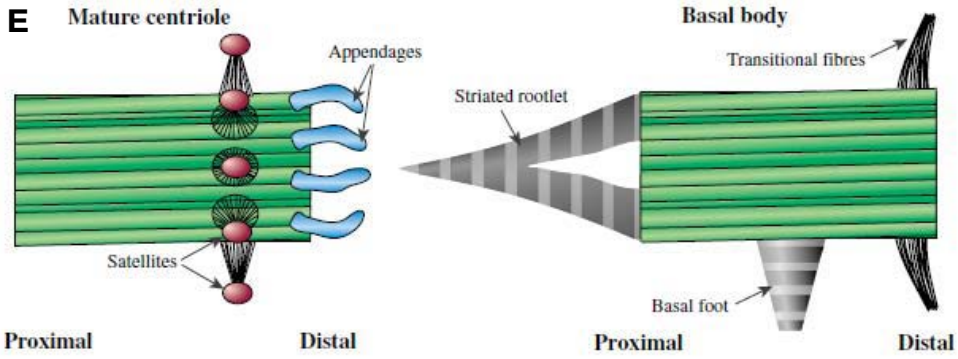

Figure 1.9 Steps of ciliogenesis in the olfactory sensory neurons (OSN)
(A) In a developing OSN, centrioles are duplicated from the mother/daughter centrioles in the cell body before migrating along the developing dendrite toward the eventual dendritic knob **(B)**. **(C)** In the dendritic knob, centrioles are converted into basal bodies which anchor to the plasma membrane. Ciliary axonemes then extend from the basal body and elongate the cilia, into the mucous area where odorant transduction occurs. **(E)** Schematic of longitudinal view of the mature centriole, showing the appendages, and basal body with accessory structures. Adapted from Jenkins et al. (2009) and Bettencourt-Dias and Glover (2007).

centre of the cell and are composed of bundles of thin longitudinal filaments made up primarily of the protein rootletin (Yang et al., 2006). They are thought to anchor the basal body-cilium complex in the cells and provide cilia with mechanical support in certain specialized settings. Moreover, these structures do not appear to be essential for cilia formation (Figure 1.9E) (Hagiwara et al., 2002; Hagiwara et al., 2004; Hoyer-Fender, 2010; Seeley and Nachury, 2010).

1.1.3.3 The importance of intraflagellar transport in cilia formation

Intraflagellar transport (IFT) is essential for construction of cilia and flagella. This process describes the bidirectional movements of large protein complexes, called IFT particles, along the doublet microtubules. These are essential to elongate and maintain the cilium. Electron microscopy analysis has shown that these particles are arranged in linear arrays that are sandwiched between the flagellar membrane and the axonemal outer doublet microtubules. IFT was first identified by Kozminski et al. (1993), who observed movement of IFT particles by differential interference contrast (DIC) microscopy in the biflagellate green algae, *Chlamydomonas*. Since then, it has been found to be essential for the assembly of both primary and motile cilia in many organisms including mice. In fact, IFT particle movement has been observed in the primary cilia of cultured mouse kidney cells using GFP-tagged IFT particle proteins and/or motor subunits. Furthermore, movement of some tagged-IFT particles has also been observed using time-lapse fluorescence microscopy in *Caenorhabditis elegans***.** Genes that encode IFT components are conserved among ciliated eukaryotes, but are not present in organisms that lack cilia (Hagiwara et al., 2004; Hao et al., 2009; Hao and Scholey, 2009; Pedersen and Rosenbaum, 2008; Pedersen et al., 2008).

Since cilia do not contain ribosomes, protein synthesis occurs in the cell body and ciliary proteins are transported along the cilium by plus-end directed kinesin motors in a process called anterograde transport. Conversely, proteins returning back to the cell body are transported by minus-end directed motors, primarily cytoplasmic dynein, in a process called retrograde transport. Proteins moving in the anterograde (base to tip) direction include precursors that are used to assemble the axonemal cytoskeleton, while particles moving in the retrograde (tip to base) direction include elements that are responsible for removal of turnover products that are brought back to the cell body for recycling.

IFT particles can be sub-divided into IFT-A and IFT-B complexes, containing 6 and 11 subunits, respectively**.** Whereas complex B polypeptides are required for

anterograde transport of axonemal precursors into the ciliary tip, complex A polypeptides are not essential for building of the ciliary axoneme. In fact, IFT-A is thought to play an important role in returning the IFT proteins from the ciliary tip to the cell body, as depletion of IFT-A components in *Chlamydomonas* resulted in the accumulation of IFT particles at the ciliary tip. The process of IFT starts with the assembly of IFT particles at the base of cilia, near the transition fibres. Together with the basal body, the transition fibre is thought to function as a filter for the cilium, regulating the import and export of proteins in and out of the cilium. The axonemal doublet microtubules initiate at the transition zone, extending from the A and B tubules that make up the mother centriole. Once cargos have passed through the cilium, a raft containing IFT complexes A and B, axonemal precursors, and the inactive cytoplasmic dynein, are transported in an anterograde manner along the axoneme by kinesin-II-mediated movement. At the ciliary tip, cargo proteins and IFT particles are released into the ciliary compartment and complex A and B dissociate from each other. This modification at the axoneme tip, results in the inactivation of kinesin-II and activation of cytoplasmic dynein. Ciliary turnover products (e.g. inactive kinesin-II) are, in turn, transported in a retrograde manner along ciliary axonemes by cytoplasmic dynein for recycling or degradation in the cytoplasm (Figure 1.10A and B) (Hao et al., 2009; Hao and Scholey, 2009; Mukhopadhyay et al., 2007; Pedersen et al., 2008).

1.1.3.4 Cilia assembly and disassembly

In normal dividing cells, exit from mitosis, and entry into the stationary or G_0 phase of the cell cycle, is accompanied by ciliary assembly, in which a transient cilium is formed. In contrast, exit from G_0 phase, and re-entry into the cell cycle is accompanied by ciliary disassembly. Thus ciliary assembly and disassembly must be coordinated within the cell cycle and involves reversible conversion of centrioles and basal bodies. However, little is known about the molecular switches that activate the switch from a centriole to a basal body and vice versa. Recent studies suggest that two distal centriole proteins, CEP97 and CEP110, play an important role in suppressing assembly of the ciliary axoneme. Firstly, CEP97 recruits CEP110 to the centriole, which in turn, caps the ends of the distal centriolar microtubules. Secondly, studies from Spektor et al. (2007) have shown that the CEP97 and CEP110 protein levels markedly decrease in quiescent cells, while both proteins disappear from the mother centriole, supporting the hypothesis that both proteins may prevent the mother centriole from becoming a basal body in cycling cells. Thirdly, overexpression of CEP110 in NIH3T3 fibroblast, resulted in the blockage of cilium formation, whereas CEP110 depletion in U2OS osteosarcoma

A **B**

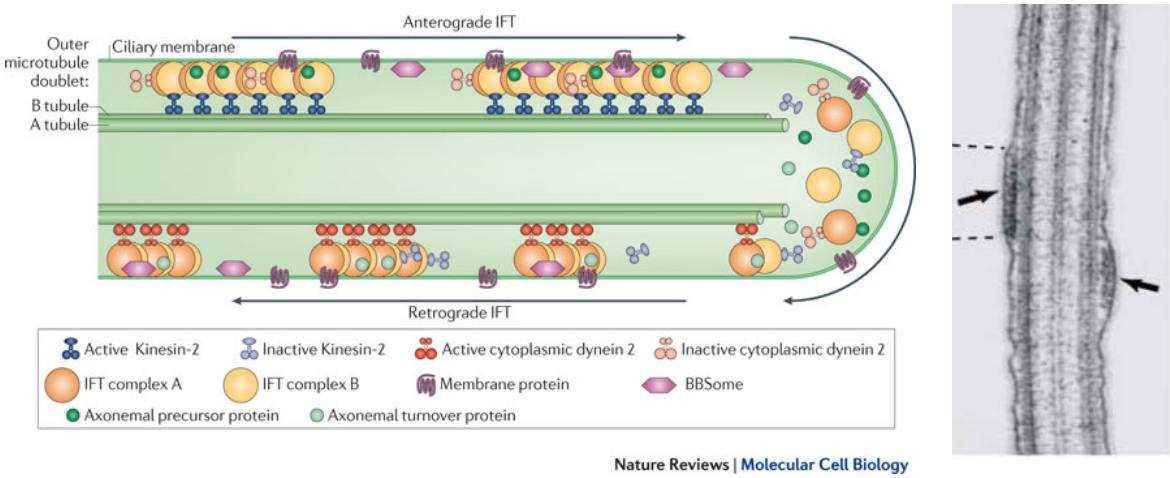

Figure 1.10 Intraflagellar transport
(A) Schematic representation of intraflagellar transport. The anterograde intraflagellar transport (IFT) motor, heterotrimeric Kinesin-2, transports IFT complexes A and B, axonemal proteins and cytoplasmic dynein 2 to the tip of cilium. During this anterograde transport, kinesin-2 is active whereas the retrograde motor, cytoplasmic dynein 2, is kept inactive to allow anterograde movement. At the ciliary tip, cargo proteins and IFT particles are released into the ciliary compartment and complex A and B dissociate from each other. Modifications at the tip of the axoneme result in the inactivation of the kinesin and facilitate the retrograde return of the raft to the base of the cilium via cytoplasmic dynein 2. This raft contains complexes A and B, inactive kinesin-II and axonemal turnover products. Subsets of IFT trains are involved in transporting membrane proteins and the BBSome (a complex comprised of at least seven Bardet–Biedl Syndrome proteins). Remodelling of IFT assemblies occurs at the turnaround phases at the tip and base of cilia. IFT rafts moving along the axoneme are shown in **(B)**. Adapted from Ischikawa & Marshall (2011) and Vlacque et al. (2008).

cells resulted in the untimely assembly of elongated structures resembling aberrant primary cilia (Kobayashi and Dynlacht, 2011; Seeley and Nachury, 2010; Spektor et al., 2007).

The disassembly of cilia can occur by either of two mechanisms: (i) deflagellation/deciliation, or (ii) resorption. Deflagellation is a drastic stress response and results in the severing of the axonemal microtubules above the transition zone in order to release the basal bodies so they can perform other roles in cell division. In contrast, resorption is a relatively slow process, coupled to the cell cycle, in which the length of the cilium or flagellum decreases gradually. Resorption normally occurs upon re-entry of quiescent cells into the cell cycle. The mechanisms that mediate ciliary disassembly are not well understood. However, evidence suggests that cilium disassembly is initially triggered by the centrosomal protein kinase, Aurora A, the activity of which regulates entry into mitosis by activating initially Plk1 and subsequently, cyclin-dependent kinase 1 (CDK1)-cyclin B. Studies from Pugacheva et al. (2007) have shown that RNAi depletion of Aurora A or its activator, HEF1, prevents the disassembly of cilia. Furthermore, injection of active Aurora A into cells led to rapid shortening of the cilium, whereas injection of an inactive Aurora A did not, suggesting that Aurora A is necessary and sufficient for ciliary disassembly to occur. On the basis of these studies, a model of cilium disassembly was proposed. Here, Aurora A kinase, acting in concert with HEF1, activates HDAC6, a deacetylase for tubulin. This, in turn, deacetylates axonemal microtubules leading to the rapid disassembly of the primary cilium. In addition to Aurora A, intraflagellar transport has also been implicated in ciliary disassembly. In fact, studies from Pan & Snell (2007) have suggested that disassembly of cilia might involve a decrease in the rate of delivery of axoneme subunit to the tip of the cilium and an increase in the rate of retrograde trafficking of disassembled cilium components (Kobayashi and Dynlacht, 2011; Pan and Snell, 2007; Pugacheva et al., 2007; Seeley and Nachury, 2010). The more drastic mechanism of deflagellation is regulated in *Chlamydomonas* by Fa2, a member of the NIMA family. Genetic studies have revealed that Fa2 is essential for calcium-activated axonemal microtubule severing during deflagellation as well as playing an important role in the cell cycle (Kobayashi and Dynlacht, 2011; Pan and Snell, 2007; Quarmby and Mahjoub, 2005; Quarmby and Parker, 2005).

1.2 Ciliary Signalling

During the last decade, the importance of cilia in a range of biological functions has begun to emerge. Recent discoveries have revealed that in addition to motility,

cilia have sensory functions that play crucial roles in cell signalling pathways and cellular homeostasis. The role of cilia as sensory organelles is perhaps best understood in the context of photoreception and olfaction. In the mammalian retina, photoreceptors sense light through a modified primary cilium that is characterized by an expanded tip called the outer segment. The outer segment is the place where the photoreceptors that initiate the reception of light are localized and where the signalling cascade is begun. For photoreceptor signalling to be maintained, retinal proteins such as rhodopsin must be constantly transported to the cilium through IFT-mediated transport. Mutations that inhibit the transport of this protein lead to retinitis pigmentosa, a common form of retinal degeneration. Similar to photoreception, olfaction occurs through signalling cascades that occur at the cilium. In the nose, specialized olfactory cilia accommodate G-protein-coupled receptors that detect and transduce odorant signals. The role of cilia in sensing light and smell is best manifested in Bardet-Biedl syndrome, a disorder associated with defects in cilia and basal bodies in which the patients cannot smell and display retinal degeneration amongst other characteristics. In addition to its chemosensory role, the primary cilium can function as a mechanosensor, sensing urine fluid flow by flexing and transducing the bending signalling through calcium influx. Together, these examples emphasize the crucial role that the primary cilium plays in human health and disease (Berbari et al., 2009; Nauli et al., 2003; Singla and Reiter, 2006).

Indeed, it is now clear that the ciliary localization of a variety of receptors, ion channels, and transporter proteins effectively positions the cilium for different types of signalling, including responses to distinct morphogens, hormones or growth factors. In fact, many key processes that occur during development are coordinated by the cilium. These include cell migration, differentiation and/or re-entry into the cell cycle, specification of the plane of cell division, and apoptosis. Some of the key signal transduction pathways coordinated by the cilium are described below.

1.2.1 The Hedgehog signalling pathway

Hedgehog family members are secreted lipoproteins that play essential roles in many processes during embryonic development. Furthermore, hedgehog signalling remains active in the adult where it is involved in the maintenance of stem cell populations. The hedgehog (Hh) gene was originally identified in 1980 by Nusslein-Volhard & Wieschaus as the “segment polarity gene” whose mutation led to segment polarity defects in *Drosophila* embryos with embryos developing as spiny

balls reminiscent of hedgehogs (Nusslein-Volhard and Wieschaus, 1980). Since then, Hh homologues have been identified in many invertebrates and vertebrates, and found to play crucial roles in controlling regulation of cell growth, survival and fate, as well as tissue patterning of almost all aspects of the body plan (Jiang and Hui, 2008; King et al., 2008; Varjosalo and Taipale, 2008).

Unlike *Drosophila,* which possesses a single Hh gene, several Hh related genes have been identified in vertebrate species. In mammals, there are three members of the *Hh* family: *Sonic hedgehog* (*Shh*), *Indian hedgehog* (*Ihh*), and *Desert hedgehog* (*Dhh*). *Shh* is the best studied and plays vital roles in embryonic development. In early embryogenesis, it controls the patterning of the left-right and dorso-ventral axes of the embryo and the distal elements of the limb, whereas in later development, *Shh* is important for the correct morphogenesis of organs such as the skin, eyes, lung, muscle and pancreas. *Dhh* is the most closely related of the mammalian *Hh* family to *Drosophila Hh* and is thought to control spermatogenesis, whereas *Ihh* is more involved in bone development (Jiang and Hui, 2008; King et al., 2008; Varjosalo and Taipale, 2008).

1.2.1.1 Mechanism of Hedgehog signalling

Once Hh is translated, it undergoes multiple processing steps before release of the active ligand from the producing cells. Studies conducted in the *Drosophila* indicate that the Hh reception system consists of two transmembrane proteins, Patched (Ptc) and Smoothened (Smo), and the downstream effectors, the Gli zinc-finger transcription factors, Gli1, Gli2, and Gli3. Ptc is a twelve transmembrane protein and acts as a Hh receptor, whereas Smo is a seven transmembrane protein that acts as a signal transducer, transducing the signal across the plasma membrane. It is thought that Ptc may inhibit Smo activity by regulating Smo trafficking. Studies have shown that in the absence of an Hh signal, Ptc localizes to the ciliary membrane and prevents the ciliary accumulation of Smo, thus keeping it in an inactive state. As result, the Gli transcription factors, predominantly Gli3, are processed to repressor forms (Gli_R) inhibiting the transcription of a subset of Hh target genes. When Hh is present, Ptc binds the ligand and exits from the cilia, losing its ability to repress Smo. As a consequence, activated Smo accumulates in the cilia and triggers a signal transduction cascade that blocks Gli_R production and promotes Gli_A activation, which, in turn, promotes target gene activation (Figure 1.11) (Anderson et al., 2008; Jiang and Hui, 2008; Kiefer, 2011b).

1.2.1.2 Hedgehog signalling and cilia

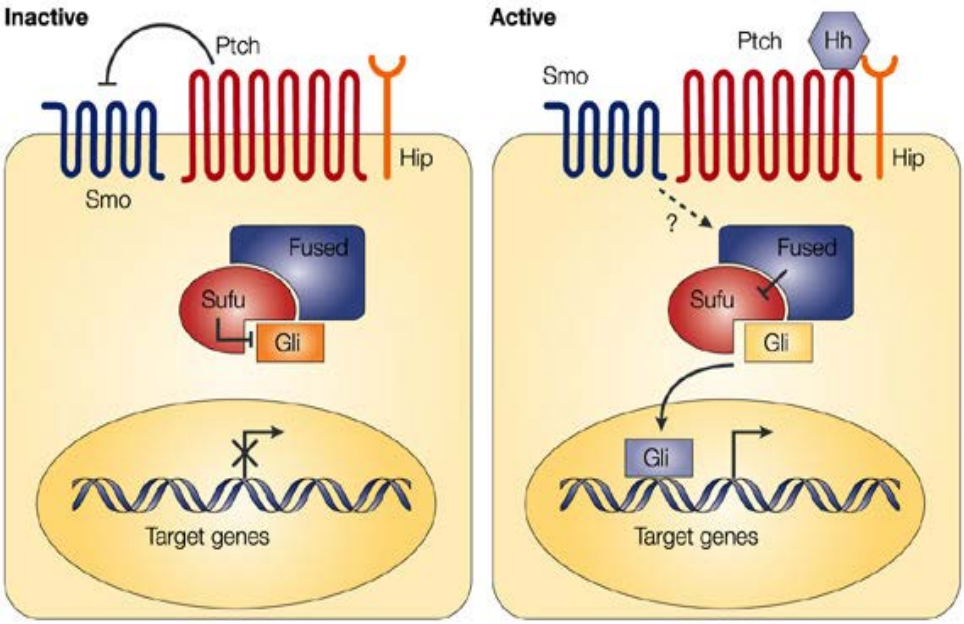

Figure 1.11 Model of Hedgehog signalling
In the absence of ligand, the Hh signalling pathway is inactive (left). In this case, the transmembrane protein receptor Patched (Ptch) inhibits the activity of Smoothened (Smo), from being transported to the tip of cilium. In addition, the transcription factor Gli, a downstream component of Hh signalling, is prevented from entering the nucleus through interactions with cytoplasmic proteins, including Fused and Suppressor of fused (Sufu). This represses the transcriptional activation of Hh target genes. Binding of Hedgehog ligand (to Ptch) induces activation of this pathway (right) by relieving the inhibitory effect of (Ptch) on Smo. Smo can now move to the cilium, thereby activating a cascade that leads to the translocation of the active form of the transcription factor Gli to the nucleus. This results in nuclear Gli activating target gene expression, including Ptch and Gli itself. Hip, a Hh binding protein that attenuates ligand diffusion is also activated. Adapted from Di Magliano and Hebrok (2003).

Since Shh signalling occurs at the primary cilium, it's not surprising that a connection between developmental defects associated with Hh signalling and primary cilia was found. This was first hinted at in 2003 by studies from Huangfu et al. (2003) who found that mice with mutations in IFT components, showed similar defects to those associated with aberrant Shh signalling, including abnormal dorsoventral patterning of the neural tube. It turns out that ciliary localization of Hh proteins is essential for correct signalling of this pathway. In fact, a point mutation that inhibits Smo localization to the cilia, compromises Smo activity, suggesting that ciliary localization of Smo is essential for its function. The advantage of using cilia for the Hh pathway is due in no small part to the many unique properties that the cilia possess, including their role as cellular antenna as they project a cell-type specific distance from the cell body, thus facilitating the reception of Hh signal. This explains why the Hh receptor Ptc, localizes to the cilium, so that it can accurately sense varying amounts of its circulating ligand, Shh. Moreover, cilia act as a subcellular compartment. The ciliary membrane and the cytoplasmic contents of the organelle are well isolated from the cell body. This provides a defined space in which signalling components are enriched, thus facilitating a rapid and efficient response. Furthermore, the IFT machinery that assembles the cilium makes it possible to transport the proteins between the cilia and the cell body in a rapid, regulated manner. We now know that this transport machinery is also essential for the mammalian Hh signalling pathway. It is thought that the trafficking of Hh pathway proteins in response to ligands is mediated by IFT proteins. In fact, genetic studies from Huangfu et al. (2003) have shown that IFT proteins function at a point downstream of the membrane proteins Ptc and Smo, and upstream of the Gli transcription factors that activate the Hh pathway. Furthermore, studies have shown that in the absence of IFT, there is no Gli activator or repressor activity with the result that there is no response to ligand. Moreover, mutations disrupting IFT in mice alter the ratio of Gli3 activator-to-repressor and result in severe polydactyly; whereas, mutant mouse embryos lacking Kif3a, subunit of kinesin-II anterograde motor, and embryos lacking *Ift88* or *Ift172* display an open neural tube, and loss of ventral cell types in the neural tube (Goetz et al., 2009; Kiefer, 2011b; King et al., 2008; Pan et al., 2005; Wong and Reiter, 2008). A hallmark of Hh signalling is the ability to control and specify distinct cell fate, in a concentration dependent manner using a single morphogen. During embryonic development, it promotes cell proliferation and differentiation in various pattern formation processes including limb formation, the determination of left-right asymmetry, and differentiation of neural tube, whereas in post-natal tissues, it directs the formation and maintenance of stem- or precursor-cell

populations. Given its important embryonic and postnatal roles, it is not surprising that defects in the Hh pathway can lead to birth defects and cancers. In fact, germline mutations that affect the Hh pathway activity are associated with developmental disorders, whereas somatic mutations that result in improper activation of this pathway, have been linked to several forms of human cancer, including basal cell carcinoma and medullobastoma (Grallert et al., 2004; Jiang and Hui, 2008; Kiefer, 2011a; Varjosalo and Taipale, 2008).

1.2.1.3 The Wnt signalling pathway

Like Hh, members of the Wnt family are secreted lipoproteins that regulate many development processes in both vertebrates and invertebrates, including cell proliferation and differentiation, polarity, and migration, all of which are fundamental to embryogenesis. The pathway was first discovered in 1987 by Cabrera and colleagues with the realization that the oncogene int1 and the *Drosophila* developmental patterning gene wingless (wg) are homologues (Cabrera et al., 1987). Wnt ligands trigger at least two distinct pathways: the canonical Wnt/β-catenin pathway and the β-catenin independent non-canonical Wnt or planar cell polarity (PCP) pathway. The canonical Wnt pathway stabilizes β-catenin and determines cell fate, whereas the non-canonical Wnt pathway is primarily involved in the organization of cytoskeletal architectures affecting cell polarity, migration and mitotic spindle orientation. Activation of both these signalling pathways is initiated by the binding of a ligand of the Wnt family to a 7-transmembrane receptor called Frizzled (Fz) (Cadigan and Peifer, 2009; He, 2008; Wallingford et al., 2002; Wang, 2009).

1.2.1.4 Mechanism of canonical Wnt signalling

As mentioned previously, the components of the Wnt signalling pathway include secreted Wnt ligands, Frizzled transmembrane receptors, the phosphoprotein Dishevelled (Dvl) and downstream effectors including-β-catenin, and the transcription factor T-cell factor/lymphoid enhancer-binding factor (TCF/LEF). Dvl is a crucial component of Wnt signalling since it determines whether the canonical or non-canonical pathway is initiated (Berbari et al., 2009; Germino, 2005). In the canonical Wnt pathway, β-catenin is the key Wnt effector, mediating all of its downstream effects. It acts as a transcription co-activator inducing cell cycle progression, proliferation and differentiation, in addition to migration and embryonic development. In the absence of a Wnt ligand, cytoplasmic β-catenin is sequestered by a complex of proteins, composed of the scaffold protein axin, the adenomatous polyposis coli (APC) tumour suppressor gene product, glycogen

synthase kinase 3β (GSK3β), casein kinase I (CKI), and protein phosphatase 2A (PP2A). GSK3β phosphorylates β-catenin at its amino terminus. The phosphorylated β-catenin is then recognized by β-TrCP, an E3 ubiquitin ligase which targets it for polyubiquitination and proteasomal destruction. Meanwhile, TCF/LEF are bound to transcriptional suppressors such as Groucho, to keep the canonical Wnt pathway inactive. Wnt ligands bind a two-part receptor, the seven transmembrane Fz and LRP5/6, both of which are required for canonical signalling. Upon ligand binding, the LRP5/6 receptor is phosphorylated on its cytoplasmic tail. This creates a binding site for axin which disrupts the complex in a process requiring Dvl. As result, β-catenin is stabilized, and translocates to the nucleus where it displaces the Groucho transcription repressor from TCF, initiating transcription of Wnt target genes (Figure 1.12) (Berbari et al., 2009; Cadigan and Peifer, 2009; Huelsken and Behrens, 2002; Wang, 2009).

1.2.1.5 Mechanism of non-canonical Wnt signalling

In contrast to the canonical pathway, the non-canonical branch of Wnt signalling is β-catenin independent and acts through various factors that include RhoA, ROCK, Jun N-terminal kinase, (JNK), calcineurin, protein kinase C (PKC) and casein kinase II (CKII) to control cell polarity. This is particularly important for PCP, which describes the polarization of epithelial cells within the plane of an epithelial sheet. PCP signals both between cells (non-autonomously), to establish asymmetric distribution of proteins, and within cells (autonomously), to reinforce and maintain this asymmetry. Thus, this intracellular communication coordinates cell movements within the same plane and orientates cells into regular, organized arrays, which are essential for the formation of complex functional structures, such as the stereocilia bundle in the inner ear, as well as photoreceptors in the eye, and kidney tubules. The PCP pathway also exists in mesenchymal cells and neural tube cells in vertebrates, where it regulates cell migration and cell intercalation, so called convergent extension movements during gastrulation and neurulation, respectively. More recent studies have also implicated the PCP pathway with cilia orientation in multiciliated cells (Huelsken and Behrens, 2002; Komiya and Habas, 2008; Veland et al., 2009; Wang, 2009). In the non-canonical Wnt/PCP pathway, Wnt signalling is transduced through Fz independent of LRP5/6 leading to the activation of Dvl. This, in turn, activates the small GTPases, Rho and Rac. Activation of Rho GTPase leads to the activation of the Rho-associated kinase (ROCK), which leads to modification of the actin cytoskeleton and cytoskeletal rearrangement, whereas activation of Rac stimulates the kinase activity of JNK,

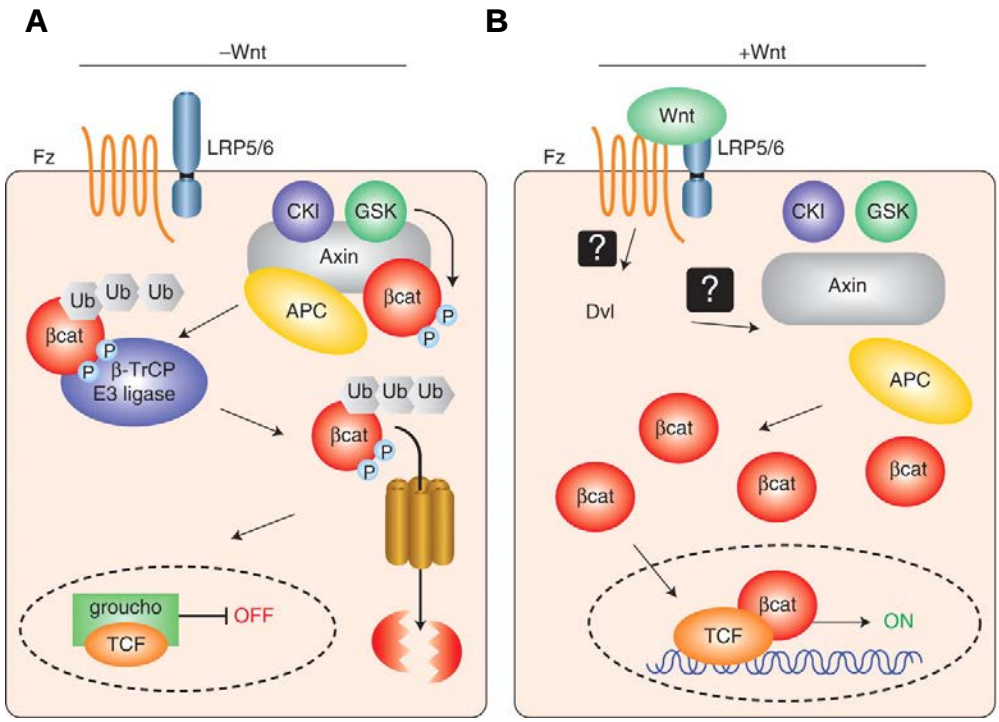

Figure 1.12 Model of Canonical Wnt signalling
(A) In the absence of Wnt ligand, cytoplasmic β-catenin is sequestered by a "destruction complex" composed of the scaffold protein axin, adenomatous polyposis coli (APC), glycogen synthase kinase 3β (GSK3β), casein kinase I (CKI), and protein phosphatase 2A (PP2A). This leads to phosphorylation of β-catenin at the amino terminus targeting it for polyubiqitination and proteasomal destruction. In the absence of β-catenin, transcription factor/ lymphoid enhancer binding factor (TCF/LEF) are bound to transcriptional suppressors such as Groucho to keep the canonical Wnt pathway inactive. **(B)** Upon ligand binding, the LRP5/6 receptor is phosphorylated in its cytoplasmic tail. This creates a binding site for axin which inactivates the disruption complex in a poorly understood process that requires Dishevelled (Dvl). As result, β-catenin is released and translocates to the nucleus where it displaces Groucho transcription repressors from TCF. This initiates transcription of Wnt target genes. Adapted from Cadigan & Peifer (2008).

resulting in a transcriptional response. Overall, the gene transcription events and cytoskeletal rearrangements stimulated by PCP signalling lead generally to the terminal differentiation of cells (Huelsken and Behrens, 2002; Veeman et al., 2003; Wang, 2009).

1.2.1.6 Wnt signalling and cilia

In addition to members of the degradation complex, GSK-3 and APC, other proteins involved in the PCP pathway, such as Inversin (Inv) and Van Gogh2 (Vangl2), are localized to the ciliary apparatus suggesting a role for cilia in the regulation of both canonical and non-canonical Wnt signalling. This hypothesis is strengthened by studies that show that levels of canonical/β-catenin signalling increase following knockdown of proteins associated with cilia in cultured cells, zebrafish or mouse embryos. Furthermore, processes that depend on non-canonical Wnt/PCP signalling, such as convergent extension movements, are also disrupted, suggesting that the primary cilium might function as a switch between canonical and non-canonical Wnt signalling pathways (Berbari et al., 2009; Veland et al., 2009).

The Wnt pathway was first linked to cilia directly by studies from Simon et al. (2005), who showed that Inversin (Inv) localizes to cilia and interacts with the Dvl component of the Wnt pathway. Inversin is the product of a gene mutated in nephronophthisis, an autosomal recessive cystic kidney disease characterized by extensive renal cysts and situs inversus. Biochemical analyses have suggested that inversin functions as a molecular switch between the two Wnt signalling pathways. In fact, inversin inhibits canonical signalling by targeting cytoplasmic Dvl for degradation, but it doesn't degrade the plasma membrane-localized Dvl, and thus, does not inhibit non-canonical signalling, indirectly promoting the non-canonical Wnt pathway (Figure 1.13) (Berbari et al., 2009; Simons et al., 2005; Singla and Reiter, 2006). It has been proposed that this switch between the canonical and non-canonical pathways is necessary to organize the shape and function of the nephron during development and that cross-talk between the non-canonical Wnt pathway and other signalling pathways is important for the continued maintenance of tubular structure, polarity and integrity in adult tissues (Kim et al., 1999; Simons et al., 2005). The first genetic evidence that hinted at a connection between cilia and Wnt signalling came from observing that knockdown of any of several genes linked with Bardet-Biedl Syndrome (BBS1, BBS4, and MKS), a disorder associated with ciliary dysfunction, results in a hyperactive Wnt response in cultured cells (Gerdes et al., 2007). Furthermore, mice with mutations in

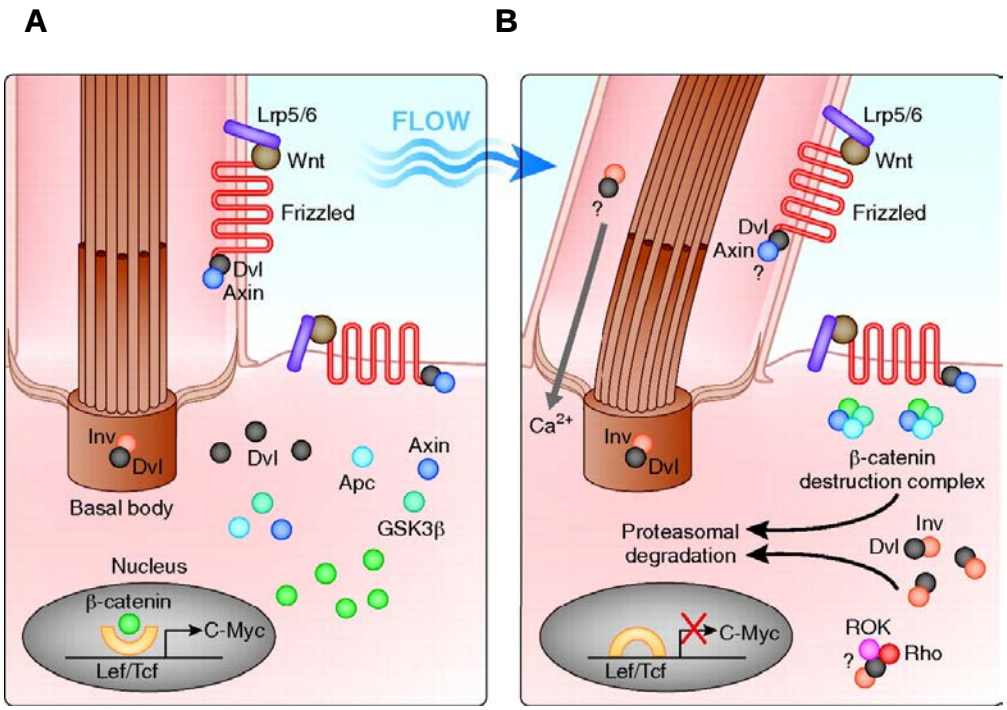

Figure 1.13 Model of mechanosensation-based Wnt signalling
(A) Wnt signalling occurs primarily through β-catenin–dependent pathways in the absence of urine flow. Upon ligand binding, frizzled receptor results in inactivation of the β-catenin destruction complex through the presence of dishevelled (Dvl). As result, β catenin levels increase and upregulate gene expression through the canonical Wnt signalling pathway. **(B)** Deflection of the primary cilium caused by flow, results in increased expression of inversin (Inv), which in turn, reduces levels of cytoplasmic Dvl by increasing its proteasomal degradation. This allows the β-catenin destruction complex to reassemble and get activated thereby switching from the canonical to the non-canonical Wnt signalling pathway. The model is consistent with the finding that overexpression of β-catenin (equivalent to canonical Wnt signalling) leads to renal cysts in a mouse model. Adapted from Hildebrandt (2009).

Bardet-Biedl Syndrome (BBS) genes, necessary for IFT and basal body function, share phenotypes with PCP mutants, including neural tube defects and disrupted cochlear stereociliary bundles. Further evidence to support the ciliary connection with the PCP came from genetic interaction of BBS genes with the PCP gene, Vangl2. Moreover, Corbit et al. (2008) showed that when the cilium is present, it significantly constrains canonical Wnt signalling in both cultured mouse embryo fibroblasts (MEFs) and embryonic stem cells. In fact, Ofd1 null cells that lack cilia are more sensitive to stimulation with exogenous Wnt ligand compared to wild-type cells. This may be due to the cilium's role in normal cells to put a brake on the Wnt/β-catenin pathway. Furthermore, suppressing expression of proteins essential for cilia formation, such as bbs1, bbs4, bbs6, and Kif3a, stabilizes β-catenin and upregulates TCF-mediated transcriptional activity, indicative of overactive Wnt/β-catenin signalling (Corbit et al., 2008; Gerdes et al., 2007; Veland et al., 2009; Wallingford and Mitchell, 2011).

1.2.2 The importance of cilia in other signalling pathways

Another signalling pathway coordinated by cilia is that mediated by the platelet derived growth factor (PDGF). PDGF was identified more than three decades ago by Kohler & Lipton, as a serum-derived growth factor for fibroblasts, smooth muscle cells and glial cells. Fibroblasts in tissues are usually in a state of growth arrest. Upon stimulation, they enter the cell cycle and migrate throughout the extracellular matrix for the purpose of wound healing or tissue organization (Goetz and Anderson, 2010; Satir and Christensen, 2007; Schneider et al., 2005). Connections between cilia and PDGF signalling were first observed by Schneider et al. (2005), who showed the ciliary localization of the platelet derived growth factor receptor α (PDGFRα) in murine embryonic fibroblasts. Binding of PDGFs to their receptors cause activation of many signalling pathways such as the Akt and ERK1/2 signalling pathways. Furthermore, activation of Akt and ERK1/2 signalling by PDGF requires the presence of primary cilia, further confirming the relationship between cilia and PDGF signalling (Schneider et al., 2005; Yang et al., 2006). Signalling via PDGFs is thought to play an essential role in cell survival, growth control and cell migration during gastrulation, fetal development and in maintenance of tissues in adults, and defects in this signalling pathway result in many diseases, including cancer, vascular disorders and fibrosis (Mans et al., 2008; Veland et al., 2009). The cilium is also thought to play an essential role in the process of mechanosensation by which cells convert mechanical force into biochemical signals. In fact, in renal epithelia, primary cilia function as mechanosensors, bending in response to fluid flow. This was first discovered in

1997 by Bowers and colleagues, who showed that the primary cilium of PtK1, a cultured renal cell line, was able to bend when the cells were submitted to flow rates comparable to those seen in renal tubules. Deflection of primary cilia in response to urine flow, leads to an increase in intracellular Ca^{2+} by activating Ca^{2+} channels; this is mediated by interaction of two transmembrane proteins, polycystin-1 and polycystin-2 (PC1 and PC2, respectively), which together form the polycystin 1/2 receptor-ion channel complex (Figure 1.14). While the function of PC1 is not clear, PC2 is a transient receptor potential (TRP)-like cation channel, and together with PC1, functions in the cilium as part of a mechanosensory system. The concentration of intracellular calcium is thought to influence several activities that are required for normal renal cell polarity, growth and differentiation. Defects in ciliary mechanosensation disrupt the mechanotransduction pathway and result in many diseases. In the kidney for example, disruptive signalling results in abnormal renal cell function, abnormal division, and ultimately, cyst formation, leading to polycystic kidney disease (PKD). Furthermore, studies have shown that cholangiocyte cilia in the liver act as mechanosensors by linking ductal bile flow to intracellular signalling via Ca^{2+} and cAMP, whereas in the bone, primary cilia act as a mechanosensor in order to maintain adult bone health and homeostasis. However, in contrast to the kidney and liver, the mechanotransduction signalling pathway in the bone is independent of intracellular Ca^{2+} release (Berbari et al., 2009; Nauli et al., 2003; Satir et al., 2010; Schwartz et al., 1997).

1.3 The Human Ciliopathies

As indicated above, mutations in genes that encode ciliary proteins give rise to a wide spectrum of disorders that together are called ciliopathies. Ciliopathies can affect either single organs or multiple organs. Furthermore, many ciliary genes are mutated in more than one ciliopathy, indicating that the mutant proteins interact with each other. Since cilia formation and function depend upon multi-subunit complexes composed of many proteins, mutation of only one protein may be sufficient to produce a defective cilium. However, there may be great variability in the phenotypic severity depending on the protein mutated. Moreover, the clinical features associated with ciliopathies are diverse reflecting the huge importance of cilia in many aspects of human physiology. These symptoms include randomization of the left-right body axis, abnormalities in neural tube closure and patterning, polydactyly, kidney, hepatic and pancreatic cyst formation, retinal degeneration, anosmia, cognitive defects and obesity. Classical examples of ciliopathies include polycystic kidney disease (PKD), primary cilia dyskinesia (PCD), Bardet-Biedl

Syndrome (BBS), orofaciodigital syndrome (OFD) and Meckel-Gruber syndrome (MKS) (Adams et al., 2008; Baker and Beales, 2009; Berbari et al., 2009; D'Angelo and Franco, 2009).

In this section, I will introduce some of these cilia-related disorders and their mechanisms.

1.3.1 Polycystic kidney disease

Polycystic kidney diseases are a group of human genetic disorders affecting more than 12 million people worldwide. PKD is more common than cystic fibrosis, muscular dystrophy, Down's syndrome, sickle cell anemia and hemophilia combined. It is characterized by the accumulation of fluid-filled cysts in the kidney and other organs, eventually leading to end-stage renal disease (ESRD). Renal cyst formation occurs in all regions of nephrons and is characterized by increased cell proliferation and apoptosis. Human PKD occurs in two forms, an autosomal dominant (ADPKD) and autosomal recessive (ARPKD) form. Both forms of PKD initiate early in life; however, whereas ARPKD patients develop ESRD shortly after birth, the ADPKD patients reach ESRD by the fifth decade of life as, in these patients, cyst formation is slower. ADPKD is one of the most common monogenic disorders of the kidney, with an incidence of 1:400-1:1000, accounting for 10% of all end-stage renal patients. It is a systemic disorder affecting multiple organs. In fact, in addition to renal cysts, ADPKD patients have cysts in the liver, pancreas and other organs, as well as cardiovascular defects and increased risk of aneurysm. In contrast to ADPKD, ARPKD is much rarer, affecting 1:20,000 individuals and is associated with a high level of mortality in affected newborns.

In 85% of cases, ADPKD is caused by mutation in the PKD1 gene, and in 15% of cases by mutation in the PKD2 gene. PKD1 and PKD2 encode two large primary cilium membrane proteins, called polycystin 1 (PC1) and polycystin 2 (PC2). PC1 is an integral membrane protein consisting of a large extracellular N-terminal domain, followed by 11 transmembrane domains, and a short intracellular C-terminus (Figure 1.14C). The extracellular domain of PC1 is thought to facilitate cell-cell and cell-matrix interactions whereas the intracellular domain is involved in the activation of downstream signalling cascades, protein-protein interaction and G-protein activation. In addition to its ciliary localization, PC1 also localizes to the plasma membrane and adherent cell junctions, and it is thought to function as a receptor that receives and transduces extracellular signals into the cell. PC2 consists of 6 transmembrane domain and intracellular N- and C-termini, and is

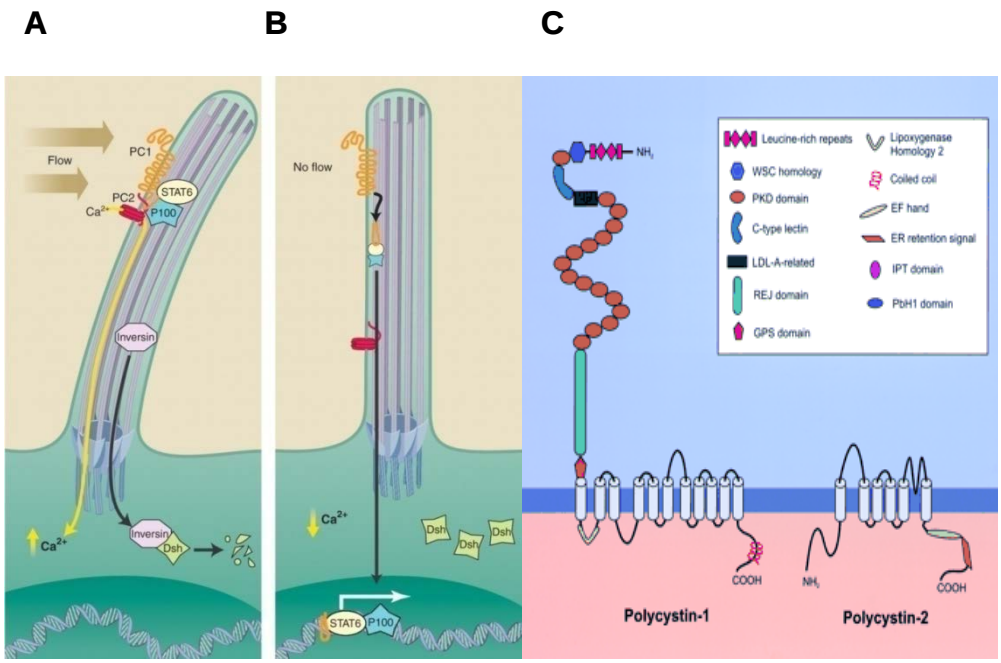

Figure 1.14 The role of PC1 and PC2 in mechanosensation-based cilia signalling

(A) Urine flow within the nephron causes deflection of the primary cilium which is detected by two transmembrane proteins, PC1 (orange) and PC2 (red). Flow induces Ca^{2+} influx through PC2 and maintains STAT6 (yellow) and P100 (turquoise) in a complex bound to the tail of PC1. Flow also leads to up-regulation of Inversin (purple), which targets cytoplasmic Dsh (green) for degradation by the proteasome. **(B)** In the absence of flow, Ca^{2+} influx is reduced and the tail of PC1 is cleaved, allowing P100 and STAT6 to translocate to the nucleus and activate transcription. Lack of flow also results in reduction of Inversin levels, which stabilizes Dsh levels and permits β-catenin to initiate transcription of canonical Wnt pathway target genes. This pathways may also be activated in the absence of PC1, PC2, or the cilium itself, leading to unregulated cell proliferation and formation of cysts. **(C)** Schematic diagram showing the structure of PC1 and PC2. Dark blue line indicates the membrane bilayer. Tan background indicates cytosol. Light blue background indicates extracellular space or ER lumen. Protein motifs are identified in the figure legend. Adapted from Singla & Reiter (2006) and Igarashi and Somlo (2002).

homologous to the transient potential receptor (TRP) protein superfamily, a diverse group of voltage-independent cation-permeable channels expressed in most mammalian cells. Localization studies have revealed that PC2 is localized to cilia, but is also found at the ER. It is thought to be required for entry of calcium into the cell upon mechanosensation. Studies from Qian et al. (1997) and Wright et al. (2005) have revealed that PC2 interacts with PC1. Together, PC1 and PC2 form a mechanosensory complex that translates the deflection of primary cilium of renal epithelial cells into signals associated with cell growth and differentiation. Also present in the complex with PC1 and PC2 are other proteins such as the STAT6 transcription factor, and its coactivator P100. In normal kidney epithelial cells, urine flow causes the bending of the primary cilia. This is detected by PC1 and PC2, which respond to this stimulus by generating Ca^{2+} influx through the cilium and into the renal epithelia cells, and by inhibiting the regulated intramembrane proteolysis (RIP) of PC1. Under the "no flow" response, the cilium straightens, blocking Ca^{2+} influx and activating the RIP of PC1, which releases a portion of the PC1 cytoplasmic tail. This, together with STAT6 and P100, translocate to the nucleus where they activate transcription leading to unregulated cell proliferation and cyst formation (Figure 1.14A and B). ARPKD is caused by mutation in a single gene, *PKDH1* (polycystic kidney and hepatic disease gene 1) that encodes a ciliary protein named polyductin/fibrocystin (FC-1). FC-1 contains a long extracellular N-terminal domain, one transmembrane domain, and a short intracellular C-terminal domain. Localization studies have shown that FC-1 localizes to the renal primary cilia and the centrosomes, and it has been proposed to play a role in collecting duct cell differentiation by interacting with PC2 and regulating its function (Cardenas-Rodriguez and Badano, 2009; Li et al., 2005; Nauli et al., 2003; Pazour et al., 2002; Qian et al., 1997; Singla and Reiter, 2006; Tobin and Beales, 2009; Torres and Harris, 2007).

1.3.1.1 Bardet-Biedl Syndrome

Bardet–Biedl Syndrome (BBS) is a genetic autosomal recessive ciliopathy that was first described in 1986 by Laurence and Moon with a description of a child with obesity, visual impairment, and mental disabilities, and was the first disease to be studied in detail whose origin lay in ciliary dysfunction. It has thus become a model ciliopathy. Just like other ciliopathies, BBS affects many body systems. It is principally characterized by retinal degeneration, cognitive impairment, obesity, renal cystic disease, polydactyly, male hypogonadism and occasionally situs inversus. To date, 14 genes have been identified (BBS1–*12,* Meckel syndrome 1 [*MKS1*] and centrosomal protein 290 kDa/nephronophthisis 6 [*CEP290/NPHP6*]),

whose mutations are associated with this syndrome. These encode proteins that are mostly localized to the cilia/basal body/centrosome complex. In addition to localization studies, results from animal models have provided further evidence of a functional link between the cilium and BBS proteins. Studies in worms have shown that homologues of the BBS7 and BBS8 proteins play an important role in coordinating the movement of IFT subcomplexes A and B. In line with this, loss of *bbs7* and *bbs8* in *C. elegans* causes IFT subcomplexes A and B to separate and move at different rates, most likely because each complex is moved by a different type of kinesin. According to this hypothesis, a model was proposed in which BBS7 and BBS8 might function as a bridging factor between the two IFT subcomplexes, thus stabilizing and coordinating transport. This might explain why BBS phenotypes are less severe than IFT knockouts (Blacque et al., 2004). Moreover, in humans, BBS4 has been found to interact with PCM-1, a centrosomal protein involved in centriolar replication, and with the p150Glued subunit of dynactin, that plays an important role in retrograde motor function. In fact, studies from Kim et al. (2004) have shown that RNAi silencing of BBS4 caused PCM-1 mislocalization to the cytoplasm, loss of microtubule anchoring from the centrosome, and arrest of cell division. Thus, it has been proposed that BBS4 functions as an adaptor protein that is important for loading cargo (e.g. PCM-1) onto IFT particles in preparation for its transport along the ciliary axonemes (Badano et al., 2006; Bisgrove and Yost, 2006; Kim et al., 2004; Zaghloul and Katsanis, 2009).

Further insight into how BBS proteins behave, at the molecular level, came from studies by Nachury et al. (2007), who showed that several of the BBS proteins form a complex, termed the ‘‘BBSome’’. This includes at least seven highly conserved BBS proteins (BBS1, BBS2, BBS4, BBS5, BBS7, BBS8 and BBS9). Of particular importance, BBS9 is observed to interact with all other subunits and may therefore act as a central organizer of the BBSome. However, the most striking ciliary defects occur when BBS1 and BBS5 proteins are depleted in cells. One theory suggests that the BBSome is transported to the basal body by the centriolar satellites where it associates with the ciliary membrane. In addition, it has been shown that the BBSome can associate with Rab8, a member of the Rab family of Ras-like small GTPases, which is a key regulator of vesicle trafficking. Rab8 itself enters the ciliary membrane and promotes ciliogenesis, therefore, it has been proposed that pathogenesis in BBS might be caused by defects in vesicular transport to the cilium (Nachury et al., 2007; Kim et al., 2004; Kim et al., 2008; Blacque & Leroux., 2006). Thus, two different mechanisms may explain the role of BBS proteins in ciliary function. One suggests that BBS proteins are necessary for

microtubule-based transport along the cilium; the other that BBS proteins function as a complex mediating vesicle transport from the cytoplasm to the cilium. The participation of BBS proteins in multiple large complexes may also explain the genetic heterogeneity, the lack of phenotype-genotype correlations, and the oligogenic nature of BBS.

1.3.1.2 Alström syndrome

Alström syndrome (ALMS) is a rare recessive disorder that is very similar to BBS. ALMS is caused by mutations in a novel gene called ALMS1, whose function is not yet known. It is characterized by several phenotypes reminiscent of BBS, including retinal degeneration, obesity and diabetes. However, polydactyly, dilated cardiomyopathy, hepatic and renal dysfunction, short stature, and male hypogonadism may also be present. Just like other ciliopathy proteins, ALMS1 protein localizes to centrosomes and to the base of the cilia, thus suggesting a ciliary role and a possible explanation for the phenotypic overlap with BBS. Studies from Hearns et al. (2005) showed that the ALMS phenotype may be due to defects in ciliary function rather than abnormal ciliary structure, as fibroblasts with disrupted ALMS1 had morphologically normal cilia. Interestingly, database searches suggest that ALMS1 is restricted to vertebrates and therefore is not required for ciliogenesis in invertebrates (Bisgrove and Yost, 2006; Hearn et al., 2005; Tobin and Beales, 2009).

1.3.1.3 Nephronophthisis

Nephronophthisis (NPHP) is an autosomal recessive cystic kidney disease and is the most frequent genetic cause of ESRD in children and young adults. Depending on time of onset of ESRD, NPHP is classified as adolescent, juvenile or infantile. The initial symptoms of NPHP are relatively mild and often start at approximately 6 years of age. These mainly include polyuria, polydipsia, secondary enuresis, and anemia, which occur as a consequence of salt wasting and an inability to concentrate urine, implicating dysfunction of the renal cortical collecting duct. In contrast to PKD, which is characterized by enlarged kidney cysts, NPHP cysts are usually small and the overall size of the kidney is normal or diminished (Figure 1.15). In fact, the term “nephronophthisis” means disappearance of nephrons and, in this disease, cysts arise from loss of normal tissue rather than abnormal cell proliferation. Other NPHP characteristics include degradation of tubular basement membranes, tubulointerstitial nephropathy/fibrosis, and corticomedullary cysts. Despite the fact that NPHP describes a renal histopathology, about 10% of NPHP cases also present with extrarenal manifestations that can be associated with other

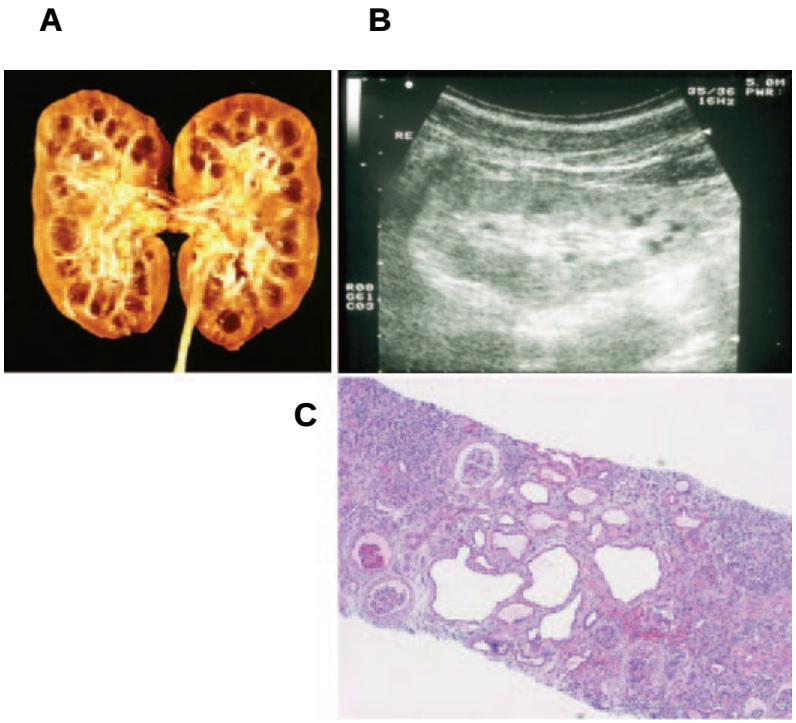

Figure 1.15 Morphology of nephronophthisis
(A) Macroscopic pathology reveals cysts that arise from the corticomedullary junction of normal-sized kidneys. **(B)** Renal ultrasound shows increased echogenicity, loss of corticomedullary differentiation, and the presence of corticomedullary cysts. In contrast to PKD, kidneys are not enlarged. **(C)** Renal histology in NPHP shows the characteristic triad of renal tubular cysts, tubular membrane disruption, and tubulointerstitial cell infiltrates with interstitial fibrosis and periglomerular fibrosis. Adapted from Hildebrandt and Zhou (2009).

syndromes such as retinitis pigmentosa, described as Senior-Løken syndrome (SLSN), cerebellar vermis hypoplasia known as Joubert syndrome (JBTS), congenital ocular motor apraxia type Cogan, cognitive impairment, hepatic fibrosis, phalangeal cone-shaped epiphyses in Mainzer-Saldino, and situs inversus. NPHP has also been described in cases of Bardet-Biedl syndrome (BBS), Ellis-van Creveld syndrome (EVC), Jeune asphyxiating thoracic dystrophy (JATD), Alström syndrome (ALMS), and Meckel-Gruber syndrome (MKS) (Adams et al., 2008; Hildebrandt et al., 2009; Hildebrandt and Zhou, 2007; Saunier et al., 2005; Simms et al., 2011; Veland et al., 2009; Yoder et al., 2002). NPHP is genetically heterogenous. To date, 13 genes have been identified as mutated in NPHP: *NPHP1/nephrocystin-1, NPHP2/inversin, NPHP3, NPHP4/nephroretinin, NPHP5/IQCB1, NPHP6/CEP290, NPHP7/GLIS2, NPHP8/RPGRIP1L, NPHP9/Nek8, NPHP10/SDCCAG8, NPHP11/TMEM67/MKS3, NPHPL1/XPNPEP3,* and *TTC21B,* which collectively account for approximately 30% of patients (Table 1.1). The proteins encoded by these genes are generally referred to as nephrocystins and all localize to the cilium or the basal body, resulting in the hypothesis that this cystic kidney disease too is a ciliopathy (Figure 1.16) (Hildebrandt and Otto, 2005; Saunier et al., 2005; Simms et al., 2011).

(I) ***NPHP1*** was the first NPHP gene identified and accounts for 20-25% of known cases of NPHP, whereas the other genes contribute less than 3% each. *NPHP1* encodes nephrocystin-1, a protein that is localized to the transition zone of primary cilia in renal and respiratory epithelia, but is also located at adherens junctions and focal adhesions, which are involved in cell–cell and cell–basement membrane contacts, respectively. Studies have shown that nephrocystin-1 interacts with various other syndrome-related proteins, such as those encoded by the *NPHP2, NPHP3* and *NPHP4 genes*, as well as proteins important in maintaining the cytoskeleton, including jouberin, ack, filamin A and B, tensin (actin binding), *β*-tubulin and protein tyrosine kinase2B (PTK2B).

(II) The ***NPHP2*** gene was identified as the human orthologue of the murine Inv (inversin) gene that encodes the Inversin protein. In contrast to *NPHP1, NPHP2* mutations are rare and cause infantile *NPHP* (type 2) which are characterised by an earlier presentation of established renal failure (ERF) (at approximately 3 years of age), with enlarged kidneys on ultrasound. Other clinical features of *NPHP2* include retinitis pigmentosa, although this is uncommon. Inversin localizes to the proximal region of the cilium where it may interact directly with the microtubule axoneme. In addition, Inversin plays important roles in Wnt signalling, acting as a

Disease	Gene & Chromosome localization	Protein & Molecular weight	Cellular Localization of Protein	Renal symptoms	Extrarenal associations
Autosomal dominant PKD1	*PKD1* 16p13.3	Polycystin-1 460 kDa	Primary cilia Focal adhesions Adherens junctions	Increased kidney size Echogenic kidneys Cortical cysts Cystic dilatation Severe hypertension	Liver and pancreatic cysts Intracranial aneurysms
Autosomal dominant PKD2	*PKD2* 4q21	Polycystin-2 110 kDa	Primary cilia Focal adhesions Adherens junctions	Increased kidney size Echogenic kidneys Cortical cysts Cystic dilatation Severe hypertension	Liver and pancreatic cysts Intracranial aneurysms
Autosomal recessive PKD	*PKHD1* 6p12.2	Polyductin/fibrocystin 447 kDa	Primary cilia Apical membrane	Same as autosomal dominant PKD Kidney collecting-duct ectasia	Hepatic fibrosis Facial malformations Pulmonary hypoplasia from oligohydramnios Ductal-palate malformation in the liver
NPHP1	*NPHP1* 2q13	Nephrocystin-1 83 kDa	Cilia Centrosome Cell-cell junctions Focal adhesions	Not reported	Retinitis pigmentosa Truncal cerebellar ataxia Congenital hepatic fibrosis Ocular motor apraxia type Cogan
NPHP2	*INVS* 9q31	Inversin 118 kDa	Cilia Centrosome Cell-cell junctions Nucleus	Increased kidney size Cortical cysts Cystic dilatation Severe hypertension	Liver and pancreatic cysts Intracranial aneurysms
NPHP3	*NPHP3* 3q22.1	Nephrocystin-3 150.8 kDa	Cilia Connecting cilia	Diffuse interstitial fibrosis Small corticomedullary cysts	Retinitis pigmentosa Leber congenital amaurosis
NPHP4	*NPHP4* 1p36	Nephroretinin 157.8 kDa	Cilia Centrosome Cell-cell junctions	Increased or normal kidney size	Retinitis pigmentosa
NPHP5	*IQCB1* 3q21.1	Nephrocystin-5 68.9 kDa	Cilia Connecting cilia	Salt wasting leading to hyponatremia and hypovolemia	Early onset retinitis pigmentosa
NPHP6	*CEP290* 12q21.3	CEP290 290 kDa	Centrosome Nucleus Connecting cilia	Polyuria and polydipsia Anemia, anorexia, nausea, metabolic acidosis, Weakness	Early onset retinitis pigmentosa Cerebellar vermis aplasia Leber congenital amaurosis
NPHP7	*GLIS2* 16p13.3	Nephrocystin-7 55.7 kDa	Cilia	ESRD: juvenile form at 13 years, adolescent form at 19 years	Not reported
NPHP8	*RPGRIP1L1* 16q12.2	Retinitis pigmentosa GTPase regulator interacting protein 1–like 1 130.5 kDa	Cilia Basal bodies Centrosome Cytoplasm	Not reported	Retinitis pigmentosa Hepatic fibrosis
NPHP9	*NEK8* 17q11.1	NIMA-related kinase 8 80 kDa	Centrosomes Cilia	Not reported	Not reported
NPHP10	SDCCAG8 1q44	Serologically defined colon cancer antigen 8 82.7 kDa	Centrosomes Cell-cell junctions	Not reported	Bardet Biedl syndrome
NPHP11	TMEM67 8q22.1	Transmembrane protein 67 111.7 kDa	Not reported	Not reported	Joubert Syndrome Hepatic fibrosis Meckel-Gruber syndrome
NPHPL1	XPNPEP3 22q13	X-prolyl aminopeptidase 3 57kDa	Mitochondria	Not reported	Cardiomapathy Seizures
NPHP JBTS	TTC21B	Intraflagellar transport protein 139 150.9 kDa	Cilia	Not reported	Joubert Syndrome Meckel-Gruber syndrome Bardet Biedl syndrome Jeune asphyxiating thoracic dystrophy

Table 1.1 Genes and Proteins Implicated in Cystic Kidney Disease
This table shows their associated symptoms and extrarenal manifestations. Adapted from Deltas and Prapagregoriou (2010).

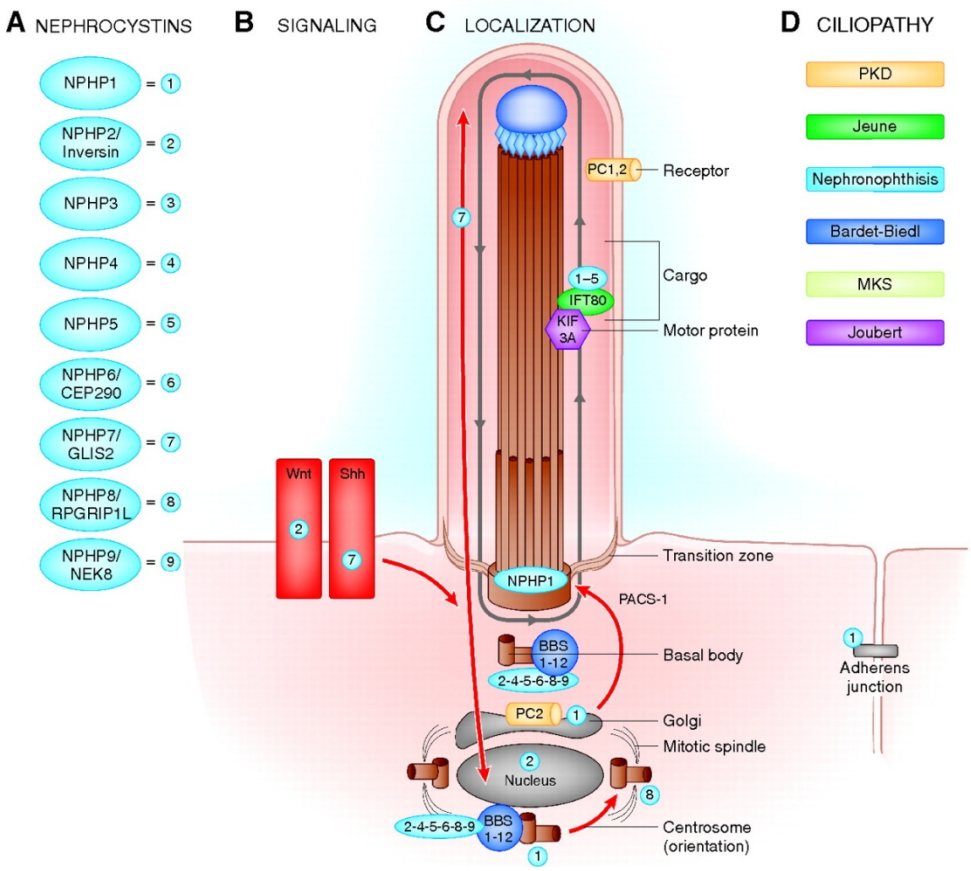

Figure 1.16 Subcellular localization of nephrocystins
(A) Nine of the twelve known NPHP nephrocystin proteins are indicated. **(B)** Sensory cilia perceive and process external signals and "nephrocystins" are involved in signalling mechanisms including Wnt signalling and sonic hedgehog signalling (Shh). **(C)** Depending on cell cycle stage, some nephrocystins localize to primary cilia, basal bodies, endoplasmic reticulum, the mitotic spindle, centrosomes, adherens junctions or focal adhesions. Many nephrocystins have been localized to more than one intracellular compartment. Arrows in the primary cilium indicate the direction of anterograde transport along the microtubule system mediated by kinesin-2 and retrograde transport by cytoplasmic dynein 1b. **(D)** Colour coding of proteins indicates the disease with which they are associated when mutated. Adapted from Hildebrandt et al. (2009).

switch between the canonical and non-canonical pathways. In fact, loss of Inversin due to *NPHP2* mutation causes activation of canonical Wnt signalling leading to cell proliferation and random oriented cell division. Furthermore, studies from Sohara et al. (2009) have shown that Inversin is essential for the localization of *NPHP3* and *NPHP9*/Nek8, but not vice versa. This indicates that Inversin plays an important function in tethering and stabilizing *NPHP3* and Nek8 in what has been called, the Inversin compartment, that sits just above the transition zone.

(III) Mutations in ***NPHP3*** are responsible for an adolescent form of the disease, which is characterized by fibrosis and retinal degeneration. Recent studies have shown that loss of *NPHP3* function in mice results in a variety of phenotypes, including situs inversus, congenital heart defects and embryonic lethality. Furthermore, truncating mutations of *NPHP3* in humans cause a similar clinical spectrum with situs inversus, polydactyly, central nervous system malformations, structural heart defects, and a wide range of congenital anomalies of the kidney and urinary tract that resemble MKS. Nephrocystin-3 interacts with nephrocystin-1 and Inversin, and can inhibit canonical Wnt signalling. In line with this, mutations in the murine ortholog of *NPHP3* cause the renal cystic mouse model mutant *pcy*, which responds to treatment with vasopressin-2-receptor antagonists.

(IV) ***NPHP4*** encodes nephroretinin, which forms complexes with other NPHP proteins involved in cell adhesion and actin cytoskeleton organization, such as nephrocystin-1, and *NPHP8*/RPGRIP1L (retinitis pigmentosa GTPase regulator interacting protein 1-like). *NPHP4* localizes to primary cilia, basal bodies and the cortical actin cytoskeleton in polarised epithelial cells, and to the centrosomes in dividing cells where it is thought to play a possible role in signal transduction, cell-cell adhesion, and actin cytoskeleton organisation. *NPHP4* mutations may cause isolated NPHP, SLSN and NPHP associated with ocular motor apraxia type Cogan.

(V) ***NPHP5*** mutations are always associated with severe retinal degeneration (early onset SLSN). The *NPHP5* protein is known to interact with the protein encoded by *RPGR* (retinitis pigmentosa GTPase regulator), an X-linked gene which when mutated causes retinitis pigmentosa in males. Both localize to the connecting cilium of the photoreceptor and primary cilium of renal epithelial cells, and may participate in a common pathway in connecting cilia of photoreceptors to primary cilia of renal epithelial cells.

(VI) The ***NPHP6/Cep290*** gene is perhaps the most important gene with respect to unifying the ciliopathies. It encodes CEP290, a centrosomal protein, deficiency of which causes a number of diseases: NPHP (type 6), JBTS (type 5), MKS (type 4), and BBS (type 14). Knockdown of *NPHP6* in zebrafish causes a wide spectrum of extrarenal features, including convergent extension defects, pronephric cysts,

retinal degeneration and hindbrain defects that are common to most of ciliopathies. Furthermore, studies from Chang et al. (2006) have shown that mutations in *NPHP6* can lead to Leber's congenital amaurosis, with a hypomorphic mutation of *NPHP6/CEP290,* the most frequent cause of Leber's congenital amaurosis.

(VII) ***NPHP7/GLS2*** encodes the Kruppel-like zinc-finger transcription factor, *GLIS2*, which localizes both to the primary cilia and the nucleus. The *NPHP7/GLIS2* gene mutations are extremely rare and have been reported in a single Oji-Cree Canadian family. There are no reports of extrarenal manifestations in these patients with the disease confined to the kidney.

(VIII) Mutations in the ***NPHP8/RPGRIP1L*** gene cause JBTS-like phenotypes (i.e. cerebro-oculo-renal syndrome) and MKS. The gene product of *NPHP8,* RPGRIP1L, interacts with nephrocystin-4 and nephrocystin-6 at the centrosome and basal body. Studies from Vierkotten et al. (2007) have shown that RPGRIP1L participates in Shh signalling through the cilium, thus affecting patterning of the developing neural tube and limb.

(IX) Another *NPHP* gene is ***NPHP9***. This encodes the Nek8 protein (never in mitosis A-related kinase 8), which was found to be mutated in the jck (juvenile cystic kidney) mouse model of cystic kidney disease. This will be described in more detail in section 1.4.15.

(X) The ***NPHP10/SDCCAG8*** was recently identified to be mutated *in* ten families with NPHP-related ciliopathies, in particular SLS and BBS. *NPHP10* gene encodes for serologically-defined colon cancer antigen 8 (SDCCAG8) protein, which colocalizes at centrosomes and cell-cell junctions with nephrocystin-5. Furthermore, studies from Siemens et al. (2011) showed that SDCCAG8 and nephrocystin-5 colocalize in the transition zone of photoreceptors. This is likely to be of functional significance and correlates with the phenotype of SLS.

(XI) Another NPHP gene is ***NPHP11/TMEM67/MKS3***, mutation of which is pleiotropic. In fact, this mutation has been identified in patients with NPHP and liver fibrosis, as well as to a number of patients suffering from different ciliopathies, including JS, MKS and COACH syndrome (cerebellar vermis hypoplasia, oligophrenia (developmental delay), ataxia, coloboma, and hypotonia).

(XII) The *NPHP-like 1* gene (***NPHPL1***) was recently identified in two consanguineous families with NPHP. It is characterized by additional extrarenal manifestations including cardiomyopathy and seizures. It codes for X-propyl aminopeptidase 3 (XPNPEP3), which unlike other NPHP gene products, does not localize to primary cilia, basal bodies or centrosomes, but to mitochondria. This is the first NPHP-associated gene so far not localized to cilia. However, it is still

possible that this enzyme may play a role in cilia function by cleaving certain cilial proteins.

(XIII) In addition to known *NPHP* genes, mutations in ***TTC21B*** gene have been recently identified in families with isolated NPHP and extrarenal manifestations including the ciliopathy, Jeune asphyxiating thoracic dystrophy (JATD). The *TTC21B* gene encodes for a retrograde intraflagellar transport protein, called intraflagellar transport protein 139 (IFT139), which is localized to the primary cilium and is essential for ciliary function.

Thus, nephronophthisis offers a clear example of the genetic and allelic heterogeneity that can be features of the ciliopathies. Considering the different subcellular localization of nephrocystins, and considering their different interacting partners, it appears that nephrocystins are involved in mediating signals from the cilia, centrosomes, cell-cell junctions and focal adhesions, and defects in these processes cause NPHP (Adams et al., 2008; Chang et al., 2006; Hildebrandt et al., 2009; Hildebrandt and Zhou, 2007; Otto et al., 2003; Simms et al., 2011; Sohara et al., 2008; Valente et al., 2006; Vierkotten et al., 2007).

1.3.1.4 Senior-Løken Syndrome

Senior-Løken Syndrome described by Senior and Løken in 1961, is a rare disorder associated with both nephronophthisis and retinal degeneration. In fact, mutations in *NPHP5* cause a severe form of retinal degeneration which leads to blindness in early infancy, called Leber's congenital amaurosis (*SLSN type 5*). Nephrocystin-5 contains an IQ domain, which directly interacts with calmodulin, and is in a complex with RPGR. Mutations in *RPGR* lead to X-linked retinis pigmentosa. Localization studies have revealed that both nephrocystin-5 and RPGR are localized in the connecting cilia of photoreceptors and in primary cilia of renal epithelia cells explaining why in Senior-Løken syndrome patients both the eye and kidney are affected (Hildebrandt et al., 2009; Hildebrandt et al., 2011; Otto et al., 2010; Simms et al., 2009).

1.3.1.5 Joubert Syndrome

Despite the fact that NPHP describes a renal histopathology, in 10% of cases, patients with NPHP also present with some extrarenal manifestations that can be associated with other syndromes such as retinitis pigmentosa (SLSN), cerebellar vermis hypoplasia (JBTS), ocular motor apraxia (Cogan type), cognitive impairment, hepatic fibrosis, phalangeal cone-shaped epiphyses (Mainzer-Saldino), and situs inversus. JBTS is an autosomal-recessive neurological disorder

characterized by hypotonia (loss of muscle tone), ataxia, developmental delay, mental retardation, and often neonatal apnea/hyperpnea (irregular breathing) and/or ocular motor apraxia (difficulties in initiating rapid horizontal eye movements). The characteristic and diagnostic symptom of JBTS is the so-called the "molar tooth sign" (MTS) that describes the cerebellar and brainstem malformation seen by magnetic resonance imaging. The MTS has greatly enhanced the diagnosis of JBTS and has identified a group of Joubert syndrome-related disorders (JSRD) with involvement of other organs (Salomon et al., 2009; Tobin and Beales, 2009). In fact, other characteristics of JBTS include central nervous system (CNS) abnormalities, ocular coloboma, retinal dystrophy, skeletal defects such as polydactyly and hepatic and renal fibrosis. These features significantly overlap with other disorders, most notably NPHP. In line with this, studies from Parisi et al. (2004) found that the NPHP1 gene is deleted in a subset of JBTS patients, further strengthening the relationship between NPHP and Joubert Syndrome. Out of the eight JBTS loci, six have been described. These include *NPHP1* (JBTS type 4), *AHI1* (JBTS type 3), *NPHP6/CEP290* (JBTS type 5), and *NPHP8/RPGRIP1L* (JBTS type 7).

JBTS3 has been shown to be caused by mutations in the Abelson helper integration site (AHI1) gene, which encodes for Jouberin, a protein localized to adherens junctions, basal bodies and primary cilia, and which interacts with nephronocystin 1. CEP290 is known to interact with and activate the cAMP–dependent transcription factor, CREB2/ATF4. Patients with NPHP6/CEP290 mutations show neurological and neuroradiological features of JBTS, but also severe retinal and renal involvement. Furthermore, mutations in the NPHP8/*RPGRIP1L* gene can cause both JBTS type 7 and Meckel-Gruber syndrome (MKS) type 5. Mutations in the ARL13B gene have recently been identified in JBTS type 8. The ARL13B gene encodes the ARL13B protein, a member of the Ras-GTPase family, which in other species is required for ciliogenesis, body axis formation, and renal function. Presently, the loci for JBTS type 1 and type 2 are not yet identified (Hildebrandt and Zhou, 2007; Louie and Gleeson, 2005; Ramamurthy and Cayouette, 2009; Simms et al., 2009; Tobin and Beales, 2009).

1.3.1.6 Meckel-Gruber Syndrome

Meckel-Gruber Syndrome (MKS) is a rare, ciliopathic, autosomal recessive disorder that leads to perinatal death as result of dysplasia and malformations in multiple organs including kidney, retina (microphthalmia), brain (occipital encephalocoele), liver (hepatic cysts) and limbs (postaxial polydactyly). So far, six loci have been

linked to MKS, of which 5 have been identified as MKS1, MKS3, MKS4, MKS5 and MKS6. All gene products encode for proteins that play a role in ciliary function. In fact, MKS1 and MKS3/meckelin interact and are required for centriole migration to the apical membrane and consequent formation of the primary cilium. Mutations in the NPHP genes *NPHP3*, *NPHP6/CEP290* and *NPHP8/RPGRIP1L*, as well as mutations in the BBS genes, *BBS2*, *BBS4* and *BBS6*, have also been found in patients with MKS, suggesting that all these conditions are connected with each other (Hildebrandt et al., 2011; Hurd and Hildebrandt, 2011; Quinlan et al., 2008; Tobin and Beales, 2009).

1.3.2 Mechanisms of ciliopathies

As emphasised throughout the introduction, a common characteristic of ciliopathies is the extensive pleiotropy they display. This is perhaps not surprising given that primary cilia are present on nearly every cell of the body and control multiple signalling pathways which play important roles in tissue development and homeostasis. In addition, the finding that mutation of the same gene may cause different phenotypes has blurred the boundaries between these diseases and led to an emerging concept of a spectrum disease. For example, if a gene defect manifests during embryo development, it will cause dysplasia, whereas if it manifests in adult tissues, it may result in degeneration of organs that had a normal architecture at birth. Most ciliopathies are also genetically heterogeneous, whereby mutations in different genes can cause the same clinical disease. The heterogeneity of the genetic locus is one of four independent mechanisms that determine the extent and severity of disease ciliopathy patients. For example, nephronophthisis results from homozygous deletion of *NPHP1*, whereas a severe Meckel's syndrome phenotype is caused by two truncating mutations of *NPHP6/CEP290.* The second mechanism is multiple allelism: two truncating mutations of *NPHP3, NPHP6, NPHP8* or *NPHP11/MKS3* cause Meckel's syndrome, but the presence of a missense mutation may favour Joubert's syndrome, which is characterized by milder phenotypes. The existence of modifier genes represents the third mechanism. For example, the presence of a heterozygous mutation in *NPHP6* or *NPHP8* in patients with homozygous *NPHP1* deletions causes additional eye or cerebella involvement. The fourth mechanism is oligogenicity. It has been proposed that the actions of two or more recessive genes with heterozygous mutations (which alone are not sufficient to result in phenotype) may result in a phenotype when the mutations act together. This is the case for some BBS and NPHP mutations. Thus, it is becoming clear that ciliopathies are not only determined by the specific gene that is mutated, its biological role and pattern of

expression, but also by the type and effect of that mutation on protein function, as well as the total number of genes mutated (Adams et al., 2008; Cardenas-Rodriguez and Badano, 2009; Hildebrandt et al., 2009).

1.3.2.1 Mechanisms of kidney cyst formation

The pathogenesis of PKD is complex and several molecular mechanisms and signalling pathways have been proposed to contribute to the initiation and progression of cyst formation. It is now becoming clear that abnormal cell proliferation and deregulated apoptosis, increased secretion of fluids into the tubular lumen, irregular cell-matrix interactions, and defective cellular polarity, all contribute to the formation of cysts. To understand how cysts are formed, we first need to look how normal renal cells are formed. Normal mature kidney cells are in a quiescent state, neither dividing nor undergoing apoptosis. However, during development, a critical balance exists between cellular differentiation, which leads to tubular heterogeneity, and proliferation, which is required for kidney growth. In cystic cells, this balance is disrupted leading to cyst formation.

Polycystin 1 and polycystin 2, the gene products of PKD1 and PKD2, respectively, play an important role in cyst formation given that they are implicated in various pathways connected to cell proliferation and differentiation, such as Wnt, Hedgehog, and G-protein signalling. As previously mentioned, the PC1/PC2 complex controls the Ca^{2+} levels in the cell, and inhibition of PC1 or PC2 expression leads to a decrease in intracellular Ca^{2+} levels, activation of transcription factors leading to cell proliferation, and ultimately cyst formation. In addition, an increase in extracellular Ca^{2+} causes the levels of cyclic adenosine monophosphate (cAMP) to increase. This activates the mitogen activated protein kinase (MAPK) pathway also promoting cell proliferation and cyst formation. Furthermore, polycystins regulate the activity of the mammalian target of rapamycin (mTOR). mTOR is a serine/threonine protein kinase which plays important roles in protein translation, cell growth and proliferation and the mTOR pathway is deregulated in various types of cancer. In fact, Wahl et al. (2006) showed that mTOR activity is elevated in cystic epithelium, and treatment of rodent PKD models with the mTOR inhibitor, rapamycin, reduced the polycystic kidney size in these animals. Therefore, disruption of cilia or mutations in PC1 are proposed to result in loss of a PC1/mTOR inhibitory complex in the cilium, which in turn leads to increased proliferation and cyst development (Chapin and Caplan, 2010; Deltas and Papagregoriou, 2010).

Perhaps even more significant than increased proliferation of tubular cells in the course of cyst formation is deregulation of planar cell polarity (PCP), which results in cystic dilation due to defective cell division and tubule lengthening. When PCP is perturbed, the tubular epithelial cells no longer divide along an axis parallel to the tubule lumen, causing tubule expansion rather than elongation (Figure 1.17). This was demonstrated by Fischer et al. (2006) who studied PCP in rat cystic kidney models and found that cells divided in an irregular manner escaping the tubular axis. It is hypothesised that in normal tubular renal epithelial cells, primary cilia sense the direction of urine flow and provide a cue for PCP and oriented cell division that is parallel to the tubular axis and leads to tubule elongation. In fact, studies from Bowser et al. (1997) and Schwarts et al. (1997) showed that in a flow gradient, as in the kidney tubule, all primary cilia align in a single direction, determining the direction in which the cilia bend. As a result, the flow, and therefore the bend, is always in the anterior-posterior direction so that the gradient of Ca^{2+} concentration or other signalling molecules along the cellular axes should be uniform from cell to cell. If the function of primary cilia or the flow sensing or responding pathway is perturbed, maloriented cell division and tubule dilation will occur, leading to cyst formation (Chapin and Caplan, 2010; Deltas and Papagregoriou, 2010; Fischer et al., 2006; Zhou, 2009).

In addition, mutation of *NPHP/inversin* also affects PCP. Simons et al. (2005) have shown that inversin inhibits canonical Wnt signalling by targeting cytoplasmic dishevelled for degradation, and concomitantly inducing PCP activity, which is necessary to maintain normal tubular development and morphology. In the absence of inversin, cysts develop as a result of unopposed canonical Wnt signalling, as is the case of NPHP type 2. The levels of inversin increase in the presence of fluid flow in cultured kidney cells, suggesting that, in the developing renal tubules, urine flow terminates canonical Wnt signalling in favour of PCP which will pattern the tubule. Thus, perturbation of fluid flow also leads to cystogenesis by decreasing the levels of inversin (Hildebrandt et al., 2009; Ross et al., 2005; Simons et al., 2005). BBS proteins also play an important role in PCP. In fact, they have been shown to modulate the balance between the canonical and non-canonical Wnt signalling. Consistent with this, perturbation of BBS proteins results in decreased PCP and the concomitant upregulation of canonical signalling through the stabilization of β-catenin (Badano et al., 2006; Cardenas-Rodriguez and Badano, 2009; Gerdes et al., 2007). These studies suggest that kidney cysts may also form from unopposed Wnt signalling that is known to suppress terminal differentiation of tubular cells.

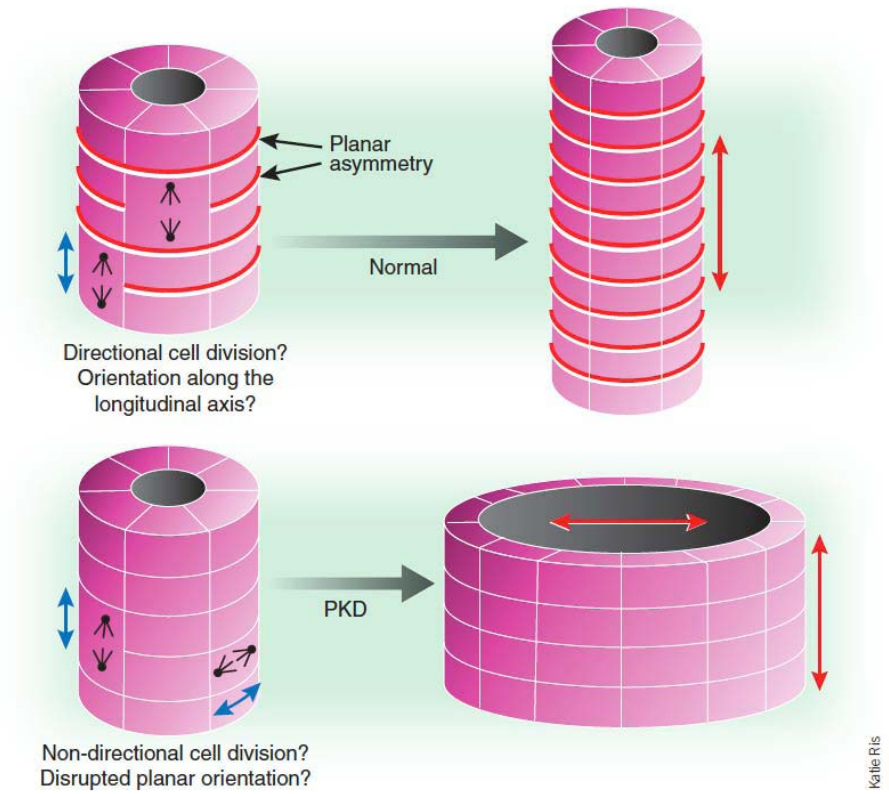

Figure 1.17 Non-canonical Wnt signalling and tubular morphogenesis

For normal solute and water transport, proper apical-basolateral polarity is essential. Tubular epithelial cells must also be correctly oriented with respect to the longitudinal axis of the tubule, especially during renal and biliary development when newly formed tubules undergo progressive lengthening. The default structure that would result from disruption of this planar orientation is predicted to be a dilated tubule or cyst. Non-canonical Wnt signalling regulates a number of processes that could help orient cells properly along the longitudinal axis. Tubular flow could be one of these signals that provide information about cellular orientation. Adapted from Germino (2005).

In addition, it has been proposed that a two-hit mechanism is required for the formation of cysts with a germ line mutation to one allele and a somatic mutation to the other. Consistent with this, kidneys in ADPKD patients, who inherit one mutated copy of PKD1 or PKD2 will develop and function normally until adulthood and, only over time, will develop cysts. This hypothesis would explain the slow progression of this disease over the course of the years (Chapin and Caplan, 2010; Zhou, 2009).

1.3.2.2 Retinal-renal involvement

Since cilia cannot synthesise proteins, protein transport into the cilium occurs through the process of IFT, an essential process for ciliogenesis. For example, photoreceptors use IFT to transport proteins and lipids between the inner and outer segments along the connecting cilium. Retinal degradation is a phenotype seen in many ciliopathies, including BBS, JBTS and SLSN. This is in large part due to defects in IFT in photoreceptors. This gives rise to retinitis pigmentosa (RP) and blindness. Despite the fact that mutations in RPGR account for approximately 20% of all RP cases, RPGR is not specific to photoreceptors and some mutations in RPGR also lead to systemic manifestations. For example, mutations in RPGR have been seen in patients with primary cilia dyskinesia (PCD), a disorder characterized by primary cilia dysfunction in cells of the respiratory and reproductive systems. In addition, mutations in RPGR interacting protein (RPGRIP), another component of the connecting cilium, have also been seen in patients with SLSN and JBTS. In fact, SLSN patients classically have both eyes and kidneys affected. This combined retinal-renal involvement most likely reflects the crucial importance of the primary cilium in photoreceptors and renal epithelial cells, and the fact that both express common proteins, such as nephrocystin-5, nephrocystin-6 and RPGRIP. In BBS patients, mislocalization of BBSome proteins and inactivation of Rab8 in photoreceptor cells leads to photoreceptor degeneration, providing a mechanism for the retinal involvement (Hildebrandt and Zhou, 2007; Ramamurthy and Cayouette, 2009; Wright et al., 2010).

1.3.2.3 Neuronal function

Many ciliopathies also exhibit defective neuronal function, such as is the case with JBTS patients who suffer from cerebellar hypoplasia, characterized by incomplete or underdevelopment of the cerebellum. Most brain cells and all neurons contain a primary cilium, which plays an essential role in many signalling pathways, including the Shh pathway. Considering that Shh signalling has a crucial role in proliferation of cerebellar neurons, it is thought that cerebellar hypoplasia occurs

due to defects in the Shh signalling. Other phenotypes of JBTS patients include the ocular motor apraxia type Cogan (associated with mutations in *NPHP1* and *NPHP4* genes), cerebellar vermis hypoplasia (JBTS), and mental retardation (*NPHP6*). These phenotypes may be explained by the fact that malformations of the cerebellum observed in JBTS consist of abnormal decussating (crossing in the brain) of neurons, defective axonal outgrowth and axon guidance, that affects the corticospinal tract and superior cerebellar peduncles, thereby explaining the motor and behavioral abnormalities. Hyperphagia-induced obesity is another characteristic seen in BBS and ALMS patients. This may be due to mislocalization of specific hormone receptors associated with feeding behavior, thus regulating the feeling of satiety and hunger. These receptors are normally found in cilia; however, in neurons of mice that have mutations in *Bbs2*, *Bbs4* or *Bbs6* genes, these receptors are mislocalized (Han and Alvarez-Buylla, 2010; Lee and Gleeson, 2010; Tobin and Beales, 2009).

1.3.2.4 Skeletal development

Many ciliopathies including BBS, MKS and JBTS, exhibit skeletal defects. Indeed, cilia play an important role in Hh signalling during bone development. This was confirmed by Koyama et al. (2007) who showed that ablation of Kif3a, a subunit of the IFT motor kinesin II, in the developing limb leads to aberrant Hh signalling (both Shh and Ihh) resulting in altered digit patterning and polydactyly. Other Shh-associated phenotypes observed in ciliopathy patients include external genitalia anomalies and craniofacial defects (Cardenas-Rodriguez and Badano, 2009; Tobin and Beales, 2009).

1.3.2.5 Situs inversus

The complete reversal of organ laterality,"situs inversus", is one of the most prominent features of ciliopathies. It results from mutations in NPHP2 gene that encodes for Inversin, which has been shown to be necessary to position cilia in cells of the ventral node (Okada et al., 1999). Indeed, disruption of Inversin in the mouse model results in defective orientation of nodal cilia. This explains the characteristic left-right specification defects of these animals (Hildebrandt et al., 2009; Simms et al., 2009; Simons et al., 2005; Tobin and Beales, 2009).

1.4 NIMA-Related Protein Kinases

NIMA (never in mitosis A) is a serine/threonine protein kinase present in the multicellular filamentous fungus, *Aspergillus nidulans,* whose activation and degradation are essential for mitotic entry and exit, respectively (Osmani et al., 1991a; Pu and Osmani, 1995). It was first identified in 1975 by Ron Morris, as a temperature-sensitive mutant that was never in mitosis (nim) when *Aspergillus* cells were incubated at the restrictive temperature. At the restrictive temperature, *nimA* mutants arrest in G2 with uncondensed chromosomes, cytoplasmic microtubule structures and duplicated, but not separated, spindle poles (SPBs). When upshifted to the permissive temperature, cells rapidly enter mitosis undergoing chromosome condensation and spindle formation. This suggests that the *nimA* mutation blocks cells at a point immediately before initiation of chromosome condensation and spindle assembly (Oakley and Morris, 1983).

NIMA is a 79 kDa protein with an N-terminal kinase and a C-terminal non-catalytic domain. The C-terminal domain contains a coiled-coil motif that is thought to be important for the formation of NIMA oligomers. This is followed by two PEST sequences that direct NIMA for degradation (Lu et al., 1994; O'Connell et al., 2003; Pu and Osmani, 1995). Analysis of mRNA and protein levels in synchronized cells showed that the expression of NIMA is cell cycle regulated with peak expression at the G2/M boundary, after which NIMA levels drop as cells progress through mitosis. These changes are paralleled by similar changes in NIMA kinase activity. However, the kinase activity of NIMA is also regulated by autophosphorylation (Lu et al., 1993; Osmani et al., 1991b; Osmani et al., 1987; Ye et al., 1995).

Evidence so far indicates that NIMA is required for initiation of many cytological aspects of mitosis. In fact, overexpression of NIMA causes induction of a pseudo-mitotic state in which chromosome condensation occurs from any stage of the cell cycle (O'Connell et al., 1994; Osmani et al., 1994). Initially, it was thought that NIMA acted independently to the master mitotic regulator, cdc2 (Osmani et al., 1991b). However, further studies revealed that NIMA may be activated by cdc2/cyclin B during mitosis initiation (Ye et al., 1995). Conversely, NIMA activity may be required to control the localization of cdc2/cyclin B. In fact, studies have shown that NIMA controls the localization of cyclin B to the SPB by promoting the nuclear uptake of cdc2-cyclin B through interaction with the nuclear pore components, SONA and SONB. This helps to trigger mitotic entry by the initiation

of chromosome condensation and spindle formation within the nucleus (De Souza et al., 2003; De Souza et al., 2000; Wu et al., 1998).

Since the discovery that NIMA plays an important role in mitotic entry in *Aspergillus*, NIMA-related kinases have been identified using homology-based screens in many different species. This includes NIM-1 from *Neurospora crassa* (Pu et al., 1995), the Nrks in trypanosomes (Gale and Parsons, 1993), Fa2p in *Chlamydomonas* (Mahjoub et al., 2002), Fin1 and Kin3 from fission and budding yeast, respectively (Jones and Rosamond, 1990; Schweitzer and Philippsen, 1992), and the mammalian Neks (Figure 1.18) (Arama et al., 1998; Cance et al., 1993; Chen et al., 1999; Holland et al., 2002; Letwin et al., 1992; Levedakou et al., 1994; Lu and Hunter, 1995; Noguchi et al., 2002; Rhee and Wolgemuth, 1997; Schultz et al., 1994; Schultz and Nigg, 1993; Tanaka and Nigg, 1999). The functions of NIMA and NIMA-related kinases are summarized in Table 1.2.

1.4.1 NIMA homologues in lower eukaryotes

The NIM-1 protein from the filamentous fungus, *Neurospora crassa*, is 75% identical within the kinase domain to NIMA. So far, it is the only known functional homologue of NIMA since it is able to complement the late G2 arrest in *nimA* temperature sensitive mutants (Pu et al., 1995).

Another member of the NIMA-related kinase family is Fa2p, from the unicellular green algae *Chlamydomonas reinhardtii.* Fa2p is one of ten NIMA-related kinases present in *Chlamydomonas* and acts during deflagellation to bring about microtubule severing. However, Fa2p mutants are not only defective in deflagellation, but also have cell cycle defects with cells being delayed at the G2/M transition (Finst et al., 1998; Mahjoub et al., 2002). Cnk2p is a second NIMA-related kinase in *Chlamydomonas* (Bradley and Quarmby, 2005). Like Fa2p, Cnk2p is thought to play dual roles in regulation of both the flagella and cell cycle. Ectopic expression of Cnk2p results in small cells with short flagella whilst RNAi depletion of Cnk2p results in large cells with long flagella. This suggests a role for Cnk2p in cell cycle control by promoting flagellar disassembly and monitoring cell size prior to commitment to mitosis (Bradley and Quarmby, 2005).

Tetrahymena, another ciliated unicellular eukaryote, has hundreds of cilia which fall into different classes depending on their location and length. So far, 39 Nek genes have been found in this organism all of which encode proteins that localize to cilia and are involved in regulating ciliary length (Wloga et al., 2006).

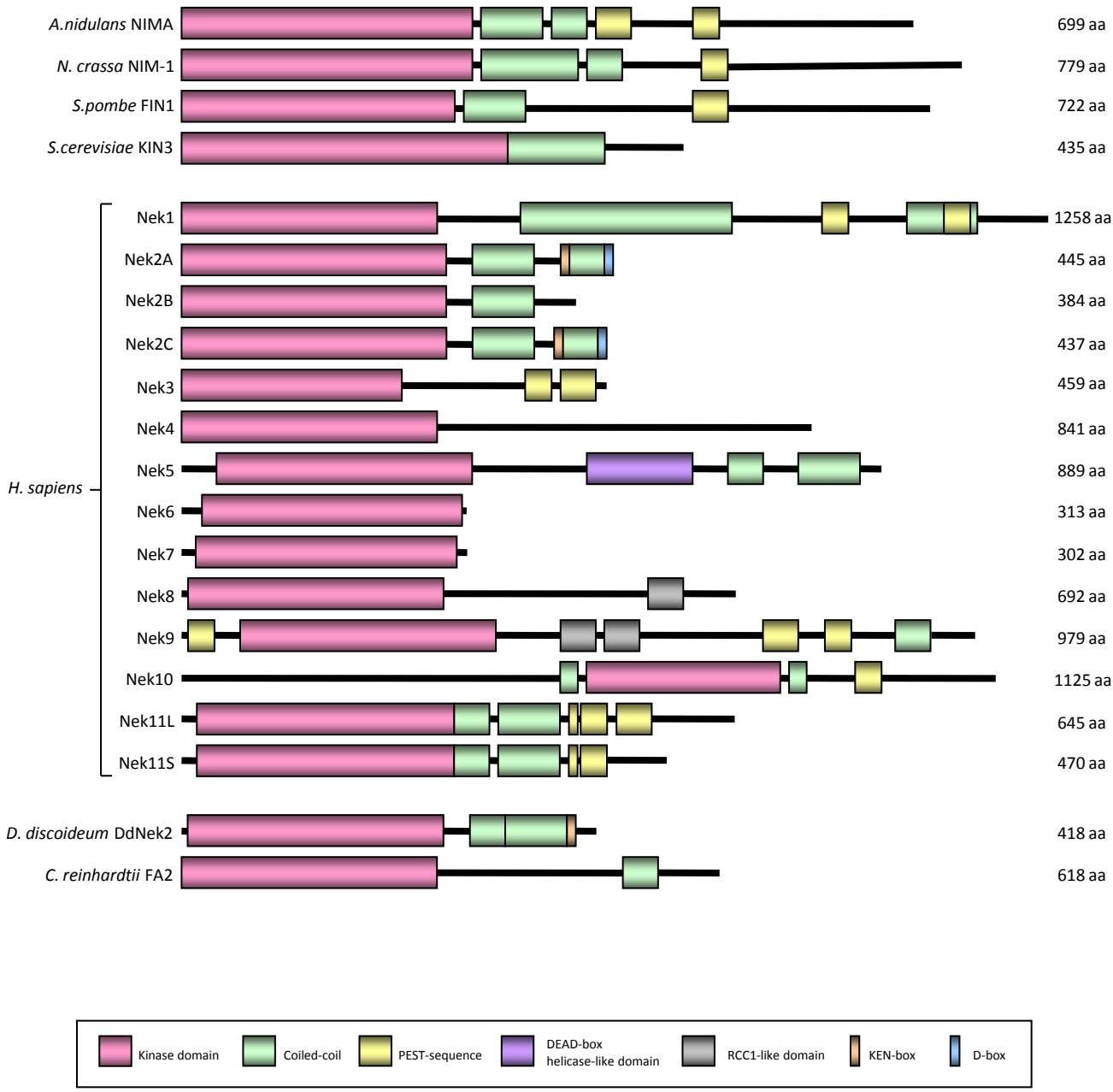

Figure 1.18 Sequence comparison of NIMA-related kinases
Schematic representation of NIMA-related kinases with their sizes indicated. The NIMA kinase family is defined by sequence homology to the *A. nidulans* NIMA kinase domain. The NIMA kinases share a conserved N-terminal catalytic domain (pink) but have divergent C-termini. The C-termini facilitate protein-protein interactions (coiled-coil, RCC1-like domain), or promote proteolytic degradation (PEST-sequence, KEN-box, D-box). There are 11 mammalian Neks, although these are likely to exist in multiple splice variants (e.g. shown for Nek2 and Nek11). Nek2 exists in three isoforms (Nek2A, Nek2B and Nek2C) and Nek11 in two isoforms (Nek11L and Nek11S). Adapted from O'Connell et al. (2003).

NIMA-Related Kinase		Function	Localization
***Aspergillus* NIMA**		Entry into and exit from mitosis Chromatin condensation Spindle formation	Spindle pole body
Chlamydomonas	**Fa2p**	Microtubule severing Regulation of the centrosome cycle?	Interphase: proximal ends of flagella Mitosis: spindle poles
	Cnk2p	Regulation of flagellar length and cell size	Ciliary axoneme
***T. brucei* NRKC**		Basal body separation and cytokinesis	Basal body
***S. pombe* Fin1**		Mitotic spindle formation Commitment to metaphase Mitotic exit	Spindle pole body and region between separating chromosomes
H. sapiens	**Nek1**	Ciliogenesis and DNA damage response	Primary cilium, basal body and centrosome
	Nek2	Centrosome disjunction Microtubule anchoring Chromatin condensation? SAC signaling?	Centrosome, nucleus
	Nek6 / Nek7	Mitotic spindle formation/function	Cytoplasm and/or nucleus, Centrosome?
	Nek8	Cytoskeletal organization Ciliary signaling	Primary cilium
	Nek9	Mitotic spindle formation and function	Centrosomes when active
	Nek11	DNA damage/replication stress response pathways	Interphase: Nucleolus Mitosis: spindle pole, microtubules

Table 1.2 Functional conservation of NIMA-related kinases
Summary of the functions and localization of the best-characterized NIMA-related kinases from different organisms.

The fission and budding yeasts (*S. pombe and S. cerevisiae,* respectively) each have one NIMA-related kinase in their genome, Fin1 and Kin3, respectively (Jones and Rosamond, 1990; Krien et al., 1998). However, kin3 mutations are not lethal and mutations or overexpression of Kin3 causes no obvious growth defects and as such its function remains unclear (Barton et al., 1992; Kambouris et al., 1993). Fin1, like Kin3 is a non-essential gene, although its mutation does delay mitotic entry (Grallert and Hagan, 2002; Krien et al., 1998). Like NIMA, the levels of Fin1 fluctuate through the cell cycle peaking after the metaphase/anaphase transition, suggesting that it may play a role in late mitosis (Krien et al., 2002). Fin1 localizes to the spindle pole body (SPB) in mitosis, as well as the region between the separating chromosomes. In line with its cell cycle dependent activity and localization, Fin1 is required for chromatin condensation and mitotic spindle formation. Moreover, Fin 1 may be involved in regulation of commitment to mitosis as well as mitotic exit (Grallert and Hagan, 2002; Grallert et al., 2004; Krien et al., 2002). Fin 1 is thought to contribute to the timing of mitotic onset as it is required to localize the polo-like kinase, Plo1, to the SPB, which activates Cdc2-cyclin B, for mitotic commitment (Grallert and Hagan, 2002; Krien et al., 1998). Fin1 regulates mitotic exit by modulating the activity of the septum initiation network (SIN) to prevent premature septation (Grallert et al., 2004). Normally, SIN pathway components are located asymmetrically on the two SPBs of fission yeast despite the fact that the yeast divides symmetrically. Indeed, the SIN pathway is only activated on one SPB and this is achieved by recruitment of Fin1 to the mature SPB. Fin1 then inhibits the SIN pathway on this SPB so that the SIN pathway is activated only in the less mature SPB. In the absence of Fin1 function, active SIN components associate with both SPBs and the signal for septation is inappropriately accelerated (Grallert et al., 2004).

These studies in lower eukaryotes suggest that members of the NIMA family play roles both within the cell cycle, notably mitosis, and at cilia/flagella. Given the widespread conservation of cell cycle control proteins in eukaryotes, it was thought that homologues of NIMA would exist in higher eukaryotes. Consistent with this, overexpression of a catalytically-inactive NimA mutant in human cells delayed entry into mitosis, suggesting that it may be interfering with the activity of an endogenous kinase or sequestering a conserved substrate (Lu and Hunter, 1995). Since then, a series of mammalian NIMA-related kinases, or Neks, have been identified using genomic and biochemical approach.

1.4.1.1 Mammalian NIMA-related kinases

The human genome contains 11 Neks named Nek1 to Nek11. Their N-terminal catalytic domains share approximately 40% homology to NIMA and 40-85% homology with each other, whereas their C-termini differ in length, sequence and domain organization. Below is a summary of what is known about the regulation and function of these kinases in human cells.

1.4.1.2 Mitotic Neks: Nek2, Nek6, Nek7 and Nek9

Among the human Neks, Nek2 is the best-characterized and is the most closely related to NIMA, being 44% identical in amino acid sequence across the catalytic domain. Like NIMA, Nek2 also has a C-terminal domain containing a coiled-coil motif through which it forms oligomers (Fry, 2002; Fry et al., 1999; O'Connell et al., 2003). Furthermore, Nek2 and NIMA show similar cell cycle dependent patterns of expression, activity and localization (Fry et al., 1998a; Fry et al., 1998b; Fry et al., 1995; Lu et al., 1993; Schultz et al., 1994). Nek2 is almost undetectable during G1 but accumulates rapidly at the G1/S transition remaining high until late in G2, suggesting that Nek2, like NIMA, may play a role at the onset of mitosis (Schultz et al., 1994). Unlike NIMA however, Nek2 is not essential for mitotic entry, but does regulate centrosome separation at the G2/M transition. Indeed, human Nek2 localizes to centrosomes via a motif in the C-terminal domain of the protein (Hames et al., 2005).

Three isoforms of Nek2 have been identified, Nek2A, Nek2B and Nek2C, that differ in their C-terminal non-catalytic region (Fardilha et al., 2004; Hames and Fry, 2002; Wu et al., 1998; Wu et al., 2007). The best described function of Nek2 is in centrosome disjunction, a step that facilitates bipolar spindle formation (Faragher and Fry, 2003; Fry, 2002). Overexpression of active Nek2 induces premature centrosome separation, whereas a catalytically-inactive mutant does not (Faragher and Fry, 2003). Consistent with this, RNAi depletion of Nek2 inhibits centrosome separation (Fletcher et al., 2005). It is thought that Nek2 promotes centrosome separation by interacting with and phosphorylating C-Nap1 and rootletin, two core components of the intercentriolar linkage that tether the two centrioles together in interphase. When phosphorylated by Nek2, C-Nap1 and rootletin dissociate from the centrosome leading to loss of centrosome cohesion (Bahe et al., 2005; Fry et al., 1998a). Recent data have shown that Nek2A also interacts with two other proteins, the Mst2 protein kinase and hSav1, which regulate Nek2 localization to centrosomes (Mardin et al., 2010). Additional centrosomal proteins have been identified as interactors and substrates of Nek2, including Ninein-like protein (Nlp) and centrobin, two large coiled-coil proteins believed to be structural components

of the PCM involved in nucleation and/or anchoring microtubules at the centrosome during interphase (Jeong et al., 2007; Rapley et al., 2005). Taken together, these studies indicate that Nek2 plays multiple roles in coordinating cell division.

Nek6, Nek7 and Nek9 also play a role in mitotic progression. Nek6 and Nek7 are highly similar in sequence showing 87% identity and are composed almost entirely of catalytic domains (Kandli et al., 2000; O'Connell et al., 2003). Initially, Nek6 was identified based on its ability to phosphorylate and activate the hydrophobic regulatory site of the p70 ribosomal S6 kinase ($p70^{S6K}$) *in vitro* (Belham et al., 2001). However, this is not thought to reflect a true physiological interaction. Instead, there is increasing evidence that Nek6 and Nek7 are required for mitotic progression downstream of another Nek kinase, Nek9, which phosphorylates the activation loop of Nek6 and Nek7 to stimulate their kinase activity (Belham et al., 2003; Roig et al., 2002). Nek9 is also likely to activate Nek6 and Nek7 through allosteric binding (Richards et al., 2009). Nek6 and Nek7 display elevated catalytic activity during mitosis and are localized to spindle poles. However, Nek6 also localizes to spindle microtubules in metaphase and anaphase and to the midbody during cytokinesis (O'Regan and Fry, 2009). Overexpression of catalytically-inactive Nek6 or Nek7 or depletion of these proteins cause cells to arrest in metaphase with reduced spindle microtubules. Meanwhile, hypomorphic mutants exhibit defects in cytokinesis that may result from a reduced density of central spindle microtubules (Kim et al., 2007; O'Regan and Fry, 2009; Yin et al., 2003; Yissachar et al., 2006).

Nek9 was originally identified in immunoprecipitates of Nek6 from HEK293 cells (Holland et al., 2002; Roig et al., 2002). Nek9 consists of an N-terminal catalytic domain that shares 33% sequence identity to NIMA and a C-terminal domain that contains an RCC1-like domain, and a predicted coiled-coil motif (Roig et al., 2002). The RCC1 domain is thought to be required for autoinhibition of Nek9. Like Nek6 and Nek7, the activity of Nek9 is increased during mitosis (Roig et al., 2005; Roig et al., 2002). Localization studies have revealed that Nek9 is diffusely distributed within the cytoplasm in interphase and mitosis (Holland et al., 2002; Pelka et al., 2007; Roig et al., 2002), although active Nek9 localizes on spindle poles during mitosis (Roig et al., 2005). Consistent with its localization and regulation, functional studies support a role for Nek9 in mitotic spindle organization. Overexpression of catalytically-inactive Nek9 and truncated Nek9 mutants caused missegregation of chromosomes. Moreover, inhibition of Nek9, resulting from

microinjection of anti-Nek9 antibodies, caused defects in mitotic spindle formation (Roig et al., 2002). In addition to association with Nek6 and Nek7, Nek9 also binds directly to components of the γ-TuRC and Bicaudal-D2 (BicD2), a coiled-coil protein implicated in dyenin-mediated microtubule-dependent transport but also microtubule anchoring at the centrosome (Fumoto et al., 2006). Nek9 also binds to DYNLL/LC8, a component of the dynein complex. This interaction regulates Nek6 binding to Nek9, thus controlling signalling transduction through the Nek9/Nek6 signalling module. Moreover, Nek9 is activated by Plk1 and this interaction has been proposed to control the centrosome separation through regulating the kinesin, Eg5 (Bertran et al., 2011; Regue et al., 2011). Together, these data suggest that Nek9 plays key roles in microtubule nucleation and anchorage as well as centrosome separation (Holland et al., 2002; Roig et al., 2005; Roig et al., 2002). Interestingly, Nek9 has also been found to bind Ran GTPase, although the significance of this remains unclear.

In summary, Nek2, Nek6, Nek7 and Nek9 coordinate the formation and maintenance of the mitotic spindle (O'Regan et al., 2007; O'Regan and Fry, 2009).

1.4.1.3 DNA damage response Neks: Nek10 and Nek11

Unlike most other NIMA-related kinases, which contain an N-terminal catalytic domain, Nek10 contains a kinase domain that is located in the centre of the protein. Nek10 also contains coiled-coiled domains flanking the catalytic domain, a putative PEST sequence in the C-terminus and 4 N-terminal armadillo repeats, which have been implicated in coordinating protein-protein interactions. Judged by sequence homology, Nek10 is most similar to Nek6 and Nek7 sharing 54% homology within the kinase domain. However, very little is known about Nek10. Recent studies have shown that Nek10 plays an important role in mediating G2/M arrest and autoactivation of MEK in response to DNA damage (Moniz and Stambolic, 2010). Overexpression of Nek10 caused an increase in ERK1/2 and MEK activation in response to UV damage, but not in response to mitogens, such as epidermal growth factor. In support of this, Nek10 depletion led to impaired MEK/ERK activation in response to UV irradiation, but not in response to mitogens (Moniz and Stambolic, 2010). It is hypothesised that Nek10 causes the activation of ERK1/2 by associating with MEK1 in a Raf-dependent manner; this causes MEK1 autophosphorylation, which in turn leads to ERK1/2 activation, and this is essential for G2/M arrest in response to UV damage (Moniz and Stambolic, 2010).

Nek11 is also implicated in checkpoint control and the DNA damage response. Nek11 is composed of an N-terminal catalytic domain and a C-terminal domain which contains predicted coiled-coil and PEST sequences (Noguchi et al., 2002). Nek11 shows cell cycle-dependent expression with low levels in G1, increasing through S and G2, and peaking at G2/M; this suggests that Nek11 may play a role in cell cycle regulation (Noguchi et al., 2002). Furthermore, Nek11 subcellular localization also changes throughout the cell cycle, localizing to the nucleus in interphase and microtubules during mitosis (Noguchi et al., 2002). Surprisingly, it was found that the kinase activity of Nek11 is highest in cells arrested in response to DNA-damaging agents and DNA replication inhibitors (Noguchi et al., 2002). Indeed, it has been recently shown that Nek11 contributes to the DNA damage induced G2/M checkpoint by regulating the phosphorylation of Cdc25A, a protein phosphatase required for activity of Cdk1 (Melixetian et al., 2009). Specifically, in response to DNA damage, Chk1 phosphorylates Nek11 causing its activation; active Nek11 then phosphorylates Cdc25A targeting it for degradation via the SCF ubiquitin ligase, thus inducing G2/M arrest. In the absence of Nek11, Cdc25A is not degraded and cells fail to arrest in the presence of DNA damage (Melixetian et al., 2009; Sorensen et al., 2010).

1.4.1.4 Ciliary Neks: Nek1 and Nek8

Nek1 was the first mammalian Nek to be characterized. It contains an N-terminal kinase domain, which shares 42% identity with NIMA, and, like NIMA, possesses a C-terminal coiled-coil domain and PEST sequences (O'Connell et al., 2003). Nek1 is highly expressed in testes and ovaries, suggesting a possible role in meiosis; but it is also highly expressed in brain, indicating a potential role in neural development (Letwin et al., 1992). However, for a long time, the function of Nek1 remained obscure until almost a decade later when two spontaneous mutations were found in the Nek1 gene in the mouse *kat* and *kat*^{2J} polycystic kidney disease models (Badano et al., 2006; Upadhya et al., 2000). This was the first clue that some of the mammalian Neks may have roles related to cilia.

Further evidence for a role for Nek1 in cystic kidney disease came from a yeast two-hybrid assay, in which it was shown that Nek1 interacts with proteins involved in PKD, such as the motor transport protein, KIF3A, and the tumour suppressor protein, tuberin (Surpili et al., 2003). More recently, Nek1 was shown to localize to primary cilia, basal bodies and centrosomes, while its overexpression was found to inhibit ciliogenesis. However, embryonic fibroblasts from *kat*^{2J} mice exhibit a reduced number of primary cilia (Shalom et al., 2008; White and Quarmby, 2008).

Interestingly, Nek1 also localizes to the nucleus, suggesting that Nek1 may transduce signals between the primary cilium and nucleus to regulate gene expression (Hilton et al., 2009). Alternatively, Nek1 may also play a role in the DNA damage response as it interacts with several proteins in DNA repair pathways (Polci et al., 2004; Surpili et al., 2003). Moreover, the expression and activity of Nek1 are stimulated following DNA damage and active Nek1 is redistributed to sites of DNA double strand breaks. In addition, interference with Nek1 function appears to make cells more sensitive to IR , while cells deficient in Nek1 fail to reliably initiate G1/S and M-phase checkpoints in response to DNA damage (Chen et al., 2008; Polci et al., 2004). Thus, Nek1 may have a dual role in both ciliogenesis and the DNA damage response.

Soon after identifying mutations in the Nek1 gene in a mouse PKD model, a mutation that causes juvenile cystic kidney disease in another mouse model, jck, was mapped to the gene encoding Nek8. Nek8 is a 692 amino acid protein with a calculated molecular weight of 79.5 kDa (Liu et al., 2002). Typically of Nek kinases, it contains an N-terminal catalytic domain and a C-terminal non-catalytic domain. The sequence of the Nek8 kinase domain is most similar to Nek2 sharing 42% amino acid identity. However, its C-terminal domain is more reminiscent of Nek9 as it possesses five predicted RCC1 repeats (Bowers and Boylan, 2004; O'Connell et al., 2003).

The jck mouse has two point mutations in Nek8, although both lie in the same codon converting glycine 448 into valine. This mutation altered the localization pattern of Nek8 from a distinctly apical localization to a diffuse cytoplasmic pattern in kidney collecting duct cells (Liu et al., 2002). Furthermore, expression of the G448V mutant or kinase domain mutants predicted to be inactive in renal epithelia cells resulted in the formation of enlarged, multinucleated cells suggestive of division failure. Meanwhile, expression of inactive Nek8 in U2OS cells led to decreased actin expression (Bowers and Boylan, 2004; Liu et al., 2002).

Confirmation of a cilia-related role for Nek8 came from showing that knockdown of Nek8 led to formation of pronephric cysts in zebrafish embryos. Indeed, injection of zebrafish embryos with a morpholino anti-sense oligonucleotide against Nek8 resulted in a PKD phenotype (Liu et al., 2002). Moreover, three mutations have been recently identified in Nek8 that are implicated in the childhood autosomal recessive kidney disease nephronophthisis, with Nek8 proposed as the candidate NPHP9 gene (Otto et al., 2008). Of the three mutations, two are heterozygous

(L330F and A497P) and one is homozygous (H425Y). Interestingly, all three mutated amino acids (L330, H425 and A497) are found in the RCC1 domain and show evolutionary conservation being identical in humans, mouse, *Xenopus* and zebrafish, with H425 also being conserved in the chordate *Ciona intestinalis* (Figure 1.20). Similar to the jck G448V mutation, the NPHP associated mutants show reduction in ciliary localization in IMCD-3 mouse kidney epithelial cells, supporting the hypothesis that mislocalization of Nek8 results in the formation of renal cysts (Otto et al., 2008; Trapp et al., 2008).

Nek8 localizes to the proximal region of the primary cilium in inner medullary collecting duct (IMCD-3) mouse kidney epithelial cell lines. More specifically, Nek8, together with another NPHP protein, Nphp3, localizes to the inversin compartment towards the proximal ends of the primary cilia where the inversin (inv/Nphp2) protein accumulates (Figure 1.19). This localization is dependent on inv, with Nek8 losing localization to the primary cilia in *inv* mutant cells, suggesting that an interaction between inv and Nek8 might exist (Shiba et al., 2010). Furthermore, localization of Nek8 to the inversin compartment is also lost in cells derived from jck mice (Liu et al., 2002). However, other studies contradict this finding indicating that cells derived from jck mice don't lose ciliary localization of Nek8, but instead Nek8 becomes localized to the entire length of the primary cilia and not just the inversin compartment (Sohara et al., 2008). Strict compartmentalization of Nek8 may be required for Nek8 to function properly, with mislocalization resulting somehow in defective ciliary signalling (Mahjoub et al., 2005; Otto et al., 2008; Trapp et al., 2008).

There is now evidence that Nek8 might also be implicated in ADPKD as Nek8 protein has been reported to interact with PC2 (Cai and Somlo, 2008). Increased expression of both PC1 and PC2 was observed in jck mouse kidney, and PC2 was abnormally phosphorylated. This was associated with lengthened cilia and ciliary accumulation of PC1 and PC2 (Sohara et al., 2008). Furthermore, the ciliary localization of Nek8 and PC1 appears to be reciprocally regulated as the expression of Nek8 is increased in cilia of *Pkd1*$^{-/-}$ kidney explants, whereas the expression of PC1 is increased in cilia of *jck* kidney explants (Cai and Somlo, 2008; Natoli et al., 2008). Together, these results suggest that Nek8 may control the targeting of the polycystins.

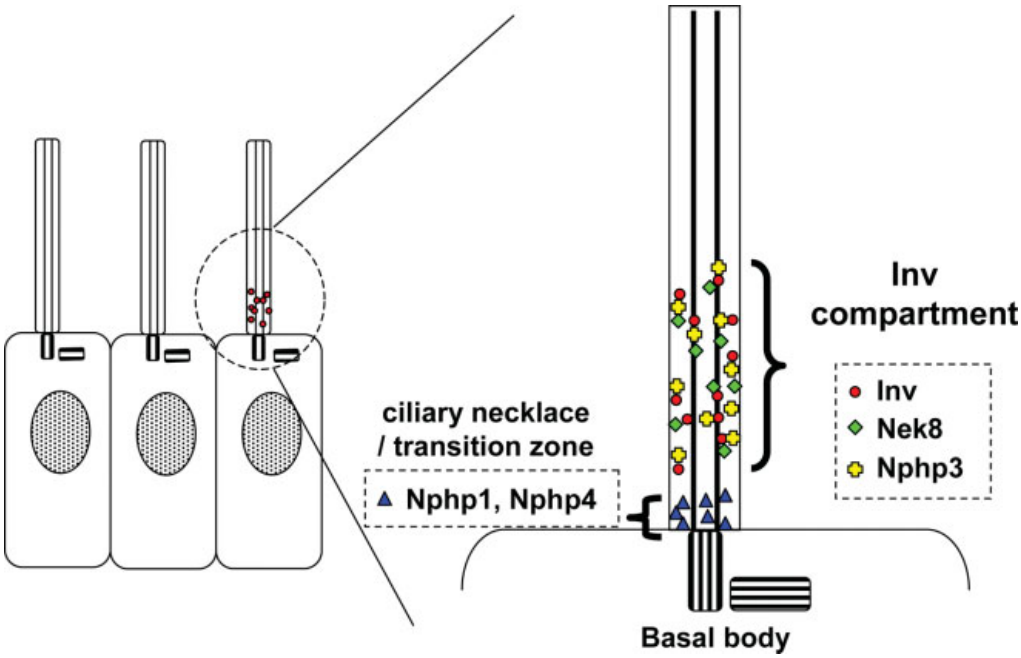

Figure 1.19 Nek8 is localized to the inversin compartment
A schematic representation of the Inversin (Inv) compartment in the primary cilium. Inv/NPHP2, NPHP3 and Nek8/NPHP9 localize at the proximal segment of the primary cilia termed the ‘‘Inv compartment’’, whereas NPHP1 and NPHP4 are detected proximal to the Inv compartment at the transition zone. Adapted from Shiba et al. (2010).

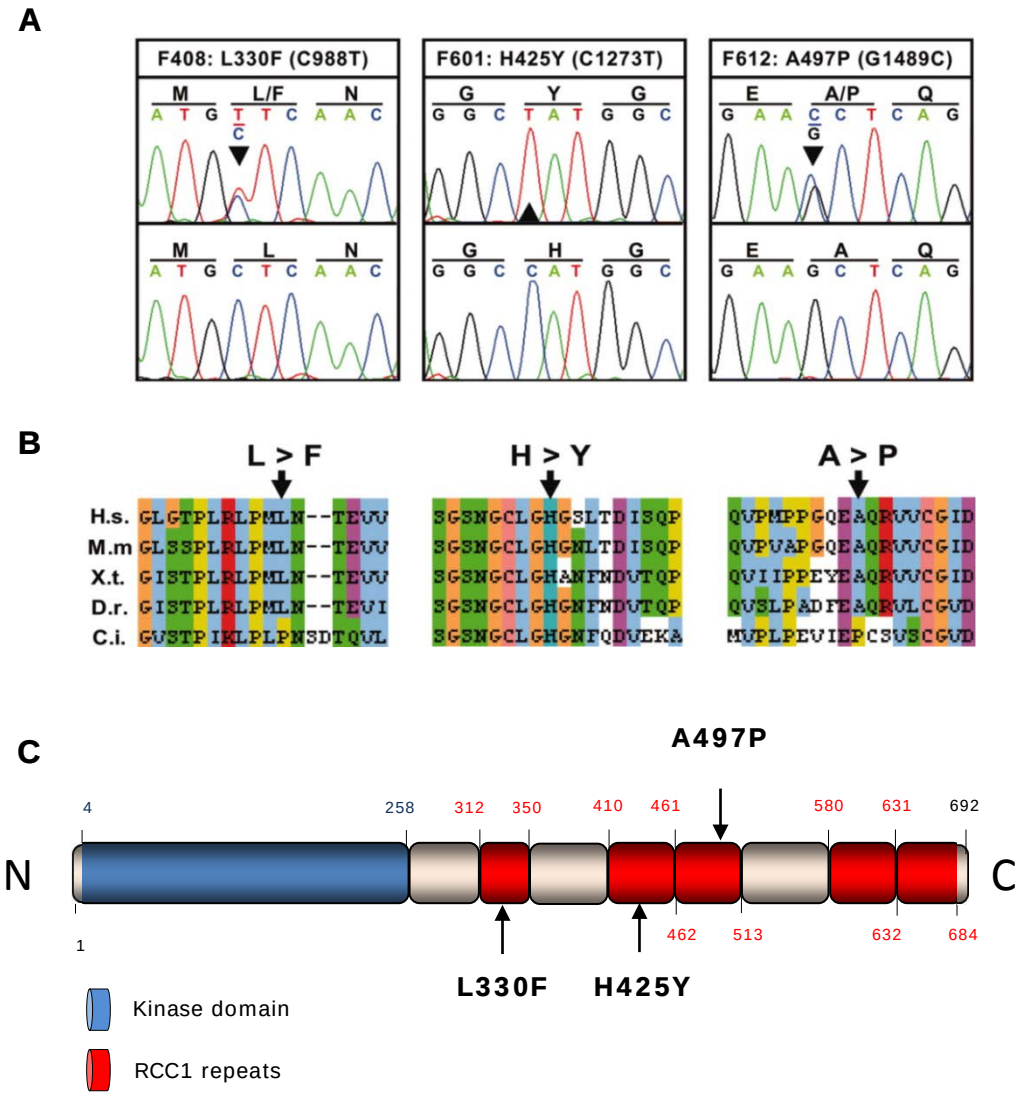

Figure 1.20 Sites mutated in human Nek8 in NPHP patients are evolutionary conserved

(A) Chromatograms of NEK8 mutations detected in 3 individuals with nephronophthisis. Family number, amino acid sequence change, and mutated nucleotide are given above sequence traces. Wild-type sequences are shown below mutated sequences. Reading frame is indicated by underlining codon triplets in the upper panel, and mutated nucleotides are indicated by an arrowhead. L330F and A497P mutations are heterozygous while H425Y is homozygous. **(B)** Alignment of the Nek8 protein sequence mutated in NPHP patients from various species including *Homo sapiens* (H.s.), *Musculus musculus* (M.m.), *Xenopus tropicalis* (X.t.), *Danio rerio* (D.r.), and *Ciona intestinalis* (C.i.). Amino acid residues that are within the same chemical group are coded in the same colour. Mutated amino acids are indicated with arrowheads. **(C)** Schematic diagram of Nek8 showing position of the NPHP mutations. Note that all mutations are in the RCC1 domain. Adapted from Otto et al. (2008).

Overall, the role of Nek8 at the cilia is almost entirely unknown. Dysfunction of Nek8 may lead to cystogenesis by altering the structure or function of cilia. The fact that Nek8 localizes to the inversin compartment, together with the fact that Nek8 regulates polycystins localization, may suggest that the inversin compartment may be an important site for the control of protein entry into the cilium. It is thus possible that Nek8 is one of the ciliary gatekeeper proteins, and defects in Nek8 may result in aberrant trafficking of proteins which subsequently lead to defects in signalling and, ultimately to polycystic kidney disease. The observation that Nek8 may modulate ciliary targeting of PC1 and PC2 also suggests a link between NPHP and ADPKD. Furthermore, the finding that mice carrying a null mutation in Nek8 have left-right asymmetry defects supports its importance for cilia-dependent processes (Shiba et al., 2010).

1.5 Aims and Objectives

Despite structural similarities in mammalian Neks, it is clear that they do not all share the same function. While some Neks play an important role in the cell cycle, others, including Nek8, function at the cilium and play an important role during ciliogenesis. In fact, Nek8 is mutated in the *jck* mouse model of cystic kidney disease, while mutations of human Nek8 are causative for the childhood autosomal recessive kidney disease nephronophthisis, with Nek8 encoded by the NPHP9 gene. These findings, together with the fact that Nek8 and polycystin-2, a protein mutated in 15% of ADPKD cases, interact together, link Nek8 with PKD, a disease involving abnormal cell proliferation and differentiation, which is thought to result from ciliary defects. Furthermore, the reported centrosomal/basal body and ciliary location of this protein in dividing and ciliated cells, lead us to speculate that Nek8 may be involved in the biogenesis, maintenance or signalling function of primary cilia. However, despite some basic characterization of Nek8 at the molecular level, its regulation and function remain far from clear. In fact, to date, the kinase activity of Nek8 has not been reported. For this reason, it is difficult to know whether the mislocalization of certain Nek8/NPHP9 point mutants is a result of defective activity. Similarly, it is unclear what role kinase activity has in the localization of the protein, although a point mutant in the mouse Nek8 kinase that is predicted to cause loss of activity prevented Nek8 from localizing to the cilia (Trapp et al., 2008). Moreover, no substrates of Nek8 have yet been identified. As a result, the role of Nek8 in ciliogenesis remains to be defined.

The aim of this project was therefore to use a variety of biochemical and cell biology based assays to investigate the regulation and function of Nek8 with respect to cell cycle progression and ciliogenesis.

The specific experimental objectives were defined as follows:

1. To generate, affinity-purify and characterize anti-Nek8 antibodies that could be used for characterization of Nek8 localization, expression and activity. Antibodies were raised in rabbits against bacterially expressed C-terminal fragments of Nek8. Following purification, these were initially used to assess the localization of Nek8 in dividing and ciliated hTERT-RPE1 cells.

2. To investigate the effects of disease-associated mutations and mutations predicted to render the kinase catalytically-inactive on Nek8 localization during cell cycle progression and ciliogenesis in hTERT-RPE1 cells. The

localization of truncated forms of Nek8 was also assessed to map the regions required for Nek8 localization in cultured mammalian cells.

3. To define conditions required for measurement of Nek8 catalytic activity. These kinase assays were then used to measure activity of the disease-associated mutants, as well as the kinase domain and truncation mutants. In this way, we could test the hypothesis that Nek8 activity was an important determinant of its localization.

4. Finally, to investigate how Nek8 is regulated in term of expression and activity in response to the induction of ciliogenesis upon serum-starvation of hTERT-RPE1 cells.

Chapter 2

Materials and Methods

2.1 Materials

2.1.1 Suppliers and manufacturers

All chemicals were of analytical grade purity or higher and supplied by Sigma (Poole, UK), Roche (Lewes, UK), or as stated below.

Reagent	Supplier
ON-TARGET*plus* siRNA reagents Oligofectamine transfection reagent	Dharmacon (Lafayette Colorado, USA)
Nek8 Recombinant Protein	Novus Biologicals (Littleton, Colorado, USA)
ECL plus Western blotting reagent CNBr activated sepharose Deoxyribonucleotides (dATP, dCTP, dGTP, dTTP)	Amersham Pharmacia Biotech (Buckinghamshire, UK)
Annexin V/FITC apoptosis detection kit	Bender MedSystems (Burlingame, USA)
Protein A beads Poly-prep columns	BioRad (Hemel Hempstead, UK)
Chloramphenicol Hoechst 33258 Leptomycin B	Calbiochem (Nottingham, UK)
Glacial acetic acid EDTA EGTA NaCl KCl Na_2HPO_4 KH_2PO_4	Fisher Scientific (Loughborough, UK)
Bovine serum albumin (fraction V)	Fluka (Gillingham, UK)
Super RX X-Ray film	Fuji Photo Film (Tokyo, Japan)
Ethidium bromide GeneTailor site directed mutagenesis kit SuperScript III reverse transcriptase NI-NTA agarose Oligonucleotide primers DH5α-T1R max efficiency chemically competent bacteria Gateway cloning enzymes (LR and BP clonase) Protein G beads Penicillin/streptomycin Fetal bovine serum D-MEM with Glutamax Opti-MEM Oligofectamine	Invitrogen/Gibco (Paisley, UK)

Lipofectamine 2000	
GeneRuler 1 kb DNA ladder	MBI Fermentas (York, UK)
Protogel liquid acrylamide (30% w/v)	National Diagnostics (Hessle, UK)
Bacto-agar Bacto-tryptone Yeast extract	Oxoid (Basingstoke, UK)
Slide-A-Lyzer dialysis cassettes BCA protein assay reagent	Pierce (Rockford, USA)
TnT T7 quick coupled transcription/translation kit	Promega (Southampton, UK)
QIAfilter plasmid miniprep spin kit QIAfilter plasmid maxiprep kit QIAquick PCR purification kit QIAquick gel extraction kit	Qiagen (Hilden, Germany)
Restriction endonucleases Expand high fidelity DNA polymerase Rapid DNA ligation kit Shrimp alkaline phosphatase 5-Bromo-2'-deoxy-uridine Labeling and Detection Kit II	Roche (Lewes, UK)
Nitrocellulose transfer membrane	Schleicher & Schuell (Dassel, Germany)
3MM chromatography paper	Whattman International (Maidstone, UK)
Coverslips 22mm/13mm diameter, No. 1.5 Glass slides	VWR International (Lutterworth, UK)

2.1.2 Radioisotopes

Isotope	Specific Activity	Supplier
[γ-^{32}P]-ATP	167 Tbq/mmol	PerkinElmer
[^{35}S]-methionine	43.5 Tbq/mmol	NEN Life Sciences Products

2.1.3 Vectors and constructs

Vector	Application	Supplier
pETM-11	Bacterial protein expression	EMBL

pCMV-Tag-3C	Eukaryotic protein expression	Stratagene
pFLAG-CMV2	Eukaryotic protein expression	Sigma
pEGFP-T7	Eukaryotic expression vector	Fry lab

2.1.4 Antibodies

2.1.4.1 Primary antibodies

Antibody	Dilution ([Antibody])*	Supplier
Anti-FLAG Mouse monoclonal	1:1000 (0.5 µg/ml)	Sigma (Poole, UK)
Anti-GFP Mouse monoclonal	1:500 (0.25 µg/ml)	Abcam (Cambridge, UK)
Anti-GFP Rabbit polyclonal	1:1000 (0.1 µg/ml)	Abcam (Cambridge, UK)
Anti-FLAG Rabbit polyclonal	1:500	Sigma (Poole, UK)
Anti-mCherry Rabbit polyclonal	1:100	BioVision (San Francisco, USA)
Anti-α-tubulin Mouse monoclonal	1:2000 (0.3 µg/ml)	Sigma (Poole, UK)
Anti-γ-tubulin Mouse monoclonal	1:2000 (0.15 µg/ml)	Sigma (Poole, UK)
Anti-α-tubulin Rabbit polyclonal	1:200	Sigma (Poole, UK)
Anti-γ-tubulin Rabbit polyclonal	1:500	Sigma (Poole, UK)
Anti-acetylated-tubulin Mouse monoclonal	1:1000 (1 µg/ml)	Abcam (Cambridge, UK)
Anti-Nek8 R4175 Rabbit polyclonal	1:200 (2.5 µg/ml)	This work
Anti-Nek8 R4176 Rabbit polyclonal	1:200 (2 µg/ml)	This work

* Where known, final antibody concentrations are stated in brackets after the working dilution

2.1.4.2 Secondary antibodies

Antibody	Dilution ([Antibody])*	Supplier
Anti-mouse alkaline phosphatase conjugate	1:7500 (0.1 µg/ml)	Promega (Southampton, UK)
Anti-rabbit alkaline phosphatase conjugate	1:7500 (0.1 µg/ml)	Promega (Southampton, UK)
Anti-mouse horseradish peroxidase conjugate	1:1000	Sigma (Poole, UK)
Anti-rabbit horseradish peroxidase conjugate	1:1000	Sigma (Poole, UK)
Anti-mouse Alexa 488 nm	1:200 (10 µg/ml)	Invitrogen (Paisley, UK)
Anti-rabbit Alexa 488 nm	1:200 (10 µg/ml)	Invitrogen (Paisley, UK)
Anti-mouse Alexa 594 nm	1:200 (10 µg/ml)	Invitrogen (Paisley, UK)
Anti-rabbit Alexa 594 nm	1:200 (10 µg/ml)	Invitrogen (Paisley, UK)

* Where known, final antibody concentrations are stated in brackets after the working dilution

2.1.5 Bacterial strains

Strain	Genotype	Supplier
DH5α library efficiency *E. coli*	Φ80d *lacZ*ΔM15, *Rec*A1, *end*A1, A1, *gyr*A96, *thi*-1, *hsd*R17(r_K-m_K^+), *sup*E44, *rel*A1, *deo*R, [Δ*lacZYA*-argF]U169	Invitrogen
DH5α-T1^R max efficiency *E. coli*	F- φ80*lac*ZΔM15 Δ(*lac*ZYA-*arg*F)U169 *rec*A1 *end*A1 *hsd*R17(r_{k-}, m_{k+}) *pho*A *sup*E44 *thi*-1 *gyr*A96 *rel*A1 *ton*A	Invitrogen
BL21 star (DE3) *E. coli*	F- ompT hsdS$_B$ (r_B-m_B-) gal dcm rne131 (DE3)	Invitrogen

2.2 Molecular biology techniques

2.2.1 Cloning

The cloning procedure involved amplifying the insert DNA by polymerase chain reaction (PCR), digesting the purified PCR product with restriction enzymes and ligating the digested product with the appropriate vector under conditions as outlined below. A PCR screening approach was then used to identify colonies that contained the plasmid with insert DNA, after which plasmid DNA was prepared from bacterial cultures in the appropriate manner. The specific details of each stage are indicated below.

2.2.1.1 Oligonucleotide design

For PCR-based cloning, oligonucleotides were designed to be 21-30 bp in length with an AT:CG ratio of 50%, to ensure an annealing temperature of around 55-60°C. To incorporate appropriate restriction enzyme sites for cloning, additional bases were added to the 5′ ends of the oligonucleotide sequences with additional bases added to ensure the correct reading frame was maintained upon insertion into the vector, as necessary.

2.2.1.2 Polymerase chain reaction

PCR amplification was carried out using the Expand high fidelity proof-reading DNA polymerase (Roche, Lewes, UK) in order to obtain insert DNA for cloning. The volume of a standard reaction mixture was 50 µl and contained 0.1-1 µg template DNA, 0.4 µM forward primer, 0.4 µM reverse primer, 10 x PCR amplification buffer, 0.1-0.5 mM $MgCl_2$, 0.4 mM dNTPs, 1 U DNA polymerase and the appropriate volume of water to complete the reaction volume. For each set of primers and template, annealing temperatures and elongation times were employed as appropriate; however, the basic PCR reaction consisted of one cycle of denaturation at 94°C for 2 min, followed by 25 cycles of denaturation at 95°C for 30 sec, annealing at the appropriate temperature for 30 sec and elongation at 72°C for the appropriate extension time (1 min per kb), followed by one cycle of extension at 72°C for 10 min. PCR products were analyzed by agarose gel electrophoresis to assess yield.

2.2.1.3 Agarose gel electrophoresis

DNA was combined with loading buffer (50% v/v glycerol, 100 mM EDTA, 0.3% v/v bromophenol blue) in a 1:5 ratio and resolved by electrophoresis on a 1% (w/v) agarose gel made by dissolving agarose in 1x TBE (89 mM Tris-HCl, 89 mM Boric acid, 1 mM EDTA pH 8.0) supplemented with ethidium bromide (0.5 µg/ml).

2 µl of 1 kb markers were added to a separate well and electrophoresis was carried out at 80 V for 45 min. The resolved DNA was then analyzed by UV transillumination and images captured using a Gene Genuis CDC gel documentation system (Syngene, Cambridge, UK).

2.2.1.4 Purification of PCR products for cloning

Once a PCR reaction was verified to be successful, and sufficient levels of product of the appropriate size obtained, PCR products were purified for cloning using a PCR purification kit (Qiagen, Crawley, UK) according to the manufacturer's instructions. Purified DNA was eluted in 50 µl of sterile water. The product yield and DNA concentration was then assessed by agarose gel electrophoresis as described above.

2.2.1.5 Restriction enzyme digests

The appropriate restriction enzymes were used to digest the purified insert DNA and destination vectors using suitable buffer conditions and temperatures, as indicated by the manufacturer. Usually, 2 µg of DNA was incubated with 5 U of restriction endonuclease and appropriate buffer at 37°C for 2-4 hrs. The total reaction volumes were then separated in a 1% agarose gel as described in section 2.2.1.3 to allow purification of digested DNA by gel extraction.

2.2.1.6 DNA extraction from agarose gels

Following electrophoresis of the DNA to be purified, agarose gels were visualized by UV transillumination and the band that represented the DNA to be purified was excised. The DNA was then extracted from the agarose slice using the QIAquick gel extraction kit (Qiagen, Crawley, UK) according to the manufacturer's instructions. DNA was eluted in 30 µl of sterile water and DNA yield was assessed by agarose gel electrophoresis in order to determine the concentrations of DNA required for ligation.

2.2.1.7 DNA ligation

A rapid DNA ligation kit (Roche, Lewes, UK) was used to carry out ligation reactions. Typically a vector:insert molar ratio of 1:3 was used with a standard reaction mix of 75 ng vector DNA, 150 ng insert DNA and 5 U DNA ligase diluted in the appropriate volume of ligation buffer. Reactions were then incubated for 5-15 min at room temperature.

2.2.1.8 Bacterial transformation

For cloning, 100 ng of ligated DNA was added to 50 µl of DH5α competent cells, which had been defrosted on ice, and the two mixed by tapping gently on the side of the tube. This was followed by incubating the mix on ice for 30 min, transferring to a water bath at 42°C for 1 min to induce plasmid DNA uptake, and returning to the ice for a further 2 min. The cells were resuspended in 500 µl of pre-warmed Luria Bertani (LB) media (tryptone, 10 g/l, yeast extract 5 g/l, NaCl 5 g/l pH 7.0) and the transformation mix incubated at 37°C, 225 rpm for 1 hr. Following incubation, the transformation mix was briefly spun down to pellet transformed cells. These were then gently resuspended in 200 µl of remaining supernatant and cell suspension was spread onto LB agar plates containing the appropriate antibiotic for selection (tryptone 10 g/l, yeast extract 5g/l, NaCl 5 g/l, agar 2% w/v, pH 7.0 plus ampicillin 100 µg/ml, or kanamycin 50 µg/ml, as appropriate). LB agar plates were then incubated for 12-14 hrs at 37°C and colonies picked for insert screening by PCR and plasmid preparation.

2.2.1.9 DNA insert verification

The presence of the appropriate DNA insert was verified using PCR screening of colony DNA using Taq DNA polymerase (Invitrogen, Paisley, UK). Typically, a standard reaction mixture of 50 µl in volume contained, 0.4 µM forward primer, 0.4 µM reverse primer, 1x PCR amplification buffer plus $MgCl_2$ (0-5 mM $MgCl_2$), 0.4 mM dNTPs, 1 U DNA polymerase and the appropriate volume of water to complete the reaction volume. Colonies to be screened were picked and cells added directly to the PCR reaction mix. PCR reaction cycles were as described above in section 2.2.1.2. Colonies which proved positive by PCR screen were then grown up for isolation of plasmid DNA and further verification of insert by DNA sequencing.

2.2.1.10 Miniprep plasmid DNA isolation

Individual bacterial colonies were picked off LB agar plates, inoculated into 5 ml LB media containing the appropriate antibiotic and incubated at 37°C, 225 rpm for 12-16 hrs. This was followed by recovering cells by centrifugation (2500 g, 10 min) after which DNA was isolated using a Qiagen plasmid miniprep kit according to the manufacturer's instructions. DNA was eluted in 50 µl of sterile water.

2.2.1.11 DNA sequencing

Automated DNA sequencing was employed to verify the presence of the appropriate insert and the correct reading frame. This was carried out by PNACL (The Protein and Nucleic Acid Chemistry Laboratory), Leicester. The results were analyzed using CLC Free Workbench 3 software.

2.2.2 Maxiprep plasmid DNA isolation

For isolation of large quantities of high quality, pure plasmid DNA for transfection, DNA plasmids maxipreps were used. A single colony was picked from a freshly streaked selective plate and a starter culture of 5 ml LB containing the appropriate antibiotic was inoculated and incubated for 8 hrs at 37°C, 225 rpm. This was used to inoculate a 100 ml LB + antibiotic culture at a dilution of 1:1000 which was then grown at 37°C, 225 rpm for 12-16 hrs. The bacterial cells were harvested by centrifugation at 6000 g for 15 min at 4°C and plasmid DNA isolated using a QIAfilter plasmid maxiprep kit (Qiagen, Crawley, UK) according to the manufacturer's instructions. Isolated plasmid DNA was resuspended in 200 µl of sterile water and DNA concentration was determined by measuring OD_{260} (BioPhotometer plus, Eppendorf) after which DNA was diluted to a final concentration of 1 µg/µl.

2.2.3 Site-directed mutagenesis

2.2.3.1 Oligonucleotide design

For site-directed mutagenesis oligonucleotides were designed to be approximately 30 bp in length. The forward primers consisted of an overlapping region at the 5' end of 15-21 bases, the mutation site, and an extended region of at least 10 nucleotides downstream of the mutation site. The reverse primer contained a region complementary to the forward primer from the mutation site to the 5' end of the forward primer and extended beyond this for a further 10-13 bp.

2.2.3.2 Site-directed mutagenesis reaction

To induce nucleotide changes in plasmid DNA, the Genetailor^{TM} Site-Directed Mutagenesis System (Invitrogen) was used according to the manufacturer's instruction. In brief, 100 ng of target plasmid was methylated by incubation with 8 U of DNA methylase in appropriate buffer conditions for 1 hr at 37^{o}C. Methylated DNA was then amplified by PCR using the appropriate mutagenesis primers at a final concentration of 12.5 ng in a reaction mix containing 10 µM each forward and reverse primer, 10 mM dNTPs and 2.5 U Expand DNA polymerase in appropriate buffer conditions. The PCR amplification cycle was composed of denaturation at 94°C for 2 min, followed by 25 cycles of denaturation at 94°C for 30 sec, annealing at 60°C for 30 sec and elongation at 68°C for 1 min/kb template DNA, and a final elongation step of 68°C for 10 min. After amplification was confirmed by agarose gel electrophoresis, the plasmid DNA was transformed into DH5α-T1^{R}, a strain containing endonuclease McrBC that selectively cleaves the methylated DNA template, allowing only replication of the non-methylated PCR product. The

transformants containing plasmid were then grown on an appropriate selective media. The individual transformants were selected, plasmid DNA was isolated and the expected nucleotide changes confirmed by DNA sequencing.

2.3 RT-PCR

Total RNA preparation was carried out as described in section 2.4.6. RNA and was then used for first strand cDNA synthesis with Superscript III reverse transcriptase (Invitrogen) according to manufacturer's instructions. For reverse transcription, a standard reaction mixture was prepared which contained 1 µg total RNA, 2.5 µM oligo$(dT)_{20}$, 0.5 mM dNTPs, 5 mM DTT, 2 U Recombinant RNase inhibitor and 10 U Superscript III reverse transcriptase. Denaturation of RNA was then carried out by incubation at 65°C for 5 min, followed by first strand synthesis at 50°C for 60 min. The reaction was then inactivated by heating at 70°C for 15 min. For the subsequent PCR reaction, 10% of the first strand reaction was used together with 1.5 mM $MgCl_2$, 0.2 mM dNTPs, 0.4 µM each forward and reverse primer and 1 U *Taq* DNA polymerase (Invitrogen). For each set of primers and template, annealing temperatures and elongation times were employed as appropriate. However, the basic PCR reaction consisted of one cycle of denaturation at 94°C for 2 min, followed by 25 cycles of denaturation at 95°C for 30 sec, annealing at the appropriate temperature for 30 sec and elongation at 72°C for the appropriate extension time (1 min per kb), followed by one cycle of extension at 72°C for 10 min. RT-PCR products were analyzed by agarose gel electrophoresis to assess yield as described in section 2.2.1.3.

2.4 Mammalian cell culture techniques

2.4.1 Maintenance of human cell lines

All cell lines were maintained in a humidified 5% CO_2 atmosphere at 37°C and passaged upon reaching ~80% confluency. To passage, growth media was aspirated off adherent cell populations, cells were washed in 1x PBS and harvested either by incubation in 1x PBS supplemented with 0.5 mM EDTA, or by incubation in Trypsin/EDTA (Invitrogen). Cells were then seeded into fresh, pre-warmed growth media at the appropriate density. hTERT-RPE1 cells were cultured in Dulbecco's Modified Eagle's Medium (DMEM)/Ham's F12 (1:1) supplemented with 10% (v/v) heat inactivated foetal bovine serum (FBS, Invitrogen), penicillin-streptomycin (100 IU/ml and 100 µg/ml, Invitrogen) and 0.348% sodium bicarbonate solution. HEK293, U2OS and HeLa cell lines were cultured in Dulbecco's Modified Eagle's medium (DMEM, Invitrogen) supplemented with 10%

(v/v) heat inactivated FBS, penicillin-streptomycin (100 IU/ml and 100 µg/ml, respectively), and 2 mM Glutamine (Invitrogen).

2.4.2 Storage of human cell lines

All cell lines were cryopreserved in liquid nitrogen for long term storage. Briefly, cells were washed and harvested using 1x PBS and 0.5% Trypsin/EDTA before being collected by centrifugation (1100 rpm, 5 min). After a second wash, cells were resuspended in FBS supplemented with 10% (v/v) DMSO and transferred to cryotubes for freezing in steps (-20°C o/n; -80°C o/n; liquid nitrogen).

2.4.3 Transient transfection of mammalian cells

Lipofectamine 2000 transfection reagent (Invitrogen) was used to transiently transfect cultured mammalian cells with appropriate recombinant vectors. Cells were seeded at a density of $1x10^5$ cells/cm^2 in appropriate culture vessels 24 hrs prior to transfection. Transfections were then carried out according to the manufacturer's instructions with plasmid DNA and lipofectamine mixed in a 1:3 ratio in Opti-MEM and then added dropwise to cells whose normal growth media had been replaced with Opti-MEM medium without FBS or Pen/Strep. After a 4 hrs incubation period (5% CO_2, 37°C), transfection media was replaced with the appropriate complete media and cells were allowed to express recombinant protein for the appropriate length of time before processing as required.

2.4.4 Nuclear export block

Leptomycin B (20 nM; Calbiochem) was added to cells for 6 hrs to block nuclear export.

2.4.5 Preparation of cell extracts for protein analysis

hTERT-RPE1 cell lysates were prepared in NP-40 lysis buffer, whereas HEK293, U2OS and HeLa cell lysates were prepared in NEB lysis buffer (50 mM HEPES-KOH pH 7.4, 5 mM $MnCl_2$, 10 mM $MgCl_2$, 5 mM EGTA, 2 mM EDTA, 100 mM NaCl, 5 mM KCl, 0.1% (v/v) NP-40, 30 µg/ml RNase A, 30 µg/ml DNase I, 10 µg/ml leupeptin, 10 µg/ml bestatin, 10 µg/ml pepstatin, 1 mM PMSF, 20 mM β-glycerophosphate, 20 mM NaF). Briefly, cells were washed in 1x PBS, and then harvested by scrapping after adding lysis buffer directly to the plate. Lysis was carried out on ice for 30 min after which lysates were passed 10 times through a 27G needle and centrifuged at 13000 g for 10 min at 4°C to remove insoluble material. Supernatants were then either used directly as required or stored at -80°C.

2.4.6 Preparation of cell extracts for mRNA analysis

To prepare RNA for RT-PCR analysis, cells were lysed with Tri reagent (Sigma). Tri reagent was added directly to washed cells in culture vessels and the subsequent suspension collected. RNA isolation was then performed according to the manufacturer's instructions. Briefly, the suspension was separated into aqueous and organic phases by addition of bromochloropropane and centrifugation at 13000 g for 10 min at 4°C. RNA, partitioned to the aqueous phase, was then precipitated with isopropanol before washing with ethanol and solubilisation in RNase-free water. Total RNA concentration was calculated by measuring OD_{260} and samples were stored at -80°C.

2.4.7 Flow cytometry analysis

To determine cell cycle distributions, cells were harvested as appropriate (mitotic shake off for M-Phase cells or treatment with 1x PBS/EDTA for all other cell populations), pelleted by centrifugation and washed in 1x PBS before being resuspended in 1 ml 70% ice-cold ethanol to fix cells. Cells were maintained in ethanol at 4°C for a minimum of 30 min before being stained with propidium iodide. Briefly, cells were washed twice in 1x PBS to completely remove all traces of ethanol, and resuspended in 1x PBS supplemented with 200 µg/ml RNase A and 20 µg/ml propidium iodide. Cells were stained in the dark at 4°C for a minimum of 4 hrs or left O/N. Cells were then analysed via flow cytometry, using a FACScan II instrument and CellQuest Pro software (BD Biosciences).

2.4.8 BrdU labeling

For BrdU staining, cells were grown on coverslips until they reached about 50% confluency. Cell culture medium was aspirated off and BrdU labelling medium was added and cells incubated at 37°C, 5% CO_2 for 60 min. Following incubation period, cells were fixed and permeabilized with ice-cold ethanol before being processed for microscopy. In brief, cells were maintained at -20°C in ethanol for a minimum of 20 min before being rehydrated by three 5 min washes in 1x PBS. Cells were then covered with Anti-BrdU labelling solution and incubated for 60 min at 37°C. Coverslips were then washed again three times for 5 min in 1x PBS to remove unbound antibody before incubation with Anti-mouse-Ig-AP solution and incubation for 60 min at 37°C . Coverslips were then subjected to a third round of washes in 1x PBS before being covered with a sufficient amount of freshly prepared Color-substrate solution (13 µl of NBT solution and 10 µl of BCIP solution) for 30 min at room temperature and mounted on glass microscope slides

in mountant (80% (v/v) glycerol, 35 (w/v) n-propyl gallate). They were then examined using a light microscope.

2.4.9 RNA interference

Cells were seeded into a 6-well dish the day before transfection so as to reach a confluency of ~25% for transfection. 100 nM siRNAs and Oligofectamine (Invitrogen, Paisley, UK) transfection reagent were mixed according to the manufacturer's instructions and added dropwise to cells whose normal growth media had been replaced with medium without FBS or Pen/Strep. After 4 hrs incubation period (5 % CO_2, 37^oC), antibiotic free media containing 30% FBS (v/v) was added and cells incubated (5 % CO_2, 37^oC) for 72 hrs before being processed as required. Nek8 was depleted using a pool of four oligonucleotides (5'-GGGCAGAGAGCGAAGUGUA-3'; 5'-GCGAAAGGCUGACCAGAAG-3'; 5'-GUAAUUCCCUGCUGGAGGA-3'; and 5'-AGACAAAGCCCUUAUGAUC-3') with dTdT overhangs at the 3' termini (Dharmacon Scientific, UK). Control depletions were performed with GL2 siRNAs that target luciferase (Dharmacon).

2.4.10 siRNA-plasmid co-transfection

To perform siRNA-plasmid co-transfection using Lipofectamine 2000, cells were seeded in appropriate culture vessels 24 hrs prior to transfection to reach ~80% confluency on the day of transfection using media without Pen/Strep. Briefly, transfection mixes containing 1 µg plasmid DNA, 100 nM final concentration of siRNA duplex(es) and 4 µl of lipofectamine in Opti-MEM were prepared, according to the manufacturer's instructions. The DNA-siRNA-lipofectamine complexes were added dropwise to cells and following a 4 hr incubation period (5% CO_2, 37^oC), transfection media was replaced with fresh media without Pen/Strep. Cells were then returned to the incubator (5% CO_2, 37^oC) until they needed to be processed as required.

2.4.11 Induction of primary cilia formation

Primary cilia formation was induced by culturing hTERT-RPE1 cells in serum-free media for at least 48 hrs.

2.5 Indirect immunofluorescence microscopy

For indirect immunofluorescence microscopy, cells grown on acid-etched glass coverslips were fixed and permeabilized with ice-cold methanol before being processed for microscopy. In brief, cells were maintained at -20°C in methanol for a minimum of 20 min before being rehydrated by three 5 min washes in 1x PBS.

The binding of non-specific antibody was blocked by incubation for 10 min in 1x PBS supplemented with 1% (w/v) BSA. Primary antibody solution was diluted to a suitable concentration in 1x PBS supplemented with 3% (w/v) BSA before incubating coverslips with an appropriate volume (100-150 µl) for a minimum of 1 hr at room temperature. Coverslips were then washed again three times for 5 min in 1x PBS to remove unbound antibody before incubation with appropriate secondary antibodies diluted in 1x PBS supplemented with 3% (w/v) BSA and 0.3 µg/ml Hoechst 33258 in the dark for 1 hr at room temperature. Coverslips were then subjected to a third round of washes in 1x PBS before being mounted on glass microscope slides in mountant (80% (v/v) glycerol, 35 (w/v) n-propyl gallate). The coverslips were then sealed with nail polish and examined by a TE300 inverted microscope (Nikon, Kingston-upon-Thames, U.K.) using an ORCA ER CCD camera (Hamamatsu, Hamamatsu, Japan) using Openlab 5 software (Improvision, Coventry, U.K.). Adobe Photoshop 7 was used to process images and where necessary Openlab 5 or Image J software (Section 2.6.3.1) used for quantification.

2.6 Protein analysis techniques

2.6.1 SDS-PAGE

To resolve proteins the Mini Protean 2 polyacrylamide gel electrophoresis (PAGE) system (Bio-Rad) with a discontinuous Tris-HCl buffer system was used. This consisted of a stacking gel (1.5 M Tris-HCl pH 6.8, 0.4% SDS (w/v), 3.9% (v/v) acrylamide) and a resolving gel (1.5 M Tris-HCl pH 6.8, 0.4% SDS, 5-18% (v/v) acrylamide) with an SDS running buffer (0.1% SDS (w/v), 0.3% Tris (w/v), 1.44% glycine (w/v)). To achieve gel polymerization, 0.8% or 2.4% (v/v) TEMED and 0.015% or 0.045% (v/v) APS was added to the stacking and resolving gels, respectively. According to the size of protein to be resolved, the percentage of acrylamide in the resolving gel varied between 5 and 18%. Samples to be analyzed were mixed with 3x Laemmli buffer (62.5 mM Tris-HCl pH 6.8, 2% (w/v) SDS, 5% (v/v) β-mercaptoethanol, 10% (v/v) glycerol, 0.01% (v/v) bromophenol blue) and boiled for 5 min before being loaded into the gel. Electrophoresis was carried out at 180 V for 1 hr. Coomassie Blue staining or Western Blotting was then used to analyze the resolved proteins.

2.6.2 Coomassie blue staining

For direct visualization of protein in gels following electrophoresis, gels were immersed in Coomassie Brilliant Blue solution (0.25% (w/v) Coomassie Brilliant Blue, 40% (v/v) IMS, 10% (v/v) acetic acid) for a minimum of 30 min. The Coomassie Blue solution was then removed and protein bands were visualized by

washing repeatedly in destain solution (25% (v/v) IMS, 7.5% (v/v) acetic acid) to remove background staining, until the proteins became clearly visible. Appropriate bands were then either excised for mass spectrometry or gels were dried onto 3 MM paper (Whatmann) under a vacuum at 80°C as appropriate. Where necessary, radiolabelled proteins were visualized by autoradiography.

2.6.3 Western blotting

For immunodetection of proteins, semi-dry electrophoretic blotting was used to transfer resolved proteins to nitrocellulose. Briefly, the resolving gel, ProTran nitrocellulose membrane (Schleicher and Schuell), and 3MM chromatography paper were equilibrated in transfer buffer (25 mM Tris, 192 mM glycine, 10% (v/v) methanol). The gel was then placed on the membrane and sandwiched between the buffer-soaked blotting paper. Transfer was carried out in a TE 77 semi-dry transfer unit (Amersham) for 1 hr at 1 mA/cm^2 membrane. Following transfer, the ponceau red solution (0.1% (w/v) Ponceau S, 5% (v/v) acetic acid) was used to visualize the position of size markers and allow lanes to be marked. To block non-specific antibody binding, membranes were incubated in 5% (w/v) non-fat milk power in 1x PBS-Tween (PBS-T; 137 mM NaCl, 2.7 mM Na_2HPO_4, 1.4 mM KH_2PO_4, 0.1% (v/v) Tween-20) for 30 min, prior to antibody incubation. The blocked membrane was then incubated with primary antibody at the appropriate dilution in 5% non-fat milk powder/PBS-T for 1 hr at room temperature or overnight at 4°C. This was followed by three repeated washes of membranes in PBS-T to remove unbound antibody and incubation with a horseradish peroxidase-conjugated secondary antibody for a further hour at room temperature. Membranes were then washed a further three times to remove unbound secondary antibody and developed using ECL Plus Western blotting detection solution (Thermo Scientific), and proteins visualized on X-ray films.

2.6.3.1 Quantification of Western blot band intensities

For comparative quantification of protein band intensities on Western blots, ImageJ software was used. Briefly, the nitrocellulose membrane or X-ray film was scanned using an Epson 2600 scanner and Adobe Photoshop 7 software (Adobe). A region of interest of fixed size that encompassed the band of interest was then selected using ImageJ and pixel intensity within this region of interest calculated for each band to be analyzed, with background intensity subtracted.

2.6.4 Immunoprecipitation

Immunoprecipitation experiments were carried out on whole cell lysates (see section 2.4.5 for cell lysis) using the appropriate rabbit polyclonal or mouse monoclonal antibody bound to protein A beads or protein G sepharose, respectively. Briefly, 500 µl cell lysate suspended in NEB buffer was incubated with 10 µl of washed beads at 4°C for 1 hr with rotation to pre-clear the lysate of any proteins that bound non-specifically to the beads. The pre-cleared supernatant was removed and incubated on ice for 1 hr with the appropriate antibody; after which it was rotated at 4°C for 1 hr with 40 µl washed beads. Beads were then washed 3x with NEB buffer, resuspended with 3x Laemmli buffer and analyzed by SDS-PAGE and Western blotting.

2.6.5 *In vitro* kinase assays

Kinase assays were performed with 5-10 µl of washed immune complex beads prepared as described above. Briefly, beads were incubated with 5 µg of the appropriate substrate and 1 µCi of [γ-^{32}P]-ATP in 40 µl kinase buffer (50 mM Hepes-KOH pH 7.4, 5 mM $MnCl_2$, 5 mM β-glycerophosphate, 5 mM NaF, 4 µM ATP, 1 mM DTT) for 30 min at 30°C. Reactions were stopped by addition of 50 µl 3x Laemmli buffer and analysed by SDS-PAGE and autoradiography. Protein bands were excised from dried gels to quantify the phosphorylation of substrate by scintillation counting. Excised bands were immersed in 3 ml Optiphase HiSafe 2 liquid scintillant (Wallace-Perkin Elmer) and quantified in a LS6500 scintillation analyzer (Beckman Coulter) to determine the incorporation of ^{32}P.

2.7 Recombinant protein expression and purification

2.7.1 Recombinant protein expression in *E. coli*

For expression of recombinant proteins in *E. coli,* DNA sequences were amplified by PCR, subjected to restriction digest and inserted into the pETM-11 bacterial expression vector as described in section 2.2.1. Ligated plasmids were transformed into *E. coli* Rosetta 2(DE3) (Novagen) competent cells. 1 µg of DNA was added to 50 µl of chemically competent Rosetta cells, which had been defrosted on ice, and the slurry was mixed by gently tapping the side of the tube. The mix was incubated on ice for 2 min, heat shocked at 42^{o}C for 30 sec to induce plasmid DNA uptake, and returned to the ice for a further 2 min. 250 µl of pre-warmed LB media was added to the cells and the transformation mix was incubated at 37^{o}C, 225 rpm for 1 hr. Following incubation, 100 µl of the cell suspension was spread onto LB agar plates containing the appropriate antibiotic for selection (chloramphenicol, 34 µg/ml, and ampicillin, 100 µg/ml). Plates were incubated for 12-14 hrs at 37^{o}C. Individual colonies were used to inoculate 100 ml of LB

supplemented with the appropriate antibiotic (chloramphenicol, 34 µg/ml, and ampicillin, 100 µg/ml). Cultures were grown at 37°C, 225 rpm until an A_{600} of ~0.6 was reached. The temperature was then adjusted to 22°C and expression was induced using 400 µM isopropyl 1-thio-β-D-galactopyranoside (IPTG) for 6 hrs. Cells were collected by centrifugation and the recombinant protein purified as below.

2.7.2 Recombinant protein purification

Pelleted cells expressing His-tagged proteins were resuspended in lysis buffer (100 mM NaH_2PO_4, 10 mM Tris-Cl, 8 M urea, pH 8.0) at 5 ml per gram wet weight, and lysed by gently rocking at room temperature for 30 min. The lysate was then clarified by centrifugation at 10000 g for 30 min at room temperature and the clarified lysate loaded onto a nickel column and subjected to two rounds of washing with lysis buffer supplemented with 8 M urea, pH 8.0. Bound protein was then eluted in low pH lysis buffer (pH 4.5) supplemented with 8 M urea in several 500 µl fractions. Protein recovery was determined by SDS-PAGE and Coomassie Blue analysis of 10 µl aliquots of each fraction and those containing highest protein levels were pooled and dialyzed in 1x PBS.

2.7.3 Quantification of protein concentration

Total protein levels were determined using the bicinchoninic acid (BCA) assay (Pierce), which relies on the reduction of Cu^{2+} to Cu^{+} in an alkaline solution with concentration-dependent detection of the monovalent copper ions. Briefly, 5 µl of the protein solution (or appropriate dilutions of the protein solution) were incubated with 1 ml of BCA assay reagent at 37°C for 30 min. Following 5 min cooling period, A_{562} was measured. A serial dilution of BSA standards was prepared and analyzed alongside the protein samples to allow construction of a standard curve from which the protein concentration of the samples could be determined.

2.8 Antibody generation and purification

2.8.1 Antibody generation

For production of antibodies against Nek8, rabbits were immunized with a His-tagged C-terminal fragment of Nek8 that included part of the RCC1 domain spanning amino acids 259 to 550. This fragment was expressed in *E. coli* strain Rosetta 2 (DE3) and individual colonies were used to inoculate cultures of LB supplemented with the appropriate antibiotics (chloramphenicol, 34 µg/ml, and kanamycin, 50 µg/ml). Cultures were grown at 37°C, 225 rpm until an OD_{600} of ~ 0.6 was reached. The temperature was then adjusted to 22°C, and expression was

induced using 400 µM IPTG for 6 hrs. Cells were then collected by centrifugation and bacterial cells were resuspended in denaturing lysis buffer (100 mM NaH_2PO_4, 10 mM Tris, 8 M urea) adjusted to pH 8.0, and lysed by rotating for 15-60 min at room temperature until solution became translucent. The lysate was then centrifuged at 1000 g for 30 min at room temperature to pellet the cellular debris, and the cleared lysate was mixed with 50% Ni-NTA slurry and rotated at room temperature for 1 hr. The lysate-resin mixture was then loaded onto a column and subjected to two round of washing with lysis buffer with pH adjusted to 6.3. Bound proteins were then eluted in lysis buffer with pH adjusted to 5.9 in four 500 µl fractions, followed by elution in lysis buffer with pH adjusted to 4.5 in an additional four 500 µl fractions. Protein recovery after elution was determined by SDS-PAGE and Coomassie Blue analysis of aliquots of each fraction. Aliquots containing highest protein levels were pooled and the pooled purified protein fractions were analyzed on SDS-PAGE and Coomassie Blue analysis. The total concentration was determined by comparison against BSA standards.

2.8.2 Antibody purification

Antibodies were purified by first eluting with a low pH (pH 2.5) glycine buffer and then with a high pH (pH 7.5) triethylamine (TEA) buffer by Cambridge Research Biochemicals. Following elution, the purified antibody fractions were rapidly neutralized and two distinct elutions of purified antibodies in glycine and TEA buffers were obtained. The reactivity of these was tested by Western blotting of HEK293 cell lysates and immunofluorescence microscopy of methanol-fixed hTERT-RPE1 cells, as described in sections 2.6.3 and 2.5, respectively.

2.8.3 Statistical test

Statistical analysis was performed using the T-test from GraphPad Software, Inc (GraphPad Prism 5). A P-value of <0.05 was considered statistically significant.

Chapter 3

Generation of antibodies against Nek8

3.1 Introduction

Nek8 is a serine/threonine kinase that encodes a 692 amino-acid protein with a calculated molecular weight of 79.5 kDa (Liu et al., 2002). The *jck* mouse model of cystic kidney disease contains a missense mutation (G448V) in Nek8 (Liu et al., 2002), while mutations in human Nek8 are implicated in the childhood autosomal recessive kidney disease, nephronophthisis, with Nek8 proposed as the candidate NPHP9 gene (Otto et al., 2008). These findings, together with the fact that Nek8 and polycystin-2 (a protein mutated in 15% of autosomal dominant polycystic kidney disease (ADPKD) cases) form a complex (Sohara et al., 2008), strongly links Nek8 with PKD, a disease involving abnormal cell proliferation and differentiation. Importantly, localisation studies have shown that Nek8 localises to the centrosomes in dividing cells and to the cilium in ciliated cells (Mahjoub et al., 2005). This further strengthens the ciliary hypothesis of cystic kidney disease (Kolb and Nauli, 2008). Nek8 is also overexpressed in primary human breast tumors (Bowers and Boylan, 2004), and may play an important role in cell cycle progression since it shares considerable homology with the Nek9 protein kinase, which is involved in mitotic progression. Although these data direct us towards the existence of a possible pathway linking Nek8 with cilia and the cell cycle, much remains to be determined about these relationships i.e. mode of regulation, downstream targets, as well as the basic biochemistry of this kinase. Such analyses require the availability of highly specific antibodies to Nek8, yet to date there is no commercial Nek8 antibody available. This limitation led us to design and generate a specific Nek8 antibody that could be used for Western blotting, immunofluorescence microscopy and immunoprecipitation experiments. Those would serve to enable us to investigate the distinct functions of Nek8 protein.

In this chapter, I describe the expression of protein fragments of Nek8 in bacteria, their purification and their use for immunization of rabbits. The sera generated from these rabbits were characterized by Western blotting and immunofluorescence microscopy using untransfected cells and cells overexpressing Nek8. Finally, I present the characterization of purified Nek8 antibodies and the localization of endogenous Nek8 in dividing and ciliated cells.

3.2 Results

3.2.1 Generation of rabbit polyclonal antisera against human Nek8

Nek8 is a typical member of the human NIMA-related protein kinase family. It consists of an N-terminal catalytic domain and a C-terminal domain that contains five predicted RCC1 (regulator of chromatin condensation-1) repeats (Liu et al., 2002) (Figure 3.1A). For generation of a specific Nek8 polyclonal antibody, we decided to avoid the kinase domain corresponding to amino acid residues 4-258 since all NIMA-related protein kinases share homology with this domain. We therefore designed a construct corresponding to the RCC1 sequence encompassing amino acid residues 270-550 (Figure 3.1A). This region was named Nek8-Fragment 1 (Nek8-F1) and was cloned into a His-tagged bacterial expression vector to produce DNA encoding His-tagged Nek8-F1. The advantages of the His-tag are its small size (6 consecutive histidine residues) and the ability to purify the proteins under native and denaturing conditions. To determine the optimal conditions of expression and solubilisation of the recombinant protein, we tested different IPTG concentration (100 to 400 µM), temperature (22 to 37^{o}C), time of induction (3 to 16 hrs), and lysis method (sonication/liquid homogenization and lysis buffer). The best protein expression levels were obtained using 400 µM IPTG at 22^{o}C for 6 hrs. His-Nek8-F1 recombinant protein was then prepared with denaturing buffer and a sonication. Following optimization of His-Nek8-F1 expression and solubilisation, the His-Nek8-F1 recombinant protein was expressed and purified on a large scale using Ni-NTA agarose, and used as an antigen for immunization of rabbits (Figure 3.1B).

Prior to immunization, however, sera from a number of rabbits were analyzed by immunofluorescence microscopy of methanol-fixed hTERT-RPE1 cells to check that they did not naturally cross-react with centrosomes and cilia (Figure 3.2A). This is an important consideration as Nek8 has been reported to localize to the centrosomes in dividing cells and cilia in ciliated cells, and many rabbit sera show reactivity to centrosomes prior to immunization (Kim et al., 2004; Romio et al., 2004). Furthermore, to ensure no reactivity of pre-immune sera with proteins around the predicted molecular weight of Nek8 (80 kDa), Western blot analysis was performed in whole cell lysate prepared from hTERT-RPE1 cells (Figure 3.2B). Based on the data from these experiments, rabbits 4175 and 4176 were selected for immunization with the Nek8 antigen. Rabbit immunization was carried by Cambridge Research Biochemicals and immune sera sent to Leicester for characterization.

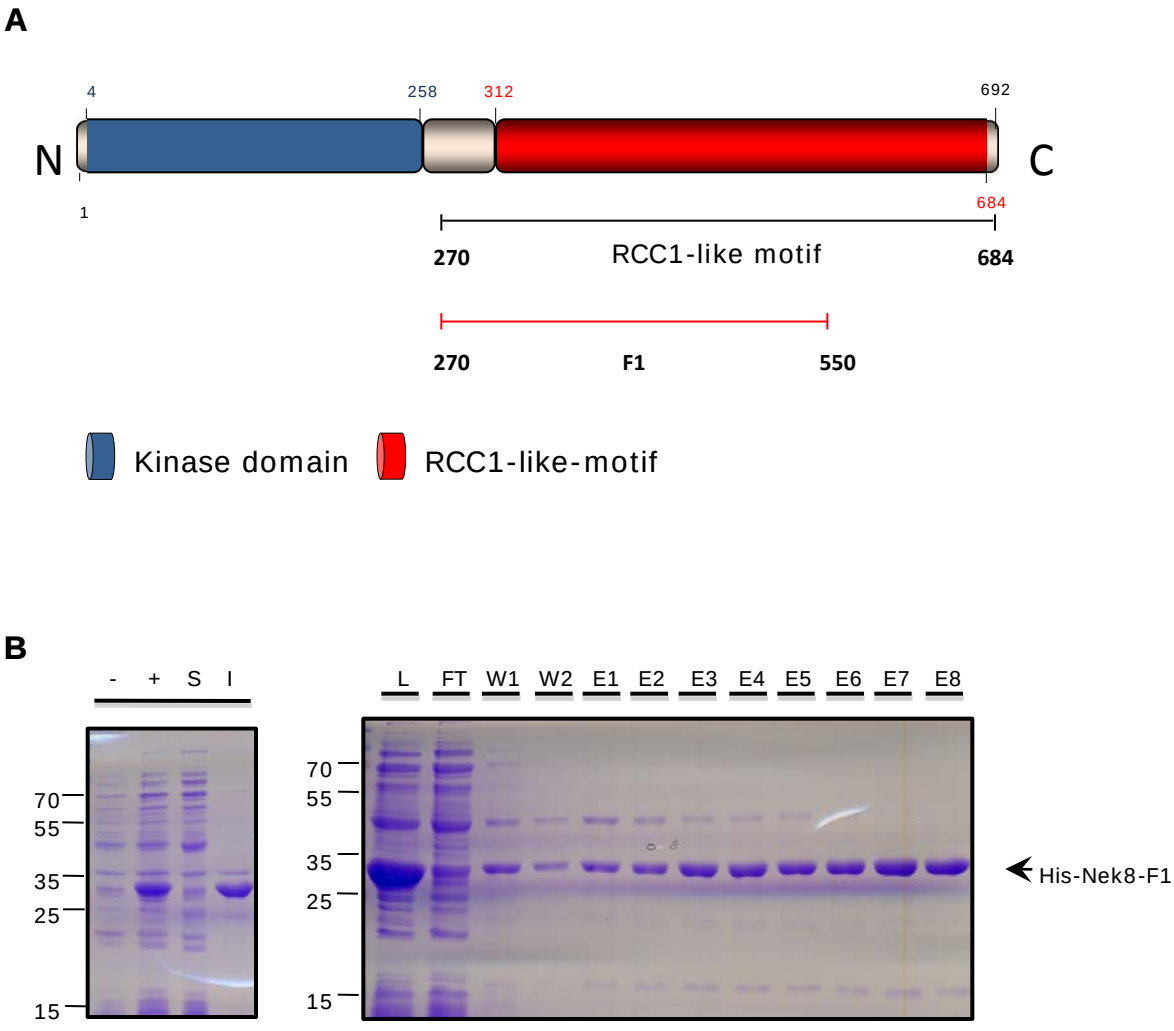

Figure 3.1 Generation of Nek8 antigen for antibody generation **(A)** Schematic representation of full-length Nek8 protein. Red line represents the region expressed as a His-tagged recombinant protein and used as an antigen for immunisation of rabbits for antibody generation. The blue box indicates the kinase domain and the red box represent the RCC1-like motif. Amino acid numbers are indicated. **(B)** Expression and purification of the His-Nek8-F1 recombinant protein. The non-induced (-), induced (+), soluble (S), insoluble (I), lysate (L), flow-through (FT), washes (W1-W2) and elution fractions (E1-E8) were analysed by SDS-PAGE and Coomassie Blue staining. Molecular weights (kDa) are indicated on the left. Black arrowhead indicates predicted molecular weight of His-Nek8-F1 (35 kDa).

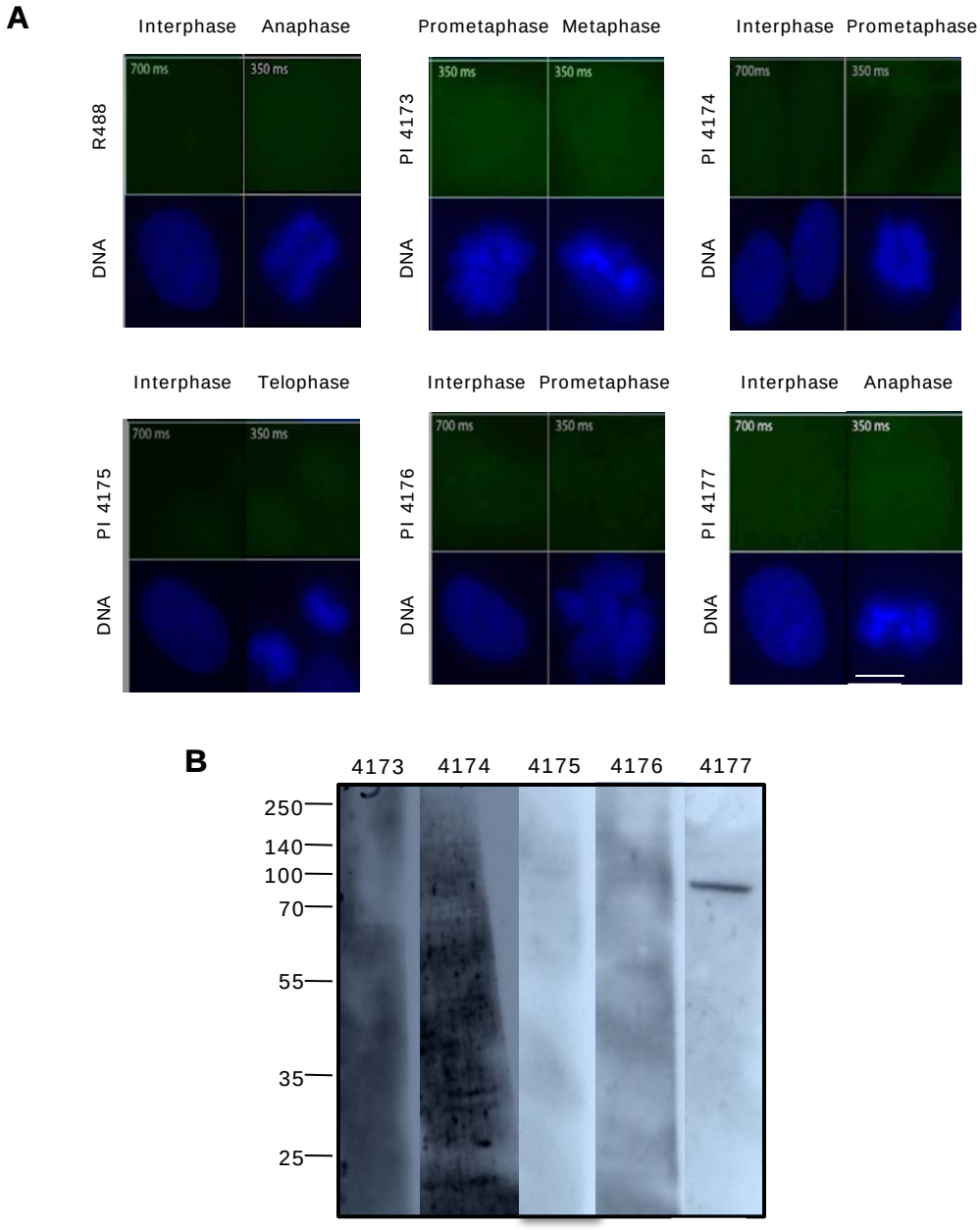

Figure 3.2 Characterisation of pre-immune rabbit sera
(A) Reactivity of the pre-immune sera from rabbits was characterised by immunofluorescence microscopy in hTERT-RPE1 cells. Cells were processed for immunofluorescence microscopy with the appropriate rabbit sera used at 1:250. DNA was stained with Hoechst 33258. Images show the results obtained for the pre-immune sera (PI) of rabbits 4173, 4174, 4175, 4176 and 4177, through different stages of the cell cycle (indicated on top of the panels). R488 represents the secondary antibody above that was used as a control. Images were taken at 700 ms for interphase cells and 350 ms for mitotic cells. Scale bar, 5 µm. **(B)** Western blot analysis of reactivity of the pre-immune (PI) sera from rabbits 4173, 4174, 4175, 4176 and 4177, used at 1:250, against whole cell lysates of hTERT-RPE1 cells. Molecular weights (kDa) are indicated on the left.

3.2.2 Characterization of Nek8 antisera from immunized rabbits

Each rabbit (R4175 and R4176) was subjected to five cycles of immunization and bleeding. Sera from each rabbit were first tested by Western blot analysis of extracts from untransfected HEK293 cells or cells transfected with GFP-Nek8 (Figure 3.3A and 3.3B). They were also tested by immunofluorescence microscopy of methanol fixed untransfected hTERT-RPE1 cells (Figures 3.4A and 3.4B). Reactivity with tagged Nek8 protein allowed us to confirm that the antibodies were capable of detecting the correct target even in the early stages of immunization when the titre of antibody was low.

For Western blot analysis, the Nek8 antisera were used at a 1:250 dilution. This revealed a major band in extracts prepared from GFP-Nek8 transfected cells which corresponded to the predicted molecular weight of GFP-Nek8 (106 kDa) (Figures 3.3A and 3.3B). This band was not detected with the preimmune sera and its size was equivalent to the band detected by an anti-GFP antibody, thus establishing it as GFP-Nek8. Importantly, the intensity of this band increased from bleeds one to the final (5^{th}) bleed for antisera from both rabbit 4175 and 4176 (Figures 3.3A and 3.3B). Moreover, a band of the predicted size of endogenous Nek8 (80 kDa) was detected clearly in both untransfected and GFP-Nek8 transfected cell extracts from bleed 3 to the final bleed for both rabbits 4175 and 4176 (Figures 3.3A and 3.3B). Similar to the exogenous Nek8 protein, this endogenous protein showed increased reactivity from bleed 3 to the final bleed (Figures 3.3A and 3.3B). There was very little other reactivity in these antisera, suggesting a strong positive response to the immunizations, although the final bleeds of both rabbits R4175 and R4176 did detect some lower molecular weight bands, one of which was of approximately 55 kDa, raising the possibility of an alternative version of the Nek8 protein, perhaps as a result of alternative splicing or protein modification.

Immunofluorescence microscopy analysis with the Nek8 antisera at a 1:250 dilution and anti-γ-tubulin antibodies to detect centrosomes confirmed that neither preimmune sera from R4175 and R4176 obviously stained the centrosome (Figures 3.4A and 3.4B). However, immunofluorescence microscopy analysis with post-immunization sera from both rabbits, 4175 and 4176, showed strong consistent colocalization with the centrosomal γ-tubulin stain in interphase cells (Figures 3.4A and 3.4B). Furthermore, post-immunization sera from both rabbits also stained the nucleus and, more weakly, the cytoplasm, suggesting that Nek8 might also play a role in the nucleus and cytoplasm.

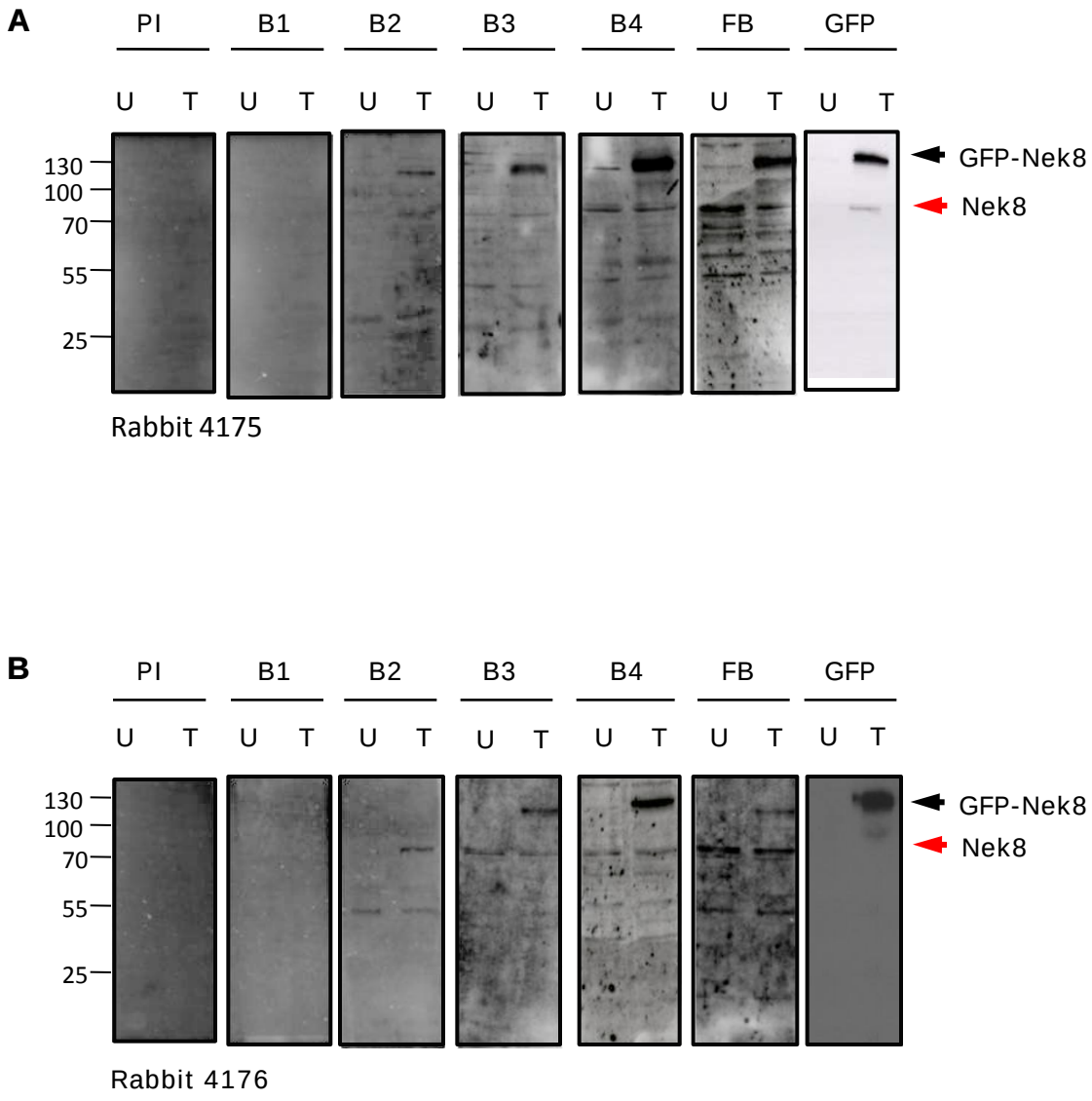

Figure 3.3 Characterisation of Nek8 antisera by Western blot analysis

Reactivity of the sera taken from rabbit 4175 **(A)** and 4176 **(B)** was tested by Western blot, used at 1:250, against untransfected (U) and GFP-Nek8 transfected (T) HEK293 whole cell lysates. PI, pre-immune sera; B1 to B4, antisera from bleeds 1 to 4, respectively; FB, final bleed; GFP, anti-GFP antibody. Molecular weights (kDa) are indicated on the left of each panel. Black arrowhead indicates predicted molecular weight of GFP-Nek8 (106 kDa), red arrowhead indicates predicted molecular weight of endogenous Nek8 (79.6 kDa).

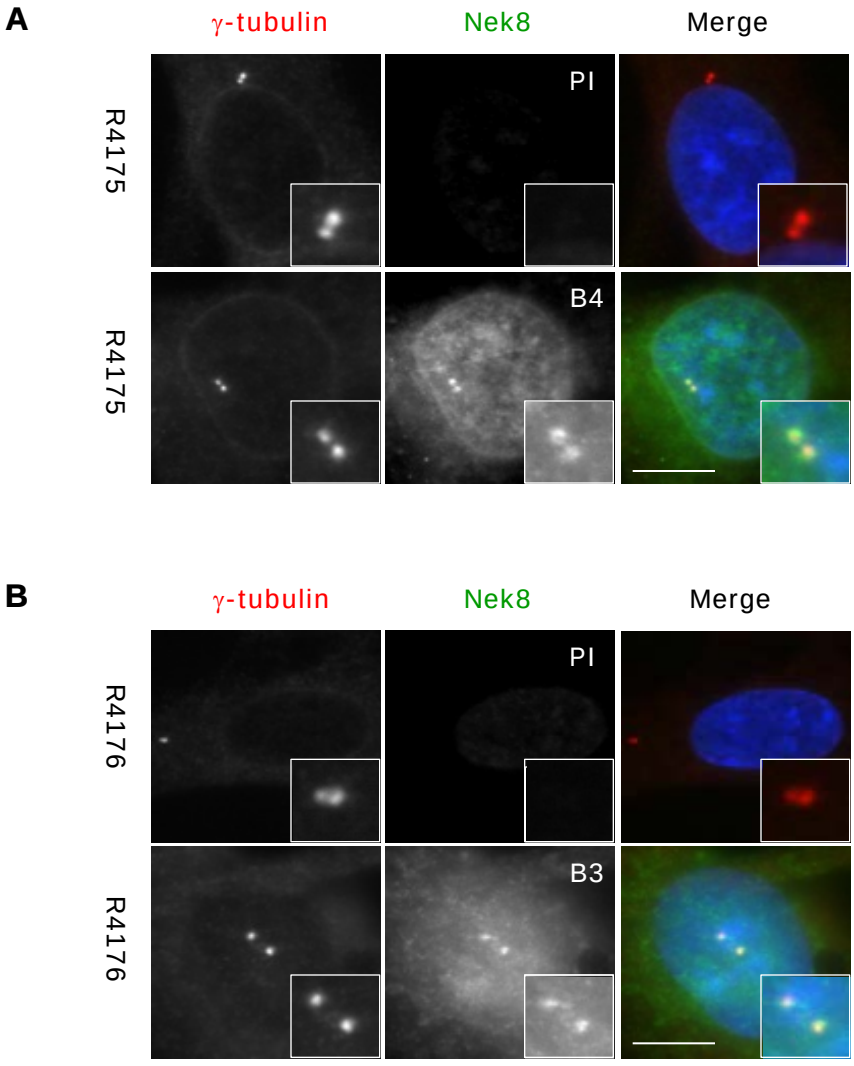

Figure 3.4 Characterisation of Nek8 antisera by immunofluorescence microscopy in dividing hTERT-RPE1 cells
Reactivity of rabbit antisera 4175 **(A)** and 4176 **(B)** was tested by immunofluorescence microscopy in asynchronous hTERT-RPE1 cells. Cells were methanol-fixed before being processed for immunofluorescence microscopy with γ-tubulin antibodies (red on merge) and the appropriate rabbit antisera as indicated (green on merge). DNA was stained with Hoechst 33258 (blue on merge). Rabbit sera was used at a dilution of 1:250. PI, pre-immune sera; B3 and B4, antisera from bleeds 3 and 4, respectively. Insets show magnified views of centrosomes. Scale bars, 10 µm.

In addition to being a centrosomal protein, Nek8 has been reported to localize to the proximal region of cilia, specifically in the inversin compartment where the NPHP2 protein inversin is localized (Omran, 2010; Shiba et al., 2010). For this reason, sera from both rabbits were also tested by immunofluorescence microscopy of ciliated hTERT-RPE1 cells. To promote ciliogenesis, untransfected hTERT-RPE1 cells were serum starved for 72 hrs. Cells were then co-stained with acetylated-tubulin antibodies to detect basal bodies and cilia (Figure 3.5A and 3.5B). Immunofluorescence microscopy analysis confirmed that antisera from both rabbits detected localization of Nek8 in the proximal region of cilia (Figure 3.5A and 3.5B). Taken together, these data indicate that Nek8 antibodies were successfully generated in both rabbits.

3.2.3 Characterization of affinity-purified Nek8 antibodies

The final bleeds from rabbits 4175 and 4176 were purified on His-Nek8-F1 antigen-bound sepharose beads by Cambridge Research Biochemicals. Antibodies were recovered by first eluting with a low pH glycine buffer (pH 2.5) and then with a high pH triethylamine (TEA) buffer (pH 11). Following elution, the purified antibody fractions were rapidly neutralized. We were then provided with two distinct elutions of purified antibodies in glycine and TEA buffers, respectively. The reactivity and specificity of the affinity-purified Nek8 antibodies was tested by Western blot analysis using asynchronous HEK293 whole cell lysates from untransfected cells and cells transfected with GFP-Nek8 constructs, as well as indirect immunofluorescence microscopy using methanol-fixed untransfected hTERT-RPE1 cells and hTERT-RPE1 cells transfected with GFP-Nek8.

Western blot analysis of both glycine and TEA elutions of Nek8 purified antibodies from both rabbits (αR4175 and αR4176) detected bands in extracts of cells expressing GFP-Nek8 which corresponded with the predicted molecular weight of GFP-Nek8 (106kDa). However, the TEA elutions of both antibodies did not detect the endogenous Nek8 which has a predicted molecular weight of 80 kDa (Figure 3.6). The glycine elutions of both αR4175 and αR4176 also detected bands of the expected size of endogenous Nek8 protein both in untreated and transfected cell extracts (Figure 3.6). Some additional lower molecular weight bands were also detected by both glycine purified antibodies, again raising the possibility of an alternative version of the Nek8 protein.

Immunofluorescence microscopy analysis revealed that glycine elutions of αR4175 and αR4176 failed to recognize endogenous Nek8 (Figure 3.7A and B). Similarly,

TEA elutions of both antibodies also failed to detect endogenous Nek8 (data not shown). However, both purified antibodies could recognize transfected GFP-tagged full-length Nek8 (Figure 3.8A and B). The fact that the purified antibodies detected exogenous but not endogenous Nek8 may be explained by low levels of endogenous Nek8 in the cell, in which case a higher concentration of purified antibodies might be needed to detect endogenous Nek8. As result of these studies, the glycine elutions of both αR4175 and αR4176 were used for Western blot analysis of endogenous Nek8, while sera from bleed 3 of rabbits R4175 and R4176 were used for immunofluorescence microscopy studies of endogenous Nek8.

Finally, to confirm the specificity of these Nek8 antibodies, hTERT-RPE1 cells were transiently transfected with a pool of siRNAs oligonucleotides designed to specifically knockdown Nek8. Non-specific siRNA against GAPDH was used as a negative control for Western blot analysis and non-specific siRNA against firefly luciferase (GL2) was used as a negative control for immunofluorescence microscopy studies (Elbashir et al. 2001). Western blot analysis of extracts prepared from hTERT-RPE1 cells transfected with these siRNAs for 72 hrs confirmed the specific detection of Nek8 by the affinity-purified antibodies (Figure 3.9). Meanwhile, depletion of the Nek8 protein followed by immunofluorescence microscopy with the crude sera resulted in loss of both centrosomal and ciliary staining in dividing and ciliated hTERT-RPE1 cells, respectively, confirming the specificity of antibodies using this technique (Figures 3.10A and B).

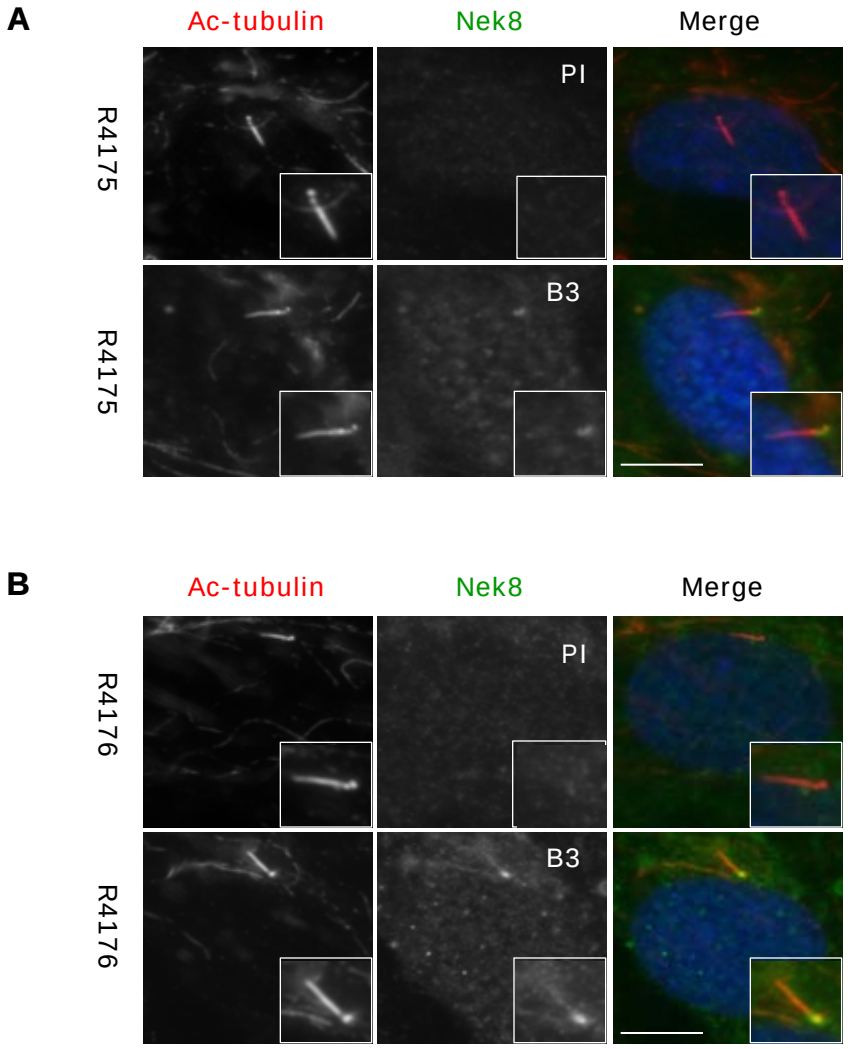

Figure 3.5 Characterisation of Nek8 antisera by immunofluorescence microscopy in ciliated hTERT-RPE1 cells
Reactivity of rabbit antisera 4175 **(A)** and 4176 **(B)** raised against the His-Nek8-F1 protein was tested by immunofluorescence microscopy in ciliated hTERT-RPE1 cells. Cells were then serum starved for 72 hours to promote ciliogenesis. They were methanol-fixed before being processed for immunofluorescence microscopy with acetylated-tubulin antibodies (red on merge) and the appropriate rabbit antisera as indicated (green on merge). DNA was stained with Hoechst 33258 (blue on merge). Rabbit sera was used at a dilution of 1:250. PI, pre-immune sera; B3, antisera from bleeds 3. Insets show magnified views of centrosomes. Scale bars, 10 µm.

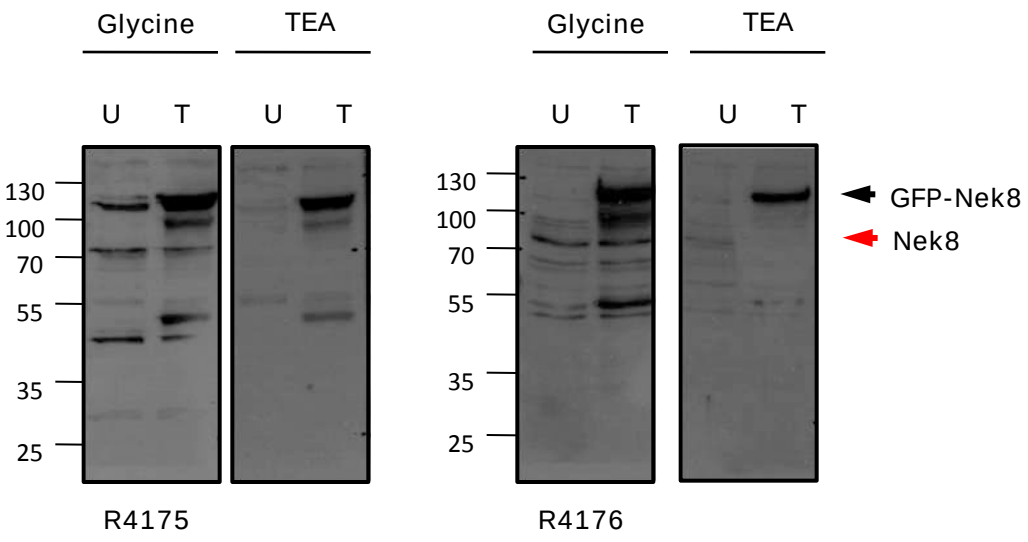

Figure 3.6 Characterisation of affinity purified Nek8 antibodies by Western blot analysis
Reactivity of glycine and TEA elutions of antibodies purified from R4175 and R4176 was tested by Western blot against untransfected (U) and GFP-Nek8 transfected (T) HEK293 whole cell lysates. Molecular weights (kDa) are shown on the left of each panel. Black and red arrowheads indicate the predicted size of GFP-Nek8 (106 kDa), and endogenous Nek8 (79.6 kDa), respectively. Purified antibodies were used at a concentration of 5 µg/ml.

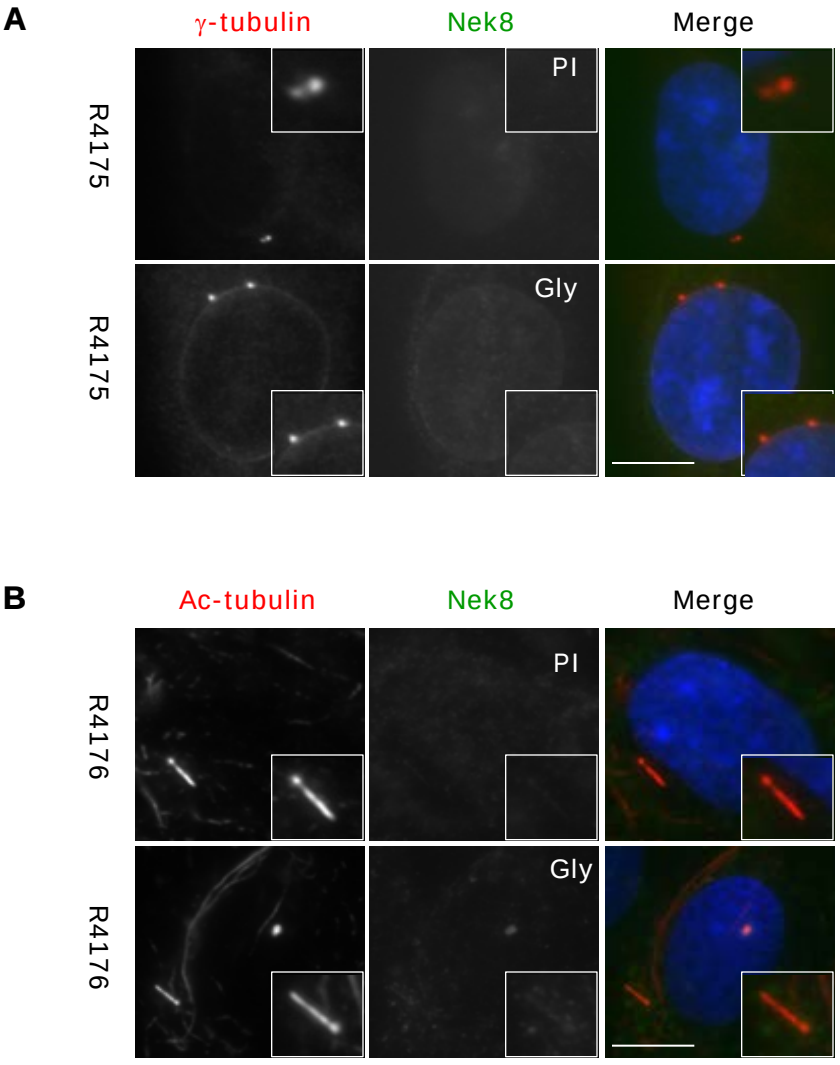

Figure 3.7 Characterisation of affinity purified Nek8 antibodies by immunofluorescence microscopy

Reactivity of the glycine elutions of purified Nek8 antibodies was characterised by immunofluorescence microscopy on asynchronous dividing **(A)** or serum starved **(B)** hTERT-RPE1 cells. Asynchronous dividing cells were methanol fixed before being processed for immunofluorescence microscopy with γ-tubulin antibodies (red on merge) or acetylated tubulin antibodies in serum starved hTERT-RPE1 cells (red on merge) and the appropriate purified Nek8 antibody as indicated (green on merge). DNA was stained with Hoechst 33258 (blue on merge). Purified antibodies were used at a concentration of 5 µg/ml. Scale bars, 10 µm. Insets show magnified views of centrosomes.

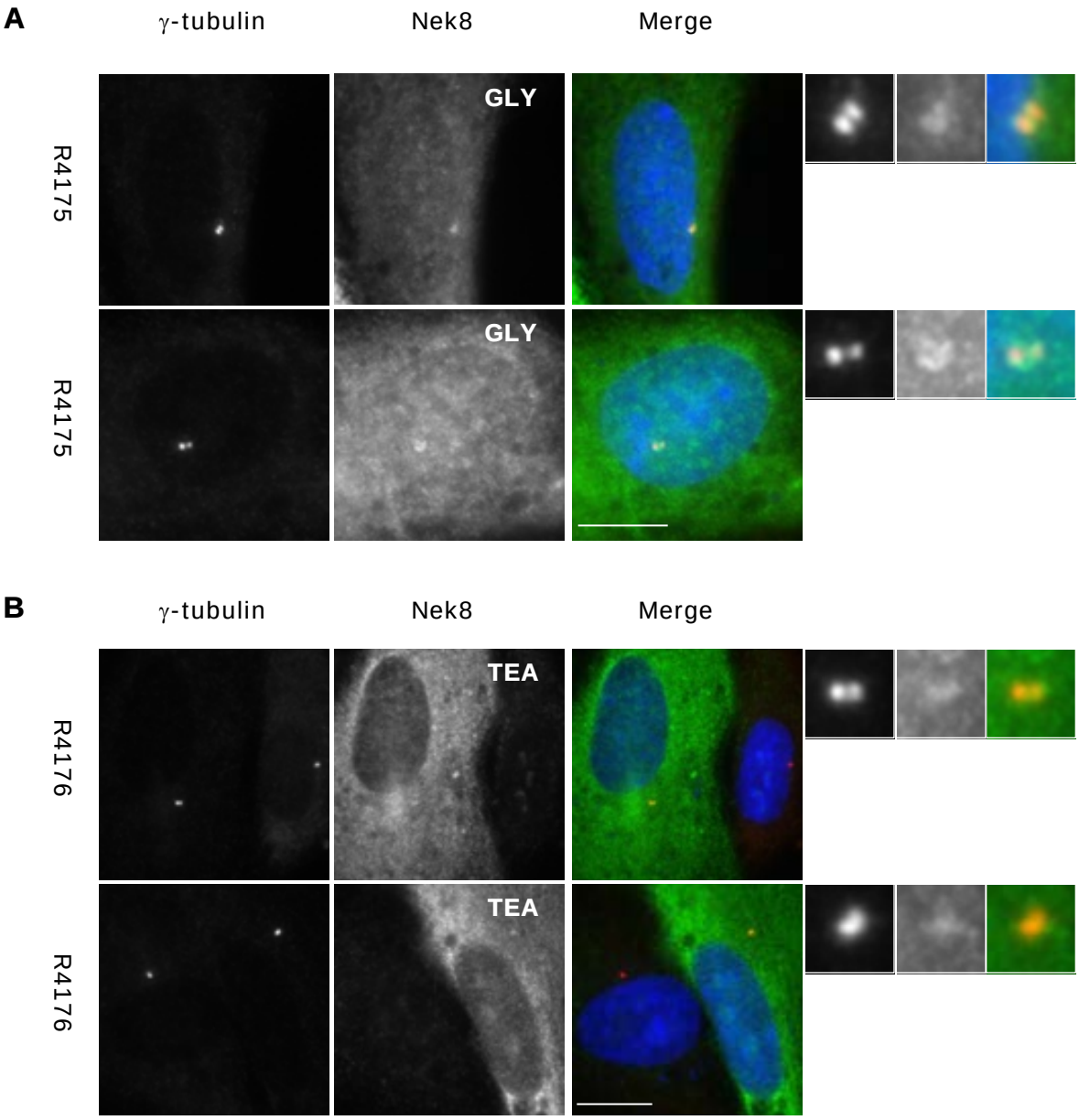

Figure 3.8 Characterisation of affinity purified Nek8 antibodies by immunofluorescence microscopy on transfected GFP-Nek8 hTERT-RPE1 cells

Reactivity of the glycine **(A)** and TEA elutions **(B)** of purified Nek8 antibodies was characterised by immunofluorescence microscopy in hTERT-RPE1 cells transfected with GFP-Nek8. Cells were methanol fixed before being processed for immunofluorescence microscopy with γ-tubulin antibodies (red on merge) and the appropriate purified Nek8 antibody as indicated (green on merge). DNA was stained with Hoechst 33258 (blue on merge). Purified antibodies were used at a concentration of 5 µg/ml. Scale bars, 10 µm. Insets show magnified views of centrosomes.

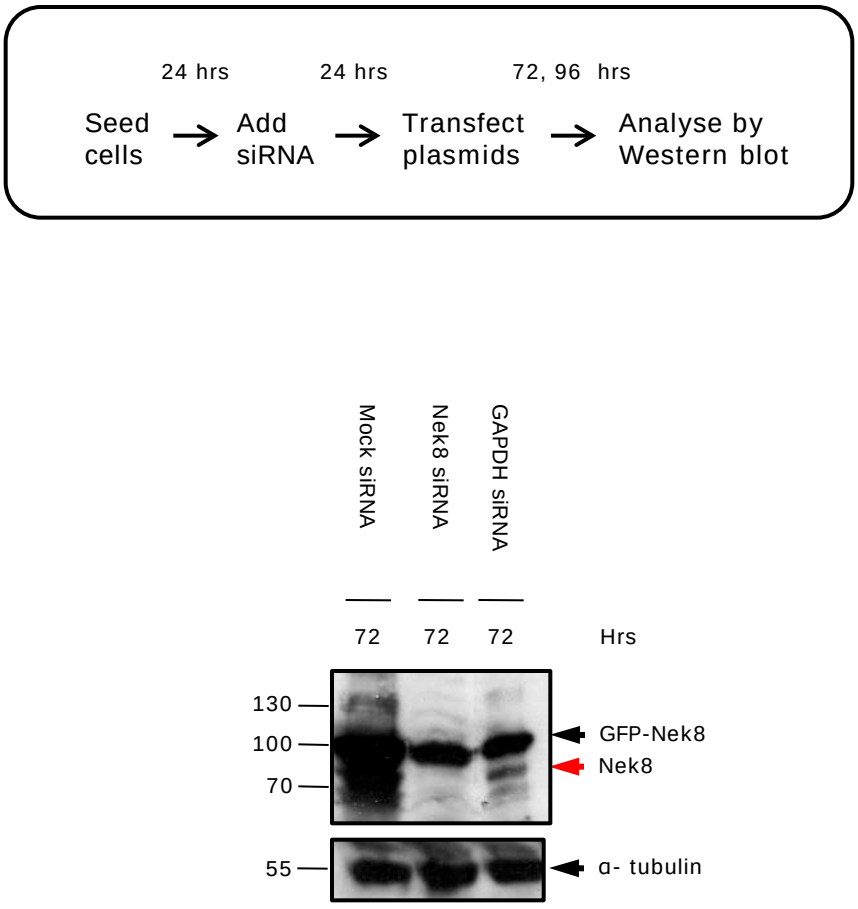

Figure 3.9 Characterising Nek8 siRNA oligos
hTERT-RPE1 cells were transfected with a pool of either four Nek8 siRNA oligonucleotides or GAPDH siRNA for 24 hours and then recombinant Nek8 was transfected in the siRNA treated cells. Cells were harvested 72 hours following plasmid transfection, lysed and analysed by SDS-PAGE and Western blot with anti-Nek8 antibody (R4176 glycine elution). Black and red arrowheads indicate the predicted size of GFP-Nek8 (106 kDa), and endogenous Nek8 (79.6 kDa), respectively. Nek8 antibodies were used at a concentration of 5 µg/ml.

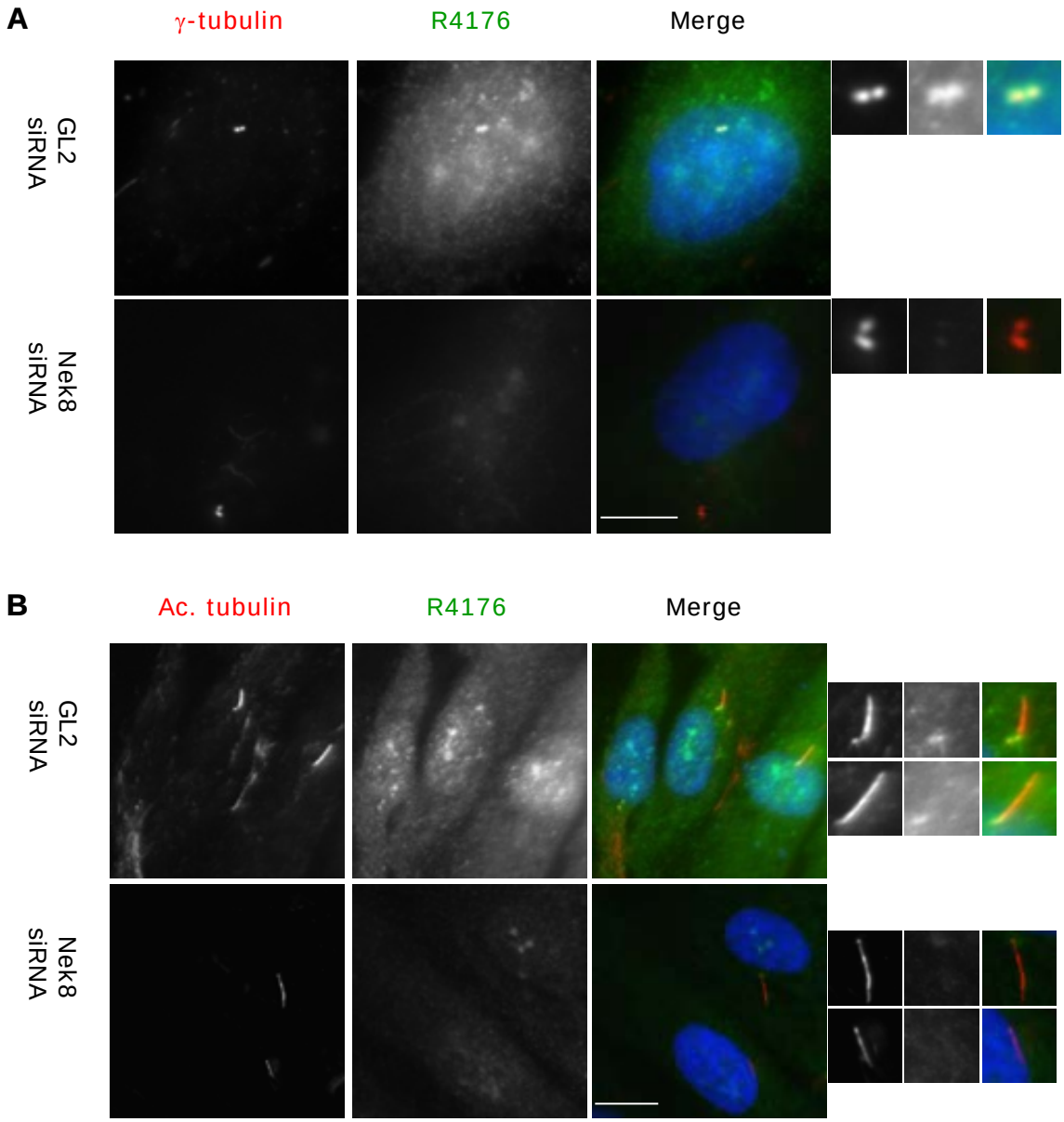

Figure 3.10 RNAi knockdown of Nek8 leads to loss of centrosome and cilia staining

(A) hTERT-RPE1 cells were either transfected with a pool of four Nek8 siRNA oligonucleotides or GL2 specific RNA oligos for 72 hours before being pre-extracted then methanol fixed and immunostained with anti-γ-tubulin antibodies to detect centrosomes and with bleed 3 of rabbit 4176 (green in merge) to detect the Nek8 protein. **(B)** As in A, only that cells were serum starved for 72 hours to promote ciliogenesis. Cilia was co-stained with acetylated tubulin antibodies. Insets show enlargements of the centrosome **(A)** and the cilium **(B)**. DNA was stained with Hoechst 33258 (blue in merge). Scale bars, 10 μm

3.3 Discussion

Aspergillus NIMA is a serine-threonine protein kinase whose activation and degradation are essential for mitotic entry and exit, respectively (Osmani et al., 1991; Pu and Osmani, 1995). Eleven mammalian NIMA-related kinases or Neks have been identified. Of these, Nek8, was found to be mutated in the *jck* (juvenile cystic kidneys) mouse and so appears to be involved in ciliogenesis (Liu et al., 2002). Furthermore, it might play an important role in cell cycle control, since it shares considerable homology with the Nek9 protein kinase, which is involved in mitotic progression. However, the downstream targets, interactors, mode of action and function of Nek8 during cell cycle and ciliogenesis remain to be determined. This led us to generate antibodies that were specific to Nek8 and which would enable us to further explore the properties of this protein.

Since Nek8 shares a significant degree of sequence identity in the kinase domain not only with other Neks, but also other serine/threonine kinases, a fragment corresponding to the divergent RCC1 domain of the protein was expressed in bacteria and used for antibody production. Several attempts to express GST-tagged Nek8 fragments in bacteria ran into the problem that the proteins were insoluble. We therefore decided to use His-tagged fragments that could be purified under denaturing conditions. Most successful was a fragment encoding the N-terminal half of the RCC1-like domain. Two rabbits were immunized with this His-tagged Nek8-F1 protein and yielded sera that recognized recombinant GFP-tagged-Nek8 and endogenous Nek8 proteins by Western blotting. However, bleed 5 of both rabbits (R4175 and R4176), which was chosen for antibody purification, also detected some lower molecular weight bands, one of which was of approximately 55 kDa, raising the possibility of an alternative version of this protein.

Following purification, both glycine and TEA elutions of both anti-Nek8-antibodies appeared to detect recombinant GFP-tagged Nek8 protein in extracts from cells expressing GFP-Nek8. However, while the TEA elutions of both antibodies failed to detect the endogenous Nek8, the glycine elutions of both antibodies detected bands of the expected size of endogenous Nek8 protein both in untreated and transfected extracts. The lower molecular weight bands seen with the Nek8 unpurified antisera were also detectable following purification of both Nek8 antisera. The observed bands were smaller than the endogenous Nek8 protein, again raising the possibility that these might represent alternative versions of Nek8 perhaps as a result of alternative splicing or post-translation modification. Unlike the immune sera of both rabbits, which specifically detected Nek8 colocalizing with

centrosomes in dividing hTERT-RPE1 cells and the proximal region of cilia in ciliated hTERT-RPE1 cells, all the purified antibodies (i.e. both the glycine and TEA elutions of both R4175 and R4176) failed to detect endogenous Nek8 by immunofluorescence microscopy. The most likely explanation for this loss of reactivity is that endogenous Nek8 might be present at very low levels in the cell and therefore a higher concentration of purified antibodies would be needed to detect endogenous Nek8. Nevertheless, as the crude sera from each Nek8 antibody gave a positive stain, these were used in all microscopy experiments. Thus, antibodies specific to human Nek8 that could be used for Western blot and immunofluorescence microscopy analysis have been generated. The specificity of these antibodies was further supported by analysis of lysates which had been prepared from cells depleted of Nek8 by RNAi. This resulted in loss of an 80 kDa band by Western blot with the purified antibodies and loss of centrosome and cilia staining by immunofluorescence microscopy with the crude sera. A primary goal had therefore been achieved with the generation of antibodies specific for Nek8 that would allow characterization of the expression, activity and localization of this protein kinase in cell cycle progression and ciliogenesis.

Chapter 4

Regulation of Nek8 localization in dividing and ciliated cells

4.1 Introduction

Many of the proteins which carry mutations that cause cystic kidney disease localize to the cilium or centrosomes, where they normally function (Hildebrandt and Otto, 2005). One of the mutated proteins associated with the formation of renal cysts in both humans (in NPHP type 9) and mice (in the juvenile cystic kidney (jck) model) is Nek8 (Liu et al., 2002; Otto et al., 2008). Consistent with the hypothesis of ciliary disease, localization studies have shown the murine Nek8 (mNek8) localizes to centrosomes in proliferating cells and at the base of the primary cilia in ciliated cells (Liu et al., 2002; Mahjoub et al., 2005; Otto et al., 2008; Sohara et al., 2008). Most specifically, studies from Mahjoub et al. (2005) have reported that endogenous mNek8 localizes to the proximal region of the primary cilia in an inner medullary collecting duct (IMCD-3) cell line, which is consistent with studies showing that Nek8 localizes to the proximal region of the primary cilia in mouse kidney tubules (Sohara et al., 2008).

So far, three independent mutations have been found within the human Nek8 gene in NPHP patients. These all lie within the region encoding the RCC1 domain: L330F, H425Y and A497P (Otto et al., 2008). These residues show evolutionary conservation and are present in mouse, *Xenopus* and zebrafish Nek8, with the H425 also conserved in the chordate *Ciona intenstinalis* (Figure 1.23A and 1.23B). Interestingly, the H425Y mutation is positioned within the same RCC1 repeat as the missense mutation G448V, found in jck mice (Liu et al., 2002) (Figures 1.23C and 4.1B).

When introduced into GFP-tagged full-length mouse Nek8 constructs and transiently expressed in IMCD-3 cells, both the H431Y (equivalent to human H425Y) and the G448V mutants lost ciliary localization, while the H431Y mutation also exhibited reduced centrosomal localization. In contrast, the L330F and A497P mutations localized similar to the wild-type protein (Otto et al., 2008). On the other hand, a mutation in the kinase domain of mouse Nek8 expected to render the protein catalytically inactive (K33M) also disrupted localization to the primary cilia in IMCD-3 cells (Trapp et al., 2008). More recently, a mutation has been identified in Nek8, A197P, in pancreatic cancer (Carter et al., 2010). This is interesting when considering the fact that pancreatic cancer cells lack primary cilia (Seeley et al., 2009).

Based on these studies, and given the potential role of human Nek8 in both nephronophthisis disease and cancer, we decided to first revisit the localization of

different mutant Nek8 proteins in human hTERT-RPE1 cells. Specifically, we addressed the localization of Nek8 proteins with point mutation in the catalytic or RCC1 domain, as well as isolated catalytic and non-catalytic fragment, to the centrosome, cilia and the nucleus.

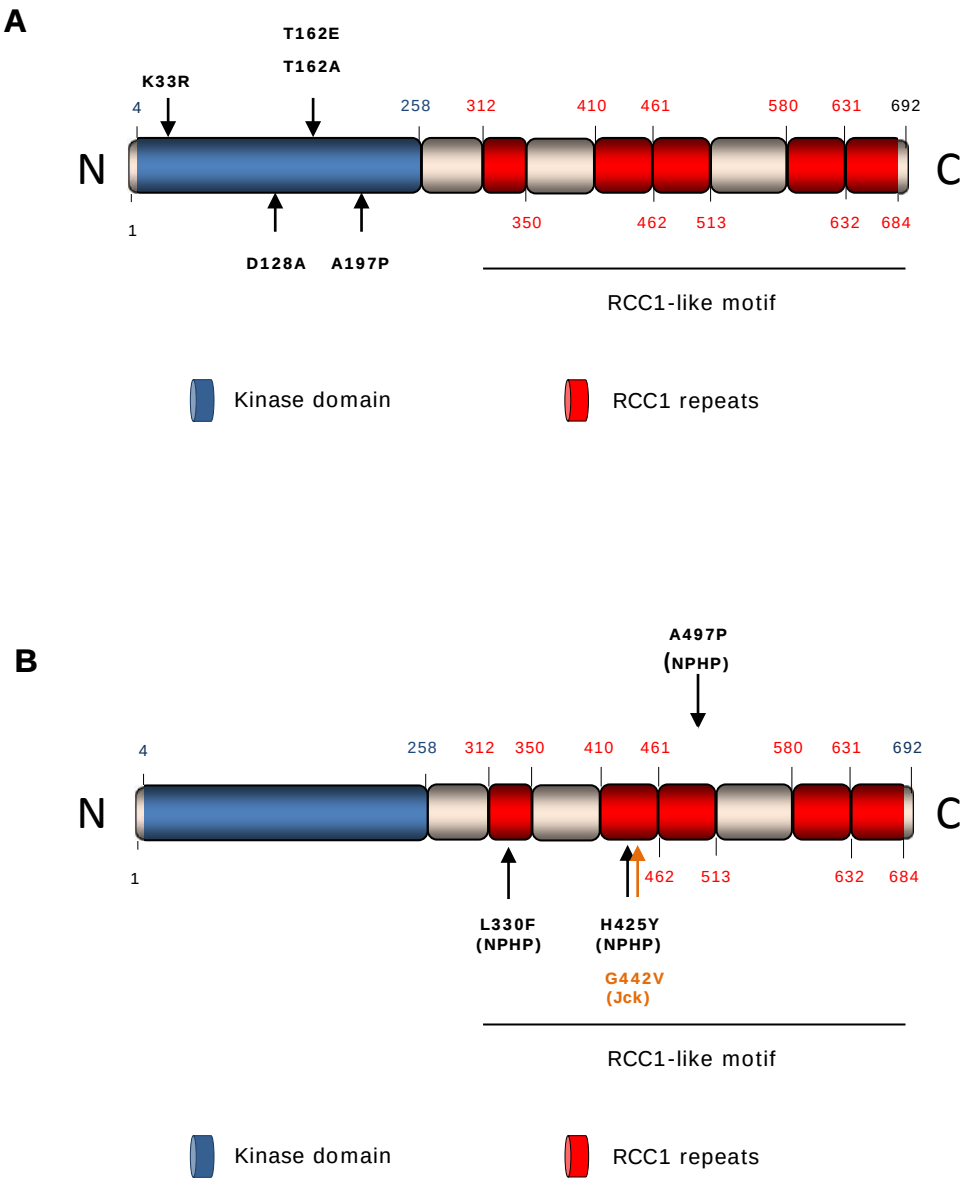

Figure 4.1 Schematic diagram of Nek8 showing sites of mutations analyzed in this study

Schematic diagram of the Nek8 protein showing the position of the catalytic-site mutants **(A)** and the disease-associated mutants **(B)** studied here.

4.2 Results

4.2.1 Recombinant Nek8 localizes to centrosomes

To begin to explore the localization of recombinant Nek8 proteins, GFP-Nek8 and Flag-Nek8 constructs were generated and transiently expressed in hTERT-RPE1 cells. For this purpose, a cDNA clone containing the full-length human Nek8 sequence was obtained from the German cDNA Consortium (RZPD) (clone DKFZp434NO419) as the template. This clone was verified by sequencing in both directions and contains a complete open reading frame (ORF) encoding a protein of the correct predicted length of 692 amino acids. The full-length ORF of Nek8 was then subcloned into the pEGFP-C1 mammalian expression vector as a HindIII/SalI fragment to generate a recombinant protein with an N-terminal GFP tag. In addition, it was also cloned into the pFLAG-CMV2 mammalian expression vector as an EcoRI/SAll fragment to generate a recombinant protein with an N-terminal Flag tag. These tags would allow the study of recombinant Nek8 localization in hTERT-RPE1 cells.

In order to confirm expression of the recombinant protein and also to confirm that the recombinant protein was of the expected size, we next prepared lysates of transfected cell populations and subjected them to SDS-PAGE and Western blotting with anti-GFP or anti-Flag antibodies, as appropriate. This confirmed that the proteins were expressed with a high degree of efficiency and were of the expected size for GFP-Nek8 (106 kDa) and Flag-Nek8 (80 kDa). The identity of the GFP-Nek8 protein was further confirmed by blotting with anti-Nek8 antibodies (Figures 4.2A and 4.2B, respectively).

To examine the localization of these recombinant proteins, the GFP-Nek8 and Flag-Nek8 constructs were transiently transfected into hTERT-RPE1 cells. Cells were allowed to express the recombinant protein for 24 hrs before being fixed and permeabilized using ice-cold methanol. They were then processed for immunofluorescence microscopy with anti-γ-tubulin antibodies to mark the centrosomes and anti-GFP or anti-Flag antibodies to detect the GFP-Nek8 or Flag-Nek8, respectively.

In addition to a general cytoplasmic and/or nuclear stain (see later); the most obvious conclusion from the immunofluorescence microscopy analysis was that GFP-Nek8 shows a strong, distinct localization to centrosomes in proliferating hTERT-RPE1 cells (Figure 4.2C). Localization of Nek8 to centrosomes was confirmed in hTERT-RPE1 cells expressing full-length Flag-Nek8 (Figure 4.2D). This

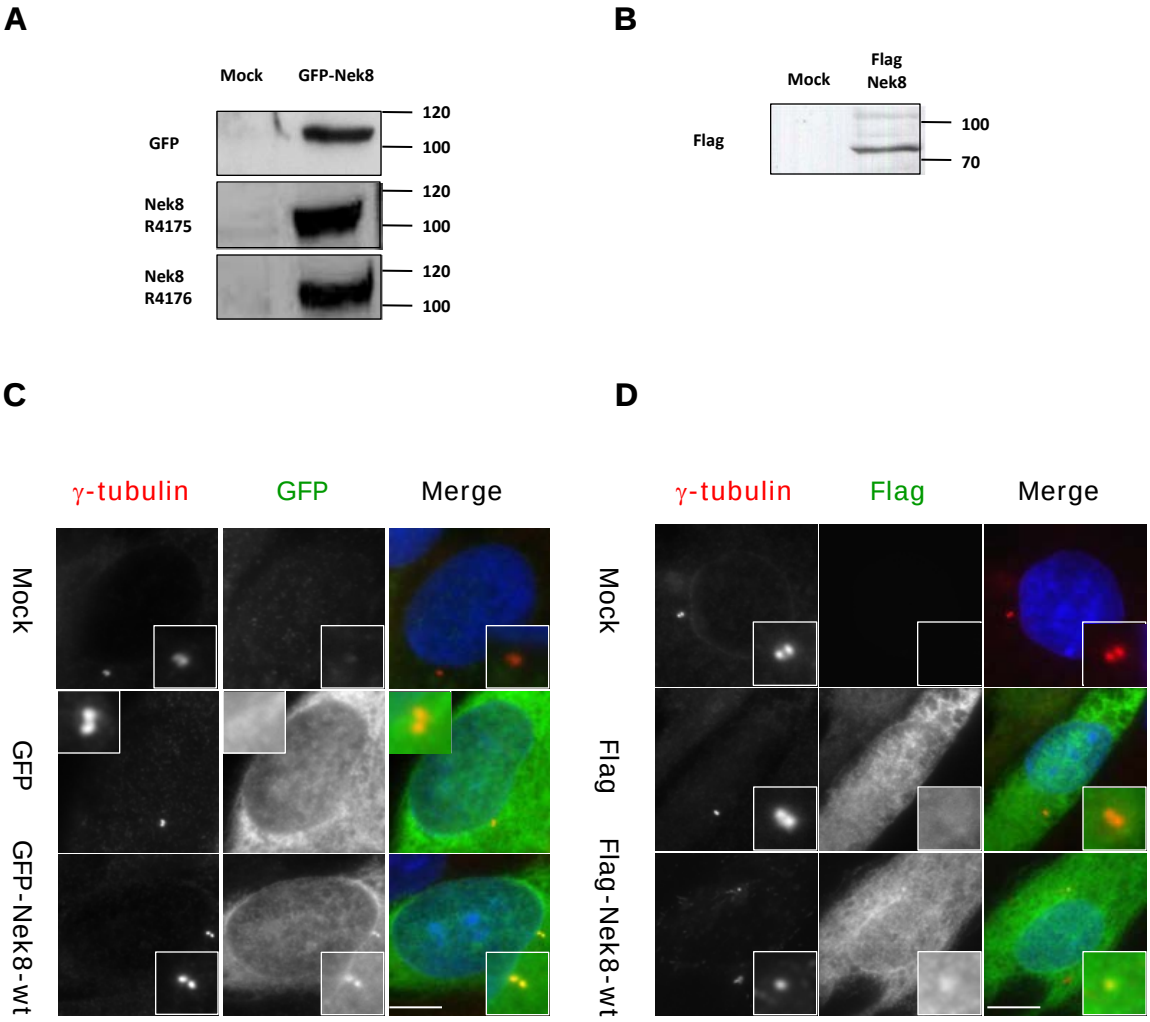

Figure 4.2 Recombinant Nek8 is localized to centrosomes
(A & B) hTERT-RPE1 cells were either mock transfected or transiently transfected for 24 hours with either GFP-Nek8 **(A)** or Flag-Nek8 **(B)**. Cells were then lysed and subjected to SDS-PAGE and Western blotting with anti-GFP or anti-Nek8 antibodies **(A)** and anti-Flag antibodies **(B)**. Molecular weights (kDa) are indicated on the right. **(C)** hTERT-RPE1 cells were either mock transfected or transiently transfected for 24 hours with GFP alone or GFP-tagged Nek8 full length construct. These were fixed in methanol and co-stained with GFP antibodies to detect the recombinant Nek8 (green in merge) and γ-tubulin to detect the centrosome (red in merge). **(D)** As for C, except using Flag-tagged Nek8 and Flag antibodies. Insets show enlargements of the centrosome. DNA was stained with Hoechst 33258 (blue in merge). Scale bars, 10 μm.

is consistent with the centrosomal localization described in IMCD-3 cells expressing murine GFP-Nek8 (Otto et al., 2008), confirming the potential role of Nek8 at the centrosome. This data also confirms the localization pattern of endogenous Nek8 presented in chapter 3.

4.2.2 Catalytic-site mutants of Nek8 lose localization to centrosomes

To determine whether centrosome localization of Nek8 requires kinase activity, we generated the double mutant K33R/D128A carrying mutations in both the invariant lysine and aspartic acid residues within the active site (Hanks and Hunter, 1995). We also generated the T162A mutation in the threonine residue commonly phosphorylated within the activation loop. The cognate mutation inactivates other Nek kinases (Noguchi et al., 2002; O'Regan and Fry, 2009; Twomey et al., 2004). We also generated a T162E mutation to mimic potential phosphorylation at this site. Mutations were introduced by PCR-based mutagenesis of the GFP-Nek8 construct using the Gene Tailor^{TM} site-directed mutagenesis system (Invitrogen) and confirmed by DNA sequencing.

To examine the localization of these recombinant proteins, the wild-type and mutant Nek8 constructs were transiently transfected into hTERT-RPE1 cells for 24 hrs before being fixed and permeabilized using ice cold methanol and processed for immunofluorescence microscopy with anti-γ-tubulin antibodies to mark the centrosomes and anti-GFP antibodies to detect the recombinant protein.

Immunofluorescence microscopy analysis revealed that the Nek8-K33R/D128A and Nek8-T162A mutants showed no centrosomal localization. In contrast, the wild-type Nek8 and the Nek8-T162E mutant strongly localized to centrosomes (Figures 4.3 and 4.7A). These results are consistent with those of Trapp et al. (2008), who showed that the predicted kinase-deficient mutant Nek8-K33M fails to localize to centrosomes in mouse cells (Trapp et al., 2008). Taken together, these studies in human and mouse cells provide persuasive evidence that mutations in the catalytic domain of Nek8 affect Nek8 centrosomal localization, possibly by interfering with the Nek8 catalytic activity, although, at the moment, there is no evidence that correct localization of Nek8 to centrosomes depends on Nek8 kinase activity.

4.2.3 Some but not all Nek8 disease-associated mutants fail to localize to the centrosome

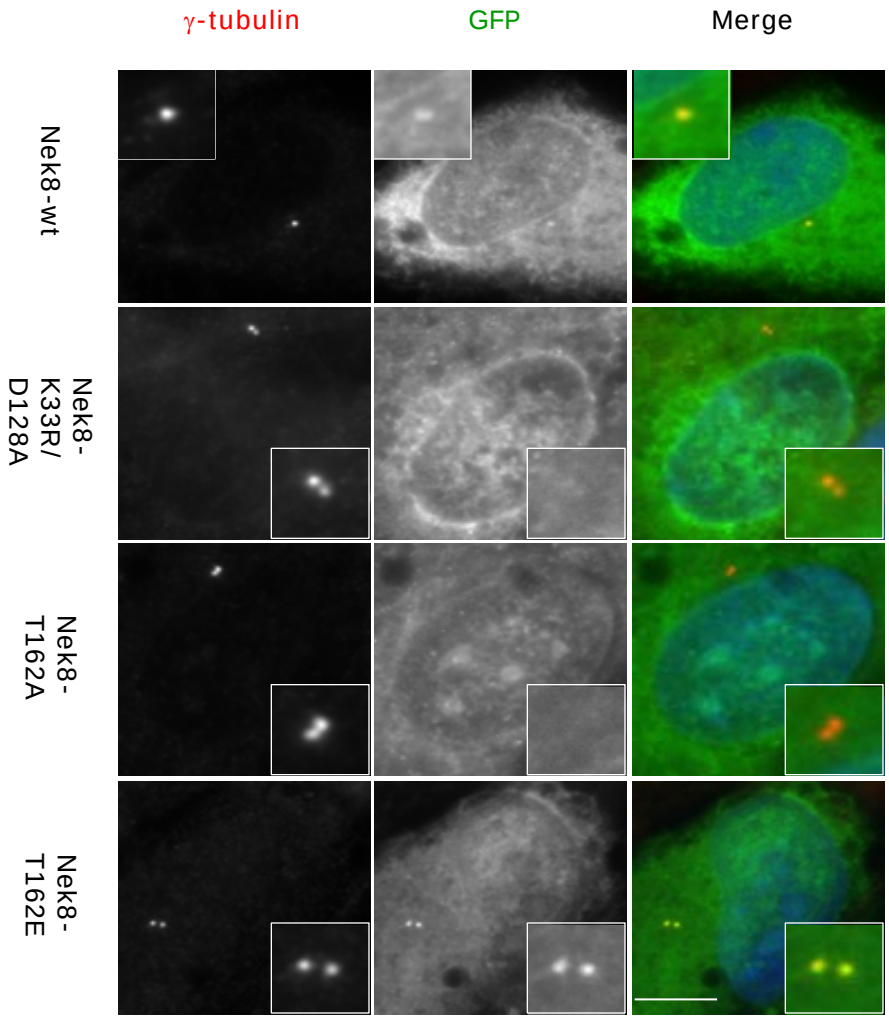

Figure 4.3 Catalytic-site mutants of Nek8 lose localization to centrosomes

hTERT-RPE1 cells were either mock transfected or transiently transfected for 24 hours with GFP-Nek8 constructs as indicated. They were fixed in methanol and co-stained with GFP antibodies to detect the recombinant Nek8 (green in merge) and γ-tubulin to detect the centrosome (red in merge). Insets show enlargements of the centrosome. DNA was stained with Hoechst 33258 (blue in merge). Scale bar, 10 μm.

We next looked at the localization of Nek8 carrying known NPHP mutations, as well as the equivalent mutation G442V found in the jck mouse and the A197P mutation found in pancreatic cancer. Again, these mutations were introduced into full-length GFP-tagged human Nek8 using the GeneTailor^{TM} site-directed mutagenesis system (Invitrogen) and all constructs were confirmed by DNA sequencing. These mutants were then transiently transfected into hTERT-RPE1 cells for 24 hrs before being fixed and permeabilized using ice cold methanol and processed for immunofluorescence microscopy with anti-γ-tubulin antibodies to mark the centrosomes and anti-GFP antibodies to detect the recombinant Nek8 proteins. Immunofluorescence microscopy analysis revealed that whereas the L330F and A497P mutants still strongly localized to centrosomes, the H425Y and G442V mutants, lost centrosomal localization (Figure 4.4). In fact, only 4% of cells expressing GFP-Nek8-H425Y and 1% of cells expressing GFP-Nek8-G442V exhibited localization to centrosomes compared with 62% of cells expressing wild-type GFP-Nek8 (Figure 4.7B). Similarly, the Nek8-A197P mutant also lost centrosomal localization with only 8% of cells exhibiting centrosomal localization (Figures 4.4 and 4.7B). This agrees with data from Otto et al. (2008) who showed that the L336F and A503P mutants in mouse, which correspond to L330F and A497P in humans, respectively, did not alter localization to centrosomes, as opposed to the H431Y mutant, equivalent to H425Y mutant in humans, which decreased centrosomal localization in IMCD-3 cells. However in this study we also show that centrosomal localization is lost in cells expressing the equivalent jck mutation, G442V. This is in contrast to the finding from Trapp et al. (2008) who reported that Nek8 is localized to the centrosomes in cells from jck mice. From this study, we conclude that the A197P, H425Y and G442V mutations prevent the localization of this protein at the centrosome.

4.2.4 The RCC1 domain of Nek8 is required for centrosomal localization

The above data has established that both endogenous and recombinant Nek8 are localized to the centrosomes in dividing cells, and that mutations in either the catalytic or non-catalytic domain can disrupt this localization. To further understand the functional targeting domain of Nek8, a series of truncated fragments of Nek8 were constructed and expressed in cells. The kinase domain (FK; encompassing amino acids 4-258), the C-terminal RCC1-like domain (RCC1; encompassing amino acids 270-692), as well as two other fragments that divide the RCC1 domain, F1 (encompassing amino acids 270-550), and F2 (encompassing amino acids 551-692), were generated in the GFP-tag containing vector pLEICS-021 by the Protex facility, University of Leicester (Figure 4.5A).

To confirm that recombinant proteins of the expected size were produced, lysates of transfected hTERT-RPE1 cells were subjected to SDS-PAGE and Western blotting with an anti-GFP antibody. This confirmed that all four truncated proteins were expressed with a high degree of efficiency and of the expected size; these were GFP-Nek8-FK (55 kDa), GFP-Nek8-F1 (58 kDa), GFP-Nek8-F2 (42 kDa), and GFP-Nek8 RCC1-(75 kDa) (Figure 4.5B and 4.5C).

We next examined the localization of these GFP-Nek8 truncated proteins. To do this, the constructs were transiently transfected into hTERT-RPE1 cells for 24 hrs before being fixed and permeabilized using ice cold methanol and processed for immunofluorescence microscopy with anti-γ-tubulin antibodies to mark the centrosomes and anti-GFP antibodies to identify the GFP-Nek8 truncated proteins.

Immunofluorescence microscopy analysis revealed that the RCC1 domain of Nek8 is sufficient for Nek8 centrosomal localization since it localized to the centrosomes, whereas the catalytic domain Nek8-FK did not. Furthermore, the RCC1 domain needs to be intact as the Nek8-F1 and Nek8-F2 fragments did not localize to centrosomes (Figure 4.6). Specifically, 22% of cells expressing Nek8-F1, 18% of cells expressing F2 and 6% of cells expressing FK showed localizations to the centrosomes in hTERT-RPE1 cells, as compared with 78% of cells expressing-full length Nek8 and the Nek8-RCC1 domain (Figure 4.7C).

4.2.5 Nek8 is localized to the proximal region of the cilia

It has also been reported that Nek8 localizes to the proximal region of the cilia, adjacent to the basal bodies, in post-mitotic ciliated cells (Otto et al., 2008; Shiba et al., 2010; Trapp et al., 2008). This proximal region of the cilium is also known as the “inversin compartment”, as it is the site of localization of the NPHP2/inversin protein. Based on these studies, we next reviewed the localization of recombinant Nek8 in hTERT-RPE1 cells grown under conditions to promote ciliogenesis. For this, the GFP-Nek8 and Flag-Nek8 constructs were transiently transfected into hTERT-RPE1 cells for 4 hrs and serum starved for 48 hrs before being fixed and permeabilized using ice-cold methanol and processed for immunofluorescence microscopy with anti-acetylated tubulin antibodies to mark the cilia, and anti-GFP or anti-Flag antibodies to identify GFP-Nek8 or Flag Nek8, respectively. Consistent with previous studies, immunofluorescence microscopy of serum starved transfected hTERT-RPE1 cells revealed that both GFP-Nek8 and Flag-Nek8 localized to the proximal region of primary cilia (Figure 4.8A and B, respectively).

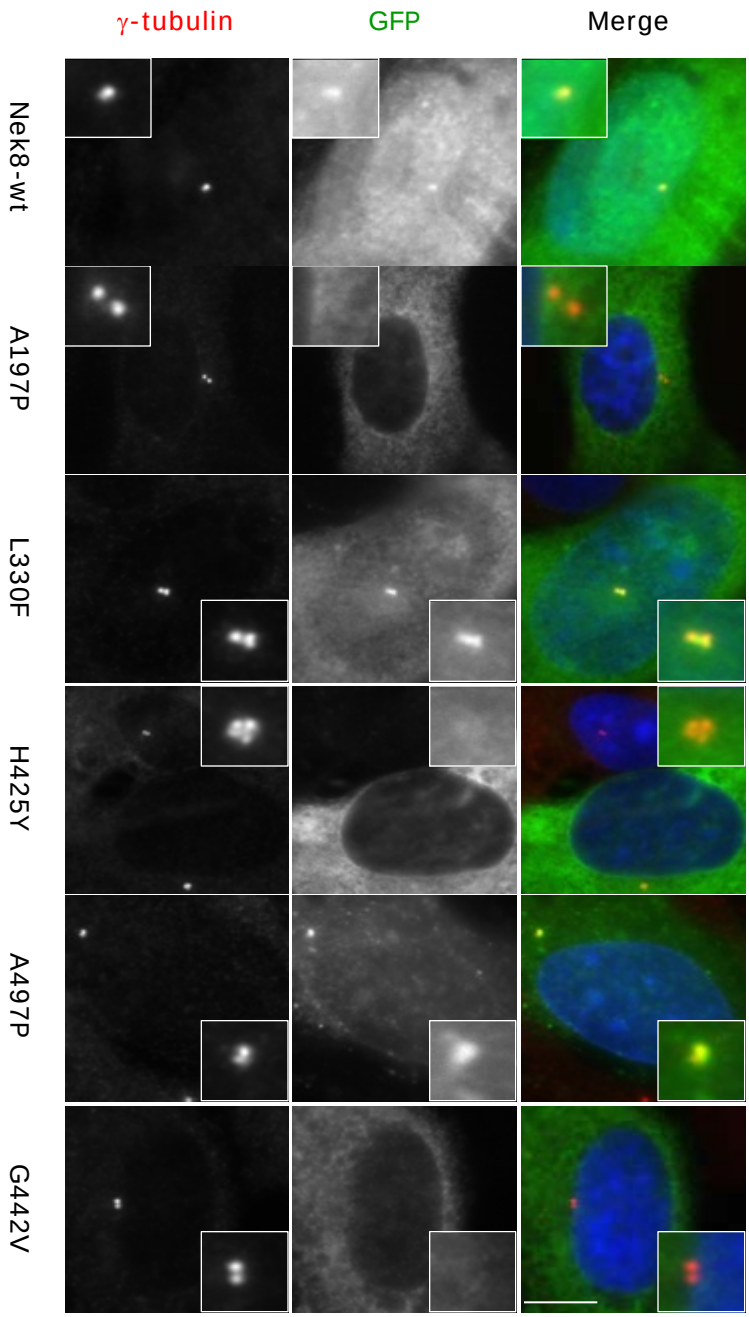

Figure 4.4 Some but not all disease-associated Nek8 mutants fail to localize to centrosomes

hTERT-RPE1 cells were either mock transfected or transiently transfected for 24 hours with GFP-Nek8 constructs as indicated. They were fixed in methanol and co-stained with GFP antibodies to detect the recombinant Nek8 (green in merge) and γ-tubulin to detect the centrosome (red in merge). Insets show enlargements of the centrosome. DNA was stained with Hoechst 33258 (blue in merge). Scale bar, 10 µm.

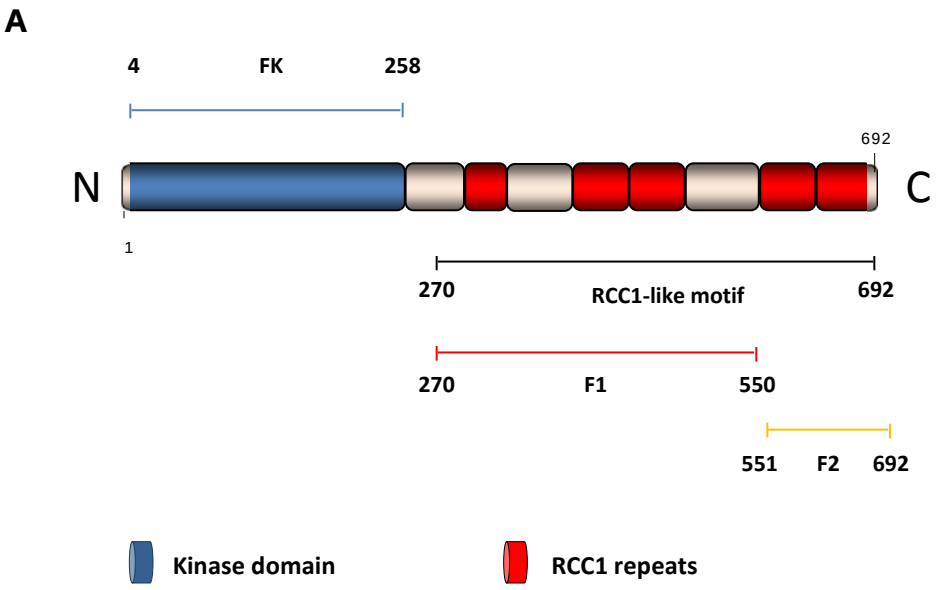

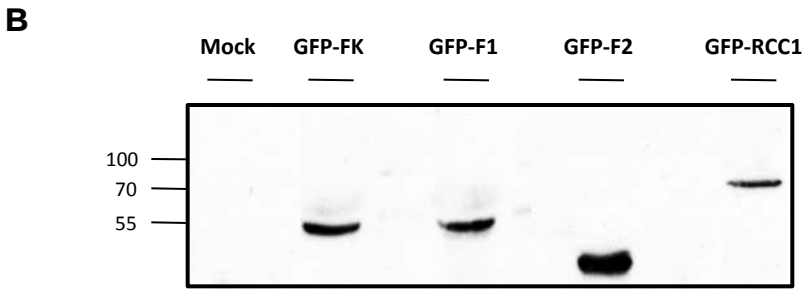

Figure 4.5 Expression of Nek8 truncated fragments in hTERT-RPE1 cells

(A) Schematic diagram of Nek8 truncated fragments. **(B)** Representative anti-GFP Western blot of hTERT-RPE1 cells that were either mock transfected or transiently transfected for 24 hours with GFP-tagged Nek8 kinase domain (FK), fragment 1 (F1), fragment 2 (F2), RCC1 domain (RCC1). Note that all bands were of expected size. Molecular weights (kDa) are indicated on the left.

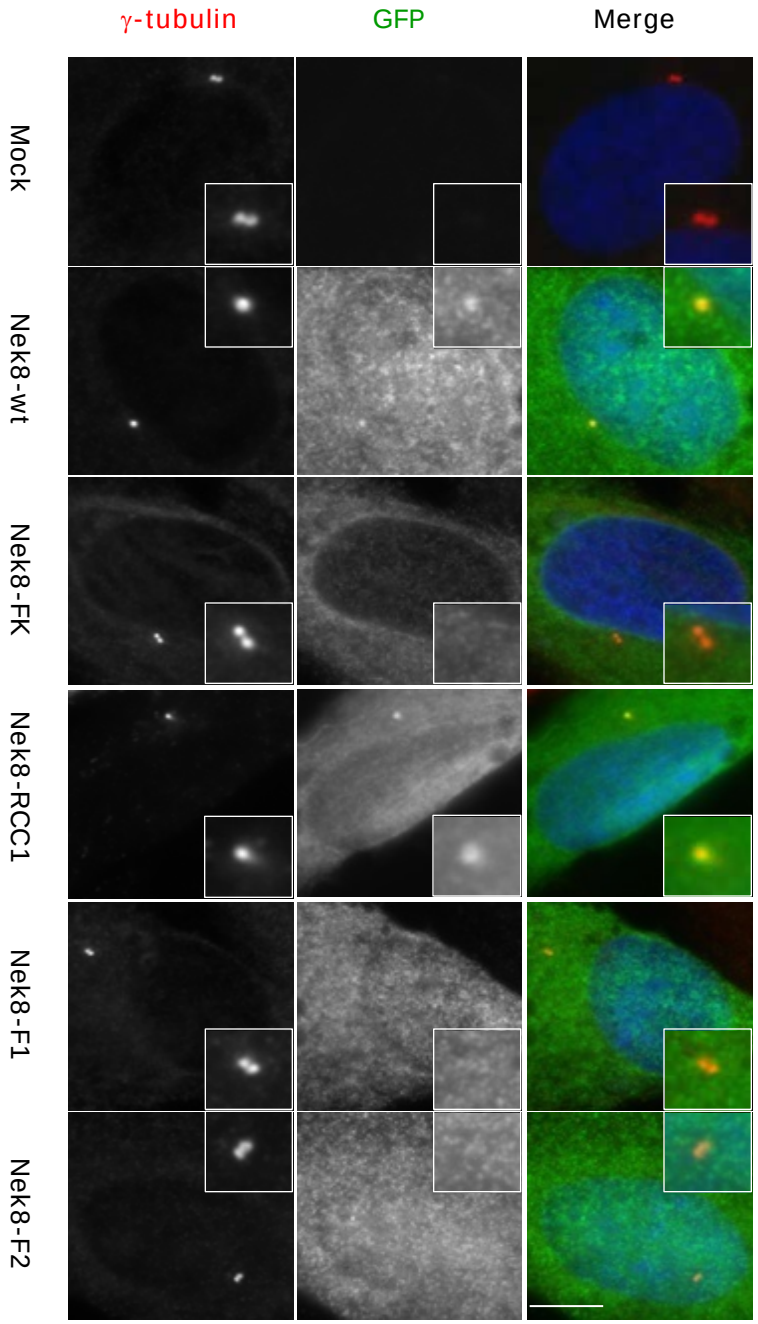

Figure 4.6 The RCC1 domain of Nek8 is responsible for localisation of Nek8 to the centrosome

hTERT-RPE1 cells were either mock transfected or transiently transfected for 24 hours with GFP-Nek8 truncated constructs as indicated. They were fixed in methanol and co-stained with GFP antibodies to detect the recombinant Nek8 (green in merge) and γ-tubulin to detect the centrosome (red in merge). Insets show enlargements of the centrosome. DNA was stained with Hoechst 33258 (blue in merge). Scale bar, 10 µm.

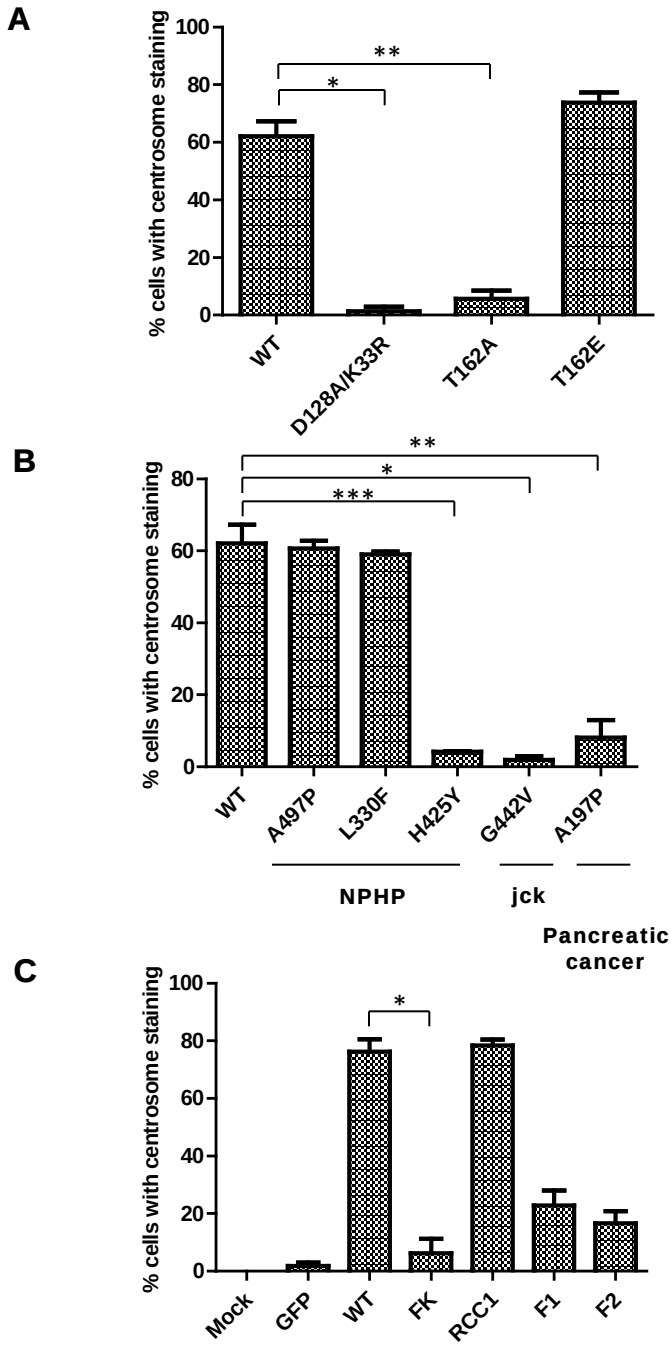

Figure 4.7 Quantification of centrosome localization of Nek8 mutants and Nek8 truncated forms

Dividing hTERT-RPE1 cells were quantified for centrosomal localization of GFP-Nek8 catalytic–site mutants **(A)**, disease mutants **(B)** and truncated forms of Nek8 **(C)**. Data represent mean (± S.E.) of three separate experiments where at least 45 cells were counted. P values are shown for specific pairwise comparison (*, $p<0.0001$; **, $p=0.0007$; ***, $p=0.0004$)

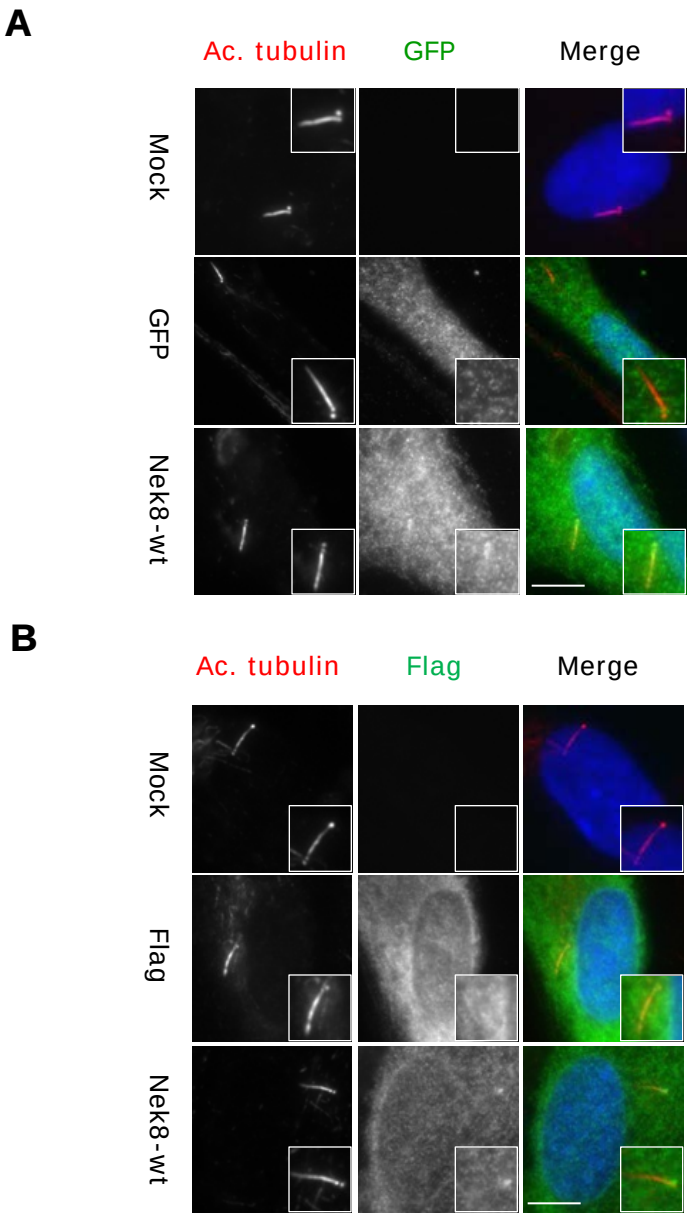

Figure 4.8 Recombinant Nek8 is localized to the proximal region of cilia

(A) hTERT-RPE1 cells were either mock transfected or transfected with GFP-alone or GFP-Nek8-wt for 4 hours and serum starved for 48 hours to promote ciliogenesis. These were then methanol fixed and stained with GFP antibodies to detect the recombinant Nek8 (green in merge) and acetylated tubulin to visualise the cilia (red in merge). DNA was stained with Hoechst 33258 (blue in merge). **(B)** As for A, except using Flag-tagged Nek8 and Flag antibodies. Insets show enlargements of the cilia. Scale bars, 10 µm.

4.2.6 Localization of Nek8 mutants to cilia reflects localization to the centrosome

Having established that Nek8 localizes at the proximal region of the primary cilium, in serum starved hTERT-RPE1 cells, we next examined whether this was also the case for first, the catalytic-site mutants and, second, the disease associated mutants. To this end, cells were transiently transfected for 4 hrs with GFP-tagged Nek8 constructs and serum starved for 48 hrs to promote ciliogenesis. They were then fixed and processed for immunofluorescence microscopy with anti-GFP antibodies to detect the recombinant Nek8, as well as anti-acetylated-tubulin antibodies to detect primary cilia.

A highly similar pattern of localization to the cilium was observed for the mutants as seen at the centrosome in dividing hTERT-RPE1 cells. Immunofluorescence microscopy analysis revealed that the kinase-deficient mutants of Nek8, K33R/D128A and T162A, did not localize to the cilium in ciliated hTERT-RPE1 cells (Figures 4.9), in line with studies that showed that the kinase-deficient mutant, Nek8-K33M, fails to localize to cilia (Trapp et al., 2008). In contrast, the Nek8-T162E mutant strongly localized to the proximal region of primary cilia, further supporting the importance of kinase activity for correct Nek8 localization in cells. It is noteworthy, though, that a somewhat reduced fraction of cells expressing the Nek8-T162E mutant exhibited localization to the cilium compared with the GFP-Nek8-wt (Figure 4.12A).

We next looked at the ciliary localization of the NPHP-disease associated mutants, A497P, L330F, H425Y, as well as the jck-equivalent mutant, G442V. The ciliary localization of the pancreatic cancer-associated mutant, A197P was also observed. For this, cells were treated as for the kinase domain mutants. Again, results correlated with those found for centrosomal localization in proliferating hTERT-RPE1 cells, with only the H425Y and G442V mutants losing ciliary localization (only 7% of the H425Y and 17% of the G442V localized to the primary cilia) as opposed to the A497P and L330F mutants which localized to the proximal region of the primary cilia in the majority of cells (63% and 59%, respectively) (Figures 4.10 and 4.12B). Loss of ciliary localization was also observed with the A197P mutant, consistent with it losing localization to the centrosome in proliferating hTERT-RPE1 cells.

We next looked at ciliary localization of Nek8 truncated forms (FK, RCC1, F1 and F2) using the same approach as above. Immunofluorescence microscopy revealed

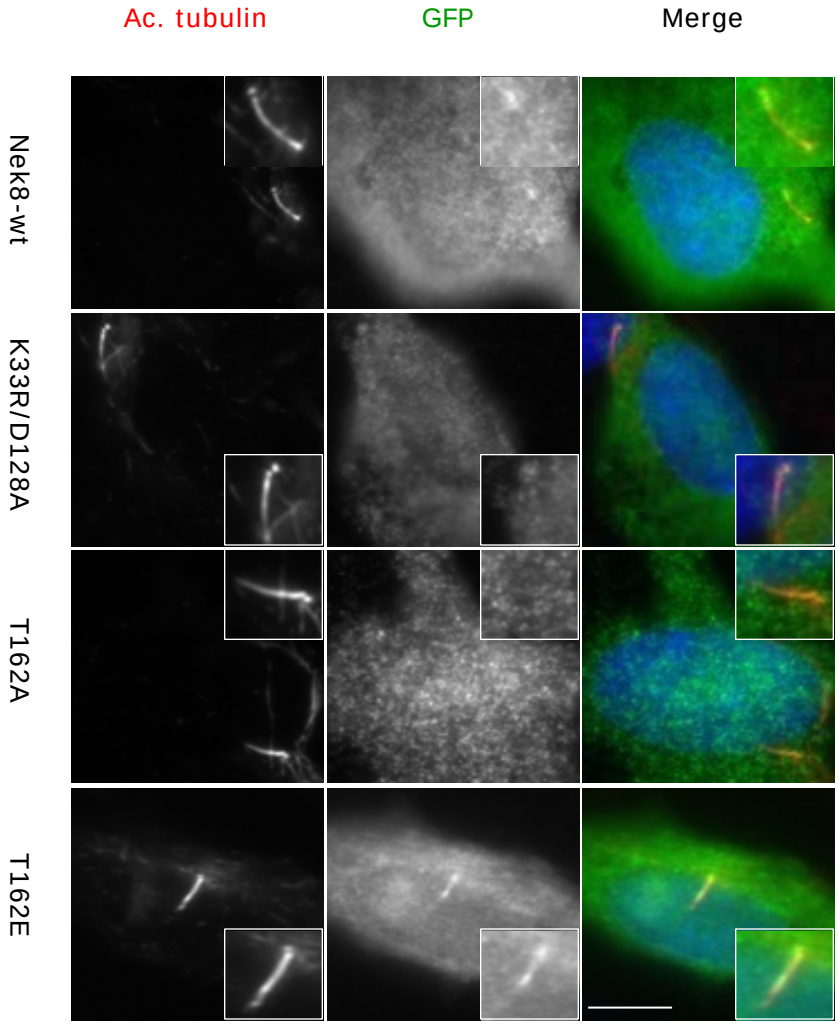

Figure 4.9 Catalytic-site mutants of Nek8 lose localization to the cilia

hTERT-RPE1 cells were transiently transfected for 4 hours with GFP-Nek8 constructs as indicated and were serum starved for 48 hours to promote ciliogenesis. They were then methanol fixed and stained with GFP antibodies to detect the recombinant Nek8 (green in merge) and acetylated tubulin to visualise the cilia (red in merge). DNA was stained with Hoechst 33258 (blue in merge). Insets show enlargements of the cilia. Scale bar, 10 µm.

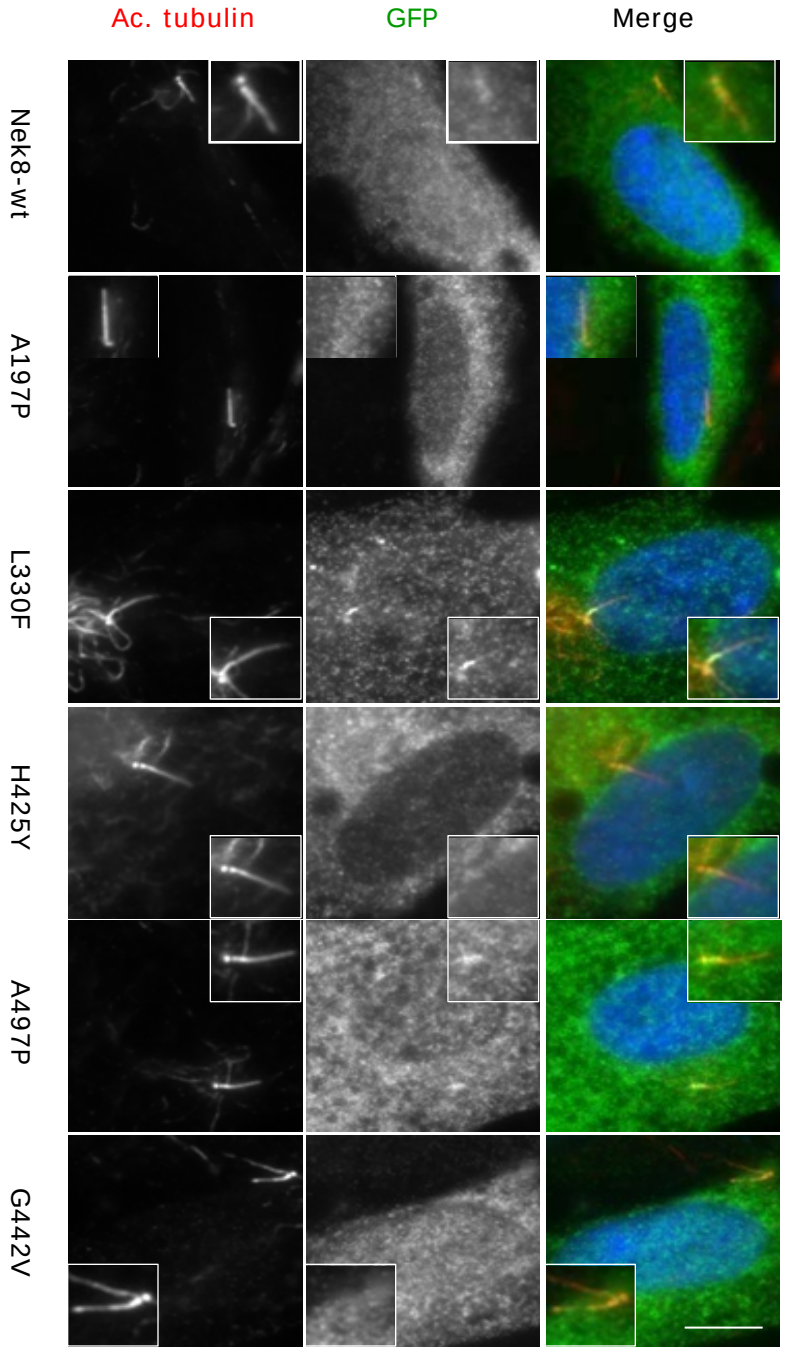

Figure 4.10 Some but not all Nek8 disease-associated mutants fail to localize to the cilia

hTERT-RPE1 cells were transiently transfected for 4 hours with GFP-Nek8 constructs as indicated and were serum starved for 48 hours to promote ciliogenesis. They were then methanol fixed and stained with GFP antibodies to detect the recombinant Nek8 (green in merge) and acetylated tubulin to visualise the cilia (red in merge). DNA was stained with Hoechst 33258 (blue in merge). Insets show enlargements of the cilia. Scale bar, 10 µm.

that the RCC1 domain of Nek8 strongly localized to the proximal region of primary cilia, unlike other truncated fragments (Nek8-FK, Nek8-F1 and Nek-F2) which exhibited reduced ciliary localization (Figures 4.11 and 4.12C). In fact, approximately 20% of cells expressing Nek8-F1 and 23% of Nek8-F2, but only 4% of cells expressing Nek8-FK showed localization to the primary cilia, as compared with 78% of the full-length and Nek8-RCC1 domain. These findings are consistent with the previous data in this chapter showing that the RCC1 domain is required for centrosomal localization.

4.2.7 Localization of Nek8 to the nucleus

Localization studies so far have revealed that Nek8 localizes to the centrosomes and the proximal region of the primary cilia in dividing and serum starved cells, respectively. However, in addition to this, we observed endogenous and recombinant Nek8 proteins localizing to the nucleus as well as cytoplasm in hTERT-RPE1 cells (Figure 4.13A-C).

As result, we next investigated the nuclear translocation of this protein. The drug Leptomycin B (LMB) binds to and inhibits CRM1, an essential protein required for nuclear export of proteins containing nuclear export signals (NES). To test the effects of LMB on the subcellular localization of Nek8, hTERT-RPE1 cells were transiently transfected with GFP-Nek8 and then treated for 6 hrs with LMB, 24 hrs post-transfection. Following fixation in ice-cold methanol, cells were processed for immunofluorescence microscopy with anti-GFP antibodies. In cells treated with LMB, the relative intensity of GFP-Nek8 within nuclei, as compared to the cytoplasm, was significantly increased in comparison to untreated cells, indicating that this protein accumulated in the nucleus in response to LMB treatment (Figure 4.13D). This suggests that Nek8 either has a functional NES that is blocked by LMB or that Nek8 exit the nucleus via interaction with another NES-bearing protein.

We therefore assessed the cytoplasmic-nuclear distribution of the catalytic-site and disease mutant forms of Nek8. To do this, constructs were transiently transfected in dividing hTERT-RPE1 cells for 24 hrs before being fixed and permeabilized using ice cold methanol and processed for immunofluorescence microscopy with anti-γ-tubulin antibodies to mark centrosomes and anti-GFP antibodies to identify GFP-Nek8. Results showed all catalytic-site mutants of Nek8 localized to both the cytoplasm and nucleus (Figures 4.14 and 4.17A), suggesting that Nek8 kinase activity is not important for this distribution. Strikingly, though, the H425Y and

G442V mutants had clearly reduced nuclear localization, with the A197P mutant completely losing Nek8 localization to the nucleus (Figures 4.15 and 4.17B).

From this data we conclude that the H425Y and G442V mutations found in the same RCC1 repeat, together with the A197P mutation, affect localization of Nek8 to the nucleus. This unexpected finding strengthens the importance of these Nek8 disease mutations and suggests that they may interfere with an important role in signalling between the cilia and nucleus.

We then examined the nuclear localization of the truncated forms of Nek8 (FK, RCC1, F1 and F2). Immunofluorescence microscopy analysis revealed that the RCC1 domain alone is sufficient for Nek8 nuclear localization, as more than 80% of cells expressing the Nek8-RCC1 domain showed localization to the nucleus (Figures 4.16 and 4.17C). Similarly, both individual parts of the RCC1 domain, F1 and F2, exhibited nuclear localization. However, this may be due to their small size and thus capability for unrestricted diffusion through nuclear pores. In contrast, the kinase domain alone was predominantly cytoplasmic with less than 20% of cells showing localization to the nucleus (Figures 4.16 and 4.17C).

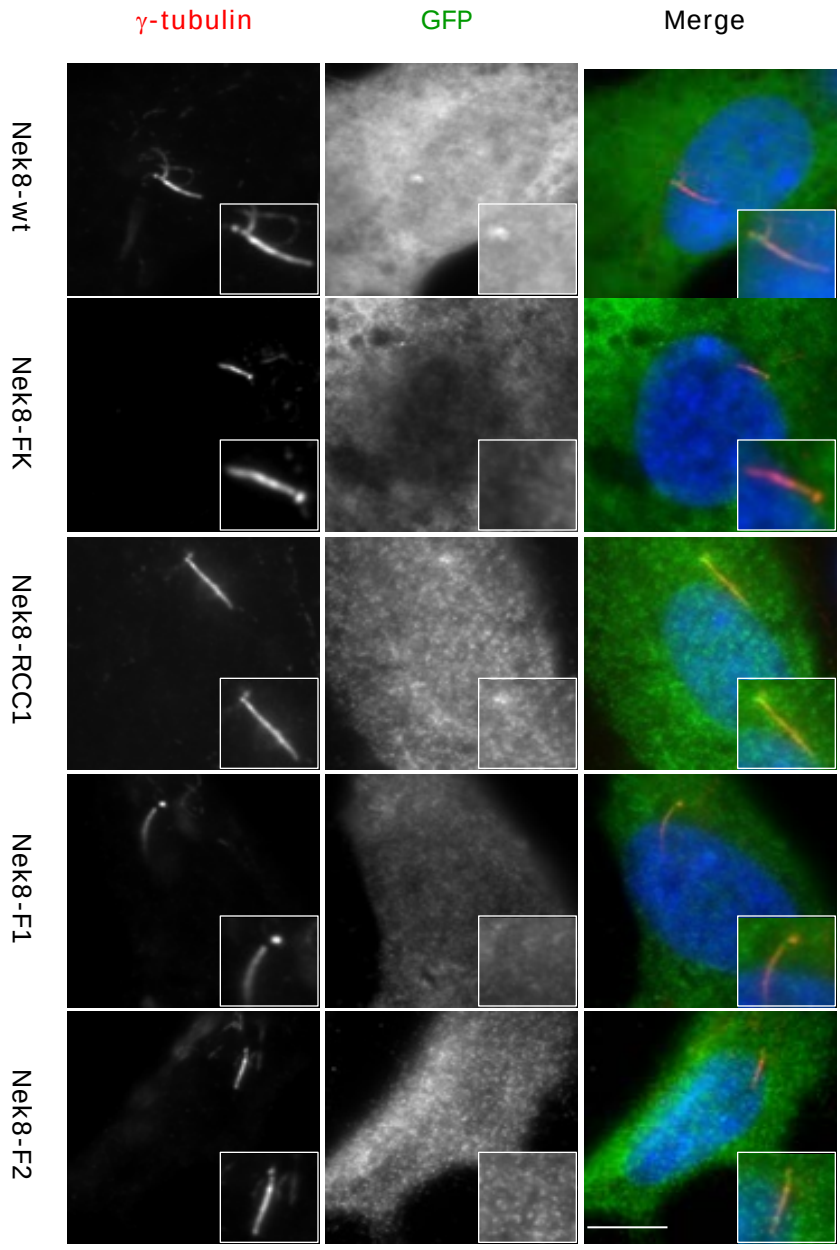

Figure 4.11 The RCC1 domain of Nek8 determines Nek8 ciliary localization

hTERT-RPE1 cells were transiently transfected for 4 hours with GFP-Nek8 truncated constructs and serum starved for 48 hours to promote ciliogenesis. Cells were then methanol fixed and stained with GFP antibodies to detect the recombinant Nek8 (green in merge) and acetylated tubulin to visualise the cilia (red in merge). DNA was stained with Hoechst 33258 (blue in merge). Insets show enlargements of the cilia. Scale bar, 10 µm.

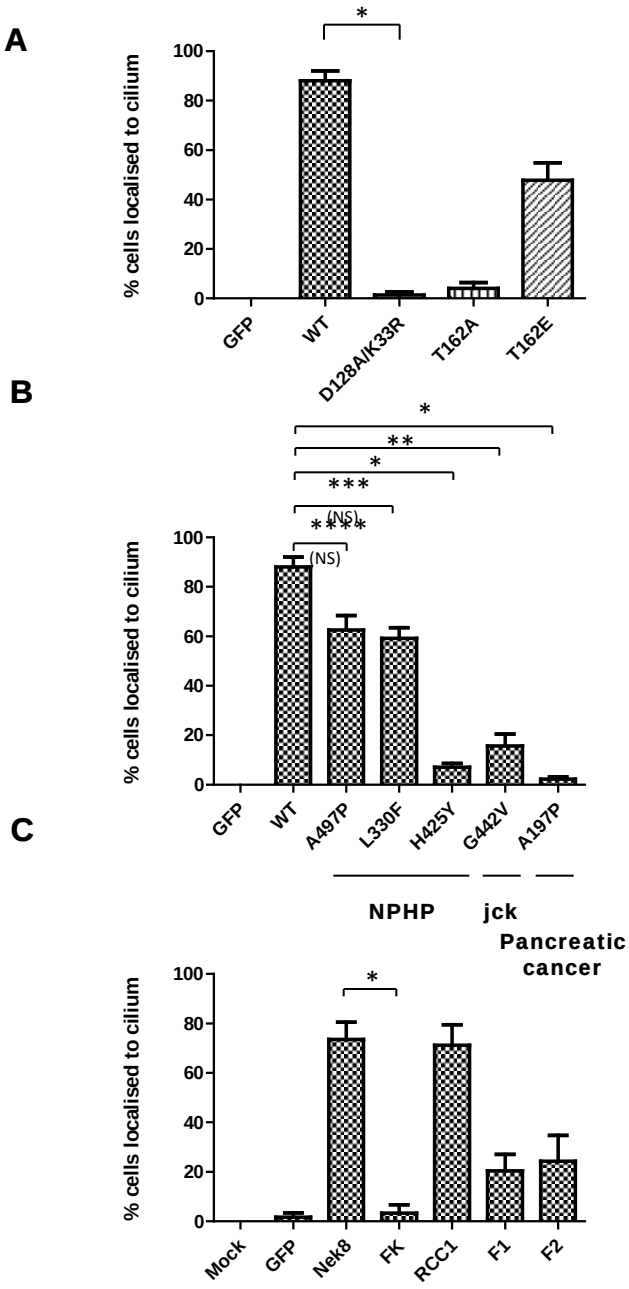

Figure 4.12 Quantification of ciliary localization of Nek8 mutants and truncated Nek8 proteins

Ciliated hTERT-RPE1 cells were quantified for ciliary localization of GFP-Nek8 catalytic-site mutants **(A)**, disease-associated mutants **(B)** and GFP-Nek8 truncated constructs **(C)**. Data represent mean (± S.E.) of three separate experiments where at least 48 cells were counted. P values are shown for specific pairwise comparison (*, $p<0.0001$; **, $p=0.0003$; ***, $p=0.07$, ****, $p=0.08$; NS= non significant.

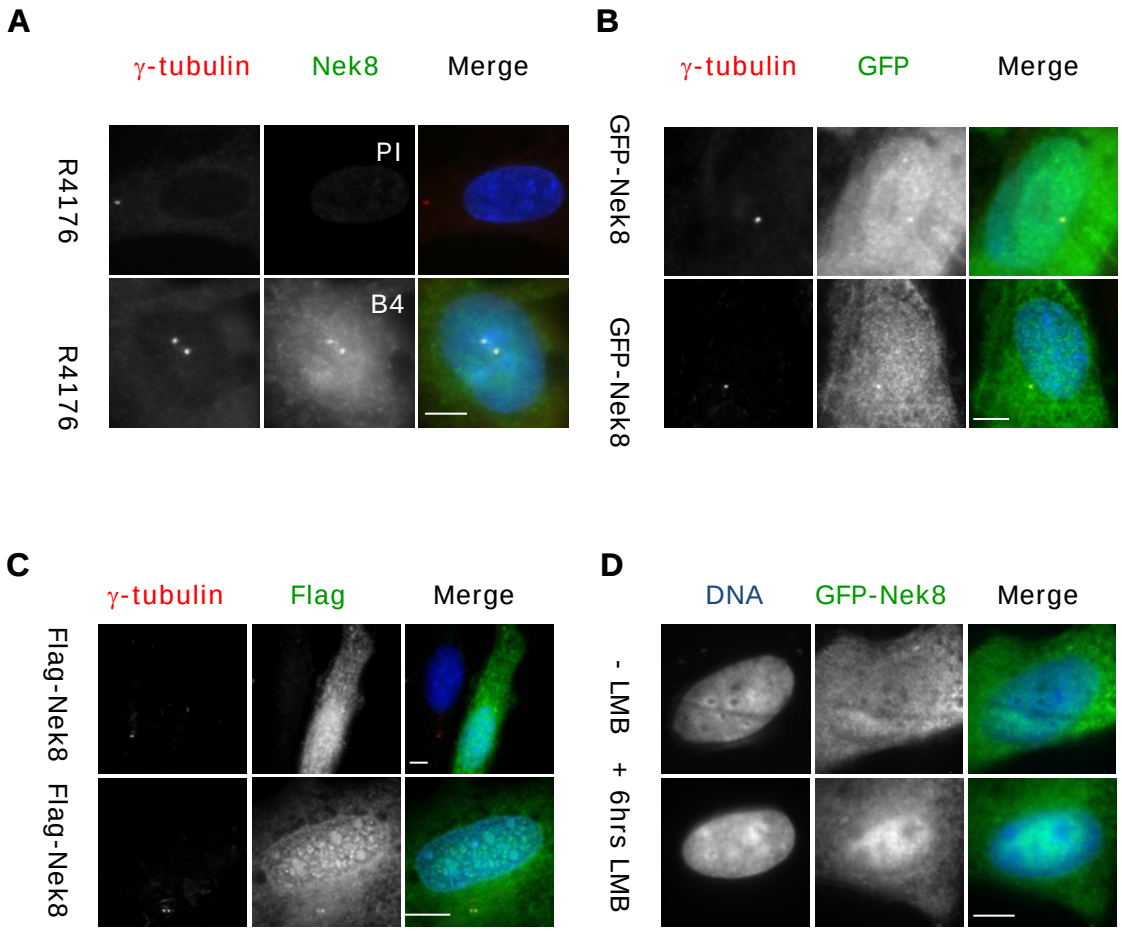

Figure 4.13 Nek8 is also localized to the nucleus and cytoplasm

(A) Untransfected hTERT-RPE1 cells were methanol fixed and stained with Nek8 antibodies to detect endogenous Nek8 (green in merge) and γ-tubulin to detect the centrosome (red in merge). PI, pre-immune sera; B4, antisera from bleed 4. **(B)** hTERT-RPE1 cells were transiently transfected for 24 hours with GFP-Nek8. These were then fixed in methanol and co-stained with GFP antibodies to detect the recombinant Nek8 (green in merge) and γ-tubulin to detect the centrosome (red in merge). **(C)** As for B, expect using Flag-tagged Nek8 and Flag antibodies. **(D)** hTERT-RPE1 cells were transiently transfected with GFP-Nek8 for 24 hours and then treated with leptomycin B (LMB) for 6 hours before being fixed and permeabilize in ice-cold methanol and co-stained with GFP antibodies to detect the recombinant Nek8 (green in merge). DNA was stained with Hoechst 33258 (blue in merge). Scale bars, 10 μm.

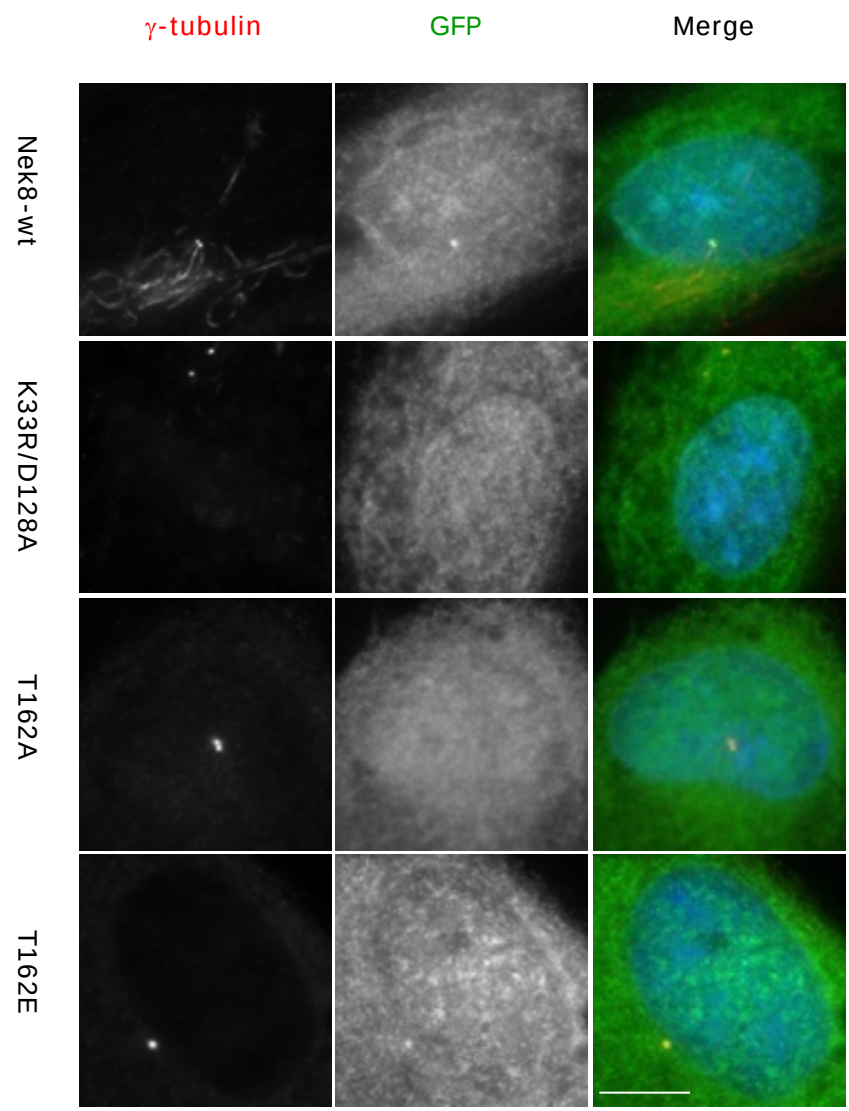

Figure 4.14 Localization of wild-type and catalytic-site mutants of Nek8 to the nucleus
hTERT-RPE1 cells were transiently transfected for 24 hours with GFP-Nek8 constructs as indicated. These were fixed in methanol and co-stained with GFP antibodies to detect the recombinant Nek8 (green in merge) and γ-tubulin to detect the centrosome (red in merge). DNA was stained with Hoechst 33258 (blue in merge). Scale bar, 10 µm.

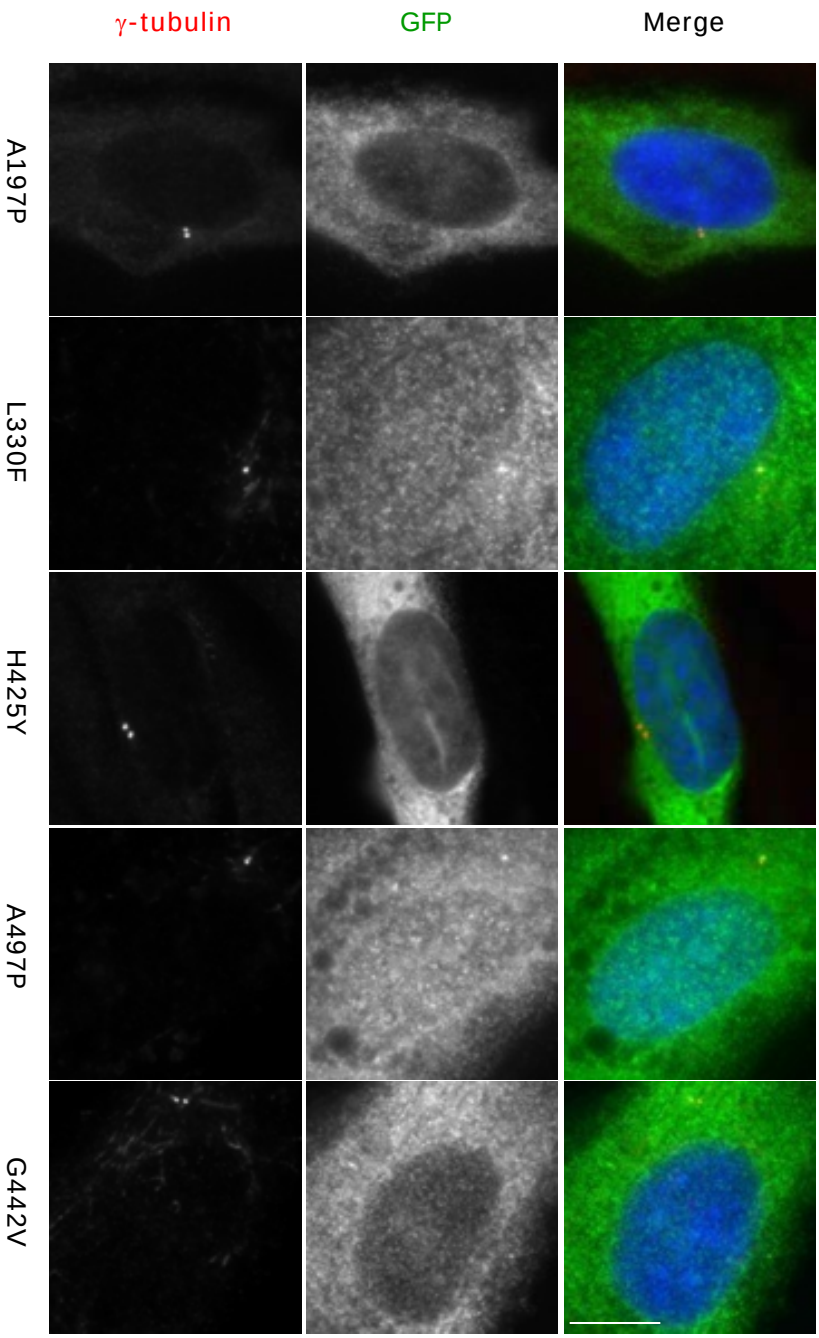

Figure 4.15 Some but not all Nek8 disease-associated mutants fail to localize to the nucleus
hTERT-RPE1 cells were transiently transfected for 24 hours with GFP-Nek8 constructs as indicated. These were fixed in methanol and co-stained with GFP antibodies to detect the recombinant Nek8 (green in merge) and γ-tubulin to detect the centrosome (red in merge). DNA was stained with Hoechst 33258 (blue in merge). Scale bar, 10 µm.

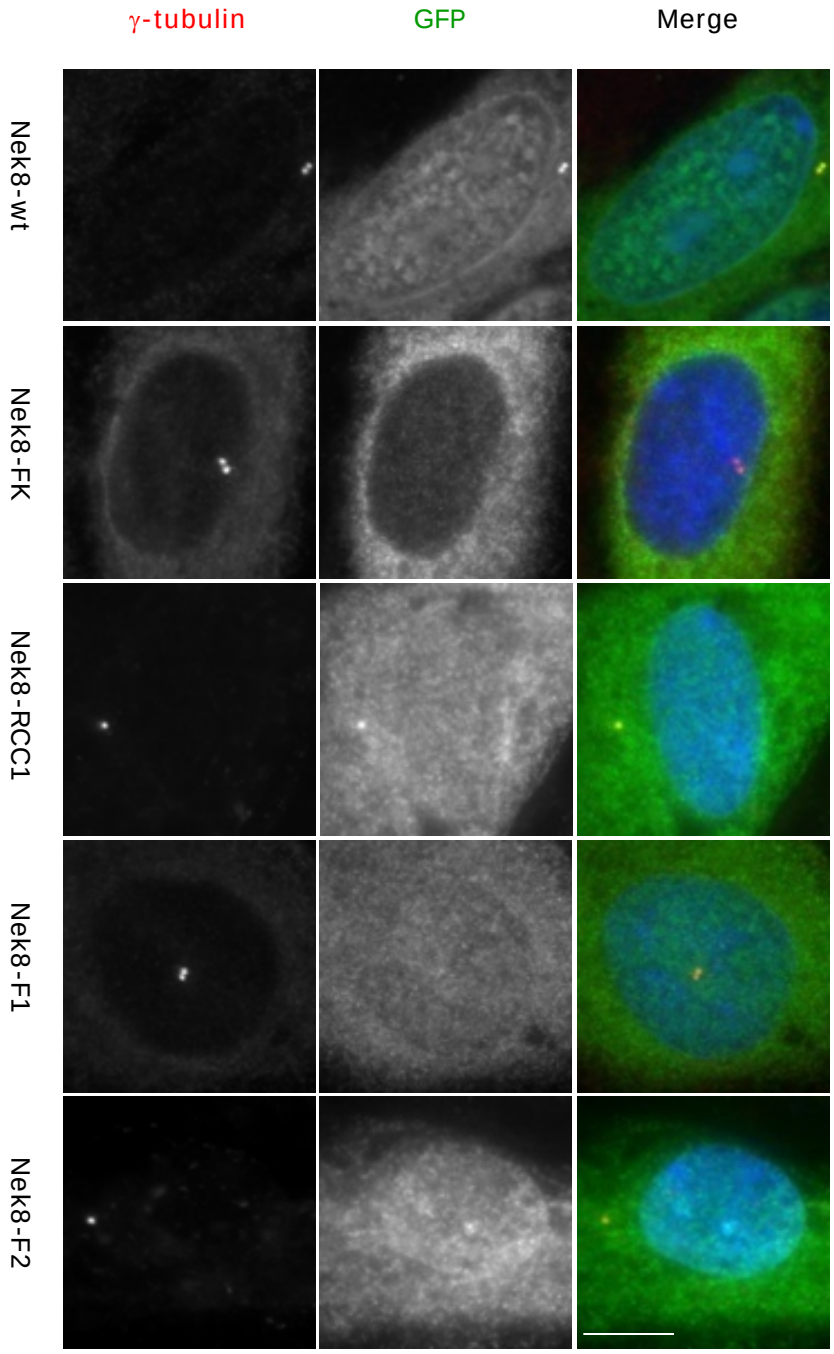

Figure 4.16 The RCC1 domain of Nek8 is required for Nek8 nuclear localization

hTERT-RPE1 cells were transiently transfected with GFP-tagged versions of Nek8. These were co-stained with GFP antibodies to detect the recombinant truncated Nek8 (green in merge) and with γ-tubulin to detect the centrosome (red in merge). DNA was stained with Hoechst 33258 (blue in merge). Scale bar, 10 µm.

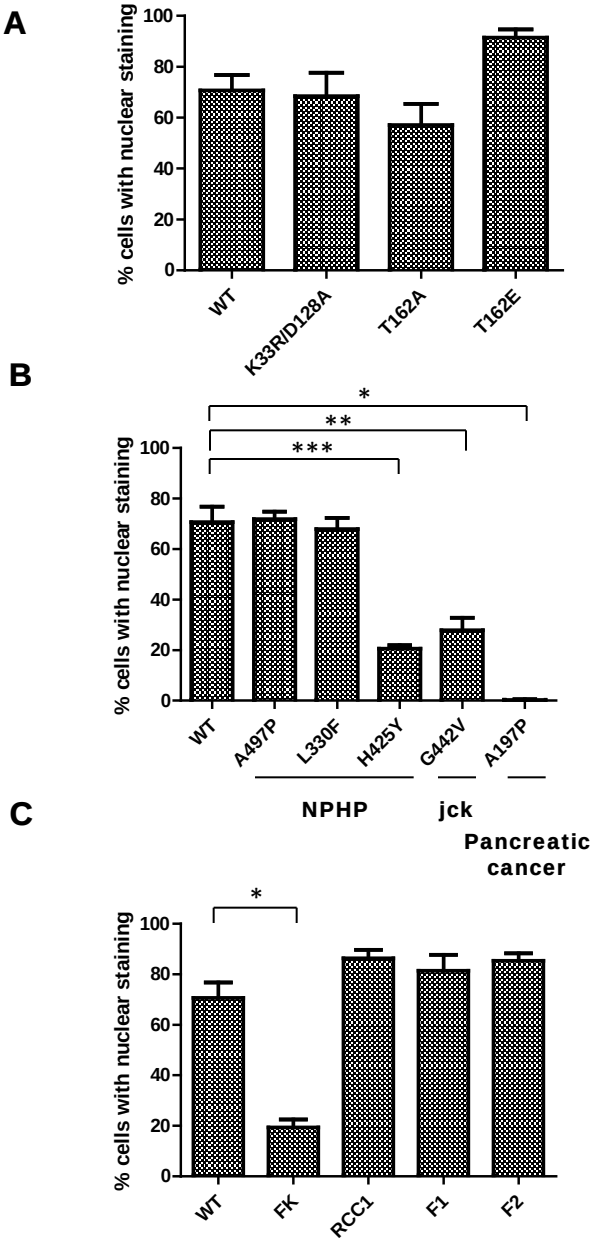

Figure 4.17 Quantification of Nek8 nuclear localization
Dividing hTERT-RPE1 cells were quantified for nuclear localization of GFP-Nek8 catalytic–site mutants **(A)**, disease mutants (*, $p<0.0001$; **, $p=0.005$; ***, $p=0.001$) **(B)** and truncated forms of Nek8 (*, $p=0.0017$) **(C)**. Data represents mean (± S.E.) of three separate experiments where at least 45 cells were counted. P values are shown for specific pairwise comparison.

	Constructs	Centrosome	Cilium	Nucleus	
	WT	+	+	+	
Truncated constructs	FK	-	-	-	
	RCC1	+	+	+	
	F1	-	-	+	
	F2	-	-	+	
Disease-mutants	L330F	+	+	+	Heterozygous
	H425Y*	-	-	-	Homozygous
	A497P	+	+	+	Heterozygous
	G442V*	-	-	-	Homozygous
	A197P	-	-	-	Heterozygous
Kinase-domain mutants	K33R/ D128A	-	-	+	
	T162A	-	-	+	
	T162E	+	+	+	

Figure 4.18 Subcellular localization of truncated and mutant forms of Nek8

L330F, H425Y, A497P (green) are nephronophthisis mutants; G442V (purple) is the jck mouse mutant; A197P (orange) is the pancreatic cancer mutant; K33R/D128A, and T162A (blue) are presumptive kinase-deficient mutants and T162E (blue) is the presumptive kinase-active mutant. Note that L330F, A497P and A197P are heterozygous while the H425Y and G442V are homozygous, and are found in the same RCC1 motif.

4.3 Discussion

A primary cilium is an antenna-like structure extending from the surface of most vertebrate cells. While scientists had long considered the primary cilia to be a functionless vestige, recent work has shown they have important roles in the control of cell proliferation and in signalling pathways during development. In fact, defects in genes that encode proteins associated with the primary cilium, the basal body or the centrosome, give rise to human disorders called ciliopathies (Baker and Beales, 2009; Marshall, 2008). The growing list of ciliopathies includes diseases such as nephronophthisis (NPHP), polycystic kidney disease (PKD), Bardet-Biedl syndrome (BBS), oral-facial digital syndrome type 1 (OFD1) and Joubert syndrome (JBTS) that affect many organ systems (Fliegauf et al., 2007; Satir et al., 2010).

So far, positional cloning has identified eleven genes that when mutated cause nephronophthisis (Hildebrandt et al., 2009; Hildebrandt et al., 1997; Mollet et al., 2002; Olbrich et al., 2003; Otto et al., 2002; Otto et al., 2005; Otto et al., 2003; Saunier et al., 1997). These include Nek8 that has been found to be mutated at three different highly conserved amino acids, L330F, H425Y and A497P in human NPHP patients (Otto et al., 2008). Nek8 is therefore also now referred to as NPHP9. Interestingly, the H425Y mutation is positioned close to the missense mutation, G448V, which causes renal cyst disease in jck mice (Liu et al., 2002).

In the previous chapter, we confirmed using antibodies that we raised to Nek8 that the endogenous Nek8 protein localizes to the centrosome in dividing cells and to the basal body in ciliated cells. Here, we begin to explore the determinants for this localization by examining the localization of a series of mutant Nek8 constructs.

As expected, examination of the subcellular distribution of recombinant GFP or Flag-tagged Nek8 showed that the full-length, wild-type protein, localized to centrosomes and basal bodies in proliferating and ciliated hTERT-RPE1 cells, respectively. Indeed, our results are consistent with recent studies that indicate that Nek8 is restricted to the basal bodies and proximal region of the primary cilia in ciliated cells (Mahjoub et al., 2005; Sohara et al., 2008). Interestingly, other NPHP proteins (NPHP1, NPHP2/inversin, NPHP4, NPHP6, NPHP9, and NPHP11) are also localized to the base of primary cilia (Mollet et al., 2005; Olbrich et al., 2003; Otto et al., 2005; Otto et al., 2008). This may well be orthologous to the transition zone that lies between the basal body and flagellar axoneme in lower eukaryotes such as *Chlamydomonas*. It is thus possible that Nek8 might be one of the

gatekeeper proteins of this ciliary compartment that controls the passage of proteins into the cilium.

We next examined whether this localization pattern was affected in catalytic-site and disease-associated mutant forms of Nek8. Immunofluorescence microscopy revealed that both catalytic-site and disease mutations affected the subcellular localization of Nek8 in both proliferating and ciliated hTERT-RPE1 cells. Firstly, the K33R/D128A and T162A mutations that are expected to lead to loss of kinase activity did not localize to centrosomes or cilia. In contrast, the T162E mutant behaves like the wild-type protein and localized to centrosomes and cilia. This is consistent with studies from Trapp et al. (2008) who found that the K33M mutation also lost centrosomal and ciliary localization in IMCD-3 cells. Together, these data provide persuasive evidence that only an active Nek8 kinase can localize at centrosome and cilia. Dependence on kinase activity for correct subcellular localization to the cilia has also been demonstrated for another family member, Nek1, which carries the causal mutation in the kat (kidney, anemia, testes) mouse model of cystic kidney disease (Smith et al., 2006; Upadhya et al., 2000). Interestingly, this even suggests a functional similarity in the role of Nek1 and Nek8 in ciliogenesis.

Loss of ciliary and centrosomal Nek8 localization was observed for the pancreatic cancer mutant, A197P. It is possible that this mislocalization may alter the kinase activity or uncouple it from regulation, ultimately leading to the pancreatic cancer. Indeed, many cancer associated mutations located at the catalytic domain, such as the Aurora A mutant V174M, mislocalize and alter the kinase activity of the protein (Bibby et al., 2009).

The NPHP-associated mutation, H425Y, and the jck-associated mutation, G442V, also mislocalized, which can explain the disease phenotype. However, the other NPHP-associated mutants, L330F and A497P, did not affect localization to the centrosome or proximal region of the primary cilia, suggesting that if these cause disease, it may be due to loss of function, despite correct localization. This corresponds with data from Otto et al. (2008), who showed reduced ciliary localization only for the mutant construct H431Y, with no ciliary reduction observed in A503P and L336F compared with the wild-type Nek8 in mouse cells. In contrast, the effect of the jck missense mutation on Nek8 localization in mouse is not clear. Confusingly, one study has reported that Nek8 is localized throughout the length of the primary cilia in jck mouse (Sohara et al., 2008), whilst another report showed

loss of Nek8 from primary cilia of cultured kidney cells taken from the jck mouse (Smith et al., 2006). Yet another study has shown the jck mutant protein to localize to centrosomes in IMCD-3 cells (Otto et al., 2008). We show that in dividing or ciliated hTERT-RPE1 cells, the GFP-Nek8-G442V mutant does not localize to the centrosome or cilia. These discrepancies may result from differences in cell type or differentiation status, or possibly levels of expression. The fact that both the H425Y and G442V mutations are positioned within the same RCC1 repeat of human Nek8, and both lead to loss of centrosomal and ciliary localization in our hands, underlines the importance of this specific region of the protein for correct subcellular localization.

There are a number of possible explanations for this result. The first is that this region of the RCC1-like domain is required for Nek8 kinase activity. Alternatively, it may form part of a targeting motif that enables interaction with other core centrosomal proteins. These mutations could of course also lead to misfolding of the Nek8 protein. We therefore looked at the localization of isolated Nek8 domains. We found that the RCC1-like domain alone is sufficient for localization to the cilia and centrosome, whereas each part of the RCC1 domain, F1 and F2 alone, and the kinase domain alone, are not. Since the RCC1-like domain is likely to fold into a beta-propeller structure, then one can imagine that the F1 and F2 fragments would not fold properly, which explains their mislocalization. However, the mislocalization of the kinase domain alone is difficult to reconcile with our earlier findings that Nek8 kinase activity plays a crucial role for Nek8 localization to centrosomes and cilia. Clearly, our data suggests that both kinase activity, as well as the RCC1-like domain, contribute to the correct localization of Nek8. Identifying proteins that interact with Nek8 will give us more insights into how the G442V and H425Y mutations alter the localization of Nek8 and why both the kinase activity as well as the RCC1-like domain is required for correct Nek8 localization in cells. More fundamentally, identifying interacting partners of Nek8 will help to specify the role of Nek8 in cilia.

Apart from ciliary and centrosomal localization of Nek8, we also observed Nek8 localizing to the nucleus both in proliferating and ciliated hTERT-RPE1 cells. This is not entirely unexpected since some ciliary proteins, for example those involved in the non-canonical Wnt signalling pathway, are known to traffic to the nucleus and alter transcriptional programmes. Indeed, in this study we also identified the RCC1-like domain as responsible for nuclear localization as the kinase domain alone was cytoplasmic. Again, this suggests that the RCC1-like domain interacts

with proteins involved in nuclear trafficking. What is surprising, however, is that those Nek8 mutations that lead to loss of centrosomal and ciliary localization (i.e. A197P, H425Y and G442V), also lead to loss of nuclear localization. However, in this case kinase activity is not required and the kinase domain mutants localized to the nucleus similar to the wild-type protein. Intriguingly, it is possible that nuclear localization of Nek8 is controlled by Ran through interaction with the Nek8 RCC1-like domain. This might explain why the mutants, H425Y and G442V, lose nuclear localization. This hypothesis is also supported by Dishinger et al. (2010) who speculate that there may be potential similarities between the ciliary gateway and the nuclear pore complex that regulates nuclear entry via a nuclear-cytoplasmic gradient of the small GTP-ase Ran. Ran is also found in cilia and might regulate the targeting of Nek8 to cilia via a similar ciliary-cytoplasmic gradient (Dishinger et al., 2010). To test this possibility, direct interaction studies would be required between Nek8 and Ran proteins.

Chapter 5

Nek8 kinase is activated upon serum starvation

5.1 Introduction

So far, our studies have shown that expression of Nek8 mutants whose kinase activity is expected to be compromised results in aberrant localization of Nek8; this falls in line with results from Mahjoub et al. (2005). We have also seen that certain disease-associated mutants are mislocalized but not others. This could reflect a difference in kinase activity of these mutants. However, confirmation of this hypothesis is hampered by the lack of activity data. To overcome this problem we wished to establish conditions for measurement of Nek8 catalytic activity and then use this assay to measure activity of the kinase-domain mutants, the disease-associated mutants and the truncated forms of Nek8. This would be a very important step in understanding the mechanisms by which Nek8 is regulated and dissecting the underlying role of Nek8 in ciliogenesis and cystic kidney disease in humans. Furthermore, to better understand these mechanisms, I also attempted to identify biological substrates of Nek8.

One of the principle regulatory mechanisms in eukaryotic cells is post-translational modification of proteins. Protein phosphorylation in particular, is one of the most important and well-studied post-translational modifications and plays critical roles in the regulation of many cellular processes including cell cycle control, growth, apoptosis and differentiation (Meng et al., 2008). Protein phosphorylation is catalyzed by protein kinases, whilst dephosphorylation is catalyzed by protein phosphatases. However, these enzymes themselves are subject to regulatory phosphorylation events. For example, in many kinases, phosphorylation occurs within a particular loop in the catalytic domain known as the activation loop (also called the T-loop). This consists of a flexible region of 20-25 amino acids whose beginning and end are typically marked by conserved DFG and APE motifs (Johnson et al., 1996). Phosphorylation of residues within the activation loop can lead to activation of the kinase by either stabilizing the active conformation or destabilizing the inactive conformation, thus ensuring the correct positioning for substrate binding and phosphate transfer to occur (Johnson et al., 1996). This was first described in protein kinase A (PKA) in which this loop spans amino acids 184 to 208 and includes Thr-197 which serves as an autophosphorylation site. Since then, many other protein kinases have been identified which are activated by phosphorylation of their T-loop residues. Examples of these kinases include Plk1, Pak1 and Nek6, which are activated by phosphorylation of T210, T212, and S206, respectively (Belham et al., 2003; Jang et al., 2002; Mattison et al., 2007). Similar to these kinases, Nek8 contains a threonine, T162, within its T-loop that may be subject to phosphorylation.

This explains why we had used a mutagenesis approach to test the potential role of T162 in Nek8 localization. We had also generated a mutant that changed two crucial residues in the catalytic site, K33R and D128A. This putative inactive mutant would act as a control in our establishment of the assay for Nek8 activity.

The aim of this chapter was therefore to establish conditions for measuring the kinase activity of recombinant Nek8 protein expressed in cultured cells and use these to measure the activity of potentially deficient Nek8 mutants. Finally, we would examine whether there was any change in Nek8 activity during the process of ciliogenesis.

5.2 Results

5.2.1 Establishment of an assay for Nek8 protein kinase activity

To date, the kinase activity of Nek8 has not been reported and its substrates have not been identified. As we wanted to explore the mechanism of Nek8 regulation and how kinase activity might be important for Nek8 function, we first needed to establish conditions under which Nek8 activity could be measured. For this purpose, we began by performing an in vitro kinase assay using a commercial source of purified GST-tagged Nek8 kinase expressed in wheat germ extract that was available from Abnova Corporation. To provide the first set of clues as to its kinase activity and substrates, we decided to take a broad analysis testing different conditions and substrates. With regard to substrates, *Aspergillus* NIMA, as well as most known mammalian Neks, phosphorylate β-casein in vitro (Fry et al., 1995; Letwin et al., 1992; Lu et al., 1993; Minoguchi et al., 2003; Osmani et al., 1991). Indeed, Nek6 and Nek7 have been reported to phosphorylate β-casein, whereas Nek9 whilst still able to phosphorylate β-casein, has been shown to phosphorylate MBP and different histones more strongly (Roig et al., 2002).

However, in contrast to NIMA kinase activity which requires Mg^{2+} in order to coordinate the ATP, the mammalian Neks tend to have a preference for Mn^{2+} (Fry et al., 1995; Holland et al., 2002; Letwin et al., 1992; Minoguchi et al., 2003), although the kinase activity of some Neks is activated using both Mg^{2+} and Mn^{2+}. Here, in order to establish our own assays, β-casein, histone H1 and MBP were tested as substrates for Nek8 kinase activity in the presence of either Mg^{2+} or Mn^{2+} divalent cations.

GST-Nek8 was first incubated in a kinase buffer containing β-casein, histone H1 or MBP as a substrate incubated with ^{32}P-γ-ATP for 30 min at 30^{o}C. Analysis of substrate phosphorylation by SDS-PAGE, Coomassie Blue staining and autoradiography demonstrated that whilst Nek8 could phosphorylate all three substrates in the presence of 4 μM ATP, histone H1 and MBP are the best substrates for Nek8 kinase (Figure 5.1A and B). In attempts to increase the amount of substrate phosphorylation by Nek8, we tested whether preincubating the purified Nek8 protein with cold ATP would activate the kinase. The related kinase, Nek9, which is structurally very similar to Nek8, was shown to require pre-incubation with ATP to activate the kinase, presumably by autophosphorylation, before it was capable of phosphorylating exogenous substrates (Roig et al., 2002). In the case of Nek8, though, we did not find that pre-incubation of the commercial

kinase with ATP significantly changed its activity towards these proteins (Figure 5.2A and B).

5.2.2 Assay for Nek8 activity from transfected cells

We then moved on to measure the kinase activity of recombinant GFP-tagged Nek8 expressed in HEK293 cells. As controls, we generated two different mutants; the first, Nek8-K33R/D128A, had changes in two key catalytic residues that we predicted would lead to loss of activity, and the second, Nek8-T162E, which would be constitutively active if phosphorylation of T162 in the Nek8 activation loop is sufficient to activate the kinase.

GFP-tagged wild-type Nek8 and K33R/D128A were expressed in HEK293 cells for 24 hrs after which cell lysates were prepared. Samples of the lysates were analyzed by SDS-PAGE and Western blotting with anti-GFP antibodies, and 20 µg of total protein lysate was then subjected to immunoprecipitation with anti-GFP antibodies. To confirm successful immunoprecipitation, samples of the immune complexes were analyzed by SDS-PAGE and Western blotting with anti-GFP antibodies. The remaining immune complexes were then used in a kinase assay with histone H1 as substrate. Analysis of histone H1 phosphorylation by SDS-PAGE, Coomassie Blue staining and autoradiography demonstrated similar levels of phosphorylation with both the wild-type and kinase deficient K33R/D128A Nek8 in the presence of either Mg^{2+} or Mn^{2+} divalent cations (Figure 5.3A and C). However, kinase assays using purified GST-Nek8 indicated that despite phosphorylating histone H1 in the presence of either Mg^{2+} or Mn^{2+}, there was a 5-fold increase in the phosphorylation of histone H1 in the presence of Mg^{2+} compared with Mn^{2+} divalent cations, suggesting that unlike other Nek kinases, Nek8 tends to have a preference for Mg^{2+} cations (Figure 5.4). The fact that similar levels of phosphorylation with both the wild-type and kinase deficient K33R/D128A Nek8 were observed from Nek8 immunoprecipitates, indicates that this kinase activity is most likely not due to Nek8 but to a contaminating protein kinase. In contrast, GFP-Nek7 but not the inactive mutant, Nek7-K75M, strongly phosphorylated β-casein (Figure 5.3B).

We therefore made a number of changes to our assay system to try and identify specific Nek8 activity. We started by washing the Protein G coupled to sepharose beads more extensively during the immunoprecipitation of Nek8. Immunoprecipitation was also carried out overnight, instead for 2 hrs; this resulted in more Nek8 protein being precipitated. We avoided freeze-thaw cycles during the

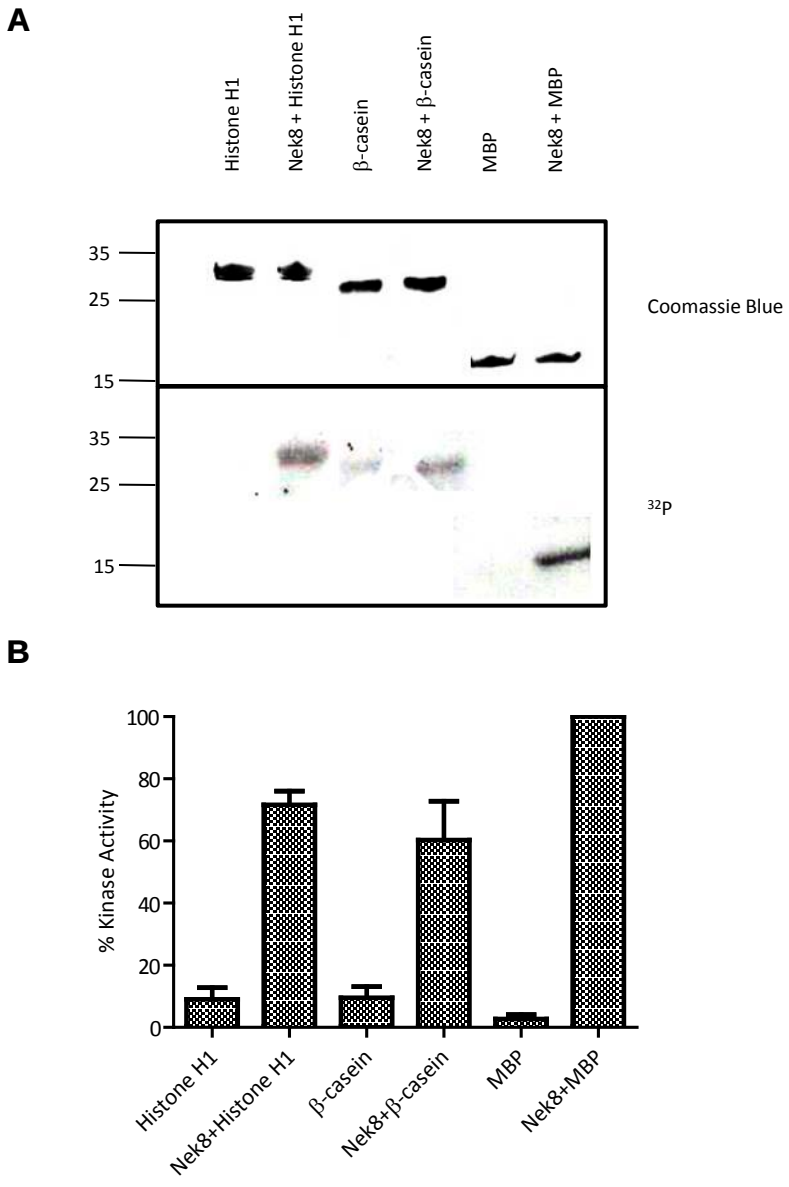

Figure 5.1 Activity of commercial GST-Nek8 against model substrates

(A) The kinase activity of commercial GST-Nek8 was tested by incubation with histone H1, β-casein or MBP and [γ^{32}P]-ATP at 30°C for 30 min. Samples were analyzed by SDS-PAGE, Coomassie Blue staining and autoradiography (^{32}P). Molecular weights (kDa) are shown on the left. **(B)** Scintillation counting was used to determine the kinase activity of Nek8 against the different substrates relative to phosphorylation of MBP. Data represent means (± S.E.) of three separate experiments.

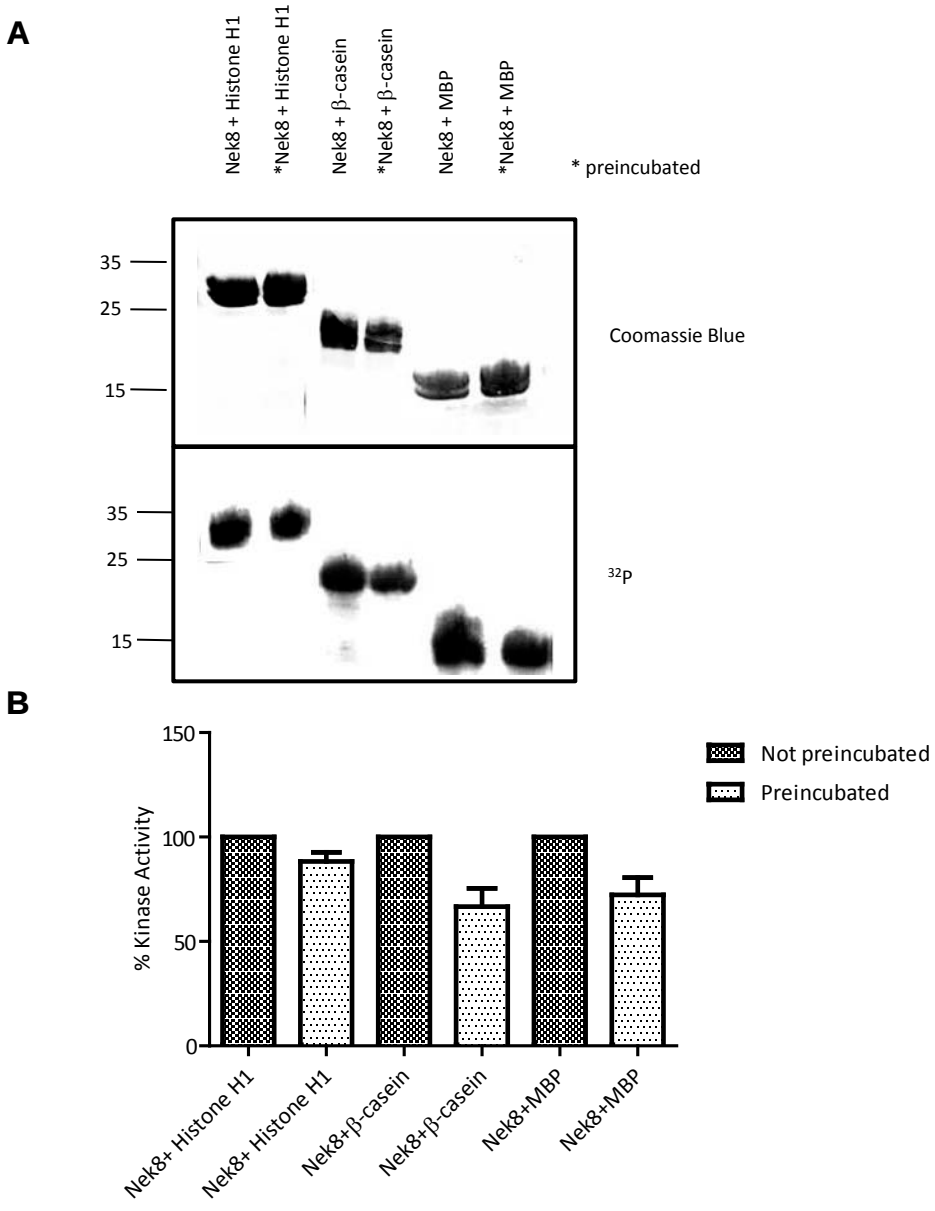

Figure 5.2 Preincubation with ATP does not increase Nek8 kinase activity

(A) To observe whether preincubation with ATP increases the kinase activity of Nek8, purified GST-Nek8 was incubated with or without 4 μM ATP for 1 hour at 25°C in phosphorylation buffer. Kinase assays were then initiated by the addition of [γ^{32}P]-ATP and either histone H1, β-casein or MBP. After 1 hour at 30°C, ^{32}P incorporation was stopped by addition of SDS sample buffer. Reactions were analysed by SDS-PAGE, Coomassie Blue staining and autoradiography (^{32}P). Molecular weights (kDa) are shown on the left. **(B)** Scintillation counting was used to determine the kinase activity of Nek8 against the different substrates relative to phosphorylation of histone H1. Data represent means (± S.E.) of three separate experiments.

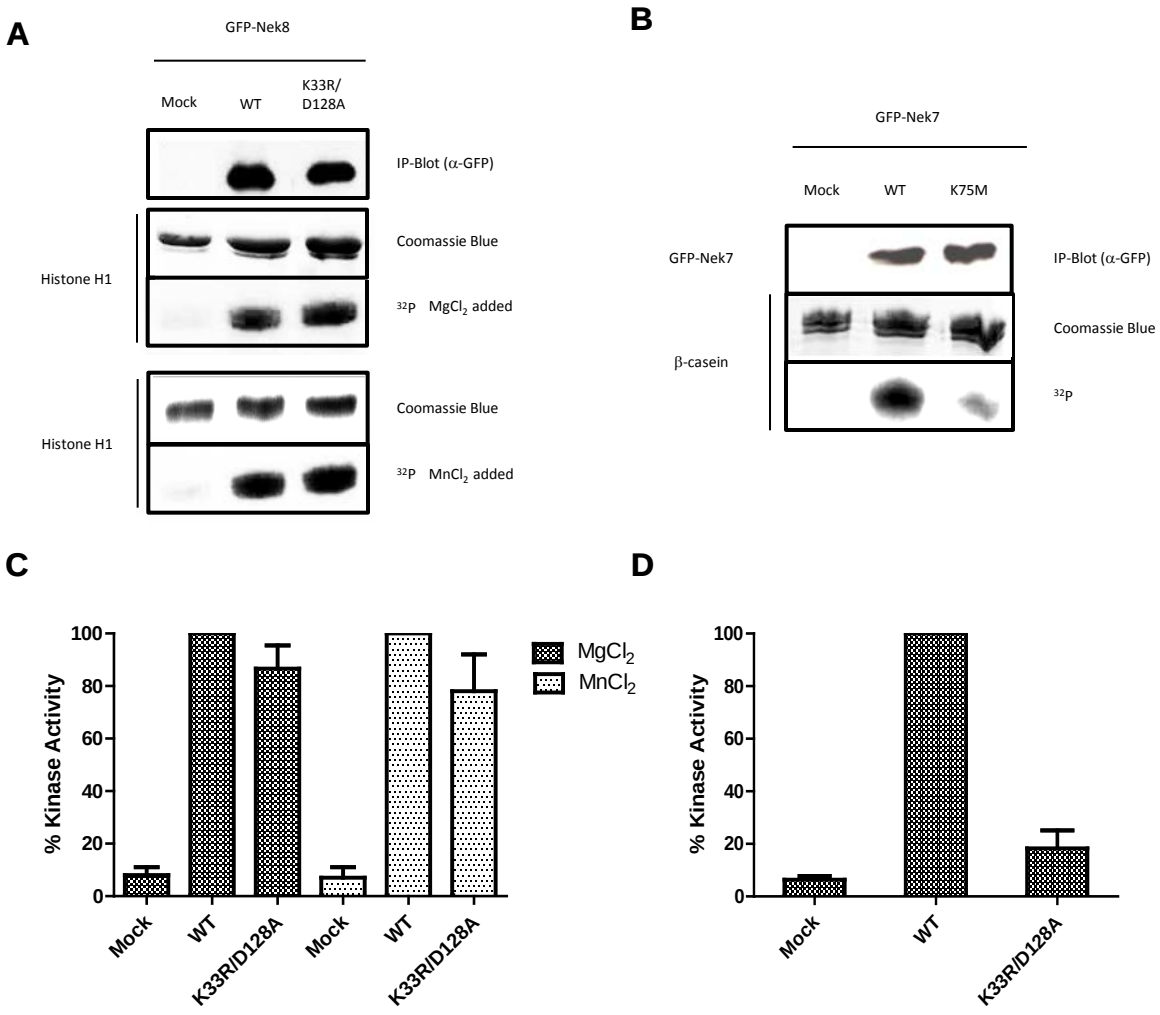

Figure 5.3 Lack of specificity of Nek8 activity in early assays
HEK293 cells were either mock transfected or transiently transfected with GFP-tagged Nek8 **(A)** or GFP-tagged Nek7 **(B)** for 24 hours before cells were lysed and subjected to immunoprecipitation with anti-GFP antibodies. The amount of kinase precipitated was determined by Western blot with anti-GFP antibodies (IP-Blot) and the immunoprecipitates used for kinase assays. The ability of Nek8 to phosphorylate histone H1 with Mn^{2+} or Mg^{2+} as a cofactor was tested. Proteins were incubated in kinase buffer containing Mn^{2+}-[γ^{32}P]-ATP or Mg^{2+}-[γ^{32}P]-ATP for 30 min at 30°C and analyzed by SDS-PAGE, Coomassie Blue staining and autoradiography (^{32}P). For GFP-Nek7, it has previously been established that this phosphorylates β-casein in the presence of Mn^{2+}. In each case, a protein carrying mutations in key catalytic residues (K33R/D128A for Nek8, and K75M for Nek7) was used as a negative control. Percentage activity of the GFP-Nek8 protein with the Mn^{2+} cofactor and Mg^{2+} cofactor **(C)** and of GFP-Nek7 **(D)** is shown. Data represent means (±S.E.) of three separate experiments.

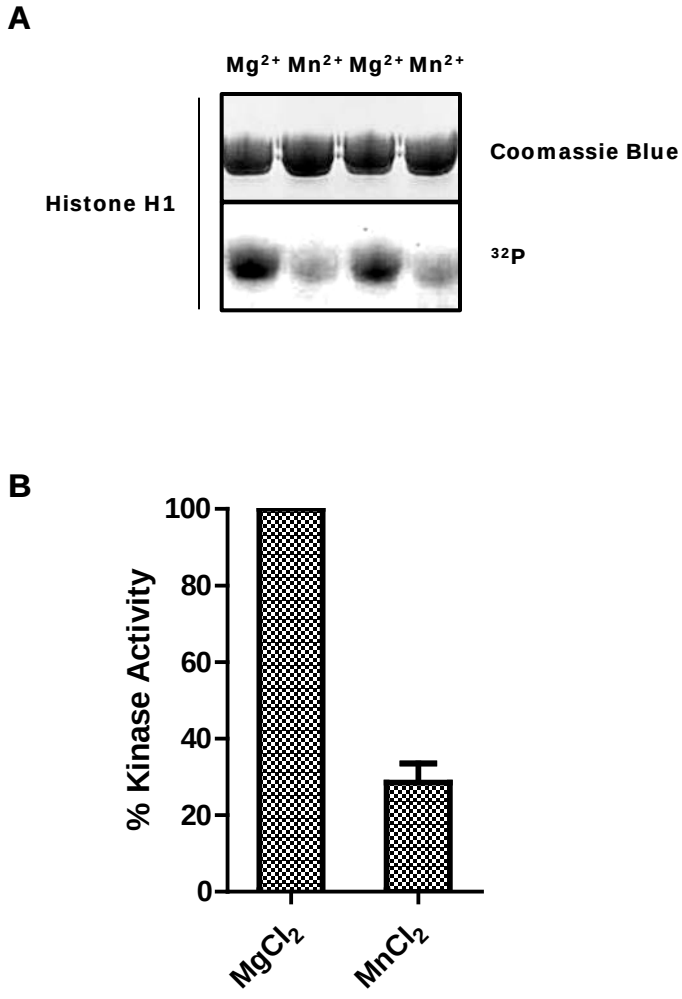

Figure 5.4 Activity of commercial GST-Nek8 with divalent cations

The ability of commercial GST-Nek8 to phosphorylate histone H1 with Mn^{2+} or Mg^{2+} as a cofactor was tested. Proteins were incubated in kinase buffer containing Mn^{2+}-[γ^{32}P]-ATP or Mg^{2+}-[γ^{32}P]-ATP for 30 min at 30°C and analyzed by SDS-PAGE, Coomassie Blue staining and autoradiography (^{32}P). **(B)** Scintillation counting was used to determine the kinase activity of Nek8 against histone H1 with Mn^{2+} relative to Mg^{2+}. Data represent means (± S.E.) of six separate experiments.

immunoprecipitation that had been present in previous experiments, and we washed the immunoprecipitates more extensively in kinase buffer before the kinase reaction. Importantly, we ensured that samples remained on ice throughout the immunoprecipitation, thus preserving Nek8 kinase activity. Under these reaction conditions, we then re-tested the kinase activity of Nek8 using either β-casein, histone H1 or MBP as substrates. Analysis of substrate phosphorylation by SDS-PAGE, Coomassie Blue staining and autoradiography demonstrated that wild-type Nek8 phosphorylated all three substrates. Similarly, the active mutant T162E phosphorylated all three substrates to a greater extent than wild-type Nek8. In contrast, the double mutation K33R/D128A showed almost no kinase activity against histone H1, and very little activity against β-casein. However, MBP was phosphorylated to a similar extent by the inactivated and wild-type Nek8 (Figure 5.5B and C). A possible explanation of this result is that immunoprecipitation of Nek8 may pull down other kinases that are able to phosphorylate MBP better than histone H1 and β-casein. Therefore, all further assays were performed with histone H1 as a substrate for Nek8.

5.2.3 NPHP disease mutants of Nek8 are active

We then used this assay to determine the kinase activity of the three NPHP disease mutants of Nek8, L330F, H425Y and A497P, previously identified in an analysis of 188 NPHP patients (Otto et al., 2008). These had been generated as GFP-tagged full-length Nek8 constructs for expression in cells. In addition, we had generated a Nek8-G442V mutation, which was equivalent to the G448V mutation identified in *jck* mice, an A197P mutation, which is an amino acid change reported as a potential driver mutation in pancreatic cancer (Carter et al., 2010), and a T162A mutation to block phosphorylation at this site within the activation loop. Following transient expression in HEK293 cells, these proteins were immunoprecipitated with anti-GFP antibodies before immune complexes were used in kinase assay with histone H1 as substrate. For controls, wild-type and the catalytically-inactive mutants (Nek8-K33R/D128A and T162A) were compared alongside. All the NPHP disease mutants, as well as the jck equivalent mutation, G442V, exhibited similar activity to the wild-type protein (Figure 5.6A and B). The A197P pancreatic cancer mutant had slightly reduced activity; in contrast the T162A mutant was completely inactive. This was surprising given that some of these mutants, A197P, H425Y and G442V, were mislocalized and that we had shown activity is a key determinant of Nek8 localization. These data suggests that mislocalization is rather a result of disruption of the centrosome targeting motif present in the RCC1 domain. We conclude that Nek8 activity is most likely regulated through activation loop

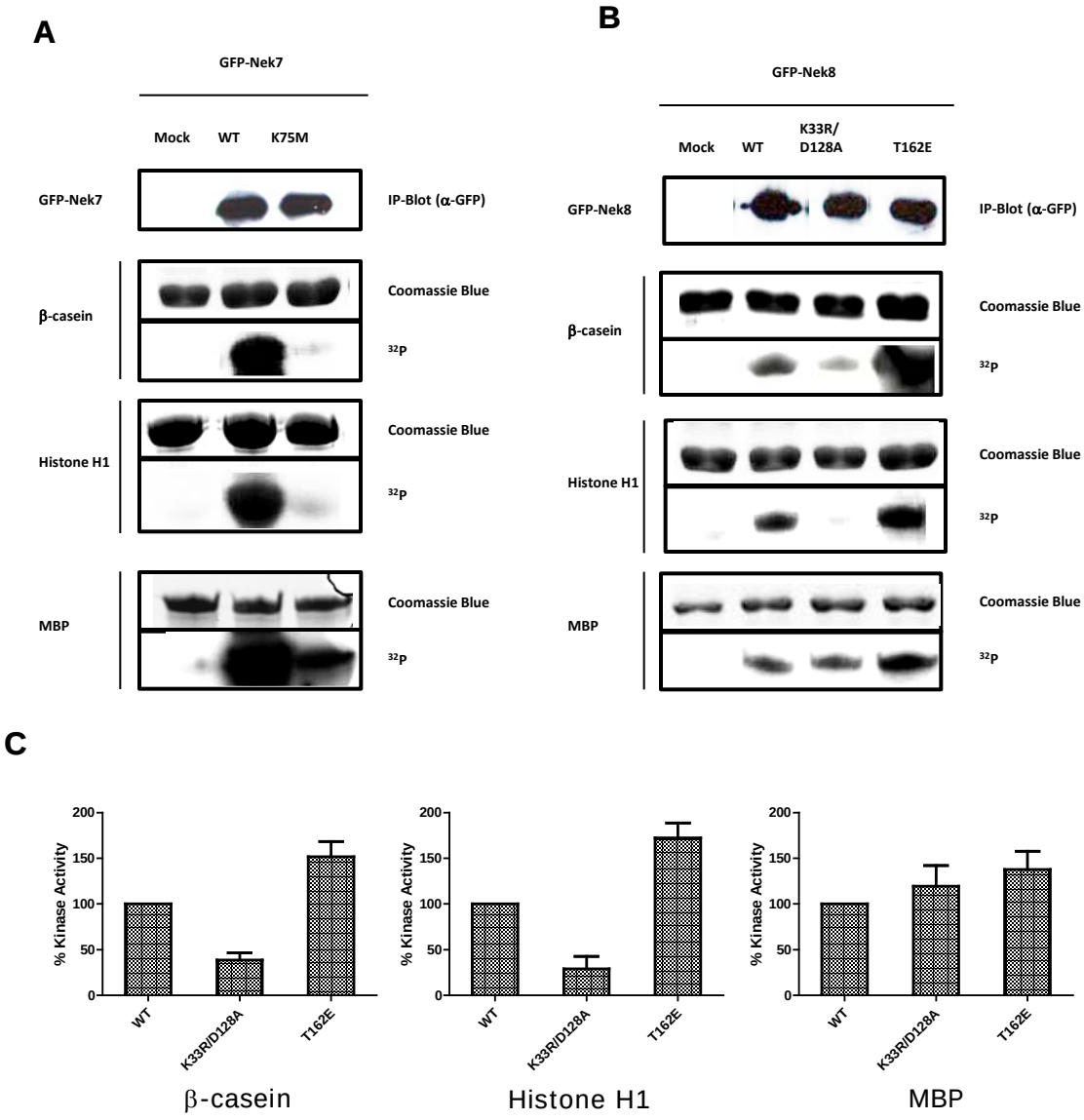

Figure 5.5 Detection of specific Nek8 activity verses β-casein and histone H1

HEK293 cells were either mock transfected or transiently transfected with GFP-tagged Nek7 **(A)** or Nek8 **(B)** for 24 hours before cells were lysed and subjected to immunoprecipitation with anti-GFP antibodies. The amount of kinase precipitated was determined by Western blot with anti-GFP antibodies (IP-Blot) and the immunoprecipitates used for kinase assays with β-casein, histone H1 or MBP as substrates. Inactive mutants as described in Fig. 5.3 were included as indicated. Samples were analyzed by SDS-PAGE, Coomassie Blue staining and autoradiography (^{32}P). **(C)** The kinase activity of the Nek8 proteins relative to the wild-type against the different substrates are shown. Data represent means (± S.E.) of three separate experiments. Differences in assay conditions from those used in Fig. 5.3 are explained in the text.

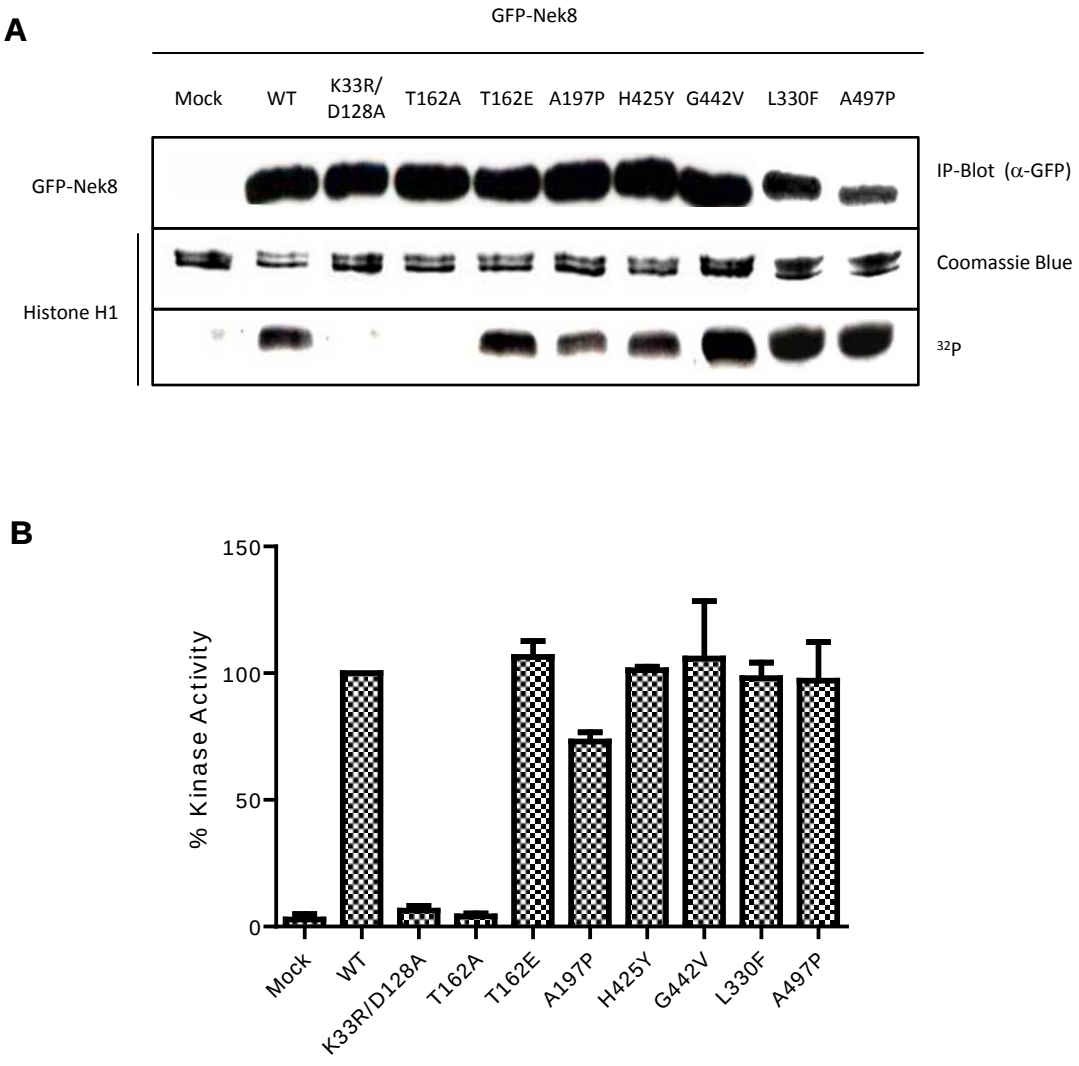

Figure 5.6 Nek8 disease mutants are active
HEK293 cells were either mock transfected or transiently transfected with the GFP-tagged Nek8 wild-type protein or the Nek8 kinase domain and disease mutants for 24 hours before cells were lysed and subjected to immunoprecipitation with anti-GFP antibodies. The amount of kinase precipitated was determined by Western blot with anti-GFP antibodies (IP-Blot) and the immunoprecipitates used for kinase assays with histone H1 as a substrate. Samples were analyzed by SDS-PAGE, Coomassie Blue staining and autoradiography (^{32}P). **(B)** The kinase activity of the mutant Nek8 proteins relative to the wild-type protein are shown. Data represent means (± S.E.) of three separate experiments.

phosphorylation and that the NPHP disease mutants identified to date do not lead to loss of kinase activity.

5.2.4 Kinase activity of Nek8 truncated fragments

Having determined the relative activities of the Nek8 disease-associated mutants, we then examined the kinase activity of the isolated catalytic, Nek8-FK, and non-catalytic, Nek8-RCC1, domains. To this end, GFP-tagged truncated Nek8 constructs were expressed in HEK293 cells for 24 hrs, cells were lysed and recombinant proteins immunoprecipitated with anti-GFP antibodies before immune complexes were used in kinase assays with histone H1 as substrate (Figure 5.7). The Nek8-FK fragment phosphorylated histone H1 and exhibited kinase activity to a similar level as the Nek8- wild-type protein. In contrast, the Nek8-RCC1 domain did not show kinase activity and was unable to phosphorylate histone H1 (Figure 5.7A and B). Hence, we conclude that the kinase domain alone is active and appears not to be inhibited or activated by the RCC1 domain.

5.2.5 Nek8 phosphorylates the RCC1 domain

Identification of physiological substrates of any kinase is key to understanding its function. To date, though, no substrates of Nek8 have been described. As our model for Nek8 localization suggested a Nek8-kinase dependent conformational change, we decided to test whether the RCC1 domain itself might be a target for Nek8. As it had not been possible to express this domain in native conditions in bacteria, the GFP-tagged Nek8-RCC1 protein was expressed in HEK293 cells for 24 hrs, cells were lysed and the recombinant protein immunoprecipitated with anti-GFP antibodies. The immune complexes were then used as a substrate in a kinase assay with purified GST-Nek8. Analysis of samples by SDS-PAGE, Coomassie Blue staining and autoradiography revealed that the RCC1 domain acted as an excellent substrate for Nek8, whilst Nek8 did not phosphorylate GFP alone (Figure 5.8A and B). Hence, the RCC1 domain could be a bona fide physiological substrate of Nek8.

5.2.6 Serum starvation induces Nek8 activation

We next tested whether conditions that induced ciliogenesis might also influence Nek8 activity. For this, hTERT-RPE1 cells were either mock transfected or transfected with GFP-Nek8-wt or catalytically-inactive GFP-Nek8-K33R/D128A for 48 hrs. For the final 24 hrs, cells were either left in normal serum-containing media or put into serum-free media. Cells were then lysed and subjected to immunoprecipitation with anti-GFP antibodies, after which immunoprecipitates were used for kinase assays with histone H1 as substrate. Surprisingly, serum

starvation stimulated Nek8 activity in hTERT-RPE1 cells with the Nek8-wt protein being 5 fold more active after serum starvation than before serum starvation (Figure 5.9A and B). In fact, in dividing hTERT-RPE1 cells, the Nek8-wt protein showed similar basal activity to the K33R/D128A, suggesting that this activity was caused by a contaminating kinase. Hence, we conclude that in dividing hTERT-RPE1 cells, there is only a basal level of Nek8 activity, but the protein is activated upon serum withdrawal.

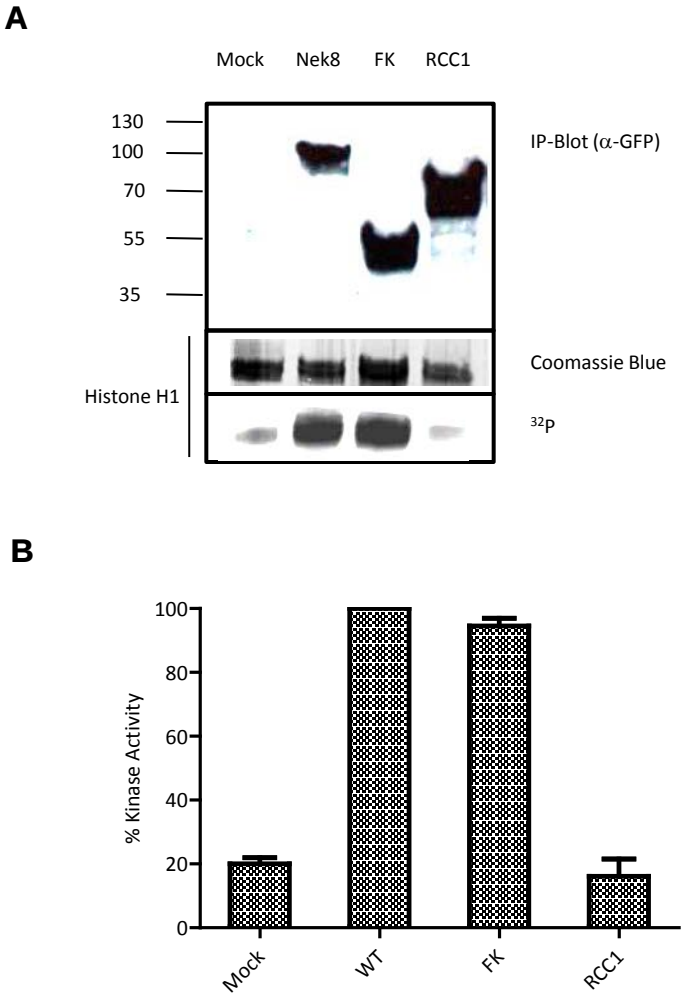

Figure 5.7 The kinase domain of Nek8 has similar activity to the full-length protein

(A) Kinase assays were performed and analysed as described in Fig. 5.5 on immunoprecipitates prepared from HEK293 cells that were either mock transfected or transfected for 24 hours with wild-type Nek8, the kinase domain fragment (FK) or the RCC1 domain fragment (RCC1). Molecular weights (kDa) are shown on the left. **(B)** The kinase activity of the different Nek8 proteins relative to the wild-type is indicated. Data represent means (± S.E.) of three separate experiments.

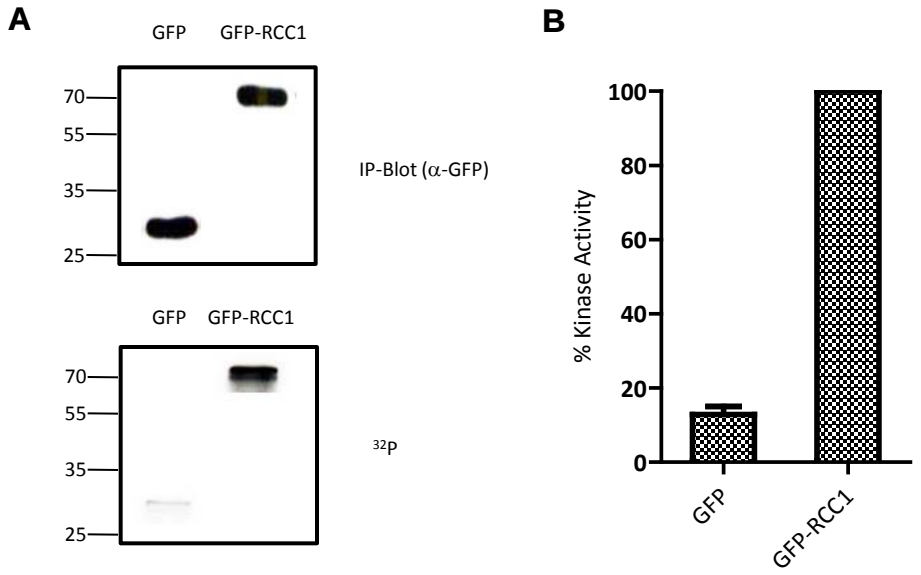

Figure 5.8 Nek8 phosphorylates the RCC1 domain
(A) HEK293 cells were either transiently transfected with GFP-alone or GFP-Nek8-RCC1 for 24 hours before cells were lysed and subjected to immunoprecipitation with anti-GFP antibodies. The amount of kinase precipitated was determined by Western blot with anti-GFP antibodies (IP-Blot) and the immunoprecipitates used for kinase assays. The ability of commercial GST-Nek8 to phosphorylate GFP-alone and GFP-RCC1 was tested. Proteins were incubated in kinase buffer containing [γ^{32}P]-ATP for 30 min at 30°C and analyzed by SDS-PAGE, Coomassie Blue staining and autoradiography (^{32}P). Molecular weights (kDa) are shown on the left. **(B)** Scintillation counting was used to determine the kinase activity of GST-Nek8 against GFP and GFP-RCC1 relative to phosphorylation of GFP-RCC1. Data represent means (± S.E.) of three separate experiments.

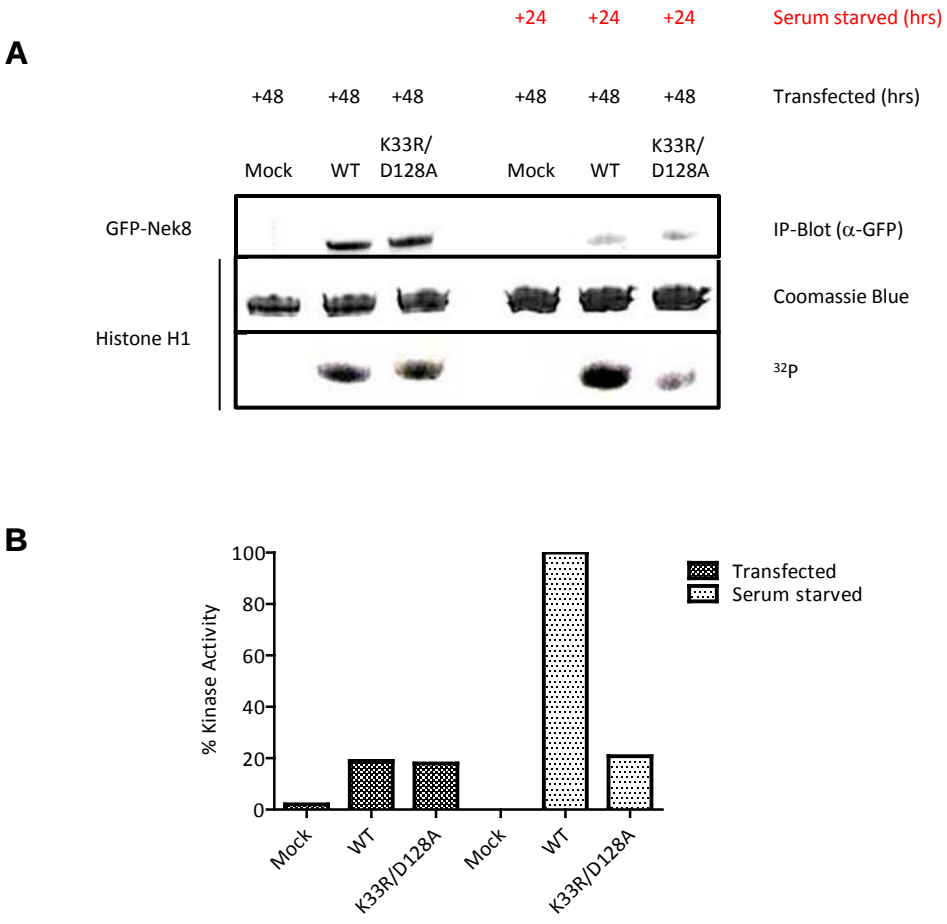

Figure 5.9 Serum starvation induces activation of Nek8
(A) hTERT-RPE1 cells were either mock transfected or transiently transfected with GFP-Nek8 or GFP-Nek8-K33R/D128A for 48 hours and either left in normal media (left three lanes) or serum-starved for the final 24 hours (right three lanes). Cells were then lysed and subjected to immunoprecipitation with anti-GFP antibodies. The amount of kinase precipitated was determined by Western blot with anti-GFP antibodies (IP-Blot) and the immunoprecipitates used for kinase assays with histone H1 as substrate. Samples were analysed by SDS-PAGE, Coomassie Blue staining and autoradiography (^{32}P). **(B)** The kinase activity of Nek8 under different conditions against histone H1 is shown relative to the activity for the wild-type kinase after serum starvation.

5.3 Discussion

Data presented in chapter 4 suggested that the subcellular localization of Nek8 to centrosomes and cilia in dividing and ciliated cells, respectively, was dependent on Nek8 activity with mutants presumed to be active, such as Nek8-T162E correctly localizing to centrosomes and cilia, and mutants presumed to be inactive, such as Nek8-K33R/D128A, losing this localization. However, to date the activity of Nek8 had not been shown. To support the hypothesis that Nek8 activity is a determinant of its localization, it was therefore important to optimize conditions that would enable the kinase activity of Nek8 to be measured. These conditions could then be further used to determine the kinase activity of the Nek8 disease-associated mutants, some of which lost centrosomal and ciliary localization. Therefore, in this chapter we aimed to carry out a detailed characterization of the kinase activity of Nek8 under different conditions.

As with *Aspergillus* NIMA, most mammalian Neks phosphorylate β-casein *in vitro*, while some can also phosphorylate histone H1 and MBP. However, although the NIMA kinase requires Mg^{2+} as a cofactor for kinase activity (Lu et al., 1993), mammalian Neks tend to have a preference for Mn^{2+} (Fry et al., 1995; Holland et al., 2002; Letwin et al., 1992; Minoguchi et al., 2003). Therefore, we first tested the kinase activity of Nek8 using different substrates and under different reaction conditions in the presence of either Mn^{2+} or Mg^{2+}. Initial attempts to measure activity of transfected GFP-Nek8 following immunoprecipitation from transfected cells proved fruitless with the precipitated wild-type GFP-Nek8 protein having no more activity than control precipitates. We therefore switched to using a commercial source of purified GST-Nek8 to optimize assays. Using this protein, we were able to demonstrate phosphorylation of histone H1, β-casein and MBP. This led us to reconsider the reaction conditions under which the kinase assays were carried out with the immunoprecipitated proteins. We started by pre-clearing the Protein G sepharose beads used for Nek8 immunoprecipitation; this would reduce non-specific binding of proteins from the cell extract. We also performed the immunoprecipitations for a longer time which resulted in an increased level of Nek8 protein being precipitated. Perhaps most importantly, we avoided freezing the cell extracts or immunoprecipitates before the kinase reaction and kept the samples on ice throughout the experiment. Finally, we increased the incubation time with ^{32}P-γ-ATP from 30 min to 1 hr at 30^{o}C, which gave Nek8 more time to phosphorylate its substrates. Under these reaction conditions, immunoprecipitation assays with GFP-Nek8 demonstrated clear activity of the wild-type protein against histone H1 and β-casein over mock-transfected samples and predicted inactive

kinases. Indeed, we found that mutation not only of key catalytic site residues (K33 and D128) but also a site on the activation loop that is often subject to phosphorylation in protein kinases, mutation of T162 to alanine in the case of Nek8, completely abolished Nek8 activity. Conversely, a T162E phosphomimetic mutant led to equivalent, possibly even elevated, Nek8 activity compared to the wild-type protein. We therefore conclude that Nek8 is almost certainly regulated in a positive manner through phosphorylation at this site.

Having established conditions for assaying Nek8 kinase activity, we next tested the kinase activity of the Nek8 disease-associated mutants. Unexpectedly, all disease mutants phosphorylated histone H1 to a similar extent as the wild-type protein. This indicates that the reason certain mutants were mislocalized was not a result of loss of activity. Interestingly, we propose that the reason two of these mutants, H425Y and G442V, failed to localize correctly was due to disruption of the centrosome targeting motif in the RCC1 domain.

Previous studies with Nek9, whose structure is very similar to Nek8, had shown that its RCC1 domain inhibits its kinase activity with Nek9 being activated upon deletion of the RCC1 domain (Roig et al., 2002). To observe whether the RCC1 domain also inhibits Nek8 catalytic activity, a truncated form of Nek8 lacking the entire RCC1 domain and representing only the kinase domain was constructed and its catalytic activity was measured compared with the full length protein. We found that the isolated kinase domain was as active as the full-length protein arguing that, unlike the related Nek9 protein, either the RCC1 domain does not act as an auto-inhibitory domain, or the auto-inhibition is fully released when the protein is expressed in cycling cells. Interestingly, though, we found that the full-length kinase was capable of phosphorylating an isolated RCC1 domain raising the prospect that this kinase undergoes autophosphorylation within this region.

Given that Nek8 plays an important role during ciliogenesis, we next measured its kinase activity under conditions that promote ciliogenesis in hTERT-RPE1 cells. Importantly, we found that in cycling hTERT-RPE1 cells, the wild-type protein did not exhibit any activity above background. However, clear activity could be measured upon serum starvation, suggesting that Nek8 may play an important role during ciliogenesis.

Taken together, data presented in this chapter not only describe conditions for assaying the activity of human Nek8, but also show important mechanisms by

which Nek8 may be regulated. We show that unlike the kinase-deficient mutant, K33R/D128A, Nek8 disease-associated mutants retain full kinase activity. Moreover, we show that activity of Nek8 is induced upon exit from the cell cycle. Importantly, Nek8 was capable of phosphorylating an isolated RCC1 domain raising the prospect that this kinase undergoes autophosphorylation within this region, as part of the activation mechanism.

Chapter 6

Nek8 is subject to proteasomal degradation upon exit from the cell cycle

6.1 Introduction

So far, our studies have shown activation of Nek8 in response to serum starvation. Interestingly, under these conditions, we also observed reduced expression of the Nek8 protein as compared to cells that were not serum starved. This phenotype was also previously seen when studying the localization of Nek8 when lower numbers of Nek8 transfected cells were seen in serum starved cells compared with dividing cells. Hence, we wanted to know whether the stability of Nek8 protein might be affected under serum-starved conditions.

In order to regulate physiological functions, cells have developed many mechanisms for controlling the levels of intracellular proteins. One of the mechanisms involves post-translational modification by ubiquitination, which can rapidly and irreversibly inactivate a protein by destroying it via the ubiquitin (Ub)-proteasome pathway (UPP). Many intracellular proteins are degraded in this way. However, some proteins are degraded by non-proteasomal pathways, such as within lysosomes.

Ubiquitin-mediated proteolysis can be roughly divided into two distinct steps: ubiquitination and proteasomal degradation. Ubiquitination involves conjugation of the highly conserved 76 amino acid protein ubiquitin to a target protein designated for degradation typically leading to its polyubiquitination. This involves a conserved mechanism involving Ub activating (E1), conjugating (E2) and ligating (E3) enzymes. In this process, the C-terminal glycine residue of Ub is coupled to a target lysine residue of the protein substrate, forming an isopeptide bond (Pickart, 2001; Glickman and Ciechanover, 2002). Specifically, the E1 enzyme activates ubiquitin by forming a thiol ester with the C-terminal glycine of ubiquitin; this requires ATP. Then the ubiquitin moiety is transferred to an E2 enzyme by transesterification. The E2 enzyme in turn either transfers the ubiquitin to an E3 enzyme that is responsible for the transfer to the final target, or it ubiquitinates the target directly under the direction of an E3 enzyme (Pickart and Eddins., 2004; Fang and Weissman., 2005). Recent studies have shown that a novel class of E4 enzymes also exists and these may be responsible for polyubiquitylation in specific cases (Hoppe, 2005). Degradation of proteins that carry polyubiquitin chains is mediated by a large multi-subunit protease complex called the 26S proteasome. This is composed of two sub-complexes: the 20S core particle and the 19S regulatory particle (Voges et al., 1999). The 19S regulatory lid of the 26S proteasome recognizes proteins containing a Lys-48 Ub polymer as substrates for

degradation by the 20S catalytic core (Baboshina and Haas, 1996; Thrower *et al.*, 2000).

Many proteins are recognized as proteasomal substrates. These include activators and inhibitors of the cyclin-dependent kinases that drive the eukaryotic cell cycle. Interestingly, Nek2 has been found to be regulated by proteolysis through proteasome. Indeed, Nek2A has been shown to be degraded by the ATPase-dependent 26S proteasome upon mitotic entry following its ubiquitination by the APC/C (anaphase promoting complex-cyclosome) E3 ubiquitin ligase (Hames et al., 2001; Fry, 2002). Importantly, NIMA is also destroyed during mitosis of *Aspergillus* cells via APC/C mediated ubiquitylation (Ye et al., 1998). We therefore also tested whether Nek8 was subject to proteasomal degradation under serum starved conditions.

6.2 Results

6.2.1 Quiescence induces proteasomal degradation of Nek8 in hTERT-RPE1 cells

Under starvation conditions, we had previously observed decreased levels of Nek8 protein as compared to cells that were not serum starved. This phenotype was also previously seen when studying the localization of Nek8 when lower numbers of Nek8 transfected cells were seen in serum starved cells compared with dividing cells. To directly test whether serum starvation induced Nek8 degradation, hTERT-RPE1 cells expressing GFP alone or GFP-Nek8 were transfected for 24 hrs and then either left in serum-containing medium or transferred to serum-free medium for another 24 hrs. Western blot analysis of whole cell extracts revealed that, while the level of GFP alone remained similar, the level of GFP-Nek8 declined significantly upon serum starvation, indicating that loss of expression is specific to Nek8 (Figure 6.1). To determine whether Nek8 downregulation is a consequence of proteolysis or translational control, serum starved cells expressing Nek8 were treated with the proteasome inhibitor, MG132, for 4 hrs following 20 hrs of serum starvation. The decrease in the Nek8 level was reduced in cells treated with the proteasome inhibitor suggesting that Nek8 is prone to proteasomal degradation under these conditions (Figure 6.1). These data were confirmed by immunofluorescence microscopy studies where quantification of the transfection efficiency revealed that there was a reduced number of GFP-Nek8 transfected cells upon serum starvation that was rescued by addition of MG132 (Figure 6.1B).

6.2.2 Proteasomal degradation of Nek8 during serum starvation is specific to cells undergoing quiescence

We wanted to know whether this degradation was a cell cycle response due to entry into quiescence, or a signalling response due to growth factor withdrawal. For this purpose, we transfected GFP-Nek8 into two cell lines, hTERT-RPE1 and NIH3T3, that we confirmed by flow cytometry and BrdU incorporation exited the cell cycle upon serum withdrawal, and two cell lines, HeLa and U2OS, that remained in the cell cycle despite serum withdrawal (Figure 6.2A and B). Strikingly, we found that the proteasomal-dependent loss of Nek8 only occurred in the cell lines that entered quiescent, and not in those that remained in the cell cycle (Figure 6.2C-E). This indicates that proteasomal degradation of Nek8 under serum starvation conditions is a specific response to entry into quiescence.

6.2.3 Endogenous Nek8 is degraded upon quiescence

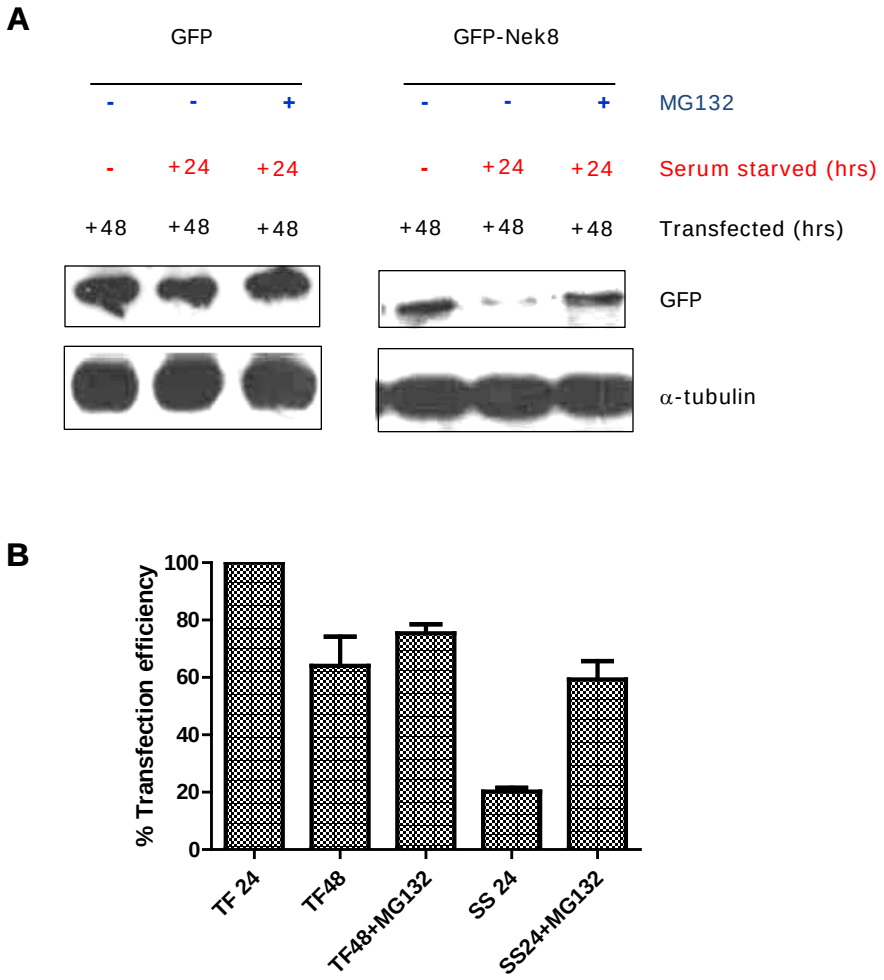

Figure 6.1 Serum starvation induces proteasomal degradation of Nek8

(A) hTERT-RPE1 cells were transfected, (TF) with GFP alone or GFP-Nek8 for the times indicated and serum starved and treated with MG132, as indicated. Samples were analysed by SDS-PAGE and Western blotting with antibodies against GFP and α-tubulin. **(B)** The transfection efficiency (% cells positive for GFP-Nek8 as determined by immunofluorescence microscopy with GFP antibodies) in hTERT-RPE1 cells was determined at the times indicated after transfection (hours), with or without serum starvation (SS) and with or without MG132 treatment, as indicated. Data represent means (± S.E.) of three separate experiments.

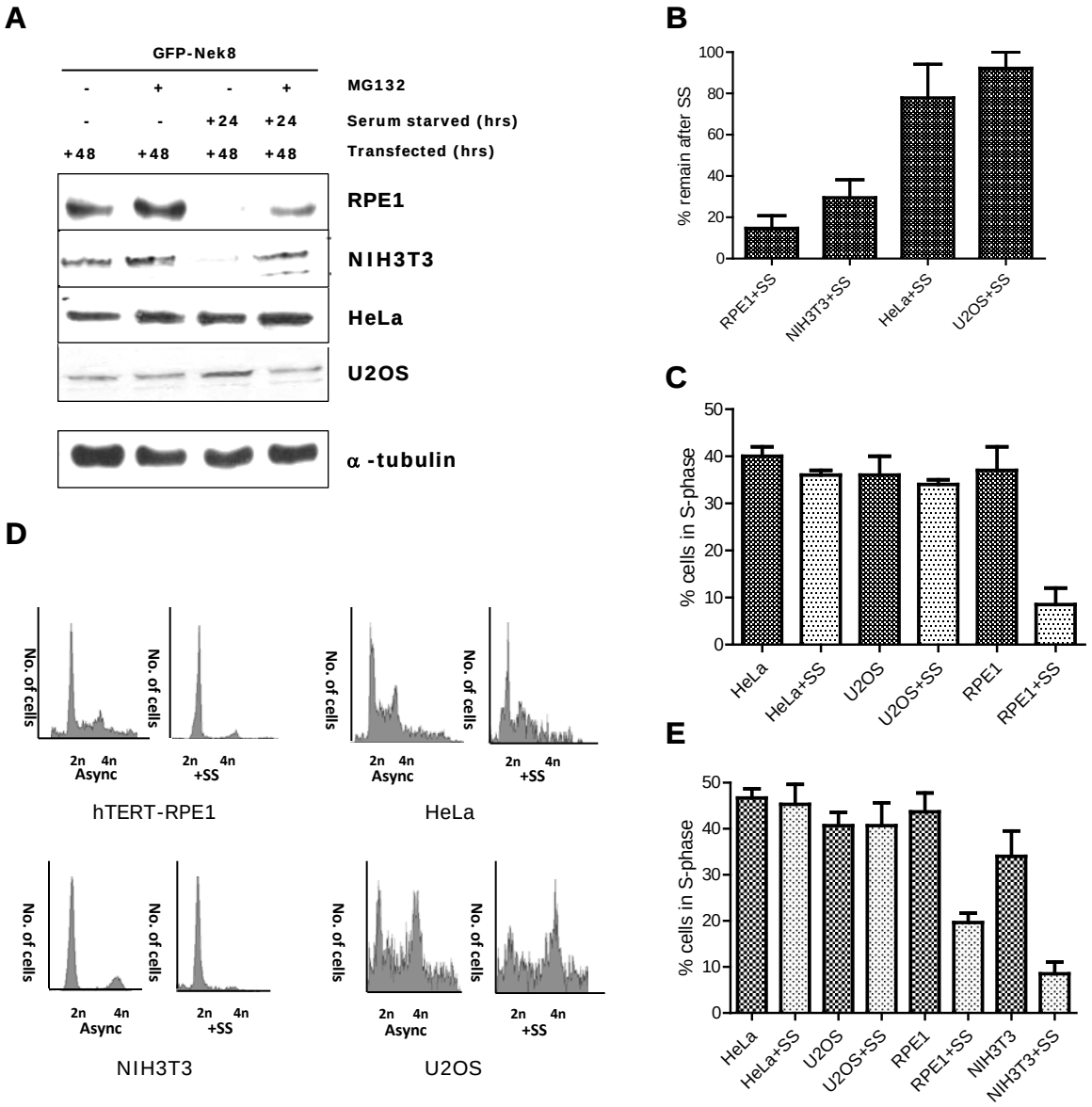

Figure 6.2 Serum starvation induces quiescence in hTERT-RPE1 and NIH3T3 cells, but not HeLa or U2OS cells

(A) GFP-Nek8 was transfected into hTERT-RPE1, NIH3T3, HeLa and U2OS cells. They were then incubated for 48 hours with transfer into serum-containing or serum-free media for the last 24 hours. MG132 was also added during the last 4 hours where indicated. Extracts were prepared and analysed by SDS-PAGE and Western blotting with antibodies against GFP. Western blots were also performed with α-tubulin antibodies on samples prepared from hTERT-RPE1 cells. **(B)** Extracts were analysed for the amount of protein remaining after serum starvation (SS), as compared to in the presence of serum, by SDS-PAGE and Western blotting with anti-GFP antibodies. **(C)** To determine whether the different cell lines remained in the cell cycle upon serum starvation, cells were serum starved for 24 hours and then pulse-labelled with BrdU for 4 hours. They were then analysed by immunofluorescence microscopy using anti-BrdU antibodies and the % of labelled cells, representing those in S-phase, were scored. **(D)** The effect of serum starvation on cell cycle progression in the different cell lines was also analysed by flow cytometry analysis. The flow cytometry profiles of asynchronous cells (async) and cells that had been serum starved for 48 hours (+SS) are shown with the positions of 2n and 4n DNA indicated. **(E)** The histogram shows the percentage of cells in S-phase based on the flow cytometry shown in D. Data represent means (±S.E.) of three separate experiments.

Having established that quiescence induces proteasomal degradation of recombinant GFP-Nek8 protein, we next examined whether this was the case for endogenous Nek8. For this, hTERT-RPE1 cells were grown either in serum-containing or serum-free media for 24 hrs. MG132 was added to an additional serum starved sample for the last 4 hrs before harvest. Cells were then lysed and Nek8 protein levels detected using the R4176 Nek8 antibody that we had previously generated. Western blot analysis revealed that as for recombinant GFP-Nek8, protein levels of endogenous Nek8 declined significantly upon serum starvation. Furthermore, addition of MG132 rescued Nek8 expression, thus confirming that Nek8 is degraded in a proteasomal dependent manner upon entry into quiescence (Figure 6.3A and B).

6.2.4 Proteasomal degradation of Nek8 occurs via the kinase domain

To map the proteasomal degradation targeting site of Nek8, we next tested the effect of serum starvation on different Nek8 truncated constructs. For this, hTERT-RPE1 cells were transiently transfected for 24 hrs with the kinase domain alone (Nek8-FK), or two separate fragments of the RCC1 domain (Nek8-F1 and Nek8-F2) and left in serum-containing medium or transferred to serum-free medium for 24 hrs. Western blot analysis revealed that whereas the levels of GFP-alone, Nek8-F1 and Nek8-F2 remained constant in the presence and absence of serum, protein levels of Nek8-FK declined significantly, suggesting that degradation of Nek8 occurs via a targeting motif in the kinase domain (Figure 6.4C and D). Importantly, the smallest amount of Nek8-FK remaining was upshifted upon serum starvation, suggesting that Nek8-FK is also phosphorylated in response to serum starvation (Figure 6.4A and C). We propose that this may correspond to the activation of Nek8 that we also see upon serum starvation.

6.2.5 Proteasomal degradation of Nek8 is not dependent on Nek8 activity

To observe whether proteasomal degradation of Nek8 upon quiescence is dependent on Nek8 activity, we next tested the effect of serum starvation on the catalytically-inactive T162A and catalytically-active T162E mutant forms of Nek8. Western blot analysis of whole cell extracts revealed that both the inactive and active forms were degraded upon serum starvation with protein levels significantly declining following 24 hrs of serum starvation and increasing upon addition of MG132 (Figure 6.5A). However, when the construct expressing the kinase domain alone with the T162A mutant was tested, although it was degraded, no band shift was observed (Figure 6.5B). This suggests that it is the phosphorylation of the T162 site that causes the upshift as this phosphorylation cannot happen with the

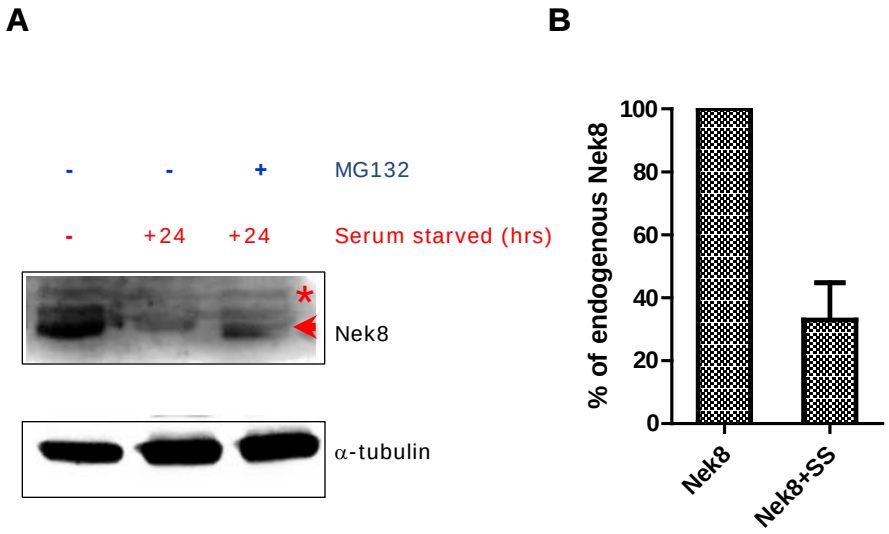

Figure 6.3 Endogenous Nek8 is degraded upon quiescence
(A) To observe degradation of endogenous Nek8, hTERT-RPE1 cells were incubated as indicated before analysis by SDS-PAGE and Western blotting with antibodies against Nek8 and α-tubulin. Nek8 antibody detected the Nek8 protein (arrowhead) and a slightly higher molecular weight cross-reacting protein (asterisk). **(B)** Extracts were analysed for the amount of protein remaining after serum starvation (SS), as compared to in the presence of serum, by SDS-PAGE and Western blotting with anti-Nek8 antibodies. Data represent means (±S.E.) of three separate experiments.

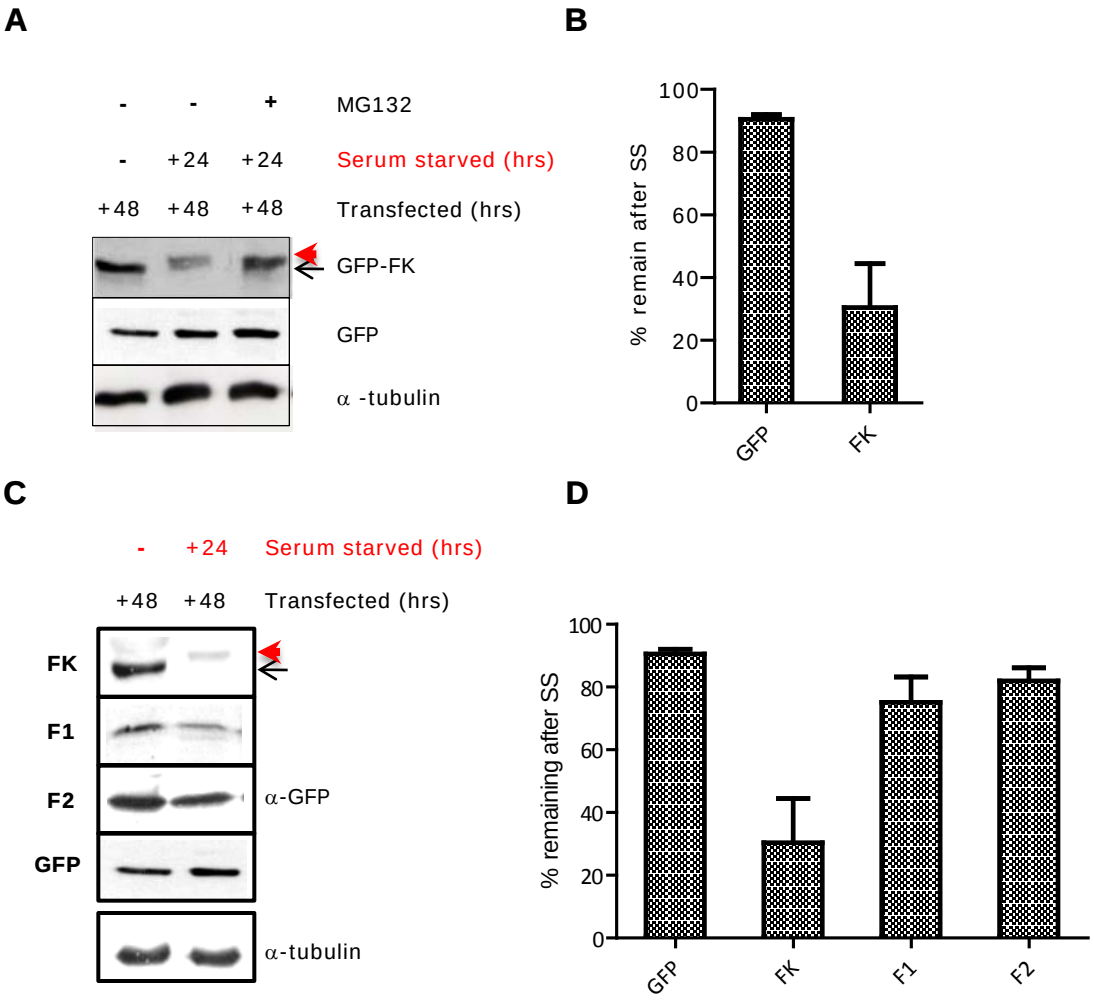

Figure 6.4 Nek8 degradation upon quiescence occurs via the kinase domain

(A) hTERT-RPE1 cells were transfected with the GFP-tagged Nek8 kinase domain alone (GFP-FK) for the times indicated and serum starved and treated with MG132, as indicated. Samples were analysed by SDS-PAGE and Western blotting with antibodies against GFP and α-tubulin. Note that FK was upshifted (arrowhead) upon serum starvation as compared to in the presence of serum (arrow). **(B)** Extracts were analysed for the amount of protein remaining after serum starvation (SS), as compared to in the presence of serum, by SDS-PAGE and Western blotting with anti-GFP antibodies. **(C)** As in A only that cells were transfected with either the GFP-tagged Nek8 kinase domain alone (GFP-FK), or the RCC1 fragments (GFP-F1 and GFP-F2). **(D)** Extracts were analysed for the amount of protein remaining after serum starvation (SS), as compared to in the presence of serum, by SDS-PAGE and Western blotting with anti-GFP antibodies. Data in B and D represent means (± S.E.) of three separate experiments.

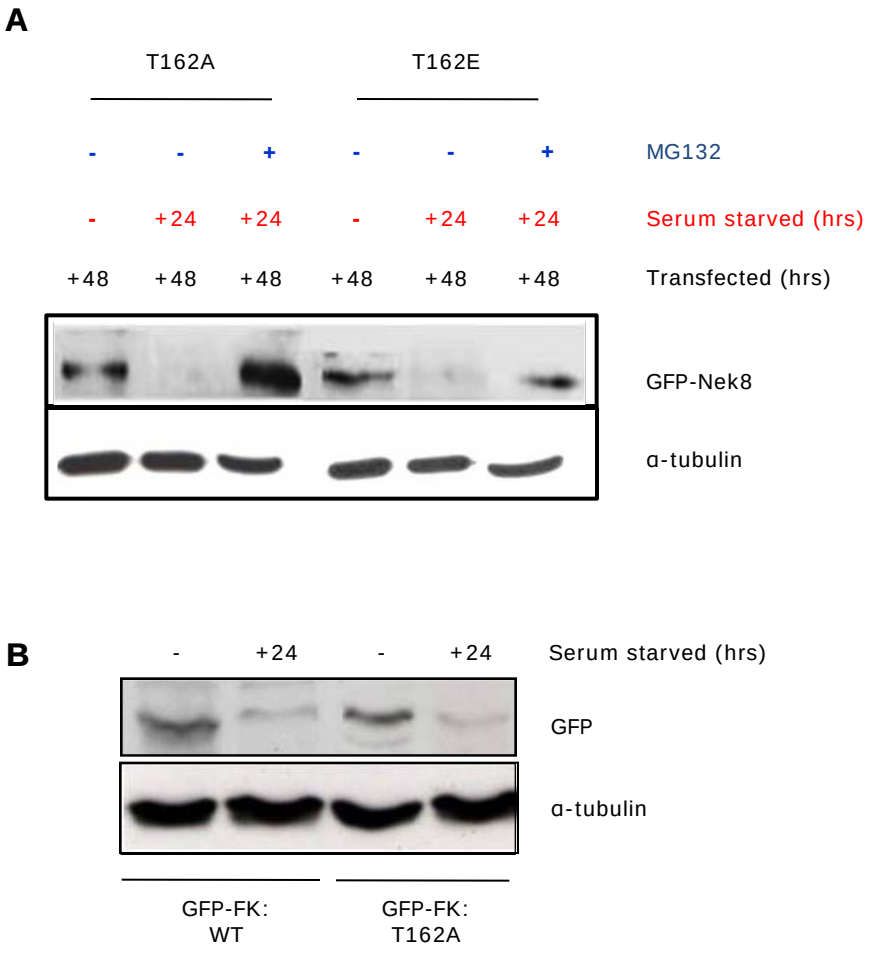

Figure 6.5 Proteasomal degradation of Nek8 is not dependent on Nek8 activity

hTERT-RPE1 cells were transfected with GFP-tagged Nek8 constructs carrying T162A or T162E mutations, as indicated. Cells were then treated as indicated before analysis by SDS-PAGE and Western blotting with antibodies against GFP and α-tubulin. **(B)** hTERT-RPE1 cells were transfected for 48 hours with GFP-tagged kinase domain constructs that were either wild-type or carried the T162A mutation. These were treated as indicated before analysis by SDS-PAGE and Western blotting with antibodies against GFP and α-tubulin.

T162A mutant. This also indicates that degradation of Nek8 is independent of Nek8 activity since the inactive mutant is also degraded. We therefore conclude that exit from the cell cycle is accompanied by proteasome mediated degradation of Nek8 that occurs via targeting of the kinase domain but in a kinase-independent manner.

6.2.6 Nek8 disease mutants are degraded upon serum starvation

Having looked at the effect of serum starvation on the Nek8 kinase domain mutants, we then looked at the protein levels of disease-associated mutant forms of Nek8 following 24 hrs of serum starvation. Similar to the wild-type Nek8, protein levels of all NPHP mutants, L330F, A497P and H425Y, the jck mutant G442V, as well as the pancreatic cancer mutant, A197P, were significantly reduced upon serum starvation (Figure 6.6). This is consistent with the fact that degradation appears to be mediated through the kinase domain and indicates that these mutations do not impede in the process of Nek8 degradation.

6.2.7 Serum starvation induces Nek8 activity in the presence of MG132

Having found that quiescence induces Nek8 activation we decided to retest the activation of Nek8 in response to serum starvation in the presence of a proteasomal inhibitor to prevent degradation. For this, hTERT-RPE1 cells were either mock transfected or transfected with GFP-Nek8-wt or with the catalytically inactive GFP-Nek8-K33R/D128A for 24 hrs and then either left in serum-containing medium for a further 24 hrs or moved to serum-free media for 24 hrs. Following 20 hrs of serum starvation, MG132 was also added for 4 hrs to prevent Nek8 degradation. Cells were then lysed and recombinant proteins immunoprecipitated with anti-GFP antibodies before immune complexes were used in kinase assays with histone H1 as substrate. Analysis of samples by SDS-PAGE, Coomassie Blue staining and autoradiography revealed that wild-type Nek8 strongly phosphorylated histone H1 under serum starvation conditions while the mock and the kinase-inactive Nek8-K33R/D128A samples did not show any kinase activity. In contrast to serum starved cells, in dividing hTERT-RPE1 cells, Nek8 failed to phosphorylate histone H1, with constructs exhibiting less than 20% kinase activity (Figure 6.7A and B). To ensure that this increase in the kinase activity was due to serum starvation and not simply addition of MG132, we repeated this experiment in dividing cells. Analysis of samples by autoradiography revealed that there was no specific phosphorylation of histone H1 under these conditions, as both the wild-type and mutant exhibited only basal levels of kinase activity (Figure 6.7C and D). Hence, this confirms that quiescence specifically induces kinase activity of Nek8.

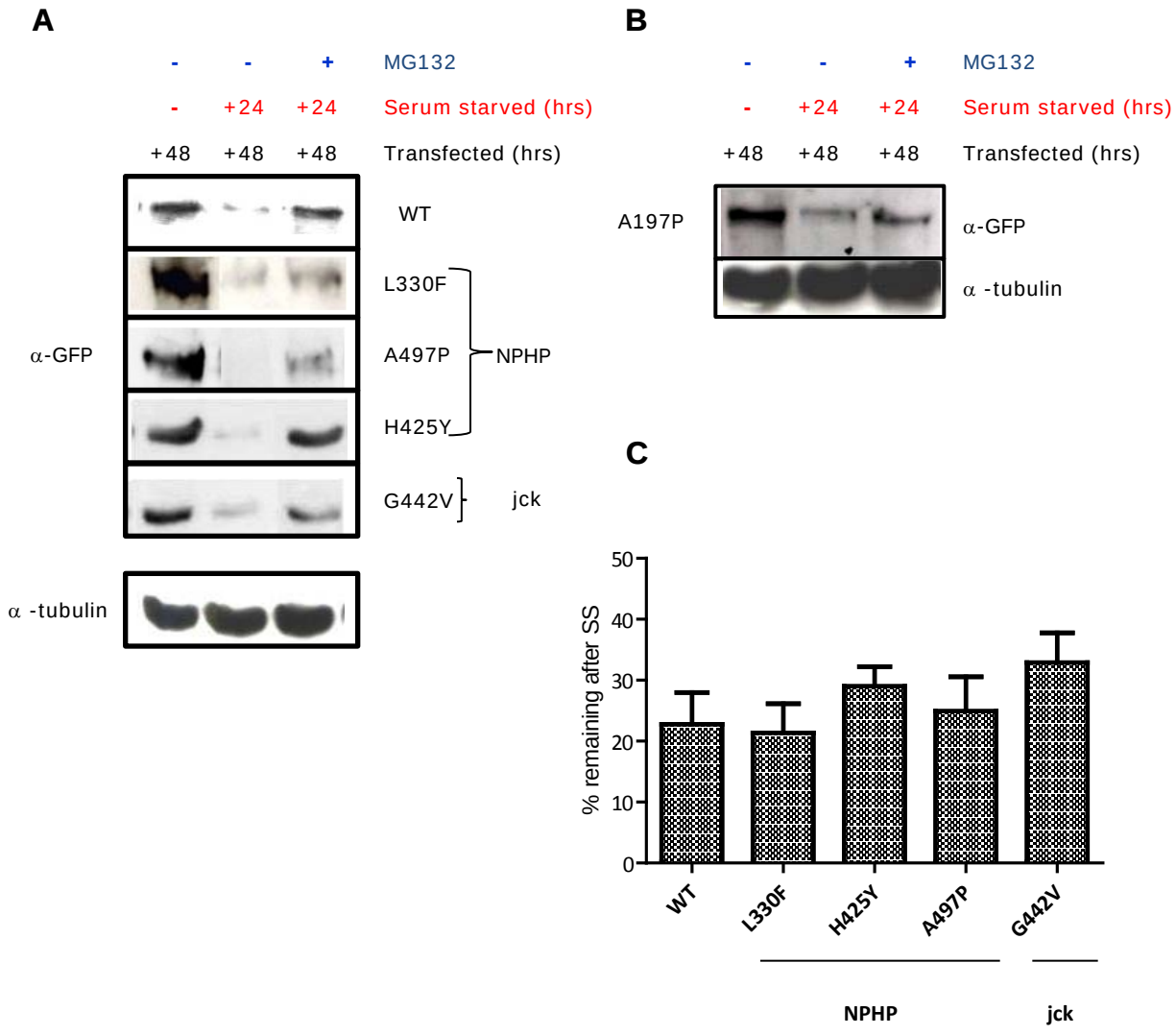

Figure 6.6 Disease-mutants of Nek8 are also subject to proteasomal degradation upon serum starvation
hTERT-RPE1 cells were transiently transfected with GFP-tagged Nek8 NPHP-mutants **(A)** or Nek8 pancreatic cancer mutant, A197P **(B)**, as indicated, for 48 hours with transfer into serum-containing or serum-free media for the last 24 hours and MG132 added for the last 4 hours where indicated. Extracts were prepared and analysed by SDS-PAGE and Western blotting with antibodies against GFP and α-tubulin. **(C)** Extracts were analysed for the amount of protein remaining after serum starvation (SS), as compared to in the presence of serum, by SDS-PAGE and Western blotting with anti-GFP antibodies. Data represent means (±S.E.) of three separate experiments.

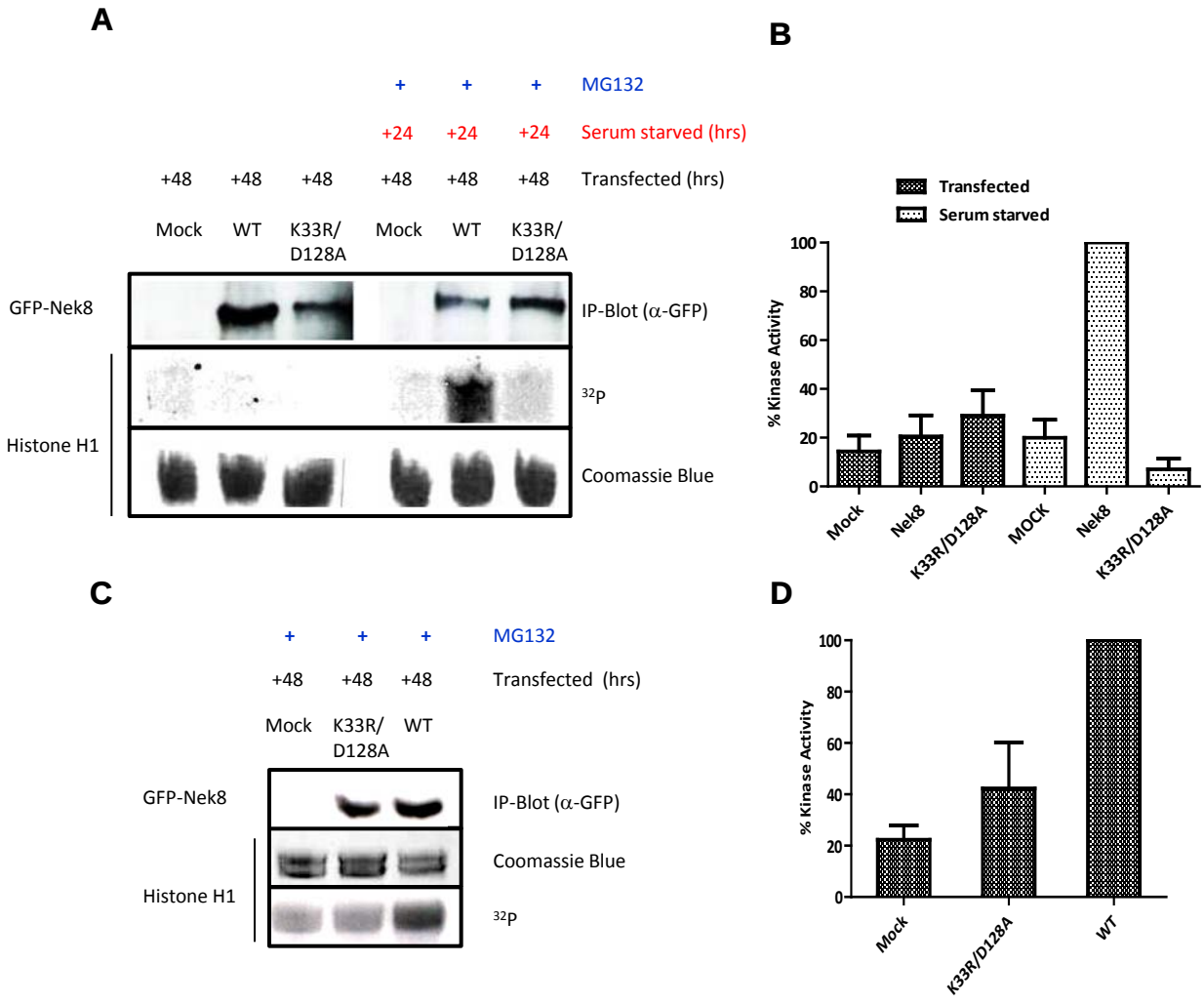

Figure 6.7 Serum starvation induces activation of stabilized Nek8
(A) hTERT-RPE1 cells were either mock transfected or transiently transfected with GFP-Nek8 or GFP-Nek8-K33R/D128A for 48 hours and either left in normal media (left three lanes) or serum-starved for the final 24 hours (right three lanes). MG132 was added for the final 4 hours to the serum-starved cells to rescue Nek8 expression. Cells were then lysed and subjected to immunoprecipitation with anti-GFP antibodies. The amount of kinase precipitated was determined by Western blot with anti-GFP antibodies (IP-Blot) and the immunoprecipitates used for kinase assays with histone H1 as substrate. Samples were analysed by SDS-PAGE, Coomassie Blue staining and autoradiography (^{32}P). **(B)** The kinase activity of Nek8 under different conditions against histone H1 is shown relative to the activity for the wild-type kinase after serum starvation. **(C & D)** The kinase activity of the samples indicated was determined as in A and B, except in this case hTERT-RPE1 cells were cycling and not serum-starved. Data represent means (±S.E.) of three separate experiments.

Finally, as we had found that Nek8 was most likely phosphorylated on T162 upon serum starvation, we asked whether this activation might at least in part be due to phosphorylation at this site. For this purpose, we tested the relative activation of the wild-type and T162 mutants upon serum starvation. Strikingly, we found that the T162A mutant exhibited very low activity in cycling cells and was not further activated by serum starvation, whereas the T162E mutant showed high activity in cycling cells but was also not further activated by serum starvation (Figure 6.8A and B). Moreover, the level of activity of the T162E mutant in cycling cells was similar to that of the wild-type protein after serum starvation. We therefore conclude that exit from the cell cycle is accompanied by activation of Nek8 that largely results from phosphorylation of T162 in the activation loop of the kinase.

6.2.8 Nek8 disease mutants are also activated upon serum starvation

Having established that serum starvation induces Nek8 activity in hTERT-RPE1 cells, we next tested whether the disease mutants were similarly activated by serum starvation. For this, hTERT-RPE1 cells were transfected with GFP-Nek8-wt or the disease mutants for 24 hrs and maintained in serum-containing media for a further 24 hrs or moved to serum-free media for 24 hrs. Following 20 hrs of serum starvation, MG132 was also added for 4 hrs to block proteasomal degradation, and cells were lysed and subjected to immunoprecipitation with anti-GFP antibodies. The amount of kinase precipitated was determined by Western blot with anti-GFP antibodies and the immunoprecipitates used for kinase assays with histone H1 as substrate. Analysis of samples by SDS-PAGE, Coomassie Blue staining and autoradiography revealed that all Nek8 disease mutants were activated to a similar level as the wild-type protein (Figure 6.9A and B). As Nek8 disease mutants were previously shown to be active in cycling HEK293 cells, together these data indicate that the NPHP disease mutations do not affect the activity or activation of Nek8.

6.2.9 Nek8 promotes microtubule acetylation but prevents ciliogenesis

Finally, having seen that Nek8 is both activated and degraded upon quiescence, we addressed whether Nek8 might be an inhibitor of ciliogenesis, in a similar manner to that reported for Nek1 (Shalom et al., 2008; White and Quarmby., 2008). For this purpose, hTERT-RPE1 cells were either transfected with GFP-Nek8 or, as controls, were mock transfected or transfected with GFP alone. After 4 hrs transfection, cells were transferred to serum-free media for 48 hrs. They were then fixed with methanol and processed for immunofluorescence microscopy with anti-acetylated tubulin to mark the cilium, and anti-GFP antibodies to identify the transfected cells. Although, as previously indicated, there was a clear reduction in

the number of cells in which we could observe GFP-Nek8 expression, it was possible to compare the frequency of ciliated cells with those expressing GFP alone. Importantly, we observed that GFP-Nek8 expression led to a clear reduction in the number of ciliated cells. Indeed, quantification of the number of cells with clearly visible cilia revealed that approximately 80% of those that were mock transfected or transfected with GFP alone possessed cilium. In contrast, this figure dropped to approximately 50% in cells expressing GFP-Nek8. This supports the notion that Nek8 may be an inhibitor of ciliogenesis (Figure 6.10A). We then asked whether, similar to Nek1, this was dependent upon kinase activity. However, in the case of Nek8, we found a similar reduction in the percentage of ciliated cells with inactive Nek8 mutants (K33R/D128A and T162A) as well as wild-type or active mutants (T162E) leading us to conclude that this is not an activity dependent response (Figure 6.10A). Similarly, expression of the NPHP disease mutants interfered with ciliogenesis (Figure 6.10B). Whilst staining cells with acetylated tubulin antibodies to detect cilia, we observed a dramatic increase in the number of cytoplasmic microtubules that stained positively for acetylated tubulin upon GFP-Nek8 expression (Figure 6.10C and E). Again, this was seen not only with the wild-type Nek8, but also the kinase-domain and NPHP disease associated mutants (Figure 6.10D, E and F). Thus, we conclude that overexpression of Nek8 in cells, whether active or inactive, suppresses ciliogenesis but also promotes microtubule hyperacetylation. It remains to be determined whether the increase in microtubule acetylation is in some way responsible for the block to cilia formation.

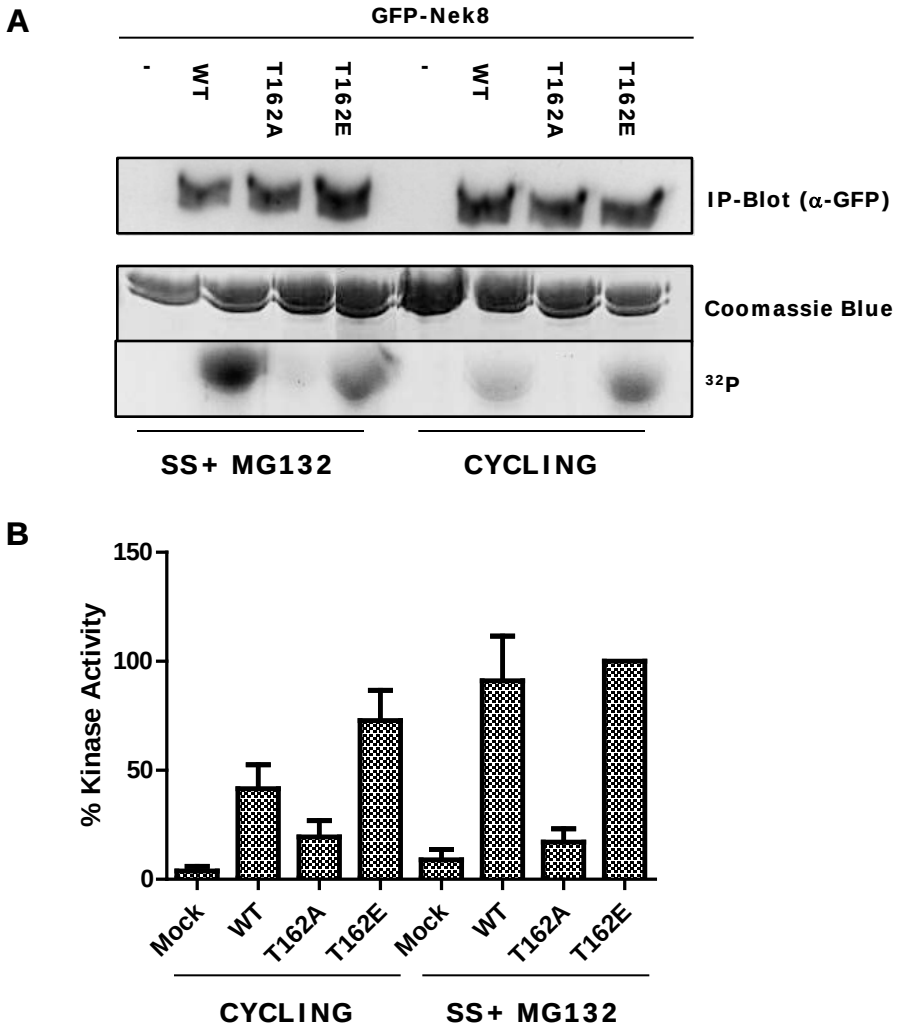

Figure 6.8 Cell cycle exit induces activation of Nek8 via phosphorylation of T162 in the activation loop of the kinase

(A) hTERT-RPE1 cells were either mock transfected or transiently transfected with GFP-Nek8 constructs for 48 hours and either left in cycling media (right three lanes) or serum-starved for the final 24 hours (left three lanes). MG132 was added for the final 4 hours to the serum-starved cells to rescue Nek8 expression. Cells were then lysed and subjected to immunoprecipitation with anti-GFP antibodies. The amount of kinase precipitated was determined by Western blot with anti-GFP antibodies (IP-Blot) and the immunoprecipitates used for kinase assays with histone H1 as substrate. Samples were analysed by SDS-PAGE, Coomassie Blue staining and autoradiography (^{32}P). **(B)** The kinase activity of Nek8 under different conditions against histone H1 is shown relative to the activity for the GFP-Nek8-T162E construct after serum starvation. Data represent means (±S.E.) of three separate experiments.

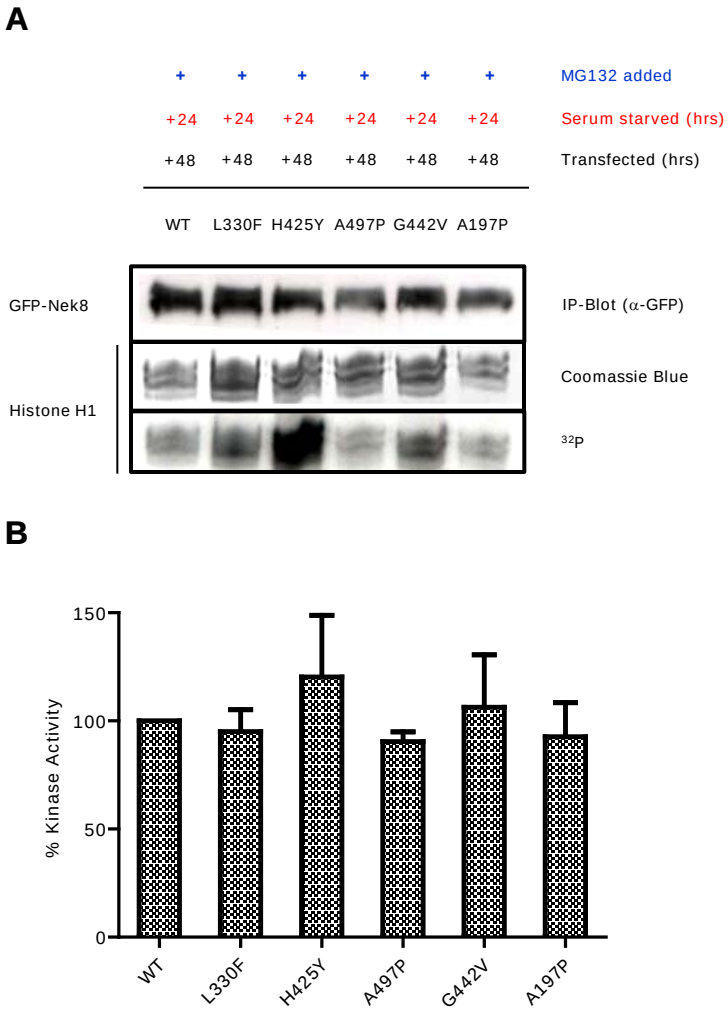

Figure 6.9 Nek8 disease mutants are active
(A) hTERT-RPE1 cells were transfected for 24 hours with different GFP-tagged Nek8 constructs as indicated and then serum starved for 24 hours. MG132 was added for the final 4 hours to the serum-starved cells to rescue Nek8 expression. Cells were then lysed and subjected to immunoprecipitation with anti-GFP antibodies. The amount of kinase precipitated was determined by Western blot with anti-GFP antibodies (IP-Blot) and the immunoprecipitates used for kinase assays with histone H1 as substrate. Samples were analysed by SDS-PAGE, Coomassie Blue staining and autoradiography (^{32}P). **(B)** The kinase activity of Nek8 under different conditions against histone H1 is shown relative to the activity for the wild-type kinase after serum starvation. Data represent means (±S.E.) of three separate experiments.

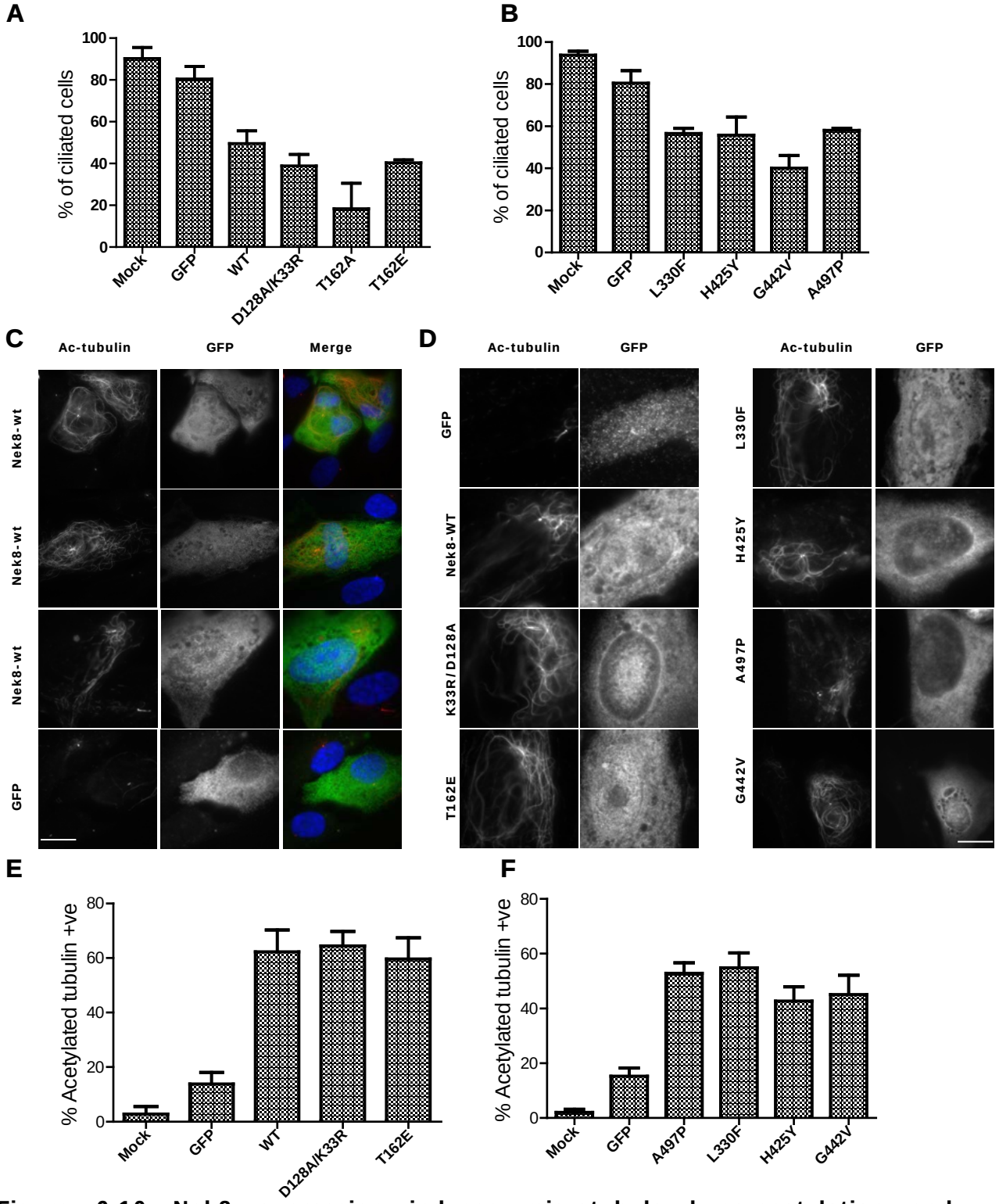

Figure 6.10 Nek8 expression induces microtubule hyperacetylation and suppresses ciliogenesis in a kinase-independent manner

(A & B) The histograms show the % of hTERT-RPE1 cells that were mock transfected or transfected with Nek8 constructs as indicated that had primary cilia following 48 hours of serum starvation. Cells were counted after immunofluorescence microscopy with antibodies against GFP to identify transfected cells and acetylated-tubulin to detect cilia. **(C & D)** hTERT-RPE1 cells were transfected with either GFP alone or GFP-tagged Nek8 constructs as indicated and then serum-starved for 48 hours. Cells were then processed for immunofluorescence microscopy with antibodies against GFP to detect the recombinant Nek8 and acetylated tubulin. Scale bars, 10 μm. **(E & F)** Histograms show the % of cells treated as in C & D that had notable cytoplasmic staining of acetylated tubulin. Data in A, B, E and F represent means (±S.E.) of three separate experiments.

6.3 Discussion

Data presented in chapter 5 showed that cell cycle exit induces activation of Nek8. In this chapter, we show that unexpectedly, serum withdrawal also induces degradation of Nek8. This degradation was also seen with endogenous Nek8 and occurred in a proteasome dependent manner since addition of the proteasome inhibitor, MG132, rescued Nek8 expression. Moreover degradation was specific to cells undergoing quiescence as degradation only occurred in hTERT-RPE1 and NIH3T3 cells that entered G0 upon serum starvation, and not in HEK293 and HeLa cells that failed to do so. The fact that Nek8 is both activated and degraded upon serum starvation, is intriguing and suggests a complex function in the initiation of ciliogenesis. It is possible that Nek8 activity may be required to initiate some aspect of the ciliogenesis programme, whereas its degradation may be required to prevent this initiation process from being maintained indefinitely.

Structure-function studies revealed that Nek8 degradation is targeted through the kinase domain, as only Nek8-FK was degraded following serum starvation, whereas other truncated forms of Nek8, Nek8-F1 and Nek8-F2, were not. However, as these truncations break the β-propeller structure, then it is difficult to draw conclusions from these data. Importantly, an upshift of the kinase domain was detected upon serum starvation. This suggests that the Nek8 kinase domain is phosphorylated at this time. Interestingly, when T162 was mutated in the kinase domain fragment, the protein was still degraded but no longer upshifted in the presence of MG132. This strongly suggests that it is phosphorylation of the T162 site that causes the upshift. However, this also indicates that degradation is independent of Nek8 activity since both the active and inactive full-length and kinase domain fragments were degraded. However, protein phosphatase treatment should be performed to confirm that the upshift is indeed due to phosphorylation. Consistent with degradation being mediated through the kinase domain, the proteins in which mutations are present in the RCC1 domain were degraded upon serum starvation.

Upon finding that the proteasomal inhibitor MG132 rescued Nek8 degradation, we revisited the finding that Nek8 is activated upon entry in quiescence by repeating this experiment but in the presence of MG132 to prevent Nek8 degradation. Consistent with previous results, serum starvation induced Nek8 activity even in the presence of MG132, whereas no activity of Nek8 was observed in cycling hTERT-RPE1 cells that were treated with MG132. This is somewhat different to the results we obtained with HEK293 cells, in which Nek8 activity was detected in the

presence of serum. This may reflect a difference in cell lines. For example, hTERT-RPE1 cells may contain an inhibitor of Nek8 that itself is degraded upon serum starvation. Alternatively, it is possible that Nek8 may need an activating protein that is present in dividing HEK293 cells but not in dividing hTERT-RPE1 cells and only appears under serum deprivation conditions.

We also investigated whether overexpression of Nek8 constructs affected ciliogenesis. Quantification of the number of cells with an obvious primary cilium in hTERT-RPE1 cells expressing GFP-Nek8 suggested a lower number than compared with mock treated cells or cells expressing GFP or GFP-Nek7. This would seem to suggest that Nek8 suppresses ciliogenesis. However, this would contradict the results from other groups who suggested no change in ciliogenesis in cells overexpressing Nek8 (Otto et al., 2008; Sohara et al., 2008). The effect that we observed was not due to catalytic activity since both the active and inactive Nek8 mutants reduced ciliogenesis compared with other controls. Ciliogenesis was also reduced in cells expressing Nek8 disease-associated mutants. Interestingly, Nek1 has been shown to inhibit ciliogenesis in the murine renal epithelial cell line, IMCD3; however, in this case, suppression was dependent on Nek1 kinase activity (White and Quarmby, 2008).

We also noticed a dramatic increase in the acetylation of cytoplasmic microtubules in those cells expressing GFP-Nek8. Again, though, this phenotype was not dependent on Nek8 kinase activity, so it is difficult to conclude that it reflects the normal function of the protein when present at physiological levels. The stimulation of microtubule hyperacetylation is nevertheless interesting in that it is also seen upon overexpression of another NIMA-related kinase, Nek3, albeit in this case it was kinase-dependent (Chang et al., 2009). The fact that microtubules of the ciliary axoneme are acetylated and that deacetylation of ciliary microtubules by HDAC6 is thought to cause ciliary retraction emphasizes the potential importance of enzymes that regulate the microtubule acetylation status for ciliogenesis (Bowers and Boylan, 2004). Based on the fact that cells expressing active or inactive Nek8 constructs have both reduced numbers of cilia and hyperacetylated microtubules, we can hypothesize that a link exists between these observations. It is possible that triggering hyperactylation of cytoplasmic microtubules suppresses the process of ciliogenesis. However, this remains to be determined.

The data presented in chapters 5 and 6 firstly demonstrate conditions for assaying the activity human Nek8. Secondly, they show that Nek8 disease-associated

mutants retain full kinase activity. Thirdly, they show that serum starvation induces proteasomal degradation of Nek8, specifically in cell lines in which serum starvation induces quiescence and ciliogenesis. Strikingly, serum starvation also induces Nek8 activation, whilst maintained expression of Nek8 appears to suppress ciliogenesis. Taken together, these findings not only reveal important mechanisms through which Nek8 activity and localization are regulated, but suggest that Nek8 itself may act, albeit in a kinase-independent manner, as an inhibitor of ciliogenesis.

Chapter 7

Final Discussion

The NIMA-related protein kinase family represents one of the least studied groups of protein kinases. Yet, it is becoming clear that different members of this play important roles in the regulation of the cell cycle, centrosome biology, as well as ciliogenesis. Moreover, their deregulation may contribute to the progression of various human diseases. Whilst, several Neks are overexpressed in cancer cells, mutations in Nek8 are associated with a rare form of the juvenile renal cystic disease, nephronophthisis. However, the signalling cascades through which Nek8 propagates its effects remain elusive. Indeed, despite some basic characterization of Nek8 at the molecular level, its regulation and function are far from clear, and the role of Nek8 in ciliogenesis remains to be defined. In this thesis, I present data from a series of biochemical and cell biology experiments aimed at investigating the regulation and function of Nek8 with respect to cell cycle progression and ciliogenesis.

7.1 Nek8 localizes to the centrosomes and proximal region of cilia in dividing and ciliated cells, respectively

The development of an antibody specific to Nek8, together with the generation of epitope-tagged Nek8 constructs, has enabled the subcellular localization of Nek8 to be examined. Data presented here indicate that in addition to nuclear localization (see 7.4), both recombinant and endogenous Nek8 localize to centrosomes and cilia in dividing and ciliated cells, respectively. Centrosomal and ciliary localization of Nek8 had been previously reported by other studies (Mahjoub et al., 2005; Shiba et al., 2010; Sohara et al., 2008) providing support to the ciliary hypothesis of cystic kidney disease. Here, we show that in human hTERT-RPE1 cells Nek8 is localized to the primary cilium, specifically to the proximal region of the cilium, known as the inversin compartment, that sits just above the transition zone (Shiba et al., 2010; Sohara et al., 2008). The inversin compartment is so-named as it is the site at which another NPHP disease gene, Inv/NPHP2 is localized. In fact, Inv/NPHP2 appears to anchor NPHP3 and Nek8/NPHP9 to this location (Shiba et al., 2010). Other proteins encoded by NPHP disease genes, including NPHP1, NPHP4 and NPHP8/RPGRIP1L, localize more precisely to the transition zone, below the inversin compartment. Moreover, in *Chlamydomonas*, the NPHP6/CEP290 homologue localizes to the wedge-shaped structures that connect the flagellar membrane with the axonemal microtubule doublets in the transition zone; and mutation leads to an abnormal distribution of proteins within the flagella (Craige et al., 2010). This has led to the hypothesis that the NPHP proteins may exist in one or several complexes around the transition zone that act as gatekeepers to control

protein entry and exit from the cilium (Hu and Nelson, 2011; Omran, 2010). Mislocalization may prevent the proper interaction between Nek8 and its substrates or effector molecules resulting in aberrant ciliary trafficking and signalling. This in turn may affect many downstream events such as cell cycle progression, ultimately leading to polycystic kidney disease. Indeed, it is tempting to speculate that many of these NPHP proteins, including Nek8, are present in a large complex, the "NPHP-some", similar to the BBSome in which many of the BBS proteins are found. Loss of any one of these components may cause the complex to fall apart explaining the phenotypic overlap that arises due to mutations in the different NPHP genes.

7.2 Establishment of an assay for Nek8 protein kinase activity

To explore the mechanism of Nek8 regulation and whether kinase activity was important for Nek8 function, it was critical to establish conditions for measuring Nek8 activity. Kinase activity of neither human nor murine Nek8 had previously been shown (Bowers and Boylan, 2004; Liu et al., 2002). Using a commercial source of purified GST-tagged Nek8 kinase expressed in wheat germ extract, we found that Nek8 phosphorylates myelin basic protein (MBP), histone H1 and β-casein as model substrates in the presence of 4 mM ATP and either 5 mM $MnCl_2$ or $MgCl_2$. Moreover, the kinase activity of recombinant GFP-tagged Nek8 expressed in HEK293 cells could also be measured following immunoprecipitation with anti-GFP antibodies. In this case it was important to avoid freezing extracts prior to immunoprecipitation as this led to much reduced activity (data not shown). The wild-type, but not the catalytically-inactive mutant D128A/K33R, phosphorylated β-casein and histone H1, whilst the Nek8 mutant, T162E, showed elevated activity against these substrates. MBP, on the other hand, was equally phosphorylated by all three Nek8 constructs suggesting that this phosphorylation may be due to a contaminating kinase. We therefore demonstrated, firstly, that Nek8 is active as a serine/threonine protein kinase and, secondly, both histone H1 and β-casein are suitable exogenous substrates for monitoring Nek8 kinase activity *in vitro*. Based on a comparison of various biochemical parameters, as well as a survey of other Neks, we conclude that human Nek8 is quite similar to other Neks. In fact, β-casein and histone H1 have been found to be suitable exogenous substrates for most Neks; for example, Nek1, Nek2, Nek3, Nek6 and Nek7 all phosphorylate β-casein, whilst Nek11 phosphorylates histone H1 and MBP (Fry et al., 1995; Holland et al., 2002; Letwin et al., 1992; Lu et al., 1993; Minoguchi et al., 2003; Osmani et al., 1991). Interestingly, Nek9 which is structurally very similar to Nek8, phosphorylates histone H1 and MBP, whilst β-casein is phosphorylated much less

well (Roig et al., 2002). In terms of biochemical properties, one striking difference between the mammalian Neks and *Aspergillus* NIMA concerns their response to Mn^{2+}; whereas most Neks are stimulated by this divalent cation, NIMA is inhibited (Fry et al., 1995; Holland et al., 2002; Letwin et al., 1992; Minoguchi et al., 2003). Here, we show that Nek8 is capable of phosphorylating better its substrates in the presence of Mg^{2+} suggesting that, like NIMA, Nek8 tends to have a preference for Mg^{2+} cations.

Using the experimental assay developed here, we then tested the activity of the known NPHP disease point mutants of Nek8: L330F, H425Y and A497P, the jck equivalent mutation, G442V, as well as the A197P mutation, which is equivalent to an amino acid change reported in a pancreatic cancer patient. We show that all the Nek8 disease mutants are active exhibiting equivalent activity to the wild-type protein. This was quite unexpected given that previous localization studies had shown that some of these mutants, notably H425Y, G442V and A197P, behave similarly to the inactive kinase domain mutants losing localization to centrosomes and cilia. As result, they were thought to be inactive. However, this is not the case, suggesting that their mislocalization is not a consequence of loss of activity.

We next compared the activity of the full-length kinase with the isolated kinase domain. For this, GFP-tagged fragments of Nek8 representing the kinase domain alone (GFP-FK) as well as the non-catalytic RCC1-like domain (GFP-RCC1) were generated. We found that an isolated kinase domain was as active as the full-length protein arguing that, unlike the related Nek9 protein (Roig et al., 2002), either the RCC1 domain does not act as an auto-inhibitory domain, or the auto-inhibition is fully released when the protein is expressed in cycling cells. We also found that the full-length kinase was capable of phosphorylating an isolated RCC1 domain raising the prospect that this kinase undergoes autophosphorylation within this region.

7.3 Correct Nek8 localization is dependent on both catalytic-activity and its RCC1 domain

Having established an assay to measure the activity of different Nek8 constructs, we examined whether Nek8 localization was affected in catalytic-site and disease-associated mutant forms of Nek8. We found that localization to the centrosomes and cilia corresponded precisely with activity of the full-length proteins (active proteins localizing correctly and inactive proteins failing to localize). This correlates with studies from Trapp et al. (2008) who showed that the kinase-deficient murine

mNek8-K33M failed to localize to cilia in IMCD-3 cells albeit without showing that the K33M mutant was inactive (Trapp et al., 2008). Another Nek kinase, Nek1, has been shown to localize to cilia and this localization is also dependent on its kinase activity. Like Nek8, Nek1 has been shown to play an important role in ciliogenesis and cystic kidney disease. Indeed, Nek1 carries the causal mutation in the *kat* and *kat*^{2J} (kidney, anemia, testes) mouse models of cystic kidney disease (Smith et al., 2006; Upadhya et al., 2000). Together, these data suggest that Nek1 and Nek8 may function in a similar manner during ciliogenesis. However, the catalytic activity of Nek8 is not the only determinant for correct localization to centrosomes and cilia as the isolated kinase domain which retained activity failed to localize correctly. Conversely, the isolated RCC1 domain localized correctly.

Localization studies of the Nek8 disease-associated mutants revealed that, whereas some NPHP mutants, i.e. L330F and A497P, localized correctly, another NPHP mutant, H425Y, together with the jck mutant, G442V, lost centrosomal and ciliary localization. Interestingly, L330F and A497P mutations were found in the heterozygous state, whereas H425Y and G442V that lie in close proximity in the same RCC1 motif occur in the homozygous state. As NPHP is a recessive disease, it is hard to reconcile the fact that heterozygous L330F and A497P mutations alone can be causative for NPHP. Indeed, a homozygous mutation in NPHP5 was found in the same patient as the L330F mutation. On the other hand these two Nek8 mutations were not found in the control samples. It remains possible that the other Nek8 allele in the patient was mutated at a different site, as this was not measured. Equally, though, it could be that these two mutations are not after all causative for NPHP.

How these mutations cause cystic kidney disease is not clear. However, it is possible that their mislocalization disturbs the gatekeeper function of protein complexes that include some of the NPHP proteins and which localize around the transition zone (Hu and Nelson, 2011; Omran, 2010). This could lead to an imbalance in the localization of ciliary proteins that control key developmental signalling pathways, such as those mediated by the Hedgehog and Wnt ligands (Berbari et al., 2009; Goetz and Anderson, 2010; Wong and Reiter, 2008). Similarly, it could disturb signalling via the polycystins, PC1 and PC2, which are mutated in ADPKD. Indeed, Nek8 is reported to interact with the PC2 protein, while the expression and localization of PC1 and PC2 are disturbed in renal cells from the *jck* mouse (Smith et al., 2006; Sohara et al., 2008). In addition, mice that carry heterozygous mutations in both the *Pkd1* gene, that encodes PC1, and the *Nek8*

gene also develop a more aggressive form of cystic kidney disease than are seen in *Pkd1* heterozygotes alone (Natoli et al., 2008). Interestingly, Nek1 is also implicated in regulating PC2 expression, in this case through phosphorylation of an E3 ubiquitin ligase adaptor that normally targets PC2 for degradation (Yim et al., 2011).

Loss of centrosomal and ciliary localization of the H425Y mutant had previously been shown in murine IMCD-3 cells (Otto et al., 2008), whereas localization of G442V jck mutant was contradictory. One study reported that Nek8 was localized throughout the length of the primary cilia in the kidney of the jck mouse (Sohara et al., 2008), whereas another report showed loss of Nek8 from primary cilia of cultured kidney cells taken from the jck mouse (Smith et al., 2006). Furthermore, Otto et al. (2008) have shown that the jck mutant protein localizes to centrosomes in IMCD-3 cells (Otto et al., 2008). These discrepancies may reflect differences in cell lines and cell differentiation status between tissue and cultured cells. Moreover, quantitative conclusion based on protein immunofluorescence is difficult due to antibody affinities. However, the fact that the H425Y and G442V mutations are positioned within the same RCC1 repeat of human Nek8, and both lead to loss of centrosomal and ciliary localization in our studies, supports the importance of this specific region of the protein for correct subcellular localization. We propose that this region forms part of a targeting motif that enables interaction with other centrosomal proteins that ultimately recruit Nek8 to centrosomes. In this regard, it will be interesting to test whether this region is important for association with INV/NPHP2 or NPHP3, as INV/NPHP2 is required to anchor both Nek8 and NPHP3 to the inversin compartment of cilium (Shiba et al., 2010). However, mutations in the RCC1 domain may also cause misfolding of this domain such that the H425Y mutation disrupts a more distant site of interaction. Indeed, whilst the RCC1-like domain alone is sufficient for localization to the cilia and centrosomes, individual fragments of the RCC1 domain, F1 and F2, lost localization. This is not surprising since the RCC1-like domain is likely to fold into a beta-propeller structure, and one can imagine that an incomplete fragment alone would not fold properly leading to its mislocalization.

However, mislocalization of the kinase domain is difficult to reconcile with our earlier finding that Nek8 kinase activity plays a crucial role for correct Nek8 localization to centrosomes and cilia. Clearly, our data show that localization of Nek8 to centrosomes and cilia is dependent upon both its kinase activity and its C-terminal non-catalytic RCC1 domain. Interestingly, Nek8 was capable of

phosphorylating its RCC1 domain as will be discussed in more detail later. Taken together, we propose a model whereby the RCC1 domain contains the centrosome/ciliary targeting motif, but that kinase activity is also required, with autophosphorylation within the RCC1 domain potentially causing a conformational change that reveals the centrosome targeting motif in the full-length protein (Fig. 7.1).

7.4 Nek8 localizes to the nucleus

In addition to centrosomal and ciliary localization, we observed that both endogenous and recombinant Nek8 proteins also localize to the nucleus. In fact, Nek8 appears to be diffusely distributed throughout nucleoplasm. Upon inhibition of nuclear export, Nek8 concentration in the nucleus increased, suggesting that this protein kinase is likely to shuttle between the cytoplasm and nucleus. This would allow it to convey signals between the primary cilium and the nucleus. None of the mutations in the kinase domain affected nuclear localization, indicating that activity is not required for nuclear uptake or export. Furthermore, using a series of truncated mutants of Nek8, we found that the C-terminal non-catalytic RCC1 domain of Nek8 is responsible for Nek8 nuclear localization. We interpret these data to mean that one or more nuclear localization sequences are present within the non-catalytic RCC1 domain.

The nuclear localization of Nek8 would be consistent with the fact that the etiology of kidney cysts involves aberrant signalling from the primary cilium to the nucleus. In fact, signals for both proliferation and differentiation are received by the primary cilium (Caspary et al., 2007; Evangelista et al., 2008). It is therefore logical that some cystogenic proteins, possibly even Nek8, convey signals between the primary cilium and the nucleus in order to regulate gene expression. A link between Nek8 ciliary and nuclear function is further supported by the localization studies of the NPHP disease-associated mutants, H425Y and the jck equivalent, G442V. These mutants that showed loss of centrosomal and ciliary localization also lost nuclear localization. Whilst one can well imagine that centrosome and ciliary targeting are regulated by interaction with one specific partner protein, it is less obvious that the same partner would target the protein to the nucleus. However, this may yet be the case if Nek8 is part of a complex that transduces signals from the cilia, through the basal body to the nucleus. Hence, it is possible that signalling cascades between the primary cilia and the nucleus may affect both proliferation and differentiation of renal cells, ultimately leading to cystic kidney disease. Intriguingly, it is possible that the nuclear localization of Nek8 is controlled by Ran

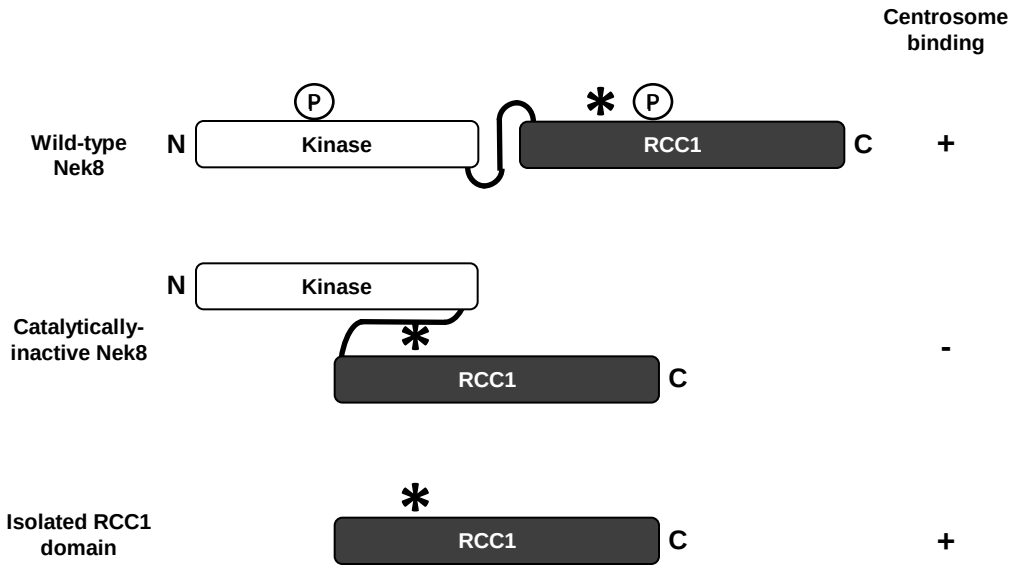

Figure 7.1 Model for control of Nek8 localization
The schematic diagram shows how both kinase activity and the non-catalytic RCC1 domain could be required for localization of Nek8 to centrosomes, cilia, and possibly, nuclei. In this model, the wild-type protein undergoes autophosphorylation within the RCC1 domain. It also requires phosphorylation within the activation loop of the catalytic domain, although whether this is an autophosphorylation event is unclear. We propose that these phosphorylation events lead to an opening up of the conformation that reveals a centrosome-targeting motif present within the RCC1 domain (*). However, a catalytically-inactive mutant cannot autophosphorylate and hence remains in the closed conformation whereby the centrosome-targeting motif is masked. In an isolated RCC1 domain, the centrosome-targeting motif would be already unmasked and therefore not require phosphorylation.

through interaction with the RCC1-like domain. This might explain why the mutants H425Y and G442V lose nuclear localization. Indeed, there are similarities between the ciliary gateway model and the nuclear pore complex that regulates nuclear entry via the nuclear-cytoplasmic gradient of the small GTPase Ran. Ran is present in cilia and could regulate Nek8 ciliary targeting through a ciliary-cytoplasmic gradient (Dishinger et al., 2010). However, at the current time we have no idea whether Nek8 can interact with Ran.

Like Nek8, polycystins have also been shown to function co-operatively in altering gene expression through cilium-to-nucleus signalling (Zhou, 2009). Similarly, Nek1, whose mutations are causal for cystic kidney disease, also localizes to the nucleus as well as the cilium making it an excellent candidate for conveying signals between primary cilia and nucleus. That Nek1 and Nek8 exhibit similar localization patterns and play an important role in polycystic kidney disease, raises the possibility that they may function in the same pathway during ciliogenesis just as Nek9, Nek6 and Nek7 cooperate in mitotic spindle organization.

7.5 Nek8 undergoes proteasomal degradation in response to entry into quiescence

During our immunofluorescence microscopy studies we had noted that it was difficult to find many transfected cells following serum starvation of hTERT-RPE1 cells. As transfected cells were common before serum starvation and there was no difficulty detecting cells transfected with GFP alone after serum starvation, this suggested that Nek8 may be degraded during serum starvation. Addition of a proteasomal inhibitor rescued Nek8 expression. Hence, Nek8 is degraded in a proteasomal dependent manner upon serum starvation. This proteasomal dependent loss of Nek8 is a cell cycle response due to entry into quiescence, as Nek8 was only degraded in NIH3T3 and hTERT-RPE1 cells, which exited the cell cycle upon serum withdrawal, and not in HeLa and U2OS cells that did not. Furthermore, this process occurs in a kinase independent manner and is not affected by Nek8 disease-associated mutants since proteasomal degradation of all full-length Nek8 constructs was observed irrespective of mutation status. The fact that quiescence induces proteasomal degradation of Nek8 suggests that maintained expression of Nek8 may be somehow detrimental to cilia organization or function. Alternatively, it is possible that Nek8 has cell cycle functions that must be switched off upon ciliogenesis. This hypothesis is supported by studies from Shiba et al (2010) who explained the ciliary localization of Nek8 as a way to

prevent it from performing unwanted functions, such as phosphorylating cytoplasmic targets that promote cell cycle progression (Shiba et al., 2010).

By carrying out structure function analysis, we were able to determine that the proteasome dependent degradation of Nek8 occurs through its kinase domain, as Nek8-FK was degraded whereas Nek8-F1 and Nek8-F2 were not. Interestingly, quiescence also led to an up-shift of the Nek8 kinase domain that was not present with the T162 mutants, suggesting that serum starvation is also accompanied by phosphorylation at this residue. We therefore conclude that exit from the cell cycle is accompanied by both phosphorylation and proteasome-mediated degradation of Nek8 that occurs via targeting of the kinase domain but in a kinase-independent manner.

7.6 Nek8 promotes microtubule acetylation but prevents ciliogenesis

Previous studies have reported that neither siRNA-mediated depletion nor overexpression of Nek8 interferes with ciliogenesis (Mahjoub et al., 2005; Otto et al., 2008; Trapp et al., 2008). Contrary to these data, we found a significant decrease in the number of GFP-Nek8 expressing hTERT-RPE1 cells that had primary cilia as compared to those expressing either GFP alone or GFP-Nek7. This might suggest that Nek8 is an inhibitor of ciliogenesis. This result was independent of kinase activity since a similar reduction in the percentage of ciliated cells was observed with the inactive Nek8 mutants K33R/D128A and T162A) as with the wild-type and the active mutant (T162E). Similarly, expression of the NPHP disease mutants led to reduction in ciliogenesis. If Nek8 is an inhibitor of ciliogenesis, then there could be several explanations for this. Nek8 could inhibit ciliogenesis by blocking the post-mitotic expression of ciliary proteins in the nucleus. Alternatively, it may interfere with assembly or docking of preciliary complexes at the centrosome. Importantly, it may also stimulate excessive ciliary disassembly leading to loss of cilia.

Interestingly, tumour cells commonly do not have cilia (Seeley et al., 2009), and Nek8 is often upregulated in cancers; for example, primary breast tumours have high levels of Nek8 (Bowers and Boylan, 2004). More recently, a new study has reported the identification of a putative driver mutation, A197P, in Nek8 in pancreatic cancer (Carter et al., 2010). We found that the A197P mutation retained Nek8 kinase activity, but failed to localize properly.

As previously mentioned, Nek1 has also been found to inhibit ciliogenesis in the murine renal epithelial cell line, IMCD3 (White and Quarmby, 2008). However, in contrast to Nek8, Nek1 inhibits cilia formation in a kinase dependent manner since overexpression of presumptive kinase-dead forms of Nek1 did not inhibit ciliogenesis (White and Quarmby, 2008). Overexpression of the mitotic kinase, Aurora A also leads to the loss of cilia in mammalian cells. This was shown to be mediated by the phosphorylation and activation of the tubulin deacetylase, HDAC6, as cilia are retained in cells with excess Aurora A if these cells are treated with HDAC inhibitors (Pugacheva et al., 2007; White and Quarmby, 2008). The hypothesis in this case is that deacetylation of ciliary microtubules promotes their instability and cilia resorption. It is unlikely that Nek8 acts in this manner though as we observed a dramatic increase in the number of cytoplasmic microtubules that stained positively for acetylated tubulin in cells expressing Nek8. Again, this was seen not only with the wild-type Nek8, but also the kinase-domain mutants and the NPHP disease associated mutants suggesting that overexpression of Nek8 in cells, whether active or inactive, promotes microtubule hyperacetylation. Nevertheless, it suggests that Nek8 may also play a role in regulating microtubule dynamics. Microtubule hyperacetylation has been previously seen with other Neks. For example, mouse embryonic fibroblast (derived from *kat* mice) in which Nek1 is mutated, displayed long, thick and usually branched structures stained by acetylated tubulin antibodies. However, these structures very rarely appeared in wild-type cells (Shalom et al., 2008). Nek3 was also shown to regulate microtubule hyperacetylation in neuronal cells in a kinase dependent manner (Chang et al., 2009). It remains to be determined whether the increase in microtubule acetylation seen upon Nek8 overexpression is in some way responsible for the block to cilia formation. It is possible that triggering hyperacetylation of cytoplasmic microtubules interferes with the process of ciliogenesis. However since this phenotype is independent on Nek8 kinase activity it is difficult to conclude that this reflects the normal function of the protein when present at physiological levels.

7.7 Nek8 kinase is activated by serum starvation

Despite undergoing proteasomal degradation, the Nek8 protein is also activated upon exit from the cell cycle. Interestingly, all three of the NPHP-disease associated mutants, together with the *jck* equivalent mutation and the pancreatic cancer associated mutation, showed equivalent activation to the wild-type upon entry into quiescence. This suggests that there is no defect in the activation of the disease-associated Nek8 mutants. The fact that Nek8 is activated during

quiescence is at first sight difficult to reconcile with the fact that Nek8 is also degraded and inhibits ciliogenesis in a kinase independent manner. So what is the function of Nek8 kinase activity and when does this activation step occur?

Here we speculate that Nek8 activity may be needed within a specific time frame during ciliogenesis, perhaps at the onset of ciliogenesis at the G1/G0 transition. Nek8 activity may stimulate the changes required to convert a centriole to basal body, thus acting as a positive regulator during the initiation of ciliogenesis. However, the initial RNAi studies performed to date do not reveal a requirement for Nek8 for ciliogenesis (Otto et al., 2008; Sohara et al., 2008). In contrast, sustained activity of Nek8 may block cilia growth thus acting as a negative regulator of ciliogenesis, explaining the need for Nek8 degradation following quiescence. Hence, both activation and degradation of Nek8 may be necessary for the formation of cilia. However, it should also be considered that the inhibition of ciliogenesis seen in GFP-expressing cells is a consequence of overexpression and, at physiological levels, Nek8 may not be an inhibitor of this process.

7.8 Concluding comments

Here, we have firstly described an assay for Nek8 kinase activity that has allowed us to explore the mechanisms through which this NPHP disease protein is regulated. We found that none of the Nek8 mutations identified in NPHP patients, nor the equivalent mutation to that found in the *jck* mouse model of juvenile cystic kidney disease, alter activity of this enzyme. However, kinase activity is required for correct localization of the protein to the centrosome in dividing cells and the proximal region of the cilia in quiescent cells. This localization is also dependent on the non-catalytic RCC1 domain, which in turn may depend upon autophosphorylation within this domain. We also conclude that the NPHP mutant, H425Y, and the jck mouse mutant, shown to lose centrosomal and ciliary localization, are most likely disrupting a centrosome/ciliary targeting motif, rather than Nek8 kinase activity. In contrast, it remains to be determined to what extent L330F and A497P are involved in the NPHP pathology. Intriguingly, we also observed a localization defect with the A197P mutant that is implicated in pancreatic cancer. Its ability to localize to the centrosome, cilium and nucleus was completely abolished. This could potentially abrogate a transcriptional programme that dictates whether cells enter quiescence or continue through the cell cycle. Indeed, defects in ciliary signalling to the nucleus have now been implicated in the development of tumours (Han et al., 2009; Wong et al., 2009). Alternatively, Nek8 could play a role at centrosomes during mitotic cell division and it is worth bearing

in mind that the development of kidney cysts reflects a loss of control over both cell cycle progression and mitotic spindle orientation (Hildebrandt and Otto, 2005; Pazour and Rosenbaum, 2004). Future studies will clearly need to address the possibility that Nek8 plays a crucial role in coordinating ciliogenesis with the mitotic cell division cycle. Finally, we show that exit from the cell cycle and initiation of ciliogenesis is accompanied by, first, activation and, second, degradation of the Nek8 protein, while activation requires autophosphorylation within the activation loop of the kinase. At the present time, the purpose of Nek8 activation and degradation remains entirely unknown. However, we can speculate that Nek8 activity may be required to initiate some aspect of the ciliogenesis programme, whereas its degradation may be required to prevent this initiation process from being maintained indefinitely. These studies therefore provide important new insights into what regulates both the activity and the localization of this cystic kidney disease protein. In the future, identification of Nek8 substrates and its regulatory proteins, together with how it cooperate with other ciliopathy-associated proteins involved in polycystic kidney disease will be crucial for the understanding of the mechanisms underlying, and connecting, these devastating human disorders.

Chapter 8

Bibliography

Adams, M., Smith, U.M., Logan, C.V., and Johnson, C.A. (2008). Recent advances in the molecular pathology, cell biology and genetics of ciliopathies. J Med Genet *45*, 257-267.

Ahmad, F.J., Yu, W., McNally, F.J., and Baas, P.W. (1999). An essential role for katanin in severing microtubules in the neuron. J Cell Biol *145*, 305-315.

Andersen, J.S., Wilkinson, C.J., Mayor, T., Mortensen, P., Nigg, E.A., and Mann, M. (2003). Proteomic characterization of the human centrosome by protein correlation profiling. Nature *426*, 570-574.

Anderson, C.T., Castillo, A.B., Brugmann, S.A., Helms, J.A., Jacobs, C.R., and Stearns, T. (2008). Primary cilia: cellular sensors for the skeleton. Anat Rec (Hoboken) *291*, 1074-1078.

A**rama, E., Yanai, A., Kilfin, G., Bernstein, A., and Motro, B.** (1998). Murine NIMA-related kinases are expressed in patterns suggesting distinct functions in gametogenesis and a role in the nervous system. Oncogene *16*, 1813-1823
.
Axelrod, J.D. (2008). Basal bodies, kinocilia and planar cell polarity. Nat Genet *40*, 10-11.

Azimzadeh, J., and Bornens, M. (2007). Structure and duplication of the centrosome. J Cell Sci *120*, 2139-2142.

Baboshina, O.V., and Haas, A.L. (1996). Novel multiubiquitin chain linkages catalyzed by the conjugating enzymes E2EPF and RAD6 are recognized by 26 S proteasome subunit 5. J Biol Chem *271*, 2823-2831.

Badano, J.L., Mitsuma, N., Beales, P.L., and Katsanis, N. (2006). The ciliopathies: an emerging class of human genetic disorders. Annu Rev Genomics Hum Genet *7*, 125-148.

Bahe, S., Stierhof, Y.D., Wilkinson, C.J., Leiss, F., and Nigg, E.A. (2005). Rootletin forms centriole-associated filaments and functions in centrosome cohesion. J Cell Biol *171*, 27-33.

Baker, K., and Beales, P.L. (2009). Making sense of cilia in disease: the human ciliopathies. Am J Med Genet C Semin Med Genet *151C*, 281-295.

Barton, A.B., Davies, C.J., Hutchison, C.A., 3rd, and Kaback, D.B. (1992). Cloning of chromosome I DNA from Saccharomyces cerevisiae: analysis of the FUN52 gene, whose product has homology to protein kinases. Gene *117*, 137-140.

Belham, C., Comb, M.J., and Avruch, J. (2001). Identification of the NIMA family kinases NEK6/7 as regulators of the p70 ribosomal S6 kinase. Curr Biol *11*, 1155-1167.

Belham, C., Roig, J., Caldwell, J.A., Aoyama, Y., Kemp, B.E., Comb, M., and Avruch, J. (2003). A mitotic cascade of NIMA family kinases. Nercc1/Nek9 activates the Nek6 and Nek7 kinases. J Biol Chem *278*, 34897-34909.

Berbari, N.F., O'Connor, A.K., Haycraft, C.J., and Yoder, B.K. (2009). The primary cilium as a complex signaling center. Curr Biol *19*, R526-535.

Bertran, M.T., Sdelci, S., Regue, L., Avruch, J., Caelles, C., and Roig, J. (2011). Nek9 is a Plk1-activated kinase that controls early centrosome separation through Nek6/7 and Eg5. EMBO J *30*, 2634-2647.

Bettencourt-Dias, M., and Glover, D.M. (2007). Centrosome biogenesis and function: centrosomics brings new understanding. Nat Rev Mol Cell Biol *8*, 451-463.

Bibby, R.A., Tang, C., Faisal, A., Drosopoulos, K., Lubbe, S., Houlston, R., Bayliss, R., and Linardopoulos, S. (2009). A cancer-associated aurora A mutant is mislocalized and misregulated due to loss of interaction with TPX2. J Biol Chem *284*, 33177-33184.

Bisgrove, B.W., and Yost, H.J. (2006). The roles of cilia in developmental disorders and disease. Development *133*, 4131-4143.

Blacque, O.E., Reardon, M.J., Li, C., McCarthy, J., Mahjoub, M.R., Ansley, S.J., Badano, J.L., Mah, A.K., Beales, P.L., Davidson, W.S.*, et al.* (2004). Loss of C. elegans BBS-7 and BBS-8 protein function results in cilia defects and compromised intraflagellar transport. Genes Dev *18*, 1630-1642.

Blagden, S.P., and Glover, D.M. (2003). Polar expeditions--provisioning the centrosome for mitosis. Nat Cell Biol *5*, 505-511.

Bloodgood, R.A. (2010). Sensory reception is an attribute of both primary cilia and motile cilia. J Cell Sci *123*, 505-509.

Bowers, A.J., and Boylan, J.F. (2004). Nek8, a NIMA family kinase member, is overexpressed in primary human breast tumors. Gene *328*, 135-142.

Bradley, B.A., and Quarmby, L.M. (2005). A NIMA-related kinase, Cnk2p, regulates both flagellar length and cell size in Chlamydomonas. J Cell Sci *118*, 3317-3326.

Cabrera, C.V., Alonso, M.C., Johnston, P., Phillips, R.G., and Lawrence, P.A. (1987). Phenocopies induced with antisense RNA identify the wingless gene. Cell *50*, 659-663.

Cadigan, K.M., and Peifer, M. (2009). Wnt signaling from development to disease: insights from model systems. Cold Spring Harb Perspect Biol *1*, a002881.

Cai, Y., and Somlo, S. (2008). Too much of a good thing: does Nek8 link polycystic kidney disease and nephronophthisis? J Am Soc Nephrol *19*, 418-420.

Cance, W.G., Craven, R.J., Weiner, T.M., and Liu, E.T. (1993). Novel protein kinases expressed in human breast cancer. Int J Cancer *54*, 571-577.

Cardenas-Rodriguez, M., and Badano, J.L. (2009). Ciliary biology: understanding the cellular and genetic basis of human ciliopathies. Am J Med Genet C Semin Med Genet *151C*, 263-280.

Carter, H., Samayoa, J., Hruban, R.H., and Karchin, R. (2010). Prioritization of driver mutations in pancreatic cancer using cancer-specific high-throughput annotation of somatic mutations (CHASM). Cancer Biol Ther *10*, 582-587.

Caspary, T., Larkins, C.E., and Anderson, K.V. (2007). The graded response to Sonic Hedgehog depends on cilia architecture. Dev Cell *12*, 767-778.

Chang, B., Khanna, H., Hawes, N., Jimeno, D., He, S., Lillo, C., Parapuram, S.K., Cheng, H., Scott, A., Hurd, R.E.*, et al.* (2006). In-frame deletion in a novel centrosomal/ciliary protein CEP290/NPHP6 perturbs its interaction with RPGR and results in early-onset retinal degeneration in the rd16 mouse. Hum Mol Genet *15*, 1847-1857.

Chang, J., Baloh, R.H., and Milbrandt, J. (2009). The NIMA-family kinase Nek3 regulates microtubule acetylation in neurons. J Cell Sci *122*, 2274-2282.

Chapin, H.C., and Caplan, M.J. (2010). The cell biology of polycystic kidney disease. J Cell Biol *191*, 701-710.

Chen, A., Yanai, A., Arama, E., Kilfin, G., and Motro, B. (1999). NIMA-related kinases: isolation and characterization of murine nek3 and nek4 cDNAs, and chromosomal localization of nek1, nek2 and nek3. Gene *234*, 127-137.

Chen, Y., Chen, P.L., Chen, C.F., Jiang, X., and Riley, D.J. (2008). Never-in-mitosis related kinase 1 functions in DNA damage response and checkpoint control. Cell Cycle *7*, 3194-3201.

Corbit, K.C., Shyer, A.E., Dowdle, W.E., Gaulden, J., Singla, V., Chen, M.H., Chuang, P.T., and Reiter, J.F. (2008). Kif3a constrains beta-catenin-dependent Wnt signalling through dual ciliary and non-ciliary mechanisms. Nat Cell Biol *10*, 70-76.

Craige, B., Tsao, C.C., Diener, D.R., Hou, Y., Lechtreck, K.F., Rosenbaum, J.L., and Witman, G.B. (2010). CEP290 tethers flagellar transition zone microtubules to the membrane and regulates flagellar protein content. J Cell Biol *190*, 927-940.

Crasta, K., Lim, H.H., Giddings, T.H., Jr., Winey, M., and Surana, U. (2008). Inactivation of Cdh1 by synergistic action of Cdk1 and polo kinase is necessary for proper assembly of the mitotic spindle. Nat Cell Biol *10*, 665-675.

Cuschieri, L., Nguyen, T., and Vogel, J. (2007). Control at the cell center: the role of spindle poles in cytoskeletal organization and cell cycle regulation. Cell Cycle *6*, 2788-2794.

D'Angelo, A., and Franco, B. (2009). The dynamic cilium in human diseases. Pathogenetics *2*, 3.

Dabdoub, A., and Kelley, M.W. (2005). Planar cell polarity and a potential role for a Wnt morphogen gradient in stereociliary bundle orientation in the mammalian inner ear. J Neurobiol *64*, 446-457.

Davenport, J.R., and Yoder, B.K. (2005). An incredible decade for the primary cilium: a look at a once-forgotten organelle. Am J Physiol Renal Physiol *289*, F1159-1169.

Dawe, H.R., Farr, H., and Gull, K. (2007). Centriole/basal body morphogenesis and migration during ciliogenesis in animal cells. J Cell Sci *120*, 7-15.

De Souza, C.P., Horn, K.P., Masker, K., and Osmani, S.A. (2003). The SONB(NUP98) nucleoporin interacts with the NIMA kinase in Aspergillus nidulans. Genetics *165*, 1071-1081.

De Souza, C.P., Osmani, A.H., Wu, L.P., Spotts, J.L., and Osmani, S.A. (2000). Mitotic histone H3 phosphorylation by the NIMA kinase in Aspergillus nidulans. Cell *102*, 293-302.

Debec, A., Sullivan, W., and Bettencourt-Dias, M. (2010). Centrioles: active players or passengers during mitosis? Cell Mol Life Sci *67*, 2173-2194.

Delgehyr, N., Sillibourne, J., and Bornens, M. (2005). Microtubule nucleation and anchoring at the centrosome are independent processes linked by ninein function. J Cell Sci *118*, 1565-1575.

Deltas, C., and Papagregoriou, G. (2010). Cystic diseases of the kidney: molecular biology and genetics. Arch Pathol Lab Med *134*, 569-582.

Dictenberg, J.B., Zimmerman, W., Sparks, C.A., Young, A., Vidair, C., Zheng, Y., Carrington, W., Fay, F.S., and Doxsey, S.J. (1998). Pericentrin and gamma-tubulin form a protein complex and are organized into a novel lattice at the centrosome. J Cell Biol *141*, 163-174.

Dishinger, J.F., Kee, H.L., Jenkins, P.M., Fan, S., Hurd, T.W., Hammond, J.W., Truong, Y.N., Margolis, B., Martens, J.R., and Verhey, K.J. (2010). Ciliary entry of the kinesin-2 motor KIF17 is regulated by importin-beta2 and RanGTP. Nat Cell Biol *12*, 703-710.

Doxsey, S. (2001a). Re-evaluating centrosome function. Nat Rev Mol Cell Biol *2*, 688-698.

Doxsey, S., Zimmerman, W., and Mikule, K. (2005). Centrosome control of the cell cycle. Trends Cell Biol *15*, 303-311.

Doxsey, S.J. (2001b). Centrosomes as command centres for cellular control. Nat Cell Biol *3*, E105-108.

Evangelista, M., Lim, T.Y., Lee, J., Parker, L., Ashique, A., Peterson, A.S., Ye, W., Davis, D.P., and de Sauvage, F.J. (2008). Kinome siRNA screen identifies regulators of ciliogenesis and hedgehog signal transduction. Sci Signal *1*, ra7.

Fang, S., and Weissman, A.M. (2004). A field guide to ubiquitylation. Cell Mol Life Sci *61*, 1546-1561.

Faragher, A.J., and Fry, A.M. (2003). Nek2A kinase stimulates centrosome disjunction and is required for formation of bipolar mitotic spindles. Mol Biol Cell *14*, 2876-2889.

Fardilha, M., Wu, W., Sa, R., Fidalgo, S., Sousa, C., Mota, C., da Cruz e Silva, O.A., and da Cruz e Silva, E.F. (2004). Alternatively spliced protein variants as potential therapeutic targets for male infertility and contraception. Ann N Y Acad Sci *1030*, 468-478.

Finst, R.J., Kim, P.J., and Quarmby, L.M. (1998). Genetics of the deflagellation pathway in Chlamydomonas. Genetics *149*, 927-936.

Fischer, E., Legue, E., Doyen, A., Nato, F., Nicolas, J.F., Torres, V., Yaniv, M., and Pontoglio, M. (2006). Defective planar cell polarity in polycystic kidney disease. Nat Genet *38*, 21-23.

Fletcher, L., Cerniglia, G.J., Yen, T.J., and Muschel, R.J. (2005). Live cell imaging reveals distinct roles in cell cycle regulation for Nek2A and Nek2B. Biochim Biophys Acta *1744*, 89-92.

Fliegauf, M., Horvath, J., von Schnakenburg, C., Olbrich, H., Muller, D., Thumfart, J., Schermer, B., Pazour, G.J., Neumann, H.P., Zentgraf, H.*, et al.* (2006). Nephrocystin specifically localizes to the transition zone of renal and respiratory cilia and photoreceptor connecting cilia. J Am Soc Nephrol *17*, 2424-2433.

Fliegauf, M., Benzing, T., and Omran, H. (2007). When cilia go bad: cilia defects and ciliopathies. Nat Rev Mol Cell Biol *8*, 880-893.

Fry, A.M. (2002). The Nek2 protein kinase: a novel regulator of centrosome structure. Oncogene *21*, 6184-6194.

Fry, A.M., Arnaud, L., and Nigg, E.A. (1999). Activity of the human centrosomal kinase, Nek2, depends on an unusual leucine zipper dimerization motif. J Biol Chem *274*, 16304-16310.

Fry, A.M., Mayor, T., Meraldi, P., Stierhof, Y.D., Tanaka, K., and Nigg, E.A. (1998a). C-Nap1, a novel centrosomal coiled-coil protein and candidate substrate of the cell cycle-regulated protein kinase Nek2. J Cell Biol *141*, 1563-1574.

Fry, A.M., Meraldi, P., and Nigg, E.A. (1998b). A centrosomal function for the human Nek2 protein kinase, a member of the NIMA family of cell cycle regulators. EMBO J *17*, 470-481.

Fry, A.M., Schultz, S.J., Bartek, J., and Nigg, E.A. (1995). Substrate specificity and cell cycle regulation of the Nek2 protein kinase, a potential human homolog of the mitotic regulator NIMA of Aspergillus nidulans. J Biol Chem *270*, 12899-12905.

Fumoto, K., Hoogenraad, C.C., and Kikuchi, A. (2006). GSK-3beta-regulated interaction of BICD with dynein is involved in microtubule anchorage at centrosome. EMBO J *25*, 5670-5682.

Gale, M., Jr., and Parsons, M. (1993). A Trypanosoma brucei gene family encoding protein kinases with catalytic domains structurally related to Nek1 and NIMA. Mol Biochem Parasitol *59*, 111-121.

Gerdes, J.M., Liu, Y., Zaghloul, N.A., Leitch, C.C., Lawson, S.S., Kato, M., Beachy, P.A., Beales, P.L., DeMartino, G.N., Fisher, S.*, et al.* (2007). Disruption of the basal body compromises proteasomal function and perturbs intracellular Wnt response. Nat Genet *39*, 1350-1360.

Germino, G.G. (2005). Linking cilia to Wnts. Nat Genet *37*, 455-457.

Glickman, M.H., and Ciechanover, A. (2002). The ubiquitin-proteasome proteolytic pathway: destruction for the sake of construction. Physiol Rev *82*, 373-428.

Goetz, S.C., and Anderson, K.V. (2010). The primary cilium: a signalling centre during vertebrate development. Nat Rev Genet *11*, 331-344.

Goetz, S.C., Ocbina, P.J., and Anderson, K.V. (2009). The primary cilium as a Hedgehog signal transduction machine. Methods Cell Biol *94*, 199-222.

Grallert, A., and Hagan, I.M. (2002). Schizosaccharomyces pombe NIMA-related kinase, Fin1, regulates spindle formation and an affinity of Polo for the SPB. EMBO J *21*, 3096-3107.

Grallert, A., Krapp, A., Bagley, S., Simanis, V., and Hagan, I.M. (2004). Recruitment of NIMA kinase shows that maturation of the S. pombe spindle-

pole body occurs over consecutive cell cycles and reveals a role for NIMA in modulating SIN activity. Genes Dev *18*, 1007-1021.

Guirao, B., and Joanny, J.F. (2007). Spontaneous creation of macroscopic flow and metachronal waves in an array of cilia. Biophys J *92*, 1900-1917.

Hagiwara, H., Harada, S., Maeda, S., Aoki, T., Ohwada, N., and Takata, K. (2002). Ultrastructural and immunohistochemical study of the basal apparatus of solitary cilia in the human oviduct epithelium. J Anat *200*, 89-96.

Hagiwara, H., Ohwada, N., and Takata, K. (2004). Cell biology of normal and abnormal ciliogenesis in the ciliated epithelium. Int Rev Cytol *234*, 101-141.

Hames, R.S., Wattam, S.L., Yamano, H., Bacchieri, R., and Fry, A.M. (2001). APC/C-mediated destruction of the centrosomal kinase Nek2A occurs in early mitosis and depends upon a cyclin A-type D-box. Embo J *20*, 7117-7127.

Hames, R.S., and Fry, A.M. (2002). Alternative splice variants of the human centrosome kinase Nek2 exhibit distinct patterns of expression in mitosis. Biochem J *361*, 77-85.

Hames, R.S., Crookes, R.E., Straatman, K.R., Merdes, A., Hayes, M.J., Faragher, A.J., and Fry, A.M. (2005). Dynamic recruitment of Nek2 kinase to the centrosome involves microtubules, PCM-1, and localized proteasomal degradation. Mol Biol Cell *16*, 1711-1724.

Han, Y.G., Kim, H.J., Dlugosz, A.A., Ellison, D.W., Gilbertson, R.J., and Alvarez-Buylla, A. (2009). Dual and opposing roles of primary cilia in medulloblastoma development. Nat Med *15*, 1062-1065.

Han, Y.G., and Alvarez-Buylla, A. (2010). Role of primary cilia in brain development and cancer. Curr Opin Neurobiol *20*, 58-67.

Hanks, S.K., and Hunter, T. (1995). Protein kinases 6. The eukaryotic protein kinase superfamily: kinase (catalytic) domain structure and classification. FASEB J *9*, 576-596

Hao, L., Acar, S., Evans, J., Ou, G., and Scholey, J.M. (2009). Analysis of intraflagellar transport in C. elegans sensory cilia. Methods Cell Biol *93*, 235-266.

Hao, L., and Scholey, J.M. (2009). Intraflagellar transport at a glance. J Cell Sci *122*, 889-892.

Hartman, J.J., Mahr, J., McNally, K., Okawa, K., Iwamatsu, A., Thomas, S., Cheesman, S., Heuser, J., Vale, R.D., and McNally, F.J. (1998). Katanin, a microtubule-severing protein, is a novel AAA ATPase that targets to the centrosome using a WD40-containing subunit. Cell *93*, 277-287.

Hashimoto, M., Shinohara, K., Wang, J., Ikeuchi, S., Yoshiba, S., Meno, C., Nonaka, S., Takada, S., Hatta, K., Wynshaw-Boris, A.*, et al.* (2010). Planar polarization of node cells determines the rotational axis of node cilia. Nat Cell Biol *12*, 170-176.

He, X. (2008). Cilia put a brake on Wnt signalling. Nat Cell Biol *10*, 11-13.

Hearn, T., Spalluto, C., Phillips, V.J., Renforth, G.L., Copin, N., Hanley, N.A., and Wilson, D.I. (2005). Subcellular localization of ALMS1 supports involvement of centrosome and basal body dysfunction in the pathogenesis of obesity, insulin resistance, and type 2 diabetes. Diabetes *54*, 1581-1587.

Helps, N.R., Luo, X., Barker, H.M., and Cohen, P.T. (2000). NIMA-related kinase 2 (Nek2), a cell-cycle-regulated protein kinase localized to centrosomes, is complexed to protein phosphatase 1. Biochem J *349*, 509-518.

Hildebrandt, F., Otto, E., Rensing, C., Nothwang, H.G., Vollmer, M., Adolphs, J., Hanusch, H., and Brandis, M. (1997). A novel gene encoding an SH3 domain protein is mutated in nephronophthisis type 1. Nat Genet *17*, 149-153.

Hildebrandt, F., Attanasio, M., and Otto, E. (2009). Nephronophthisis: disease mechanisms of a ciliopathy. J Am Soc Nephrol *20*, 23-35.
Hildebrandt, F., Benzing, T., and Katsanis, N. (2011). Ciliopathies. N Engl J Med *364*, 1533-1543.

Hildebrandt, F., and Otto, E. (2005). Cilia and centrosomes: a unifying pathogenic concept for cystic kidney disease? Nat Rev Genet *6*, 928-940.

Hildebrandt, F., and Zhou, W. (2007). Nephronophthisis-associated ciliopathies. J Am Soc Nephrol *18*, 1855-1871.

Hilton, L.K., White, M.C., and Quarmby, L.M. (2009). The NIMA-related kinase NEK1 cycles through the nucleus. Biochem Biophys Res Commun *389*, 52-56.

Hirokawa, N., Tanaka, Y., Okada, Y., and Takeda, S. (2006). Nodal flow and the generation of left-right asymmetry. Cell *125*, 33-45.

Holland, P.M., Milne, A., Garka, K., Johnson, R.S., Willis, C., Sims, J.E., Rauch, C.T., Bird, T.A., and Virca, G.D. (2002). Purification, cloning, and characterization of Nek8, a novel NIMA-related kinase, and its candidate substrate Bicd2. J Biol Chem *277*, 16229-16240.

Hoppe, T. (2005). Multiubiquitylation by E4 enzymes: 'one size' doesn't fit all. Trends Biochem Sci *30*, 183-187.

Hoyer-Fender, S. (2010). Centriole maturation and transformation to basal body. Semin Cell Dev Biol *21*, 142-147.

Hu, Q., and Nelson, W.J. (2011). Ciliary diffusion barrier: the gatekeeper for the primary cilium compartment. Cytoskeleton (Hoboken) *68*, 313-324.

Huelsken, J., and Behrens, J. (2002). The Wnt signalling pathway. J Cell Sci *115*, 3977-3978.

Hurd, T.W., and Hildebrandt, F. (2011). Mechanisms of nephronophthisis and related ciliopathies. Nephron Exp Nephrol *118*, e9-14.

Ishikawa, H., and Marshall, W.F. (2011). Ciliogenesis: building the cell's antenna. Nat Rev Mol Cell Biol *12*, 222-234.

Jang, Y.J., Lin, C.Y., Ma, S., and Erikson, R.L. (2002). Functional studies on the role of the C-terminal domain of mammalian polo-like kinase. Proc Natl Acad Sci U S A *99*, 1984-1989.

Jenkins, P.M., McEwen, D.P., and Martens, J.R. (2009). Olfactory cilia: linking sensory cilia function and human disease. Chem Senses *34*, 451-464.

Jeong, Y., Lee, J., Kim, K., Yoo, J.C., and Rhee, K. (2007). Characterization of NIP2/centrobin, a novel substrate of Nek2, and its potential role in microtubule stabilization. J Cell Sci *120*, 2106-2116.

Jiang, J., and Hui, C.C. (2008). Hedgehog signaling in development and cancer. Dev Cell *15*, 801-812.

Johnson, L.N., Noble, M.E., and Owen, D.J. (1996). Active and inactive protein kinases: structural basis for regulation. Cell *85*, 149-158.

Jones, D.G., and Rosamond, J. (1990). Isolation of a novel protein kinase-encoding gene from yeast by oligodeoxyribonucleotide probing. Gene *90*, 87-92.

Kambouris, N.G., Burke, D.J., and Creutz, C.E. (1993). Cloning and genetic analysis of the gene encoding a new protein kinase in Saccharomyces cerevisiae. Yeast *9*, 141-150.

Kandli, M., Feige, E., Chen, A., Kilfin, G., and Motro, B. (2000). Isolation and characterization of two evolutionarily conserved murine kinases (Nek6 and nek7) related to the fungal mitotic regulator, NIMA. Genomics *68*, 187-196.

Kiefer, J.C. (2011a). Primer and interviews: Diverse connections between primary cilia and Hedgehog signaling. Dev Dyn *239*, 1255-1262.

Kiefer, J.C. (2011b). Primer and interviews: The dynamic stem cell niche. Dev Dyn *240*, 737-743.

Kim, E., Arnould, T., Sellin, L.K., Benzing, T., Fan, M.J., Gruning, W., Sokol, S.Y., Drummond, I., and Walz, G. (1999). The polycystic kidney disease 1 gene product modulates Wnt signaling. J Biol Chem *274*, 4947-4953.

Kim, J.C., Badano, J.L., Sibold, S., Esmail, M.A., Hill, J., Hoskins, B.E., Leitch, C.C., Venner, K., Ansley, S.J., Ross, A.J.*, et al.* (2004). The Bardet-Biedl protein BBS4 targets cargo to the pericentriolar region and is required for microtubule anchoring and cell cycle progression. Nat Genet *36*, 462-470.

Kim, S., Lee, K., and Rhee, K. (2007). NEK7 is a centrosomal kinase critical for microtubule nucleation. Biochem Biophys Res Commun *360*, 56-62.

King, P.J., Guasti, L., and Laufer, E. (2008). Hedgehog signalling in endocrine development and disease. J Endocrinol *198*, 439-450.

Kobayashi, T., and Dynlacht, B.D. (2011). Regulating the transition from centriole to basal body. J Cell Biol *193*, 435-444.

Kolb, R.J., and Nauli, S.M. (2008). Ciliary dysfunction in polycystic kidney disease: an emerging model with polarizing potential. Front Biosci *13*, 4451-4466.

Komiya, Y., and Habas, R. (2008). Wnt signal transduction pathways. Organogenesis *4*, 68-75.

Krien, M.J., Bugg, S.J., Palatsides, M., Asouline, G., Morimyo, M., and O'Connell, M.J. (1998). A NIMA homologue promotes chromatin condensation in fission yeast. J Cell Sci *111 (Pt 7)*, 967-976.

Krien, M.J., West, R.R., John, U.P., Koniaras, K., McIntosh, J.R., and O'Connell, M.J. (2002). The fission yeast NIMA kinase Fin1p is required for spindle function and nuclear envelope integrity. EMBO J *21*, 1713-1722.

Kubo, A., Sasaki, H., Yuba-Kubo, A., Tsukita, S., and Shiina, N. (1999). Centriolar satellites: molecular characterization, ATP-dependent movement toward centrioles and possible involvement in ciliogenesis. J Cell Biol *147*, 969-980.

Lee, J.H., and Gleeson, J.G. (2010). The role of primary cilia in neuronal function. Neurobiol Dis *38*, 167-172.

Leigh, M.W., Pittman, J.E., Carson, J.L., Ferkol, T.W., Dell, S.D., Davis, S.D., Knowles, M.R., and Zariwala, M.A. (2009). Clinical and genetic aspects of primary ciliary dyskinesia/Kartagener syndrome. Genet Med *11*, 473-487.

Letwin, K., Mizzen, L., Motro, B., Ben-David, Y., Bernstein, A., and Pawson, T. (1992). A mammalian dual specificity protein kinase, Nek1, is related to the NIMA cell cycle regulator and highly expressed in meiotic germ cells. EMBO J *11*, 3521-3531.

Levedakou, E.N., He, M., Baptist, E.W., Craven, R.J., Cance, W.G., Welcsh, P.L., Simmons, A., Naylor, S.L., Leach, R.J., Lewis, T.B.*, et al.* (1994). Two novel human serine/threonine kinases with homologies to the cell cycle

regulating Xenopus MO15, and NIMA kinases: cloning and characterization of their expression pattern. Oncogene *9*, 1977-1988.

Li, Y., Wright, J.M., Qian, F., Germino, G.G., and Guggino, W.B. (2005). Polycystin 2 interacts with type I inositol 1,4,5-trisphosphate receptor to modulate intracellular Ca2+ signaling. J Biol Chem *280*, 41298-41306.

Lim, H.H., Zhang, T., and Surana, U. (2009). Regulation of centrosome separation in yeast and vertebrates: common threads. Trends Cell Biol *19*, 325-333.

Liu, S., Lu, W., Obara, T., Kuida, S., Lehoczky, J., Dewar, K., Drummond, I.A., and Beier, D.R. (2002). A defect in a novel Nek-family kinase causes cystic kidney disease in the mouse and in zebrafish. Development *129*, 5839-5846.

Loncarek, J., and Khodjakov, A. (2009). Ab ovo or de novo? Mechanisms of centriole duplication. Mol Cells *27*, 135-142.

Louie, C.M., and Gleeson, J.G. (2005). Genetic basis of Joubert syndrome and related disorders of cerebellar development. Hum Mol Genet *14 Spec No. 2*, R235-242.

Lu, K.P., and Hunter, T. (1995). Evidence for a NIMA-like mitotic pathway in vertebrate cells. Cell *81*, 413-424.

Lu, K.P., Kemp, B.E., and Means, A.R. (1994). Identification of substrate specificity determinants for the cell cycle-regulated NIMA protein kinase. J Biol Chem *269*, 6603-6607.

Lu, K.P., Osmani, S.A., and Means, A.R. (1993). Properties and regulation of the cell cycle-specific NIMA protein kinase of Aspergillus nidulans. J Biol Chem *268*, 8769-8776.

Mahjoub, M.R., Montpetit, B., Zhao, L., Finst, R.J., Goh, B., Kim, A.C., and Quarmby, L.M. (2002). The FA2 gene of Chlamydomonas encodes a NIMA family kinase with roles in cell cycle progression and microtubule severing during deflagellation. J Cell Sci *115*, 1759-1768.

Mahjoub, M.R., Trapp, M.L., and Quarmby, L.M. (2005). NIMA-related kinases defective in murine models of polycystic kidney diseases localize to primary cilia and centrosomes. J Am Soc Nephrol *16*, 3485-3489.

Mans, D.A., Voest, E.E., and Giles, R.H. (2008). All along the watchtower: is the cilium a tumor suppressor organelle? Biochim Biophys Acta *1786*, 114-125.

Mardin, B.R., Lange, C., Baxter, J.E., Hardy, T., Scholz, S.R., Fry, A.M., and Schiebel, E. (2010). Components of the Hippo pathway cooperate with Nek2 kinase to regulate centrosome disjunction. Nat Cell Biol *12*, 1166-1176.

Marshall, W.F., and Nonaka, S. (2006). Cilia: tuning in to the cell's antenna. Curr Biol *16*, R604-614.

Marshall, W.F. (2008). The cell biological basis of ciliary disease. J Cell Biol *180*, 17-21.

Mattison, C.P., Old, W.M., Steiner, E., Huneycutt, B.J., Resing, K.A., Ahn, N.G., and Winey, M. (2007). Mps1 activation loop autophosphorylation enhances kinase activity. J Biol Chem *282*, 30553-30561.

Melixetian, M., Klein, D.K., Sorensen, C.S., and Helin, K. (2009). NEK11 regulates CDC25A degradation and the IR-induced G2/M checkpoint. Nat Cell Biol *11*, 1247-1253.

Meng, L., Michaud, G.A., Merkel, J.S., Zhou, F., Huang, J., Mattoon, D.R., and Schweitzer, B. (2008). Protein kinase substrate identification on functional protein arrays. BMC Biotechnol *8*, 22.

Minoguchi, S., Minoguchi, M., and Yoshimura, A. (2003). Differential control of the NIMA-related kinases, Nek6 and Nek7, by serum stimulation. Biochem Biophys Res Commun *301*, 899-906.

Mollet, G., Salomon, R., Gribouval, O., Silbermann, F., Bacq, D., Landthaler, G., Milford, D., Nayir, A., Rizzoni, G., Antignac, C.*, et al.* (2002). The gene mutated in juvenile nephronophthisis type 4 encodes a novel protein that interacts with nephrocystin. Nat Genet *32*, 300-305.

Mollet, G., Silbermann, F., Delous, M., Salomon, R., Antignac, C., and Saunier, S. (2005). Characterization of the nephrocystin/nephrocystin-4 complex and subcellular localization of nephrocystin-4 to primary cilia and centrosomes. Hum Mol Genet *14*, 645-656.

Mogensen, M.M., Malik, A., Piel, M., Bouckson-Castaing, V., and Bornens, M. (2000). Microtubule minus-end anchorage at centrosomal and non-centrosomal sites: the role of ninein. J Cell Sci *113 (Pt 17)*, 3013-3023.

Moniz, L.S., and Stambolic, V. (2010). Nek10 mediates G2/M cell cycle arrest and MEK autoactivation in response to UV irradiation. Mol Cell Biol *31*, 30-42.

Moser, J.J., Fritzler, M.J., and Rattner, J.B. (2009). Primary ciliogenesis defects are associated with human astrocytoma/glioblastoma cells. BMC Cancer *9*, 448.

Mukhopadhyay, S., Lu, Y., Qin, H., Lanjuin, A., Shaham, S., and Sengupta, P. (2007). Distinct IFT mechanisms contribute to the generation of ciliary structural diversity in C. elegans. EMBO J *26*, 2966-2980.

Muller, U. (2008). Cadherins and mechanotransduction by hair cells. Curr Opin Cell Biol *20*, 557-566.

Natoli, T.A., Gareski, T.C., Dackowski, W.R., Smith, L., Bukanov, N.O., Russo, R.J., Husson, H., Matthews, D., Piepenhagen, P., and Ibraghimov-Beskrovnaya, O. (2008). Pkd1 and Nek8 mutations affect cell-cell adhesion and cilia in cysts formed in kidney organ cultures. Am J Physiol Renal Physiol *294*, F73-83.

Nauli, S.M., Alenghat, F.J., Luo, Y., Williams, E., Vassilev, P., Li, X., Elia, A.E., Lu, W., Brown, E.M., Quinn, S.J.*, et al.* (2003). Polycystins 1 and 2 mediate mechanosensation in the primary cilium of kidney cells. Nat Genet *33*, 129-137.

Nayak, G.D., Ratnayaka, H.S., Goodyear, R.J., and Richardson, G.P. (2007). Development of the hair bundle and mechanotransduction. Int J Dev Biol *51*, 597-608.

Nigg, E.A. (2007). Centrosome duplication: of rules and licenses. Trends Cell Biol *17*, 215-221.

Nigg, E.A., and Raff, J.W. (2009). Centrioles, centrosomes, and cilia in health and disease. Cell *139*, 663-678.

Noguchi, K., Fukazawa, H., Murakami, Y., and Uehara, Y. (2002). Nek11, a new member of the NIMA family of kinases, involved in DNA replication and genotoxic stress responses. J Biol Chem *277*, 39655-39665.

Nusslein-Volhard, C., and Wieschaus, E. (1980). Mutations affecting segment number and polarity in Drosophila. Nature *287*, 795-801.

Oakley, B.R., and Morris, N.R. (1983). A mutation in Aspergillus nidulans that blocks the transition from interphase to prophase. J Cell Biol *96*, 1155-1158.

O'Connell, M.J., Krien, M.J., and Hunter, T. (2003). Never say never. The NIMA-related protein kinases in mitotic control. Trends Cell Biol *13*, 221-228.

O'Connell, M.J., Norbury, C., and Nurse, P. (1994). Premature chromatin condensation upon accumulation of NIMA. EMBO J *13*, 4926-4937.

Okada, Y., Nonaka, S., Tanaka, Y., Saijoh, Y., Hamada, H., and Hirokawa, N. (1999). Abnormal nodal flow precedes situs inversus in iv and inv mice. Mol Cell *4*, 459-468.

Olbrich, H., Fliegauf, M., Hoefele, J., Kispert, A., Otto, E., Volz, A., Wolf, M.T., Sasmaz, G., Trauer, U., Reinhardt, R.*, et al.* (2003). Mutations in a novel gene, NPHP3, cause adolescent nephronophthisis, tapeto-retinal degeneration and hepatic fibrosis. Nat Genet *34*, 455-459.

Omran, H. (2010). NPHP proteins: gatekeepers of the ciliary compartment. J Cell Biol *190*, 715-717.

O'Regan, L., Blot, J., and Fry, A.M. (2007). Mitotic regulation by NIMA-related kinases. Cell Div *2*, 25.

O'Regan, L., and Fry, A.M. (2009). The Nek6 and Nek7 protein kinases are required for robust mitotic spindle formation and cytokinesis. Mol Cell Biol *29*, 3975-3990.

Osmani, A.H., McGuire, S.L., O'Donnell, K.L., Pu, R.T., and Osmani, S.A. (1991a). Role of the cell-cycle-regulated NIMA protein kinase during G2 and mitosis: evidence for two pathways of mitotic regulation. Cold Spring Harb Symp Quant Biol *56*, 549-555.

Osmani, A.H., O'Donnell, K., Pu, R.T., and Osmani, S.A. (1991b). Activation of the nimA protein kinase plays a unique role during mitosis that cannot be bypassed by absence of the bimE checkpoint. EMBO J *10*, 2669-2679.

Osmani, A.H., van Peij, N., Mischke, M., O'Connell, M.J., and Osmani, S.A. (1994). A single p34cdc2 protein kinase (encoded by nimXcdc2) is required at G1 and G2 in Aspergillus nidulans. J Cell Sci *107 (Pt 6)*, 1519-1528.

Osmani, S.A., May, G.S., and Morris, N.R. (1987). Regulation of the mRNA levels of nimA, a gene required for the G2-M transition in Aspergillus nidulans. J Cell Biol *104*, 1495-1504.

Otto, E., Hoefele, J., Ruf, R., Mueller, A.M., Hiller, K.S., Wolf, M.T., Schuermann, M.J., Becker, A., Birkenhager, R., Sudbrak, R.*, et al.* (2002). A gene mutated in nephronophthisis and retinitis pigmentosa encodes a novel protein, nephroretinin, conserved in evolution. Am J Hum Genet *71*, 1161-1167.

Otto, E.A., Ramaswami, G., Janssen, S., Chaki, M., Allen, S.J., Zhou, W., Airik, R., Hurd, T.W., Ghosh, A.K., Wolf, M.T.*, et al.* (2010). Mutation analysis of 18 nephronophthisis associated ciliopathy disease genes using a DNA pooling and next generation sequencing strategy. J Med Genet *48*, 105-116.

Otto, E.A., Schermer, B., Obara, T., O'Toole, J.F., Hiller, K.S., Mueller, A.M., Ruf, R.G., Hoefele, J., Beekmann, F., Landau, D.*, et al.* (2003). Mutations in INVS encoding inversin cause nephronophthisis type 2, linking renal cystic disease to the function of primary cilia and left-right axis determination. Nat Genet *34*, 413-420.

Otto, E.A., Loeys, B., Khanna, H., Hellemans, J., Sudbrak, R., Fan, S., Muerb, U., O'Toole, J.F., Helou, J., Attanasio, M.*, et al.* (2005). Nephrocystin-5, a ciliary IQ domain protein, is mutated in Senior-Loken syndrome and interacts with RPGR and calmodulin. Nat Genet *37*, 282-288.

Otto, E.A., Trapp, M.L., Schultheiss, U.T., Helou, J., Quarmby, L.M., and Hildebrandt, F. (2008). NEK8 mutations affect ciliary and centrosomal localization and may cause nephronophthisis. J Am Soc Nephrol *19*, 587-592.

Pan, J., and Snell, W. (2007). The primary cilium: keeper of the key to cell division. Cell *129*, 1255-1257.

Pan, J., Wang, Q., and Snell, W.J. (2005). Cilium-generated signaling and cilia-related disorders. Lab Invest *85*, 452-463.

Pazour, G.J., San Agustin, J.T., Follit, J.A., Rosenbaum, J.L., and Witman, G.B. (2002). Polycystin-2 localizes to kidney cilia and the ciliary level is elevated in orpk mice with polycystic kidney disease. Curr Biol *12*, R378-380.

Pazour, G.J., and Witman, G.B. (2003). The vertebrate primary cilium is a sensory organelle. Curr Opin Cell Biol *15*, 105-110.

Pazour, G.J., and Rosenbaum, J.L. (2004). Intraflagellar transport and cilia-dependent diseases. Trends Cell Biol *12*, 551-555.

Pedersen, L.B., and Rosenbaum, J.L. (2008). Intraflagellar transport (IFT) role in ciliary assembly, resorption and signalling. Curr Top Dev Biol *85*, 23-61.

Pedersen, L.B., Veland, I.R., Schroder, J.M., and Christensen, S.T. (2008). Assembly of primary cilia. Dev Dyn *237*, 1993-2006.

Pelka, P., Scime, A., Mandalfino, C., Joch, M., Abdulla, P., and Whyte, P. (2007). Adenovirus E1A proteins direct subcellular redistribution of Nek9, a NimA-related kinase. J Cell Physiol *212*, 13-25.

Pickart, C.M. (2001). Mechanisms underlying ubiquitination. Annu Rev Biochem *70*, 503-533.

Pickart, C.M., and Eddins, M.J. (2004). Ubiquitin: structures, functions, mechanisms. Biochim Biophys Acta *1695*, 55-72.

Plotnikova, O.V., Golemis, E.A., and Pugacheva, E.N. (2008). Cell cycle-dependent ciliogenesis and cancer. Cancer Res *68*, 2058-2061.

Polci, R., Peng, A., Chen, P.L., Riley, D.J., and Chen, Y. (2004). NIMA-related protein kinase 1 is involved early in the ionizing radiation-induced DNA damage response. Cancer Res *64*, 8800-8803.

Pu, R.T., and Osmani, S.A. (1995). Mitotic destruction of the cell cycle regulated NIMA protein kinase of Aspergillus nidulans is required for mitotic exit. EMBO J *14*, 995-1003.

Pu, R.T., Xu, G., Wu, L., Vierula, J., O'Donnell, K., Ye, X.S., and Osmani, S.A. (1995). Isolation of a functional homolog of the cell cycle-specific NIMA protein kinase of Aspergillus nidulans and functional analysis of conserved residues. J Biol Chem *270*, 18110-18116.

Pugacheva, E.N., Jablonski, S.A., Hartman, T.R., Henske, E.P., and Golemis, E.A. (2007). HEF1-dependent Aurora A activation induces disassembly of the primary cilium. Cell *129*, 1351-1363.

Qian, F., Germino, F.J., Cai, Y., Zhang, X., Somlo, S., and Germino, G.G. (1997). PKD1 interacts with PKD2 through a probable coiled-coil domain. Nat Genet *16*, 179-183.

Quarmby, L.M., and Mahjoub, M.R. (2005). Caught Nek-ing: cilia and centrioles. J Cell Sci *118*, 5161-5169.

Quarmby, L.M., and Parker, J.D. (2005). Cilia and the cell cycle? J Cell Biol *169*, 707-710.

Quinlan, R.J., Tobin, J.L., and Beales, P.L. (2008). Modeling ciliopathies: Primary cilia in development and disease. Curr Top Dev Biol *84*, 249-310.

Ramamurthy, V., and Cayouette, M. (2009). Development and disease of the photoreceptor cilium. Clin Genet *76*, 137-145.

R**apley, J., Baxter, J.E., Blot, J., Wattam, S.L., Casenghi, M., Meraldi, P., Nigg, E.A., and Fry, A.M.** (2005). Coordinate regulation of the mother centriole component nlp by nek2 and plk1 protein kinases. Mol Cell Biol *25*, 1309-1324.

Regue, L., Sdelci, S., Bertran, M.T., Caelles, C., Reverter, D., and Roig, J. (2011). DYNLL/LC8 protein controls signal transduction through the Nek9/Nek6 signaling module by regulating Nek6 binding to Nek9. J Biol Chem *286*, 18118-18129.

Rhee, K., and Wolgemuth, D.J. (1997). The NIMA-related kinase 2, Nek2, is expressed in specific stages of the meiotic cell cycle and associates with meiotic chromosomes. Development *124*, 2167-2177.

Richards, M.W., O'Regan, L., Mas-Droux, C., Blot, J.M., Cheung, J., Hoelder, S., Fry, A.M., and Bayliss, R. (2009). An autoinhibitory tyrosine motif in the cell-cycle-regulated Nek7 kinase is released through binding of Nek9. Mol Cell *36*, 560-570.

Rodrigues-Martins, A., Riparbelli, M., Callaini, G., Glover, D.M., and Bettencourt-Dias, M. (2007). Revisiting the role of the mother centriole in centriole biogenesis. Science *316*, 1046-1050.

Roig, J., Groen, A., Caldwell, J., and Avruch, J. (2005). Active Nercc1 protein kinase concentrates at centrosomes early in mitosis and is necessary for proper spindle assembly. Mol Biol Cell *16*, 4827-4840.

Roig, J., Mikhailov, A., Belham, C., and Avruch, J. (2002). Nercc1, a mammalian NIMA-family kinase, binds the Ran GTPase and regulates mitotic progression. Genes Dev *16*, 1640-1658.

Romio, L., Fry, A.M., Winyard, P.J., Malcolm, S., Woolf, A.S., and Feather, S.A. (2004). OFD1 is a centrosomal/basal body protein expressed during mesenchymal-epithelial transition in human nephrogenesis. J Am Soc Nephrol *15*, 2556-2568.

Ross, A.J., May-Simera, H., Eichers, E.R., Kai, M., Hill, J., Jagger, D.J., Leitch, C.C., Chapple, J.P., Munro, P.M., Fisher, S.*, et al.* (2005). Disruption of Bardet-Biedl syndrome ciliary proteins perturbs planar cell polarity in vertebrates. Nat Genet *37*, 1135-1140.

Salathe, M. (2007). Regulation of mammalian ciliary beating. Annu Rev Physiol *69*, 401-422.

Salomon, R., Saunier, S., and Niaudet, P. (2009). Nephronophthisis. Pediatr Nephrol *24*, 2333-2344.

S**ankaran, S., and Parvin, J.D.** (2006). Centrosome function in normal and tumor cells. J Cell Biochem *99*, 1240-1250.

Satir, P. (2008). Primary cilia: integral to development and disease. Dev Dyn *237*, 1953-1954.

Satir, P., and Christensen, S.T. (2007). Overview of structure and function of mammalian cilia. Annu Rev Physiol *69*, 377-400.

Satir, P., Guerra, C., and Bell, A.J. (2007). Evolution and persistence of the cilium. Cell Motil Cytoskeleton *64*, 906-913.

Satir, P., Mitchell, D.R., and Jekely, G. (2008). How did the cilium evolve? Curr Top Dev Biol *85*, 63-82.

Satir, P., Pedersen, L.B., and Christensen, S.T. (2010). The primary cilium at a glance. J Cell Sci *123*, 499-503.

Saunier, S., Calado, J., Heilig, R., Silbermann, F., Benessy, F., Morin, G., Konrad, M., Broyer, M., Gubler, M.C., Weissenbach, J.*, et al.* (1997). A novel gene that encodes a protein with a putative src homology 3 domain is a candidate gene for familial juvenile nephronophthisis. Hum Mol Genet *6*, 2317-2323.

Saunier, S., Salomon, R., and Antignac, C. (2005). Nephronophthisis. Curr Opin Genet Dev *15*, 324-331.

Schatten, H. (2008). The mammalian centrosome and its functional significance. Histochem Cell Biol *129*, 667-686.

Schneider, L., Clement, C.A., Teilmann, S.C., Pazour, G.J., Hoffmann, E.K., Satir, P., and Christensen, S.T. (2005). PDGFRalphaalpha signaling is regulated through the primary cilium in fibroblasts. Curr Biol *15*, 1861-1866.

Schultz, S.J., Fry, A.M., Sutterlin, C., Ried, T., and Nigg, E.A. (1994). Cell cycle-dependent expression of Nek2, a novel human protein kinase related to the NIMA mitotic regulator of Aspergillus nidulans. Cell Growth Differ *5*, 625-635.

Schultz, S.J., and Nigg, E.A. (1993). Identification of 21 novel human protein kinases, including 3 members of a family related to the cell cycle regulator nimA of Aspergillus nidulans. Cell Growth Differ *4*, 821-830.

Schwartz, E.A., Leonard, M.L., Bizios, R., and Bowser, S.S. (1997). Analysis and modeling of the primary cilium bending response to fluid shear. Am J Physiol *272*, F132-138.

Schweitzer, B., and Philippsen, P. (1992). NPK1, a nonessential protein kinase gene in Saccharomyces cerevisiae with similarity to Aspergillus nidulans nimA. Mol Gen Genet *234*, 164-167.

Seeley, E.S., Carriere, C., Goetze, T., Longnecker, D.S., and Korc, M. (2009). Pancreatic cancer and precursor pancreatic intraepithelial neoplasia lesions are devoid of primary cilia. Cancer Res *69*, 422-430.

Seeley, E.S., and Nachury, M.V. (2010). The perennial organelle: assembly and disassembly of the primary cilium. J Cell Sci *123*, 511-518.

Shalom, O., Shalva, N., Altschuler, Y., and Motro, B. (2008). The mammalian Nek1 kinase is involved in primary cilium formation. FEBS Lett *582*, 1465-1470.

Shiba, D., Manning, D.K., Koga, H., Beier, D.R., and Yokoyama, T. (2010). Inv acts as a molecular anchor for Nphp3 and Nek8 in the proximal segment of primary cilia. Cytoskeleton (Hoboken) *67*, 112-119.

Simms, R.J., Eley, L., and Sayer, J.A. (2009). Nephronophthisis. Eur J Hum Genet *17*, 406-416.

Simms, R.J., Hynes, A.M., Eley, L., and Sayer, J.A. Nephronophthisis: a genetically diverse ciliopathy. Int J Nephrol *2011*, 527137.

Simms, R.J., Hynes, A.M., Eley, L., and Sayer, J.A. (2011). Nephronophthisis: a genetically diverse ciliopathy. Int J Nephrol *2011*, 527137.

Simons, M., Gloy, J., Ganner, A., Bullerkotte, A., Bashkurov, M., Kronig, C., Schermer, B., Benzing, T., Cabello, O.A., Jenny, A.*, et al.* (2005). Inversin, the gene product mutated in nephronophthisis type II, functions as a molecular switch between Wnt signaling pathways. Nat Genet *37*, 537-543.

Singla, V., and Reiter, J.F. (2006). The primary cilium as the cell's antenna: signaling at a sensory organelle. Science *313*, 629-633.

Smith, L.A., Bukanov, N.O., Husson, H., Russo, R.J., Barry, T.C., Taylor, A.L., Beier, D.R., and Ibraghimov-Beskrovnaya, O. (2006). Development of polycystic kidney disease in juvenile cystic kidney mice: insights into pathogenesis, ciliary abnormalities, and common features with human disease. J Am Soc Nephrol *17*, 2821-2831.

Sobkowicz, H.M., Slapnick, S.M., and August, B.K. (1995). The kinocilium of auditory hair cells and evidence for its morphogenetic role during the regeneration of stereocilia and cuticular plates. J Neurocytol *24*, 633-653.

Sohara, E., Luo, Y., Zhang, J., Manning, D.K., Beier, D.R., and Zhou, J. (2008). Nek8 regulates the expression and localization of polycystin-1 and polycystin-2. J Am Soc Nephrol *19*, 469-476.

Sorensen, C.S., Melixetian, M., Klein, D.K., and Helin, K. (2010). NEK11: linking CHK1 and CDC25A in DNA damage checkpoint signaling. Cell Cycle *9*, 450-455.

Sorokin, S.P. (1968). Reconstructions of centriole formation and ciliogenesis in mammalian lungs. J Cell Sci *3*, 207-230.

Spektor, A., Tsang, W.Y., Khoo, D., and Dynlacht, B.D. (2007). Cep97 and CP110 suppress a cilia assembly program. Cell *130*, 678-690.

Surpili, M.J., Delben, T.M., and Kobarg, J. (2003). Identification of proteins that interact with the central coiled-coil region of the human protein kinase NEK1. Biochemistry *42*, 15369-15376.

Tanaka, K., and Nigg, E.A. (1999). Cloning and characterization of the murine Nek3 protein kinase, a novel member of the NIMA family of putative cell cycle regulators. J Biol Chem *274*, 13491-13497.

Thrower, J.S., Hoffman, L., Rechsteiner, M., and Pickart, C.M. (2000). Recognition of the polyubiquitin proteolytic signal. Embo J *19*, 94-102.

Tobin, J.L., and Beales, P.L. (2009). The nonmotile ciliopathies. Genet Med *11*, 386-402.

Torres, V.E., and Harris, P.C. (2007). Polycystic kidney disease: genes, proteins, animal models, disease mechanisms and therapeutic opportunities. J Intern Med *261*, 17-31.

Trapp, M.L., Galtseva, A., Manning, D.K., Beier, D.R., Rosenblum, N.D., and Quarmby, L.M. (2008). Defects in ciliary localization of Nek8 is associated with cystogenesis. Pediatr Nephrol *23*, 377-387.

Tsou, M.F., and Stearns, T. (2006). Mechanism limiting centrosome duplication to once per cell cycle. Nature *442*, 947-951.

Tsou, M.F., Wang, W.J., George, K.A., Uryu, K., Stearns, T., and Jallepalli, P.V. (2009). Polo kinase and separase regulate the mitotic licensing of centriole duplication in human cells. Dev Cell *17*, 344-354.

Twomey, C., Wattam, S.L., Pillai, M.R., Rapley, J., Baxter, J.E., and Fry, A.M. (2004). Nek2B stimulates zygotic centrosome assembly in Xenopus laevis in a kinase-independent manner. Dev Biol *265*, 384-398.

Upadhya, P., Birkenmeier, E.H., Birkenmeier, C.S., and Barker, J.E. (2000). Mutations in a NIMA-related kinase gene, Nek1, cause pleiotropic effects including a progressive polycystic kidney disease in mice. Proc Natl Acad Sci U S A *97*, 217-221.

Urbani, L., and Stearns, T. (1999). The centrosome. Curr Biol *9*, R315-317.

Valente, E.M., Silhavy, J.L., Brancati, F., Barrano, G., Krishnaswami, S.R., Castori, M., Lancaster, M.A., Boltshauser, E., Boccone, L., Al-Gazali, L.*, et al.* (2006). Mutations in CEP290, which encodes a centrosomal protein, cause pleiotropic forms of Joubert syndrome. Nat Genet *38*, 623-625.

Varjosalo, M., and Taipale, J. (2008). Hedgehog: functions and mechanisms. Genes Dev *22*, 2454-2472.

Veeman, M.T., Axelrod, J.D., and Moon, R.T. (2003). A second canon. Functions and mechanisms of beta-catenin-independent Wnt signaling. Dev Cell *5*, 367-377.

Veland, I.R., Awan, A., Pedersen, L.B., Yoder, B.K., and Christensen, S.T. (2009). Primary cilia and signaling pathways in mammalian development, health and disease. Nephron Physiol *111*, p39-53.

Vierkotten, J., Dildrop, R., Peters, T., Wang, B., and Ruther, U. (2007). Ftm is a novel basal body protein of cilia involved in Shh signalling. Development *134*, 2569-2577.

Voges, D., Zwickl, P., and Baumeister, W. (1999). The 26S proteasome: a molecular machine designed for controlled proteolysis. Annu Rev Biochem *68*, 1015-1068.

Wallingford, J.B., Fraser, S.E., and Harland, R.M. (2002). Convergent extension: the molecular control of polarized cell movement during embryonic development. Dev Cell *2*, 695-706.

Wallingford, J.B., and Mitchell, B. (2011). Strange as it may seem: the many links between Wnt signaling, planar cell polarity, and cilia. Genes Dev *25*, 201-213.

Wang, Y. (2009). Wnt/Planar cell polarity signaling: a new paradigm for cancer therapy. Mol Cancer Ther *8*, 2103-2109.

White, M.C., and Quarmby, L.M. (2008). The NIMA-family kinase, Nek1 affects the stability of centrosomes and ciliogenesis. BMC Cell Biol *9*, 29.

Wloga, D., Camba, A., Rogowski, K., Manning, G., Jerka-Dziadosz, M., and Gaertig, J. (2006). Members of the NIMA-related kinase family promote disassembly of cilia by multiple mechanisms. Mol Biol Cell *17*, 2799-2810.

Wong, S.Y., and Reiter, J.F. (2008). The primary cilium at the crossroads of mammalian hedgehog signaling. Curr Top Dev Biol *85*, 225-260.

Wong, S.Y., Seol, A.D., So, P.L., Ermilov, A.N., Bichakjian, C.K., Epstein, E.H., Jr., Dlugosz, A.A., and Reiter, J.F. (2009). Primary cilia can both mediate and suppress Hedgehog pathway-dependent tumorigenesis. Nat Med *15*, 1055-1061.

Wright, A.F., Chakarova, C.F., Abd El-Aziz, M.M., and Bhattacharya, S.S. (2010). Photoreceptor degeneration: genetic and mechanistic dissection of a complex trait. Nat Rev Genet *11*, 273-284.

Wu, L., Osmani, S.A., and Mirabito, P.M. (1998). A role for NIMA in the nuclear localization of cyclin B in Aspergillus nidulans. J Cell Biol *141*, 1575-1587.

Wu, W., Baxter, J.E., Wattam, S.L., Hayward, D.G., Fardilha, M., Knebel, A., Ford, E.M., da Cruz e Silva, E.F., and Fry, A.M. (2007). Alternative splicing controls nuclear translocation of the cell cycle-regulated Nek2 kinase. J Biol Chem *282*, 26431-26440.

Yang, J., Adamian, M., and Li, T. (2006). Rootletin interacts with C-Nap1 and may function as a physical linker between the pair of centrioles/basal bodies in cells. Mol Biol Cell *17*, 1033-1040.

Ye, X.S., Xu, G., Pu, R.T., Fincher, R.R., McGuire, S.L., Osmani, A.H., and Osmani, S.A. (1995). The NIMA protein kinase is hyperphosphorylated and activated downstream of p34cdc2/cyclin B: coordination of two mitosis promoting kinases. EMBO J *14*, 986-994.

Ye, X.S., Fincher, R.R., Tang, A., Osmani, A.H., and Osmani, S.A. (1998). Regulation of the anaphase-promoting complex/cyclosome by bimAAPC3 and proteolysis of NIMA. Mol Biol Cell *9*, 3019-3030.

Yim, H., Sung, C.K., You, J., Tian, Y., and Benjamin, T. (2011). Nek1 and TAZ interact to maintain normal levels of polycystin 2. J Am Soc Nephrol *22*, 832-837.

Zhou, J. (2009). Polycystins and primary cilia: primers for cell cycle progression. Annu Rev Physiol *71*, 83-113.

Yin, M.J., Shao, L., Voehringer, D., Smeal, T., and Jallal, B. (2003). The serine/threonine kinase Nek6 is required for cell cycle progression through mitosis. J Biol Chem *278*, 52454-52460.

Yissachar, N., Salem, H., Tennenbaum, T., and Motro, B. (2006). Nek7 kinase is enriched at the centrosome, and is required for proper spindle assembly and mitotic progression. FEBS Lett *580*, 6489-6495.

Zaghloul, N.A., and Katsanis, N. (2009). Mechanistic insights into Bardet-Biedl syndrome, a model ciliopathy. J Clin Invest *119*, 428-437.

Zhang, Q., Taulman, P.D., and Yoder, B.K. (2004). Cystic kidney diseases: all roads lead to the cilium. Physiology (Bethesda) *19*, 225-230.

Zhou, J. (2009). Polycystins and primary cilia: primers for cell cycle progression. Annu Rev Physiol *71*, 83-113.